Identification and characterization of vacuolar nucleotide phosphatases
and
Characterization of an engineered catabolic pathway for urea in *Arabidopsis thaliana*

Von der Naturwissenschaftlichen Fakultät der
Gottfried Wilhelm Leibniz Universität Hannover

zur Erlangung des Grades
Doktorin der Naturwissenschaften (Dr. rer. nat.)

genehmigte Dissertation
von
Nabila Firdoos, Master of Philosphy (Pakistani)

2023

The investigations described in the following thesis were conducted under the supervision of Prof. Dr. Claus-Peter Witte at the Institute of Plant Nutrition of the Gottfried Wilhelm Leibniz Universität Hannover with the financial support of the Deutsche Akademische AustauschDienst (DAAD).

Abstract

Section 1

Plants have the remarkable ability to remobilize nutrients by degrading cellular components such as damaged organelles, proteins, and RNA in vacuoles. According to the current model of RNA degradation in vacuoles, the RNA is degraded in three steps. After the transport of the RNA into vacuoles, it is first degraded to 3'-mononucleotides (3'-NMPs) by the intercellular ribonuclease RNS2. The RNA degradation products are then dephosphorylated by vacuolar acid phosphatases (AP), releasing nucleosides. These nucleosides are eventually transported by the Equilibrative Nucleoside Transporter 1 (ENT1) from vacuoles to the cytosol, where they are either degraded or salvaged to nucleotides, thereby either releasing nutrients or conserving metabolic resources. RNS2 and ENT1 were studied and characterized several years ago, but the vacuolar nucleotide phosphatases have not yet been identified.

This study focuses on the identification and characterization of the nucleotide-dephosphorylating APs from vacuoles. Three protein families, the Haloacid Dehalogenase IIIB (HADIIIB) family, the Purple Acid Phosphatase (PAP) family, and the Endonuclease (Endo) S1/P1-type nucleases were considered based on their previous identification in the vacuolar proteome or their potential to localize in the vacuole and based on their potential nucleotidase activities. In total 44 candidate proteins were then screened employing a set of selection criteria, including protein conservation in other plants, protein localization, substrate preferences, and expression profiles. Several mutant combinations were generated for the most promising candidates using T-DNA insertion lines and the CRISPR/Cas9 technique. When the final candidates (HADIIIB4 renamed to Vacuolar Nucleoside Phosphate Phosphatase 1 (VNPP1) and PAP26)) were identified, they were fully characterized *in vitro* and *in vivo*. The function of VNPP1 and PAP26 in vacuolar mononucleotide dephosphorylation could be demonstrated by the accumulation of 3'-NMPs in the corresponding mutants. Additional tissue-specific vacuolar and non-vacuolar NMP phosphatases were also discovered in the course of this work, opening the door to new research directions for investigating the significance of mononucleotide catabolism in seeds, pollen, and roots.

Zusammenfassung

Abschnitt 1

Pflanzen haben die bemerkenswerte Fähigkeit, Nährstoffe zu remobilisieren, indem sie zelluläre Komponenten wie beschädigte Organellen, Proteine und RNA in den Vakuolen abbauen. Nach dem derzeitigen Modell des RNA-Abbaus in den Vakuolen wird die RNA in drei Schritten abgebaut. Nach dem Transport der RNA in die Vakuolen wird sie zunächst durch die interzelluläre Ribonuklease RNS2 zu 3'-Mononukleotiden (3'-NMPs) katabolisiert. Die RNA-Abbauprodukte werden dann durch saure Vakuolenphosphatasen (AP) dephosphoryliert, wodurch Nukleoside freigesetzt werden. Diese Nukleoside werden schließlich durch den Equilibrative Nucleoside Transporter 1 (ENT1) aus den Vakuolen in das Zytosol transportiert, wo sie entweder weiter abgebaut oder im Salvage-Stoffwechsel zu Nukleotiden recycled werden, wodurch entweder Nährstoffe freigesetzt oder Stoffwechselressourcen geschont werden. RNS2 und ENT1 wurden bereits vor einigen Jahren untersucht und charakterisiert, aber die vakuolären Nukleotidphosphatasen sind noch nicht identifiziert worden.

Diese Studie konzentriert sich auf die Identifizierung und Charakterisierung der Nukleotid-dephosphorylierenden APs aus Vakuolen. Es wurden drei Proteinfamilien, die Haloacid Dehalogenase IIIB (HADIIIB)-Familie, die Purple-Acid-Phophatatase (PAP)-Familie und die Endonuklease (Endo) S1/P1-Typ-Nukleasen auf der Grundlage ihrer früheren Identifizierung im Vakuolenproteom oder ihres Potenzials, in der Vakuole zu lokalisieren, und aufgrund ihrer potenziellen Nukleotidase-Aktivitäten in die Untersuchungen einbezogen. Insgesamt wurden 44 Kandidatenproteine anhand einer Reihe von Auswahlkriterien wie Proteinkonservierung in anderen Pflanzen, Proteinlokalisierung, Substratpräferenzen und Expressionsprofilen untersucht. Für die vielversprechendsten Kandidaten wurden mithilfe von T-DNA-Insertionslinien und der CRISPR/Cas9-Technik mehrere Mutantenkombinationen erzeugt. Als die endgültigen Kandidaten (HADIIIB4, umbenannt in Vacuolar Nucleoside Phosphate Phosphatase 1 (VNPP1) und PAP26)) identifiziert waren, wurden diese *in vitro* und i*n vivo* vollständig charakterisiert. Die Funktion von VNPP1 und PAP26 bei der vakuolären Dephosphorylierung von Mononukleotiden konnte durch die Akkumulation von 3'-NMPs in den entsprechenden Mutanten belegt werden. Weitere gewebespezifische vakuoläre und nicht-vakuoläre NMP-Phosphatasen wurden im Rahmen dieser

Arbeit ebenfalls entdeckt, was neue Forschungsrichtungen für die Untersuchung der Bedeutung des Mononukleotid-Katabolismus in Samen, Pollen und Wurzeln eröffnet.

List of abbreviations

µM	Micromolar
35S	Cauliflower mosaic virus promoter 35S
A	Adenine
AH	Allophanate hydrolase
Amp	Ampicillin
AMP/ADP/ATP	Adenosine mono/di/tri phosphate
AP	Acid phosphates
Asp, D	Aspartic acid
AUDS	Alternative Urea Degradation System
AUDS1	Alternative Urea Degradation System 1
AUDS2	Alternative Urea Degradation System 2
B	Boron
C	Cytidine
Ca	Calcium
CDS	Coding sequences
CFP	Cyan fluorescent protein
cm	Centimeters
CMA	Chaperone-mediated autophagy
CMP/CDP/CTP	Cytidine mono/di/tri phosphate
Col-0	*Arabidopsis thaliana* ecotype Colombia-0
CRISPR	Clustered Regularly Interspaced Short Palindromic Repeats
Cu	Copper

DNA	Deoxyribonucleic acid
DW	Dry weight
Endo	S1/P1-type endonuclease
ENT1	Nucleoside Transporter 1
ER	Endoplasmic reticulum
FAD	Flavin adenine dinucleotide
Fe	Ferrum (iron)
FW	Fresh weight
G	Gram
G	Guanine
GMP/GDP/GTP	Guanosine mono/di/tri phosphate
gRNA	Guide RNA
H	Hour
HAD	Haloacid dehydrogenase
HADIIIB	Haloacid dehydrogenase sub family IIIB
K	Potassium
Kan	Kanamycin
L	Liter
LB	Lysogeny Broth
LC-MS	Liquid chromatography–mass spectrometry
LV	Lytic vacuoles
MeOH	Methanol
Mg	Milligram
Mg	Magnesium
min	Minute

mM	Millimolar
mm	Millimeter
Mn	Manganese
Mo	Molybdenum
mol	Moles
mRNA	messenger RNA
MS	Mourashige and Skoog medium
N	Nitrogen
NAD	Nicotinamide adenine dinucleotide
NASC	Nottingham Arabidopsis Stock Centre
NBPT	N-(n-butyl) thiophosphoric triamide
ncRNA	non-coding RNA
NH_3 , NH_4^+	Ammonia
Ni	Nickle
NMP	Nucleoside monophosphates
NSH	nucleoside hydrolase
P	Phosphorus
PAP	purple acid phosphatases
PCR	Polymerase chain reaction
P_i	Orthophosphate
pRCA	Promoter of *Rubisco Activase*
PSV	Protein storage vacuoles
RCA	Rubisco Activase
RNA	Ribonucleic acid
RNS2	Intercellular ribonuclease

rRNA	ribosomal RNA
Rubisco	Ribulose-1.5-bisphosphate carboxylase-oxygenase
S	Sulphur
SD	Standard deviation
SDS	Sodium dodecyl sulphate
SP	Signal peptide
tRNA	transfer RNA
U	Uracil
UC	Urea carboxylase
UCPP	Unknown phosphatases
UMP/UDP/UTP	Uridine mono/di/tri phosphate
V	Vector
v/v	Volume by volume
VSP	Vacuolar storage protein
VTS	Vacuolar targeting signal
w/w	Weight by weight
Wt	Wild type
YEB	Yeast Extract Broth
YFP	Yellow fluorescent protein
Zn	Zinc

Table of Contents

List of figures

Section 1
Identification and characterization of vacuolar nucleotide phosphatases

Section 2
Characterization of an engineered catabolic pathway for urea in *Arabidopsis thaliana*

List of tables

Section 1
Identification and characterization of vacuolar nucleotide phosphatases

Section 2
Characterization of an engineered catabolic pathway for urea in *Arabidopsis thaliana*

Section 1
Identification and characterization of vacuolar nucleotide phosphatases

1. Introduction

1.1. Ribonucleic acid

Ribonucleic acid (RNA) is an essential polymeric molecule for various biological processes, including the transmission of genetic information from deoxyribonucleic acid (DNA) to protein. RNA and DNA are collectively called nucleic acids. Generally, DNA is double-stranded and RNA is single-stranded, but there are also examples of single-stranded DNA and double-stranded RNA. Together with lipids, carbohydrates, and proteins, nucleic acids represent the four most essential molecules for all living things (Mackerell, 2004). There are three main types of RNA: messenger RNA (mRNA), ribosomal RNA (rRNA), and transfer RNA (tRNA). Additionally, small RNAs (microRNAs) have been identified and characterized that regulate gene expression and also other non-coding RNA (ncRNA) (Rathore and Pati, 2021) exists which for example has a function in the process of RNA splicing. Approximately 80% of all cellular RNA is rRNA, 15% is tRNA, and only 5% is all the other RNA, including both the mRNA and the ncRNA (Lodish et al., 2000). Each RNA type has a unique and irreplaceable function in cells. All RNA is a polymer of ribonucleotides (see 1.2). In terms of size and base sequence, mRNA is the most diverse type of RNA. The mRNA carries the genetic information that was transcribed from the DNA by RNA polymerases and processed by splicing and some RNA modification. The genetic information in mRNA is stored in the form of nucleotide triplets, the codons. Each codon specifically binds a complementary tRNA that carries an associated amino acid in the process of mRNA translation into protein at the ribosomes. The tRNA thus decodes the codon information into amino acids. However, RNA can also have structural importance. The ribosomes are made up of proteins and rRNA, which is structurally important to build functional ribosomes. As other biopolymers, RNA can also be degraded. RNA degradation is a process to control the levels of all types of RNAs in cells.

1.2.   Structure and function of the ribonucleotides

Ribonucleotides are composed of three elements: a nitrogen base, a five-carbon sugar, and a phosphate moiety (Figure 1 A). There are four different bases in RNA: adenine (A), guanine (G), cytosine (C), and uracil (U) (Figure 1 B). They form two groups depending upon the basic chemical structure. Nucleobases with one heterocyclic aromatic ring containing two nitrogen atoms are called pyrimidine bases. C and U belong to this category. On the other hand, nucleobases with two heterocyclic aromatic rings containing four nitrogen are categorized as purines. A and G are included in this group. Because amino groups can be attached to the rings aiding to create bonds to the opposite nucleobase in double-stranded DNA, pyrimidines can have up to three nitrogen atoms, and purines can contain up to five nitrogen atoms.

The majority of the nucleobases found in RNA are A, C, G, and U. They are also called primary nucleobases or canonical bases. However, also unusual nucleobases exist which carry modifications, for example additional methyl groups on the ring. Some of them are especially important for rRNA (Sharma et al., 2013) or tRNA (Dégut et al., 2016). A few of these unusual bases are also introduced via post-transcriptional modifications into mRNA, where they play a critical role in gene regulation (Kumar and Mohapatra, 2021).

The second component of the ribonuclotides is the five-carbon sugar ribose. The third component is a phosphate moiety. There can be one to three phosphate groups making a mono, di, or triphosphate, respectively (Figure 1 A). In the case of mononucleotides, the phosphate group is usually esterified to the hydroxyl group on carbon number five of the ribose making a 5'-mononucleotide (5'-NMP, Figure 1 C) but 3'-mononucleotides (3'-NMPs) also exist *in vivo* (Figure 1 D), where the phosphate group is attached to the hydroxyl group on carbon three of the ribose. If the phosphate group is entirely lacking, then the resultant molecule is called a nucleoside. In total, each mononucleotide has one phosphate and up to five nitrogen atoms (Figure 1).
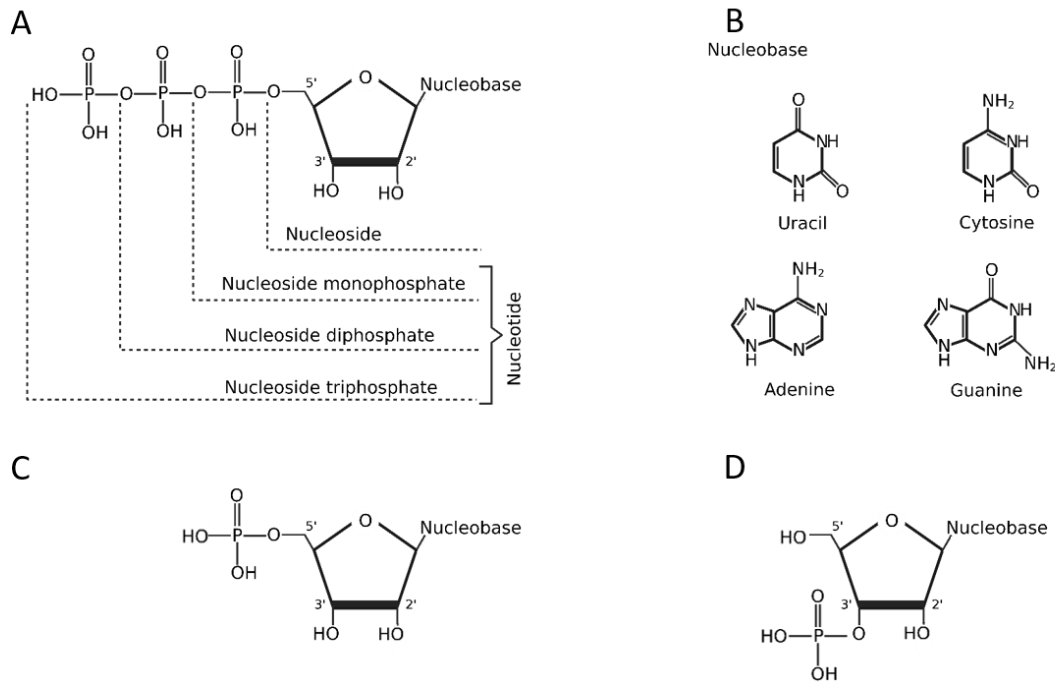
Figure 1. Molecular structure of nucleotides and nucleobases of RNA. (A) Nucleotides, (B) nucleobases present in the RNA, (C) 5' mononucleotide, and (D) 3' mononucleotide.

The nucleotides are the main building blocks of nucleic acids and are also required for molecules derived from nucleotides such as nicotinamide adenine dinucleotide (NAD) and flavin adenine dinucleotide (FAD). Nucleotides also serve as precursors to class B vitamins such as riboflavin, folate, and thiamine (Crozier A et al., 2000; Hanson et al., 2002; Herz et al., 2000). In addition, nucleotides also mediate the flow of energy within the cell. Adenosine triphosphate (ATP), for example, stores metabolic energy in its anhydride bonds and is also the so-called energy currency of the cells. AMP-amino acids and ADP-glucose serve as energetically activated precursor molecules for macromolecules such as starch and proteins. Such precursor molecules are made using the energy stored in ATP. Another example of an activated precursor molecule involving a nucleotide is UDP-glucose, which acts as a glycosyl donor in several metabolic reactions for the synthesis of cellulose, glycoproteins and sucrose (Lim and Bowles, 2004). Also the production of nucleotide-derived secondary metabolites and hormones, for example caffeine and cytokinins, relies on the availability of the corresponding nucleotides (Zrenner et al., 2006).

3

1.3.   Nitrogen and phosphorus in the plants

Plants require seventeen essential nutrients, categorized as either macronutrients or micronutrients depending on the quantitative requirement (Jones, Clain and Jeff Jacobsen, 2013). Nitrogen is the most abundant mineral element in plants as they are composed of up to 1 to 5% w/w nitrogen in the dry mass (Hawkesford et al., 2012). It is an essential part of chlorophyll, proteins, nucleic acids, ATP, and many other central molecules in plants. A limited supply can cause agricultural productivity loss (Masclaux-Daubresse et al., 2010). For carbon, hydrogen, and oxygen, plants are autotrophs and can utilize environmental carbon dioxide and water to generate reduced carbon compounds (sugars). Nitrogen is taken up by plants in inorganic from (nitrate, ammonium) from the soil solution. Because nitrogen often limits plant growth, plants are efficient in remobilizing internal nitrogen present in biological molecules, for example nucleic acids. In agricultural practice, nitrogen is often supplied as N-fertilizers such as urea. Unfortunately, a considerable part of it is not consumed by plants (Peoples et al., 1995). It either leaches to the groundwater causing pollution or it emits into the air as nitrogen oxide and produces greenhouse effects (Hirel et al., 2011). The problems associated with the nitrogen fertilizers are further elaborated in the second section of this thesis. For remobilization of nitrogen from internal sources, macromolecules containing nitrogen are catabolized in source tissues and the nutrients reallocated into new sink tissues. The degradation of macromolecules can occur in the plant vacuole and a great amount of RNA is degraded in this compartment (Hillwig et al., 2011). A recent study has highlighted that RNA and proteins are delivered to the plant vacuoles via autophagy and that these cellular components are degraded there (Hickl et al., 2021). It has also been reported that up to 4% of recycled nitrogen comes from the degradation of RNA (Melino et al., 2018).

Phosphorus is the second most abundant mineral macronutrient found in plants after nitrogen. The phosphorus concentration of the plants varies between 0.1 to 0.5% w/w in the dry mass. It is an essential part of DNA, RNA, ATP and other nucleotides as well as of phospholipids which represent the main components of the cell membrane. It only occurs in oxidized form, as phosphate, in biomolecules (Sultenfuss and Doyle, 1999). A limited phosphate supply leads to the disruption of entire cellular processes; for example, low orthophosphate (P_i) levels in the chloroplast negatively affect the ATP synthase activity (Carstensen et al., 2018) and reduce photosynthesis resulting in less production of carbohydrates (Thuynsma et al., 2016). Phosphate

is an integral part of nucleic acids (Figure 1 A) which means the transfer of genetic material from one generation to the next is dependent on phosphate. The most abundant form of phosphate in the soil is Pi while it occurs in plants also as pyrophosphate (PP$_i$), that is two phosphate groups linked by an anhydride bond. Plants take up phosphate as P$_i$ from the soil. Newer plant organs can receive phosphate either via P$_i$ uptake from the soil or from P$_i$ stored in vacuoles in older tissues or via recycling of phosphate-containing biomolecules, for example phospholipids and nucleotides from older tissues. The vacuolar phosphate reservoir serves as a buffer to maintain cellular P$_i$ homeostasis in the event of an inadequate external phosphate supply (Yang et al., 2017). A plant can be severely phosphate deficient without showing visible foliar symptoms (Carstensen et al., 2018) highlighting that internal P$_i$ distribution is quite efficient. During vacuolar nucleotide degradation, P$_i$ is released from nucleotides by so far unknown phosphatases.

1.4.   The vacuoles

Plant cells are unique in containing a large central vacuole that occupies most of the space, whereas animal cells have smaller vacuoles known as lysosomes. However, both are enriched with similar hydrolytic enzymes. The plant vacuole occupies 50 to 90% of the cell volume mainly containing sugars, proteins, ions, and sometimes pigments. The primary function of the vacuoles includes regulating the cell's turgor pressure, acting as a storage compartment, and harbouring part of the cell's degradation machinery. There are three major types of plant vacuoles (i) lytic vacuoles (LV), which contain hydrolytic enzymes and have the function of degrading and recycling the cellular waste similar as yeast vacuoles or lysosomes in mammals; (ii) protein storage vacuoles (PSV) mainly found in the seeds, where proteins are first deposited during seed development and then degraded during germination to provide essential nutrients to the embryo (Paris et al., 1996); and (iii) the central vacuole, present as a single large vacuole in most plant cells. Vacuolar proteins are encoded by the nuclear genome and translated at the rough endoplasmic reticulum (ER). After translation, the vacuolar proteins are sorted in the ER and Golgi for transport into the vacuoles (Mü, 2007). Therefore, all the vacuolar targeted proteins must contain a signal peptide for translation at the ER and they must contain vacuolar sorting signals (Robinson, 2003). A proteomic survey of the vegetative vacuole from *Arabidopsis thaliana* identified 402 proteins, although 46.5% were identified only by a single peptide hit. The groups of proteins identified include

transporters, proteins involved in stress response, cytoskeletal proteins, proteins involved in degradation, and glycosidases (Carter et al., 2004).

The vacuoles comprise the vacuolar membrane (the tonoplast) and the inner body (the lumen). The tonoplast contains two proton pumps, the vacuolar H^+-ATPase (V-ATPase) and the vacuolar H^+-pyrophosphatase (H^+-PPase) (Rea and Sanders, 1987; Figure 2). Apart from these proton pumps, the tonoplast also contains various uniporters and antiporters that allow the transport of different molecules (ions, sucrose, and other metabolites) across the tonoplast. The proton pumps are regulating the pH of the vacuoles. The pH of the endomembrane system (Golgi network, ER, and multivesicular bodies) in Arabidopsis is essential for the functionality of the different compartments. In the Arabidopsis endomembrane system, the pH ranges between 5.2 and 7.1 with the vacuoles having the lowest of these values (Shen et al., 2013). For the degradation of cellular components in the vacuole, they must be transported into this organelle. All forms of vacuoles have hydrolytic enzymes employed for catabolic processes.
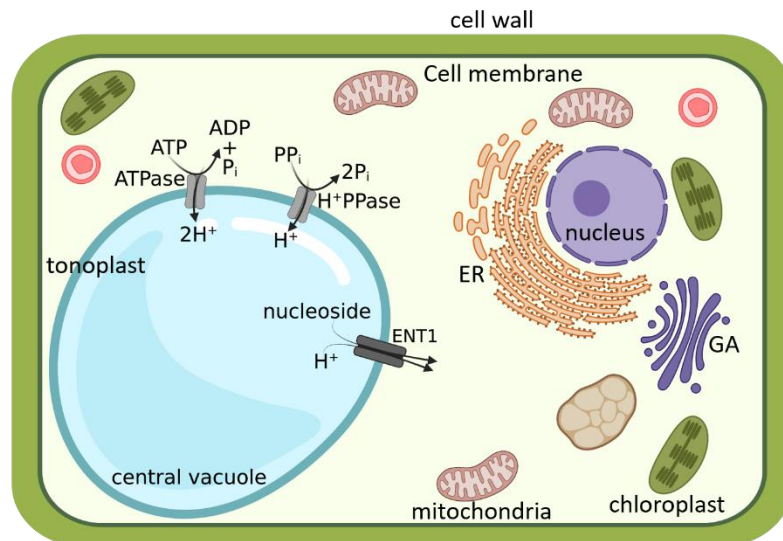
Figure 2. A representation of a typical plant cell. A plant cell contains a large central vacuole that contains 50 to 90% of the volume. Two proton pumps and the nucleoside transporter ENT1 are shown at the tonoplast. Other components of the cell include outer cell wall, and inner cell membrane, mitochondria, chloroplast, nucleus, endoplasmic reticulum (ER), and Golgi apparatus (GA).

1.4.1. The degradation of cellular components in vacuoles

Synthesis and degradation are opposing cellular processes that must be balanced to maintain metabolic homeostasis in a cell. The degradation is the breakdown of damaged or excess cellular material. The metabolites and nutrients released by degradation are used to synthesize new biomolecules in sink tissues. The degradation of macromolecules to obtain their building blocks is a more energy-efficient process compared to the *de novo* synthesis of macromolecular building blocks. For example, for the *de novo* generation of one IMP molecule, five ATP, two formate and glutamine molecules, one molecule each of glycine, aspartate, and carbon dioxide are utilized (Pedley and Benkovic, 2017). One major site for catabolic processes in a plant cell is the vacuole. The hydrolytic enzymes present in the vacuoles degrade RNA and proteins releasing nucleotides and amino acids (Sun and Brodsky, 2018; Michaeli and Galili, 2014). About 80% of the total cellular RNAase activity has been associated with the vacuole (Boller and Kende, 1979). This was later supported by other studies in which oligonucleotides of RNA were found in the vacuoles of cultured tomato cells (Abel and Glund, 1986). Recently, another study showed that RNA is delivered to the vacuoles and is degraded there (Hickl et al., 2021). How cellular components, especially the RNA, are delivered to the vacuoles is still not well characterized. However, autophagy probably plays a significant role here.

1.4.2. Major types of autophagy

Autophagy is an evolutionarily conserved degradation mechanism in all eukaryotic cells (Klionsky and Emr, 2000). It is the main mechanism of transporting cellular material to the vacuoles for degradation. Three types of autophagy are generally distinguished: (i) macroautophagy, (ii) microautophagy, and (ii) a less common type, chaperone-mediated autophagy (CMA) (Yorimitsu and Klionsky, 2005).

Macro and microautophagy transport a broad spectrum of substances to the vacuoles. Macroautophagy involves the wrapping of a double-membrane around organelles creating a structure called autophagosome. The autophagosome is transported to the vacuole and fuses with the tonoplast delivering its cargo into the vacuolar lumen. One speaks about microautophagy when cytosolic components are engulfed by an invagination of the tonoplast (Figure 3). Macroautophagy can target different damaged or excess organelles or macromolecular structures, such as ribosomes (ribophagy) (Kraft et al., 2008), the endoplasmic reticulum (reticulophagy) (Yorimitsu and

Klionsky, 2007), parts of the nucleus (piecemeal microautophagy of the nucleus) (Roberts et al., 2003), mitochondria (mitophagy) (Lemasters, 2005), and peroxisomes (micropexophagy and macropexophagy) (Farré and Subramani, 2004).

CMA is confined only to a subset of proteins that bear a particular pentapeptide motif (Nasb et al., 2021). Additionally, CMA supports the translocation of unfolded proteins across the lysosomal membrane. Since it can only translocate the unfolded protein, it is inadequate for large protein aggregates or organelles (Figure 3).
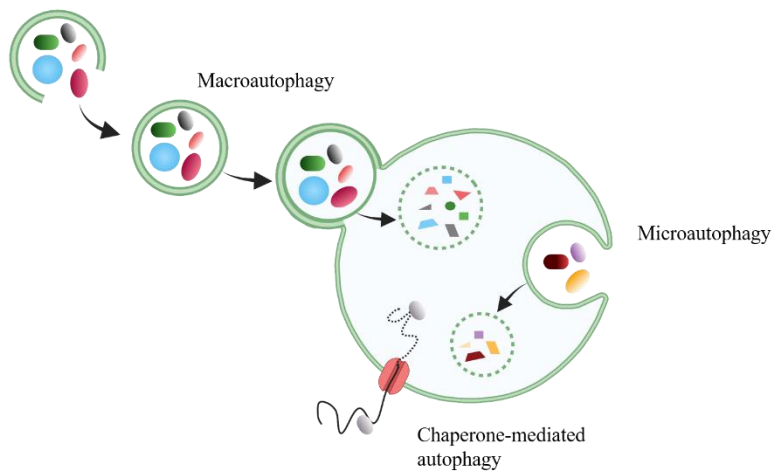
Figure 3. Scheme illustrating the three types of autophagy. In macroautophagy, the cellular material is wrapped in an autophagosome which fuses with the tonoplast. In microautophagy, the cellular material is directly engulfed by the tonoplast. During CMA an unfolded protein is transported across the tonoplast.

1.4.3. RNA transport mechanism

Most of the RNA is degraded in the vacuoles (Boller and Kende, 1979; Abel and Glund, 1986). However, the mechanisms of RNA transport into the vacuole have not been well studied and characterized. In one recent study, intact vacuoles were isolated from barley and Arabidopsis. The RNA was purified and sequenced using next-generation sequencing, and rRNA, tRNA, micro RNA, and RNA fragments of plastid origin were found there. The data indicate that bulk RNA transfer to the vacuoles and degradation in the vacuoles occurs. In mutants of *ATG5,* which is required for functional autophagy, RNA fragments of plastid origin were missing in the vacuolar RNA (Hickl et al., 2019). The data indicate that macroautophagy is the transport mechanism by which chloroplastic RNA reaches the vacuolar lumen. One recent study in yeast cells examined rapamycin-induced autophagy. Sequencing the RNA from the yeast vacuoles revealed the presence of certain mRNAs those that encode essential ribosomal and amino acid biosynthetic proteins indicating that selective mRNA degradation may occur. Such selective RNA degradation was named RNAphagy (Makino et al., 2021). Nonselective autophagy removes random cytosolic components, whereas selective autophagy removes any excess / damaged organelles, misfolded / harmful proteins and RNA. In selective autophagy, the cellular material is marked for degradation, for example by ubiquitination, and then recognized by specific receptors of the autophagosomes (Gatica et al., 2018; Johansen and Lamark, 2020; Kirkin, 2020; Hickl et al., 2021). Ribosomes can also be specifically targeted for vacuolar degradation (ribophagy) leading to the turnover of rRNA (MacIntosh et al., 2011).
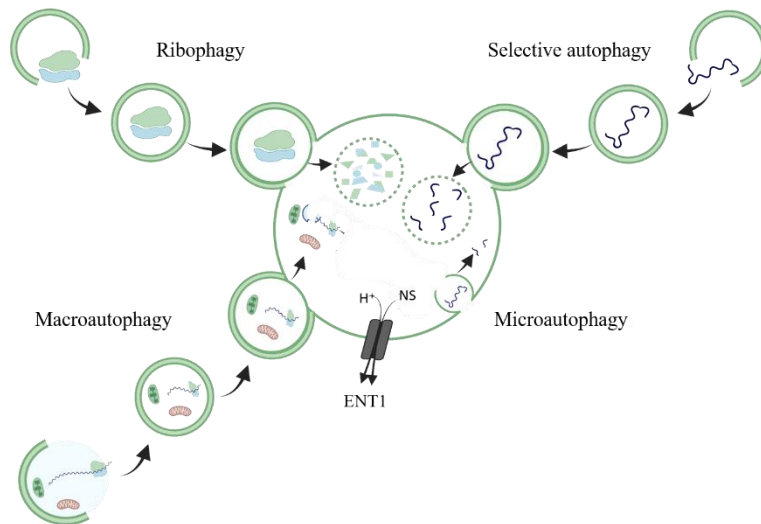
Figure 4. Suggested RNA transport pathways to the vacuole. Four different pathways are described (i) ribophagy, (ii) microautophagy, (iii) macroautophagy, and (iv) selective RNA autophagy (RNAphagy).

An exogenous import of RNA into the plant vacuoles via a form of microautophagy has been demonstrated recently. The study suggested that the RNA helicase SKI2 is a crucial factor for the ATP-dependent RNA import into the vacuoles, because *ski2* lacks the ability to import RNA into the vacuoles (Floyd et al., 2021). In summary, the RNA cargo can be delivered to the vacuole in various possible ways (i) ribophagy, (ii) microautophagy, (iii) macroautophagy, and (iv) selective RNA autophagy (RNAphagy) (Figure 4).

1.4.4. RNA degradation inside the vacuoles

As soon as the RNA has arrived in the vacuole lumen, its catabolism begins and ribonucleases and phosphatases act on it. Among these is an intercellular ribonuclease (RNS2) (Figure 5), which belongs to the T2 ribonucleases. These are acid endonucleases that do not exhibit nucleobase specificity (Irie, 1999). The RNase T2 enzymes are highly conserved in most eukaryotic species and their expression pattern suggests that they play an essential housekeeping role. RNS2 and most intracellular enzymes from the T2 family of Arabidopsis play a crucial role in rRNA degradation. RNS2 is localized in the ER, vacuoles, and other ER-derived vesicles (Hillwig et al., 2011). The mutants in *RNS2* lack this degradation activity. Over time, rRNA accumulates in the above-mentioned cell compartments in *rns2* background, and the half-life of the rRNA is longer than in

the wild-type plants. Interestingly, *rns2* plants exhibit induction of constitutive autophagy. The regular turnover of rRNA is part of the normal homeostasis of the cell and the rRNA recycling mechanism is similar in all eukaryotes suggesting it is a vital cellular function that has been maintained throughout the evolution of eukaryotes (Tatosyan et al., 2020). Although vacuolar degradation is a constitutive cellular process (Mizushima and Komatsu, 2011; Todde et al., 2009), a recent study showed that protein degradation in the vacuole of wild-type plants under sugar starvation caused by dark stress is accelerated within two days after the onset the stress. (Hirota ets al., 2018). The carbon deficiency caused by darkness is likely compensated by the induction of autophagy, which releases amino acid for respiration. The data demonstrate the importance of vacuolar-mediated degradation for the supply of nutrients under stress conditions.
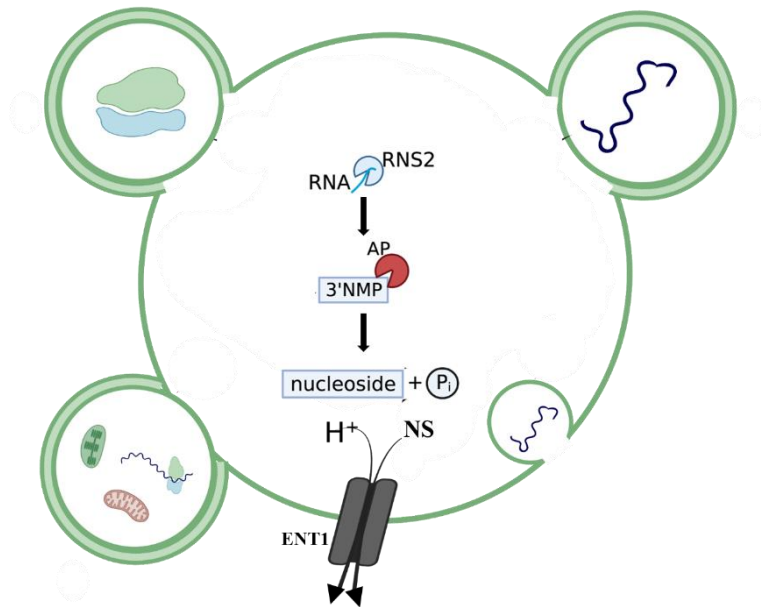
Figure 5. Model for the mechanism of RNA degradation in the vacuole. A series of catabolic processes degrade RNA in the vacuole. First, RNS2 hydrolizes RNA releasing 3'-NMPs. Unknown acid phosphates (AP) then hydrolyze the 3'-NMPs to the corresponding nucleosides. Subsequently, the nucleosides are transported out of the vacuole by the ENT1 transporter.

There is some evidence that the mononucleotides present in the vacuoles are phosphorylated at the 3'-carbon of the ribose: (i) RNS2-mediated RNA degradation results in cyclic 2'-3'-NMPs that are then converted into 3'-NMPs (Hickl et al., 2021), (ii) the oligonucleotides found in the tomato vacuoles are 3'-terminally phosphorylated (Abel et al., 1990), and (iii) the ribonuclease (Rny1) present in the yeast vacuoles generates 3'-NMPs (Huang et al., 2015).

After the degradation by RNS2 and similar RNAses, the mononucleotides are then dephosphorylated by unknown acid phosphatases (AP). Finally, the resultant nucleosides are transported out of the vacuole into the cytosol mediated by the Equilibrative Nucleoside Transporter 1 (ENT1; Bernard et al., 2011; Figure 5). In the cytoplasm, these nucleosides can either enter the catabolic pathway or can be salvaged to nucleotides.

1.5. Cytosolic degradation of the nucleosides

Nucleosides transported out of the vacuole may enter the degradation process (Figure 6). The nucleosides are mainly adenosine, guanosine, cytidine, and uridine but also rare nucleosides like pseudouridine (Chen and Witte, 2020). The adenosine and guanosine enter the purine degradation pathway, while cytidine and uridine are degraded in the pyrimidine catabolic pathway.
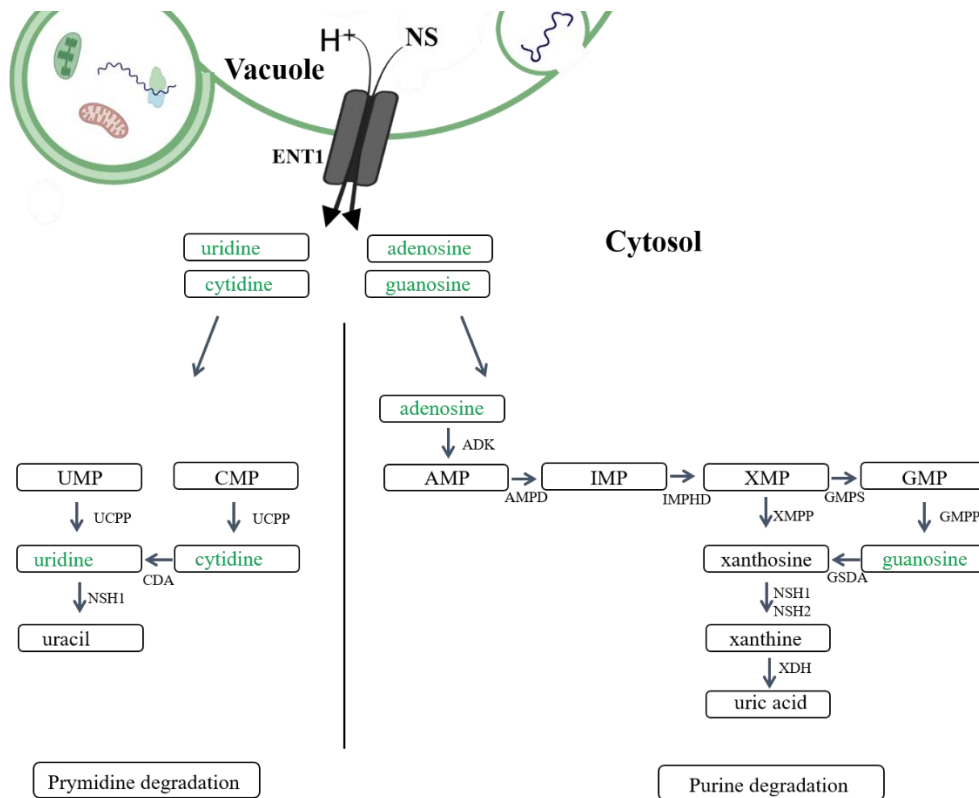
Figure 6. Overview of the degradation of purine and pyrimidine nucleotides and nucleosides. UMP, uridine-5'-monophosphate; CMP, cytidine-5'-monophosphate; UCPP, UMP-CMP phosphatase; CDA, cytidine deaminase; NSH, nucleoside hydrolase; AMP, adenosine-5'-monophosphate; ADK, adenosine kinase; IMP, inosine-5'-monophosphate; AMPD, AMP deaminase; XMP, xanthosine-5'-monophosphate; IMPHD, IMP dehydrogenase; GMP, guanosine-5'- monophosphate; GMPP, GMP phosphatase; GSDA, guanosine deaminase; XDH, xanthine dehydrogenase.

1.5.1. Pyrimidine degradation pathway

Cytosolic UMP and CMP are first dephosphorylated by yet unknown phosphatases (UCPP) to the corresponding nucleosides, uridine, and cytidine, respectively. The vacuolar nucleosides, uridine, and cytidine (color-coded green) join this pathway at this stage. Cytidine is deaminated to uridine by cytidine deaminase (CDA) (Chen et al., 2016). Interestingly, plants are unable to degrade or salvage the free nucleobase cytosine (Katahira and Ashihara, 2002). Uridine from these different sources is then hydrolyzed by a nucleoside hydrolase (NSH1) to the nucleobase uracil and ribose (Jung et al., 2009). Uracil is then completely degraded to β-alanine, CO_2, and NH_3 in three catabolic steps (Zrenner, R., and Ashihara, 2011). The pyrimidine degradation pathway is induced by nitrogen starvation and in senescence (Zrenner et al., 2009; Cornelius et al., 2011a), indicating that the nitrogen and phosphorus of the pyrimidine nucleotides are recycled.

1.5.2. Purine degradation pathway

Purine degradation is not as straightforward as pyrimidine degradation. Adenosine and guanosine (color-coded green in Figure 6) which may originate from the vacuole enter purine degradation at different stages. Adenosine cannot be degraded directly to adenine and ribose but must first be salvaged to AMP by an adenosine kinase (ADK). AMP is then deaminated to IMP by an AMP deaminase (AMPD) followed by oxidation of IMP to XMP by an IMP dehydrogenase (IMPDH; Witte and Herde, 2020). XMP can be dephosphorylated by an XMP phosphatase (XMPP; Heinemann et al., 2021) or converted to GMP by GMP synthetase (GMPS). The GMP is dephosphorylated to guanosine by an unknown GMP phosphatase (GMPP). Vacuolar guanosine enters the pathway at this stage. Guanosine is deaminated to xanthosine by a guanosine deaminase (GSDA) (Dahncke and Witte, 2013) and xanthosine is hydrolized to xanthine and ribose by a nucleoside hydrolase complex consisting of NSH1 and NSH2 (Baccolini and Witte, 2019). Subsequently, xanthine is oxidized to uric acid by xanthine dehydrogenase (XDH) (Urarte et al., 2015) and uric acid is then imported into the peroxisome, where the ring catabolism proceeds.

1.6. Candidates for the vacuolar mononucleotide phosphatases

The phosphatases that perform the dephosphorylation of mononucleotides in vacuoles have not yet been identified and characterized. Since these phosphatases possess an essential housekeeping role they must have certain characteristics. For example, they must localize inside the vacuoles, probably have a constitutive expression pattern, and should well catalyse the dephosphorylation of mononucleotides. Based on these characteristics, certain gene families may contain promising candidates.

1.6.1. Haloacid dehydrogenase phosphatases (HADIIIB)

The superfamily haloacid dehydrogenase (HAD) comprises phosphatases, P-type ATPases, phosphomannomutases, dehalogenases, and beta-phosphoglucomutases. The proteins in this family are involved diverse cellular functions ranging from nucleotide metabolism to detoxification (Burroughs et al., 2006). The sub-family IIIB contains ten members in Arabidopsis, and analyses of the vacuolar proteome indicated the presence of five of the members of this gene family in the vacuole (Carter et al., 2004; Endler et al., 2006; Shimaoka et al., 2004). Two members are classified as vacuolar storage proteins (VSPs, At5g24770 and At5g24780) possibly involved in the storage of nitrogen in protein form (Chen et al., 2012; Liu et al., 2005) but also improving the defense against plant feeding insects (Liu et al., 2005). All members of this family contain a conserved DXDXT motif. This motif serves as the intermediate acceptor for a phosphate group during catalysis and the first aspartic acid (Asp, D) residue of the motif plays a critical role for catalytic activity. When this Asp residue was replaced with glutamate in the Vacuolar Storage Protein 2 (VSP2; At5g24770) its acid phosphatase activity was lost, although the protein structure was not changed (Liu et al., 2005). That is why members of this subfamily are sometimes also referred to as the aspartate nucleophile hydrolases. All members have a signal peptide for the secretory pathway except one (Liu et al., 2005) suggesting that they might be targeted to the vacuole. The two VSPs of Arabidopsis have been characterized biochemically and only weak activities for physiological substrates have been observed (Chen et al., 2012). A recent study claims that another member, encoded at the locus At4g29260, is a VSP (VSP3) (Sun et al., 2018). This family has not yet been thoroughly characterized. Since some members of this genes family are present in the vacuoles, and contain the DXDXT signature motif that is necessary for acid

phosphatase (AP) activity some members of this gene family might be involved in the phosphatase reaction in the vacuoles.

1.6.2. Purple acid phosphatases

The purple acid phosphatases (PAPs) belong to a group of enzymes referred to as dinuclear metallohydrolases with two juxtapositioned metal binding sites. The purple color characteristic of these enzymes under certain conditions results from the interaction of bound iron with the enzyme. The PAPs have a hydrolysis function for a variety of substrates from phosphate monoesters to amides and are usually most active at acidic pH. There are well-studied PAP enzymes from mammalian, plant, fungal, and human sources (Schenk et al., 2013). Genome analysis shows that there are 29 *PAP* genes in the Arabidopsis genome (Li et al., 2002). For 28 of these *PAP* genes, transcripts have been detected in different tissues, and 11 have been reported to be up-regulated under phosphate deficiency (Del Pozo et al., 1999; Haran et al., 2000; Wang et al., 2011; Wang and Liu, 2012). Using the corresponding mutants of Arabidopsis, it has been demonstrated that PAP12 and PAP26 are the major intracellular and secreted acid phosphatases while PAP10 is primarily a secreted enzyme. During P_i-starvation conditions, AP activity is induced and secreted. This activity is believed to scavenge P_i from extra cellular spaces (Wang et al., 2014a). The PAPs have been studied in several cellular organelles, including vacuoles (Veljanovski et al., 2006), plasma membrane (Vasko et al., 2006), apoplast (Zamani et al., 2012), and dual-targeted chloroplasts and mitochondria (Zamani et al., 2012). Judging from the analysis of mutants, PAP26 appears to be one of the most important PAP enzymes. Loss of PAP26 function in Arabidopsis causes delayed leaf senescence and impairs phosphate remobilization resulting in seeds with reduced P_i content. Apparently other PAPs cannot compensate missing PAP26 function. When the plants were grown on phosphate deficient soil, PAP26 was up-regulated (Robinson et al., 2012). PAP26 was shown to be dual-targeted to the rhizosphere cell walls and to the vacuoles suggesting it has P_i remobilization function from organic sources both inside the vacuole and in the extracellular space (apoplast). Transcriptional data in senescing leaves of Arabidopsis showed that the expression patterns of PAP26 and RNS2 are similar corroborating the notion that both function in the same biological process, i.e. in phosphate remobilization (Zamani et al., 2012). Proteome analyses of intact vacuoles of Arabidopsis identified PAP26 as a vacuolar protein (Shimaoka et al., 2004; Carter et al., 2004) and subcellular localization studies demonstrated its localization in

the Arabidopsis lytic vacuoles (Hurley et al., 2010). Because of its occurrence in vacuoles and strong association with phosphate remobilization, PAP26 is one of the prime candidates for the unknown mononucleotide phosphatases in the vacuoles. This idea is supported by the observation that PAP26 has a broad substrate specificity which includes 5'-nucleotides (Veljanovski et al., 2006). However, activity on 3'-nucleotides has not yet been reported. Because other PAP phosphatases than PAP26 may also contribute to the vacuolar mononucleotide phosphatase profile, these were also considered in this study.

1.6.3. S1/P1-type endonucleases

S1/P1-type endonucleases are one of the primary nucleases for the degradation of genomic material. The Arabidopsis genome codes for five S1 endonucleases called Endo1 to Endo5 (Triques et al., 2007), which are similar in catalytic activity to the well-characterized S1 and P1 nucleases from *Penicillium citrinum* and *Aspergillus oryzae*, respectively. These bi-functional enzymes efficiently degrade single-stranded DNA (ssDNA) and RNA into 5'-nucleotides. However, they show relatively low activity with double-stranded DNA (Shishido and Ando, 1975). Interestingly, they can also act as 2'- and 3'-mononucleotide phosphatases (Fujimoto et al., 1974; Hanson and Fairley, 1969). The family is divided into two groups depending on the divalent cation required for enzyme activity; either they are Zn^{2+} (Endo3, Endo5) or Ca^{2+} (Endo1, Endo2, Endo4) dependent. The optimal pH for enzyme activity in this family ranges between 5.5 and 8.0. For all *Endo* genes except *Endo4* mRNA transcripts have been detected. *Endo1* is well expressed in senescent leaves, *Endo2* is expressed in response to biotic and abiotic stress, *Endo3* is mainly expressed in flower tissues, and *Endo5* is mainly expressed in roots (Lesniewicz et al., 2013). The subcellular localization predictions (https://suba.live/) indicate a diverse localization of the S1/P1-type endonucleases including plastids, ER, Golgi, and the cytosol. This indicates that some of these enzymes may enter the secretory pathway and therefore a localization in the vacuole is possible. The RNA is degraded in the vacuole employing ribonucleases and phosphatases and the S1 nucleases are capable of both functions while they have optimal enzyme activity at vacuolar pH. Therefore, it is possible that members of this family are located in the vacuole to function in RNA hydrolysis into 5'-NMPs and simultaneously degrade 3'-NMPs made by RNS2.

1.7. Aim of the study

The RNA degradation in the vacuoles has not been fully studied. RNA is degraded in vacuoles employing three types of enzymes: Ribonucleotides, vacuolar acid phosphatases, and nucleoside transporters. The first and last steps of this pathway are well studied and characterized a decade ago. However, the intermediate step of nucleoside monophosphate degradation still possess a gap in current model. The aim of this study was to identify possible acid phosphatases involved in the intermediate steps in the vacuoles, and determine their role *in vitro*, and characterize them *in vivo*. For this purpose, a sequence analysis was performed using known nucleotidase from *Phaseolus vulgaris* to search for such enzymes in *Arabidopsis thaliana*. Since the phosphatases are often functionally similar, two additional gene families (Purple Acid Phosphatase (PAP) family, and the S1/P1-type endonucleases) were considered in parallel based on their enzymatic activity or occurrence in the vacuoles. Specific selection criteria were then applied to the initial list of 44 candidates. The selection criteria included a wide range of techniques, from bioinformatics computer analysis to analyzing candidates in the laboratory, where candidates will be examined for their occurrence in vacuoles, substrate activity, and transcript expression. When the final candidates of the three families will be finally identified, they will be fully characterized *in vitro* and *in vivo* by expressing the enzyme, purifying it, and testing it in the enzymatic assay or by mutating the corresponding gene and analyzing the metabolic differences *in vivo*. For this purpose, not only the single mutants will be analyzed, but also higher orders if mutant combinations will also be considered and enzymes from the first and last step of the metabolic pathway will be tested together to obtain reliable and consistent data.

2. Materials and methods

2.1. Materials

2.1.1. Antibiotics

Table 1. Antibiotics.

Antibiotic	Solvent	Stock concentration (mg mL^{-1})	Working concentration (µg mL^{-1})
Ampicillin (Amp^R)	H_2O	100	100
Carbenicillin (Carb^R) Plates	H_2O	50	75
Carbenicillin (Carb^R) Liquid cultures	H_2O	50	50
Gentamycin (Gent^R)	H_2O	15	15
Kanamycin (Kan^R)	H_2O	50	50
Rifampicin (Rif^R)	DMSO[1]	50	50

[1]Dimethyl sulfoxide (DMSO)

2.1.2. Bacterial stations

Table 2. Bacterial strains.

Species	Strain	Resistance
Escherichia coli	K-12 DH10B (Invitrogen)	
Escherichia coli	BL21 (DE3) (Novagen)	
Agrobacterium tumefaciens	GV3101::pMP90RK (Koncz and Schell, 1986)	Rif^R, Gent^R, Kan^R
Agrobacterium tumefaciens	AGL-1 (Lazo et al., 1991)	Carb^R

2.1.3. Primers

Table 3. Primers used for cloning

Number	Sequence	Description
N61	TGGTTCACGTAGTGGGCCATC	Left border primer used to screen SALK T-DNA lines
P362	TGAATTCAAAATGAATCATTTGGTGATAATC	Forward primer for locus *PAP26* with *EcoRI* restriction site
P363	TCCCGGGAGTGGCGATCCAGCCAC	Reverse primer for locus *PAP26* with *XmaI* restriction site, without the stop codon
P364	TGAATTCAAAATGGCATCGGCTTTTAGATC	Forward primer for locus *ENDO1* with *EcoRI* restriction site
P365	TCCCGGGAGTGGCAGCAACACCAGC	Reverse primer for locus *ENDO1* with *XmaI* restriction site, without the stop codon
P366	TATCGATAAAATGGCAAACCAAAAAGGGTTAC	Forward primer for locus *ENDO2* with *ClaI* restriction site
P367	TCCCGGGACCGAAAATCCTGTTTAGGGTAG	Reverse primer for locus *ENDO2* with *XmaI* restriction site, without the stop codon

P368	TATCGATAAAATGGGTTGGTCGT TGAGAATG	Forward primer for locus *ENDO3* with *ClaI* restriction site
P369	TCCCGGGTGCTCTAGCAAGCTTC CGT	Reverse primer for locus *ENDO3* with *XmaI* restriction site, without the stop codon
P370	TGAATTCAAAATGAGTTCGTCGC TGCGAC	Forward primer for locus *ENDO4* with *EcoRI* restriction site
P371	TCCCGGGTGATCCAGCATGCTTA GGT	Reverse primer for locus *ENDO4* with *XmaI* restriction site, without the stop codon
P372	TGAATTCAAAATGAGATTGTGGA TTGTGAGTG	Forward primer for locus *ENDO5* with *PstI* restriction site
P373	TCCCGGGTAATCCTGCGAGCTTC G	Reverse primer for locus *ENDO5* with *XmaI* restriction site, without the stop codon
P412	TGAATTCAAAATGGCTAGATCCT TGTTG	Forward primer for locus *HADIIIB6* with *EcoRI* restriction site
P413	TCCCGGGGGCGACATAGTAGATG GAG	Reverse primer for locus *HADIIIB6* with *XmaI* restriction site, without the stop codon
P419	ACCCGGGGGCGACATAGTAGAT GGAG	Reverse primer for locus *HADIIIB5* with *XmaI* restriction site, without the stop codon
P421	ACCCGGGAACGAAGTACATAGG ATTAG	Reverse primer for locus *HADIIIB7* with *XmaI* restriction site, without the stop codon
P423	ACCCGGGGATATAATACATTGGA TTTG	Reverse primer for locus *HADIIIB1* with *XmaI* restriction site, without the stop codon
P425	ACCCGGGAGGAATGTAGTACAT GGG	Reverse primer for locus *HADIIIB4* with *XmaI* restriction site, without the stop codon
P466	ACCCGGGAGCAACATAGTACAT GGGAT	Reverse primer for locus *HADIIIB3* with *XmaI* restriction site, without the stop codon
P467	ACCCGGGGATATAATACATTGGA TTTG	Reverse primer for locus *HADIIIB2* with *XmaI* restriction site, without the stop codon
P471	AGAATTCAAAATGGACCGAACC ATGTTTC	Forward primer for locus *HADIIIB5* with *EcoRI* restriction site
P472	AGAATTCAAAATGGAAAAGTGT AGTAGAGAGACG	Forward primer for locus *HADIIIB7* with *EcoRI* restriction site

P473	AGAATTCAAAATGCGGATTCTCG TGAATC	Forward primer for locus *HADIIIB1* with *EcoRI* restriction site
P474	AGAATTCAAAATGGCGTCTCTTC GTAGC	Forward primer for locus *HADIIIB4* with *EcoRI* restriction site
P475	ACTGCAGAAAATGAGGATTTATC TGATTTTC	Forward primer for locus *HADIIIB2* with *PstI* restriction site
P476	AGAATTCAAAATGACTTTTTCTC GTAGCAG	Forward primer for locus *HADIIIB3* with *EcoRI* restriction site
P798	CCTGTAAGCAAGATAACTTTGTA CC	Primer used for screening T-DNA insertion for SALK_128131
P799	TTATTATCGTCATACGGTTCAG	Primer used for screening T-DNA insertion for SALK_087041
P1152	TCCCGGGATGGTGAGCAAG	Forward primer for locus encoding mCherry and CFP fluorescent protein with *XmaI* restriction site
P1153	ATCTAGACTTGTACAGCTCGTCC ATG	Reverse primer for locus encoding mCherry and CFP fluorescent protein with *XbaI* restriction site, without the stop codon
P1206	AATCGATAAAATGAGAGAATCG TTAG	Forward primer for locus *PAP1* with *ClaI* restriction site
P1207	AATCGATTGAAGCAAGTGTAGTT GC	Reverse primer for locus *PAP1* with *ClaI* restriction site, without the stop codon
P1208	TAAGCTTAAAATGATCGTTAATT TCTC	Forward primer for locus *PAP2* with *HindIII* restriction site
P1209	TAAGCTTTGTCTCCTCGTTCTTG	Reverse primer for locus *PAP2* with *HindIII* restriction site, without the stop codon
P1210	TAAGCTTAAAATGCACAGTCGAC TTATTC	Forward primer for locus *PAP4* with *HindIII* restriction site
P1211	TCCCGGGCAATGGGAAATAAAA ATC	Reverse primer for locus *PAP4* with *XmaI* restriction site, without the stop codon
P1212	TAAGCTTAAAATGGATAGCTTGA GAGATG	Forward primer for locus *PAP8* with *HindIII* restriction site

P1213	TCCCGGGGATATCGGAATAAACC	Reverse primer for locus *PAP8* with *XmaI* restriction site, without the stop codon
P1214	AATCGATAAAATGGGTCGTGTCC G/AAAATC	Forward primer for locus *PAP10* with *ClaI* restriction site
P1215	TCCCGGGAGAATTACAAGAAGG AG	Reverse primer for locus *PAP10* with *XmaI* restriction site, without the stop codon
P1216	TAAGCCTAAAATGAGTTCAAGAT CTGAC	Forward primer for locus *PAP12* with *HindIII* restriction site
P1217	TCCCGGGAAATGCATCAAGCC	Reverse primer for locus *PAP12* with *XmaI* restriction site, without the stop codon
P1218	TAAGCCTAAAATGAATTCTGGTC GTC	Forward primer for locus *PAP17* with *HindIII* restriction site
P1219	TCCCGGGAACAGAGGAATGAAG AAG	Reverse primer for locus *PAP17* with *XmaI* restriction site, without the stop codon
P1220	TCTGCAGAAAATGGAAAAATGG GGGATTTTG	Forward primer for locus *PAP18* with *PstI* restriction site
P1221	TCCCGGGAGGTTCCAAGAGCATT TTC	Reverse primer for locus *PAP18* with *XmaI* restriction site, without the stop codon
P1222	TAAGCCTAAAATGGCTAGGAATT TCTTGTTAG	Forward primer for locus *PAP27* with *HindIII* restriction site
P1223	TCCCGGGTGAAGCTAATGTGGTT G	Reverse primer for locus *PAP27* with *XmaI* restriction site, without the stop codon
P1224	TCTGCAGAAAATGAATTGTTCAA TCG	Forward primer for locus *PAP28* with *PstI* restriction site
P1225	TCCCGGGCTTCAGAAATGAGTCG G	Reverse primer for locus *PAP28* with *XmaI* restriction site, without the stop codon
P1227	TAAGCCTAAAATGACCTACATAT ATAGAGAC	Forward primer for locus *PAP3* with *HindIII* restriction site
P1228	ACCCGGGAGAAGCGAAATAAAG CGC	Reverse primer for locus *PAP3* with *XmaI* restriction site, without the stop codon

Table 4. Primers used for the oligonucleotide annealing

Number	Sequence[1]	Description
P1059	AATTCAAAATGGCCAGACTCAC AAGCATCATTGCCCTCTTCGCAG TGGCTCTGCTGGTTGCAGATGCG TACGCCTACCGCC	Sense strand for oligonucleotide annealing for the signal peptide (SP) of pumpkin 2S albumin protein
P1060	CCGGGGCGGTAGGCGTACGCAT CTGCAACCAGCAGAGCCACTGC GAAGAGGGCAATGATGCTTGTG AGTCTGGCCATTTTG	Antisense strand for oligonucleotide annealing for the signal peptide (SP) of pumpkin 2S albumin protein
P1061	CTAGAGGGGGGGGGAAGGCTAG GAACTTGCCTTCCATGTGCGGAA TCCGCCCACAGCGATGCGACTTC TGA	Sense strand for oligonucleotide annealing for the putative vacuolar-targeting signal (VTS) of 18-amino-acid sequence of pumpkin 2S albumin with GlyGlyGly linker sequence on N-terminus and stop codon.
P1062	CTAGTCAGAAGTCGCATCGCTGT GGGCGGATTCCGCACATGGAAG GCAAGTTCCTAGCCTTCCCCCCC CCT	Antisense strand for oligonucleotide annealing for the putative vacuolar-targeting signal (VTS) of 18-amino-acid sequence of pumpkin 2S albumin with GlyGlyGly linker sequence on N-terminus and stop codon.

[1](Mitsuhashi et al., 2000)

Table 5. Primers used for the Clustered Regularly Interspaced Short Palindromic Repeats (CRISPR) cloning.

Number	Sequence	Description
P272	TAGGTCTCCAAACGAAGACA AAAACAAAAAAAAAAGCAC CGACTCG	Reverse primer for the generation of CRISPR/Cas9 - guide-RNA_production with tRNA processing machinery (Xie et al.) modified to fit pHSE401 and internal vector of laboratory
P274	TAGGTCTCCAAACGAAGACA AAAAC	Reverse primer for the generation of CRISPR/Cas9 - guide-RNA_production with tRNA processing machinery (Xie et al.) modified to fit pHSE401 and internal vector of laboratory
P293	CGGGTCTCAGGCAGAAGACT AATTGAACAAAGCACCAGT GG	Forward primer for the generation of CRISPR/Cas9 - guide-RNA_production with tRNA processing machinery (Xie et al.) modified to fit pHSE401
P294	CGGGTCTCAGGCAGAAGACT AATTG	Forward primer for the generation of CRISPR/Cas9 - guide-RNA_production with tRNA processing machinery (Xie et al.) modified to fit pHSE401
P767	TTGAAGACAAGGAGAAGCT TTCTTCATCGGTGAT	Forward primer for the amplification of *napinA* promotor with 5'-UTR with *BpiI* restriction site from *Brassica napus* for the golden gate cloning system
P768	TTGAAGACAACATTCGTGTA TGTTTTTAATCTTG	Reverse primer for the amplification of *napinA* promotor with 5'-UTR with *BpiI* restriction site from *Brassica napus* for the golden gate cloning system
P769	TTGAAGACAAGGAGGAATA AAAGCATTTGCGTTT	Forward primer for the amplification of an egg cell specific promotor (*EC1*.2) with *BpiI* restriction site from V122 for the golden gate cloning system
P770	TTGAAGACAACATTTTCTAG ATTTCTCAACAGATTG	Reverse primer for the amplification of an egg cell specific promotor (*EC1*.2) with *BpiI* restriction site from V122 for the golden gate cloning system

P771	TTGAAGACAAGCTTGCTCAG AGCTTTCGTTCGTA	Forward primer for the amplification of rbcs-E9t Terminator with *BpiI* restriction site from V122 for the golden gate cloning system
P772	TTGAAGACAAAGCGGTTGTC AATCAATTGGCAAG	Reverse primer for the amplification of rbcs-E9t Terminator with *BpiI* restriction site from V122 for the golden gate cloning system
P773	TTGAAGACAAAATGGCCTCC GGACCCAAGAAGAAGCGC	Forward primer for the amplification of *Cas9* with a NLS and an intron with *BpiI* restriction site from V130 for the Golden Gate cloning system
P774	TTGAAGACAAAAGCTTACTT CTTCTTCTTGGCCT	Reverse primer for the amplification of *Cas9* with a NLS and an intron with *BpiI* restriction site from V130 for the Golden Gate cloning system

Table 6. Primers used forCRISPR/*Cas9* guide RNA construction

Number	Gene_Guide number _position[1]	Sequence	Description
P870	At1g04040_guide1_F	TAGGTCTCCCATCGC AGTACAGTTTTAGAG CTAGAA	CRISPR/Cas9 targeting first exon of *HADIIIB5* phosphatase At1g04040,
P982	At1g04040_guide1_R	ATGGTCTCAGATGAC GTCATGTGCACCAGC CGGGAA	CRISPR/Cas9 targeting first exon of *HADIIIB5* phosphatase At1g04040,
P872	At1g04040_guide2_F	TAGGTCTCCGTCTAA GTGTGAGTTTTAGAG CTAGAA	CRISPR/Cas9 targeting first exon of *HADIIIB5* phosphatase At1g04040,
P983	At1g04040_guide2_R	ATGGTCTCAAGACTT GCTACATGCACCAGC CGGGAA	CRISPR/Cas9 targeting first exon of *HADIIIB5* phosphatase At1g04040,
P874	At2g38600_guide1_F	TAGGTCTCCTGCGTT ACGTTGGTTTTAGAG CTAGAA	CRISPR/Cas9 targeting first exon of *HADIIIB7* phosphatase At2g38600,
P875	At2g38600_guide1_R	ATGGTCTCACGCAGA CACTGCTGCACCAGC CGGGAA	CRISPR/Cas9 targeting first exon of *HADIIIB7* phosphatase At2g38600,
P876	At2g38600_guide2_F	TAGGTCTCCCCATCA CCAGGAGTTTTAGAG CTAGAA	CRISPR/Cas9 targeting first exon of *HADIIIB7* phosphatase At2g38600,
P877	At2g38600_guide2_R	ATGGTCTCAATGGCA TGGACGTGCACCAG CCGGGAA	CRISPR/Cas9 targeting first exon of *HADIIIB7* phosphatase At2g38600,
P878	At4g29270_guide1_F	TAGGTCTCCACTACG CTAAAAGTTTTAGAG CTAGAA	CRISPR/Cas9 targeting first exon of *HADIIIB3* phosphatase At4g29270,
P879	At4g29270_guide1_R	ATGGTCTCATAGTCA ATGGCGTGCACCAG CCGGGAA	CRISPR/Cas9 targeting first exon of *HADIIIB3* phosphatase At4g29270,
P880	At4g29270_guide2_F	TAGGTCTCCTTGGAC CCTGGAGTTTTAGAG CTAGAA	CRISPR/Cas9 targeting first exon of *HADIIIB3* phosphatase At4g29270,

P881	At4g29270_guide2_R	ATGGTCTCACCAACA TTGTTGTGCACCAGC CGGGAA	CRISPR/Cas9 targeting first exon of *HADIIIB3* phosphatase At4g29270,
P882	At5g44020_guide1_F	TAGGTCTCCGAGCCA GCTCAAGTTTTAGAG CTAGAA	CRISPR/Cas9 targeting first exon of *HADIIIB6* phosphatase At5g44020,
P981	At5g44020_guide1_R	ATGGTCTCAGCTCAG GATGTTTGCACCAGC CGGGAA	CRISPR/Cas9 targeting first exon of *HADIIIB6* phosphatase At5g44020,
P884	At5g44020_guide2_F	TAGGTCTCCTCCCAA CCTAAAGTTTTAGAG CTAGAA	CRISPR/Cas9 targeting first exon of *HADIIIB6* phosphatase At5g44020,
P885	At5g44020_guide2_R	ATGGTCTCAGGGAG CTTTCAATGCACCAG CCGGGAA	CRISPR/Cas9 targeting first exon of *HADIIIB6* phosphatase At5g44020,
P886	At5g51260_guide1_F	TAGGTCTCCTCGAGT ACCCGTGTTTTAGAG CTAGAA	CRISPR/Cas9 targeting first exon of *HADIIIB2* phosphatase At5g51260,
P887	At5g51260_guide1_R	ATGGTCTCATCGAGA ATCGAATGCACCAG CCGGGAA	CRISPR/Cas9 targeting first exon of *HADIIIB2* phosphatase At5g51260,
P888	At5g51260_guide2_F	TAGGTCTCCCCTGGA GATTCGGTTTTAGAG CTAGAA	CRISPR/Cas9 targeting first exon of *HADIIIB2* phosphatase At5g51260,
P889	At5g51260_guide2_R	ATGGTCTCACAGGTC GTACAATGCACCAG CCGGGAA	CRISPR/Cas9 targeting first exon of *HADIIIB2* phosphatase At5g51260,

F = sense strand   R = antisense strand

2.1.4. Vectors

Table 7. Vectors.

Number	Identity	Description	Resistance
	pJet1.2 (Thermo scientific)	Vector used for the cloning of the blunt end PCR products	Amp^R
V36	pXCS-YFP	Binary vector used for overexpression studies of C-terminally tagged yellow fluorescent protein (YFP) proteins. Expression from the 35S promoter (Feys et al., 2005).	Amp^R Basta^R
V37	pXCS-CFP	Binary vector used for overexpression studies of C-terminally tagged cyan fluorescent protein (CFP) proteins. Expression from the 35S promoter.	Amp^R Basta^R
V69	pXCScpmv-HAStrepII	Binary vector used for overexpression studies of C-terminally tagged StrepII proteins. Expression from the of 35S promoter, enhanced by CPMV leader and tailer sequences (Cañizares et al., 2006).	Amp^R Basta^R
V113	pGTR	Vector obtained from addgene for multiple CRISP constructs contains pre-tRNA fused with guide_RNA scaffold	Amp^R
V122	pHEE2E-TRI	Expression vector used for the Cas9 protein under the control of egg cell specific promoter and rbcS-E9t terminator	Kana^R
V125	pICH41308	Cloning vector obtained from Addgene, plate position H2	Spec^R

V130	pB330p6i2xoR-ucas-U6os4	Cloning vector obtained from DNA cloning service containing coding sequence for *Cas9*	Spec^R
V132	pICH41421	Cloning vector for the golden gate cloning system containing NOS terminator	Spec^R
V134	pICH41308_ Turbo-GFP+Intron	Cloning vector for the Level-0 module for the expression of Turbo-GFP protein	Spec^R
V137	pICH41295	Cloning vector for the Level-o module for the golden gate cloning for the promoters (position G2 (vector plate))	Spec^R
V138	pICH41276	Cloning vector for the Level-o module for the golden gate cloning for the terminators (position D2 (vector plate))	Spec^R
V139	pICH41295__Pro+5U_napinA	Cloning vector for the Level-o module for the golden gate cloning containing NapinA promoter (position G2 (vector plate))	Spec^R
V140	pICH41295_Pro+5U_egg-cell-specific	Cloning vector for the Level-o module for the golden gate cloning containing egg cell specific promoter (position G2 (vector plate))	Spec^R
V141	pICH41276_rbcS-E9t	Cloning vector for the Level-o module for the golden gate cloning containing rbcS-E9 terminator (position D2 (vector plate))	Spec^R
V142	pICH87633_nos-Promotor	Cloning vector for the Level-o module for the golden gate cloning containing nos promoter and leader sequences (position D3 (plant parts kit))	Spec^R
V143	pICH43844_Basta_Resistence_Gene	Cloning vector for the Level-o module for the golden gate cloning containing Phosphinotricin-Acetyl-Transferase gene (position F10 (plant parts kit))	Spec^R
V144	pICH47742	Cloning vector obtained from Addgene, vector plate position C3	Amp^R

V145	pICH47751	Cloning vector obtained from Addgene, plate position D3 (vector plate)	Amp^R
V146	pICH47761_level_1_ pos_4	Cloning vector obtained from Addgene, plate position E3 (vector plate)	Amp^R
V147	pAGM4723	Cloning vector obtained from Addgene, plate position A5 (vector plate)	Kana^R
V148	pICH41432_ocs_Ter minator	Cloning vector obtained from Addgene, plate position D12 (Plant parts kit)	Spec^R
V149	pICH41780	Cloning vector obtained from Addgene, plate position E5 (vector plate)	Spec^R
V150	pICH41308_CDS1_C as9WT+Intron	Cloning vector for the Level-o module for the golden gate cloning containing coding sequence for Cas9	Spec^R
V181	pICH47761_napinA_t GFP_pos4_fwd	pICH47761 (E3 Vector plate) containing *napinA* promoter-TurboGFPV and vector D12 from plant parts kit	Amp^R
V182	pICH47742_Cas9WT +Intron_pos2_fwd	pICH47742 (C3 Vector Plate) containing Egg cell specific promotor-Cas9-rbcS-E9t	Amp^R
V183	pICH47732_Basta_po s1_fwd	D3(plant parts) F10(plant parts) vector containing Basta resistance gene under the control of Nos promoter and terminator	Amp^R Basta^R
V185	pDI1E	contains U6-26 promotor - insert- *Cas9*-scaffold	Amp^R
H854	pXCS _SP-mCherry-VTS	Expression of N-terminal SP and C-terminal VTS tagged mCherry *in planta*	Amp^R Basta^R

Table 8. **Constructs used and generated in this study.**

Number[1]	Vector	Cloning	Description
H854	pXCS-CFP	*EcoRI-XbaI*	Expression of N-terminal SP and C-terminal VTS tagged mCherry *in planta* (the *XbaI* site is mutated and cannot be used for further restriction digestion analysis)
H853	pXCS-CFP	*EcoRI-XbaI*	Expression of N-terminal SP and C-terminal VTS tagged CFP *in planta* (the *XbaI* site is mutated and cannot be used for further restriction digestion analysis)
H852	pXCS-CFP	*EcoRI-XbaI*	Expression of N-terminal SP and C-terminal VTS tagged CFP *in planta*. The construct could not be used the CFP in the mother plasmid V37 had a stop codon.
H851	pXCS-CFP	*EcoRI-XmaI*	Expression of N-terminal SP-tagged CFP *in planta*
H850	pJet1.2	-	Cloning of the PCR amplified product of mCherry gene from template vector V115 without the stop codon
H849	pJet1.2	-	Cloning of the PCR amplified product of CFP gene from template vector V37 without the stop codon
H846	pXCS-YFP	*EcoRI-XmaI*	Expression of C-terminal YFP-tagged HADIIIB3 *in planta*
H845	pXCS-YFP	*PstI-XmaI*	Expression of C-terminal YFP-tagged HADIIIB2 *in planta*
H844	pXCS-YFP	*EcoRI-XmaI*	Expression of C-terminal YFP-tagged HADIIIB1 *in planta*
H843	pXCS-YFP	*EcoRI-XmaI*	Expression of C-terminal YFP-tagged HADIIIB7 *in planta*
H842	pXCS-YFP	*EcoRI-XmaI*	Expression of C-terminal YFP-tagged HADIIIB5 *in planta*
H841	pXCS-YFP	*EcoRI-XmaI*	Expression of C-terminal YFP-tagged HADIIIB6 *in planta*

H212	pXCScpmv-HAStrepII	*EcoRI-XmaI*	Expression of C-terminal StrepII-tagged HADIIIB3 *in planta*
H211	pXCScpmv-HAStrepII	*PstI-XmaI*	Expression of C-terminal StrepII-tagged HADIIIB2 *in planta*
H210	pXCScpmv-HAStrepII	*EcoRI-XmaI*	Expression of C-terminal StrepII-tagged VNPP1 *in planta*
H209	pXCScpmv-HAStrepII	*EcoRI-XmaI*	Expression of C-terminal StrepII-tagged HADIIIB1 *in planta*
H208	pXCScpmv-HAStrepII	*EcoRI-XmaI*	Expression of C-terminal StrepII-tagged HADIIIB7 *in planta*
H207	pXCScpmv-HAStrepII	*EcoRI-XmaI*	Expression of C-terminal StrepII-tagged HADIIIB5 *in planta*
H206	pXCScpmv-HAStrepII	*EcoRI-XmaI*	Expression of C-terminal StrepII-tagged HADIIIB6 *in planta*
H205	pJet1.2	-	Cloning of the PCR amplified product of locus *HADIIIB3* from young seedlings of Col-0 (wild type)
H204	pJet1.2	-	Cloning of the PCR amplified product of locus *HADIIIB2* from young seedlings of Col-0 (wild type)
H203	pJet1.2	-	Cloning of the PCR amplified product of locus *HADIIIB4* from young seedlings of Col-0 (wild type)
H202	pJet1.2	-	Cloning of the PCR amplified product of locus *HADIIIB1* from young seedlings of Col-0 (wild type)
H201	pJet1.2	-	Cloning of the PCR amplified product of locus *HADIIIB7* from young roots of Col-0 (wild type)
H200	pJet1.2	-	Cloning of the PCR amplified product of locus *HADIIIB5* from young seedlings of Col-0 (wild type)

H199	pJet1.2	-	Cloning of the PCR amplified product of locus *HADIIIB6* from young seedlings of Col-0 (wild type)
H161	pXCS-YFP	*EcoRI-XmaI*	Expression of C-terminal YFP-tagged chimera PAP26 *in planta*
H160	pXCScpmv-HAStrepII	*EcoRI-XmaI*	Expression of C-terminal StrepII-tagged chimera PAP26 *in planta*
H155	pXCS-YFP	*EcoRI-XmaI*	Expression of C-terminal YFP-tagged ENDO5 *in planta*
H154	pXCS-YFP	*EcoRI-XmaI*	Expression of C-terminal YFP-tagged ENDO4 *in planta*
H153	pXCS-YFP	*ClaI-XmaI*	Expression of C-terminal YFP-tagged ENDO3 *in planta*
H152	pXCS-YFP	*ClaI-XmaI*	Expression of C-terminal YFP-tagged ENDO2 *in planta*
H151	pXCS-YFP	*EcoRI-XmaI*	Expression of C-terminal YFP-tagged ENDO1 *in planta*
H148	pXCS-YFP	*EcoRI-XmaI*	Expression of C-terminal YFP-tagged VNPP1 *in planta*
H147	pXCScpmv-HAStrepII	*EcoRI-XmaI*	Expression of C-terminal StrepII-tagged ENDO5 *in planta*
H139	pJet1.2	-	Cloning of the PCR amplified product of *ENDO5* gene from young seedlings of Col-0 (wild type)
H138	pJet1.2	-	Cloning of the PCR amplified product of *ENDO4* gene from young seedlings of Col-0 (wild type)
H137	pJet1.2	-	Cloning of the PCR amplified product of *ENDO3* gene from young seedlings of Col-0 (wild type)
H136	pJet1.2	-	Cloning of the PCR amplified product of *ENDO2* gene from young seedlings of Col-0 (wild type)

H135	pJet1.2	-	Cloning of the PCR amplified product of *ENDO1* gene from young seedlings of Col-0 (wild type)
H1099	pXCS-YFP	*PstI-XmaI*	Expression of C-terminal YFP-tagged PAP28 *in planta*
H1098	pXCS-YFP	*ClaI-XmaI*	Expression of C-terminal YFP-tagged PAP27 *in planta*
H1097	pXCS-YFP	*ClaI-XmaI*	Expression of C-terminal YFP-tagged PAP18 *in planta*
H1096	pXCS-YFP	*ClaI-XmaI*	Expression of C-terminal YFP-tagged PAP17 *in planta*
H1095	pXCS-YFP	*ClaI-XmaI*	Expression of C-terminal YFP-tagged PAP12 *in planta*
H1094	pXCS-YFP	*ClaI-XmaI*	Expression of C-terminal YFP-tagged PAP10 *in planta*
H1093	pXCS-YFP	*HindIII-XmaI*	Expression of C-terminal YFP-tagged PAP8 *in planta*
H1092	pXCS-YFP	*HindIII-XmaI*	Expression of C-terminal YFP-tagged PAP4 *in planta*
H1091	pXCS-YFP	*HindIII-XmaI*	Expression of C-terminal YFP-tagged PAP3 *in planta*
H1090	pXCS-YFP	*HindIII-HindIII*	Expression of C-terminal YFP-tagged PAP2 *in planta*
H1089	pXCS-YFP	*ClaI-ClaI*	Expression of C-terminal YFP-tagged PAP1 *in planta*
H1088	pJet1.2	-	Cloning of the PCR amplified product of *PAP28* gene from young seedlings of Col-0 (wild type)
H1087	pJet1.2	-	Cloning of the PCR amplified product of *PAP27* gene from young seedlings of Col-0 (wild type)
H1086	pJet1.2	-	Cloning of the PCR amplified product of *PAP18* gene from young seedlings of Col-0 (wild type)

H1085	pJet1.2	-	Cloning of the PCR amplified product of *PAP17* gene from young seedlings of Col-0 (wild type)
H1084	pJet1.2	-	Cloning of the PCR amplified product of *PAP12* gene from young seedlings of Col-0 (wild type)
H1083	pJet1.2	-	Cloning of the PCR amplified product of *PAP10* gene from young seedlings of Col-0 (wild type)
H1082	pJet1.2	-	Cloning of the PCR amplified product of *PAP8* gene from young seedlings of Col-0 (wild type)
H1081	pJet1.2	-	Cloning of the PCR amplified product of *PAP4* gene from young seedlings of Col-0 (wild type)
H1080	pJet1.2	-	Cloning of the PCR amplified product of *PAP3* gene from young seedlings of Col-0 (wild type)
H1079	pJet1.2	-	Cloning of the PCR amplified product of *PAP2* gene from young seedlings of Col-0 (wild type)
H1076	pJet1.2	-	Cloning of the PCR amplified product of *PAP1* gene from young seedlings of Col-0 (wild type)
H1071	pAGM4723	*BpiI-BpiI*	Level 2 vector with two guide RNA targeting *HADIIIB1* from the construct H1062
H1070	pAGM4723	*BpiI-BpiI*	Level 2 vector with two guide RNA targeting *HADIIIB2* from the construct H1061
H1069	pAGM4723	*BpiI-BpiI*	Level 2 vector with two guide RNA targeting *HADIIIB6* from the construct H1060
H1068	pAGM4723	*BpiI-BpiI*	Level 2 vector with two guide RNA targeting *HADIIIB3* from the construct H1059
H1067	pAGM4723	*BpiI-BpiI*	Level 2 vector with two guide RNA targeting *HADIIIB7* from the construct H1058
H1066	pAGM4723	*BpiI-BpiI*	Level 2 vector with two guide RNA targeting *HADIIIB5* from construct H1057
H1062	pICH47751	*BsaI-BsaI*	Level 1 vector with two guide RNA targeting *HADIIIB1* from the construct H1053

H1061	pICH47751	*BsaI-BsaI*	Level 1 vector with two guide RNA targeting *HADIIIB2* from the construct H1052
H1060	pICH47751	*BsaI-BsaI*	Level 1 vector with two guide RNA targeting *HADIIIB6* from the construct H1051
H1059	pICH47751	*BsaI-BsaI*	Level 1 vector with two guide RNA targeting *HADIIIB3* from the construct H1050
H1058	pICH47751	*BsaI-BsaI*	Level 1 vector with two guide RNA targeting *HADIIIB7* from the construct H1049
H1057	pICH47751	*BsaI-BsaI*	Level 1 vector with two guide RNA targeting *HADIIIB5* from construct H1048
H1053	pDI1E	*BpiI-BpiI*	Level 0 vector with two guide RNA targeting *HADIIIB1*, guide array 1 was prepared by annealing primers (P1052+P1053) and guide array 2 was prepared by annealing (P1054+P1055). Both guide RNA targeting same gene in the first exon.
H1052	pDI1E	*BpiI-BpiI*	Level 0 vector with two guide RNA targeting *HADIIIB2*, guide array 1 was prepared by annealing primers (P886+P887) and guide array 2 was prepared by annealing (P888+P889). Both guide RNA targeting same gene in the first exon.
H1051	pDI1E	*BpiI-BpiI*	Level 0 vector with two guide RNA targeting *HADIIIB6*, guide array 1 was prepared by annealing primers (P882+P981) and guide array 2 was prepared by annealing (P884+P885). Both guide RNA targeting same gene in the first exon.
H1050	pDI1E	*BpiI-BpiI*	Level 0 vector with two guide RNA targeting locus *HADIIIB3*, guide array 1 was prepared by annealing primers (P878+P879) and guide array 2 was prepared by annealing (P880+P881). Both guide RNA targeting same gene in the first exon.
H1049	pDI1E	*BpiI-BpiI*	Level 0 vector with two guide RNA targeting locus *HADIIIB7*, guide array 1 was prepared by annealing primers (P874+P875) and guide array 2 was prepared by annealing

| | | | (P876+P877). Both guide RNA targeting same gene in the first exon. |
| H1048 | pDI1E | *BpiI-BpiI* | Level 0 vector with two guide RNA targeting locus *HADIIIB5*, guide array 1 was prepared by annealing primers (P870+P982) and guide array 2 was prepared by annealing (P872+P883). Both guide RNA targeting same gene in the first exon. |

[1]Laboratory's internal refrence number

2.1.5. Media for the bacteria

Table 9. Media for the bacteria.

Medium	Composition
Lysogeny Broth (LB)	1.0% (w/v) tryptone; 0.5% (w/v) yeast extract; 1.0% (w/v) NaCl, pH 7.0 (adjusted with NaOH); to prepare solid media 1.5% (w/v) agar.
Yeast Extract Broth (YEB)	0.5% (w/v) meat extract; 0.1% (w/v) yeast extract; 0.5% (w/v) pepetone; 0.5% (w/v) sucrose; 2 mM $MgSO_4$, pH 7.2 (adjusted with NaOH); to prepare solid media 1.5% (w/v) agar.

2.1.6. Media for the plants

Table 10. Media for plants

Medium	Composition
Half-strength Murashige Skoog (MS)	2.45 g L^{-1} MS salt including vitamins and MES buffer; pH 5.7 (adjusted with KOH), 0.8% (w/v) phytoagar.
Modified Hoagland solution	1.50 mM KNO_3; 0.75 mM $Ca(NO_3)_2$; 0.75 mM $MgSO_4$; 0.50 mM $(NH_4)_2SO_4$; 0.50 mM K_2HPO_4; 0.50 mM KCl; 0.10 mM Fe-EDTA; 50 μM H_3BO_3; 20 μM $ZnSO_4$; 10 μM $MnSO_4$; 1 μM $CuSO_4$; 1 μM Na_2O_3Si; 0.1 μM Na_2MoO_4; pH 5.7, adjusted with HCl.

2.1.7. Plant lines

Table 11. Plant lines

Number[1]	Name	Locus identifier	Ecotype	Line
-	Wild type	-	Col-0	-
KO200	*HADIIIB4/VNPP1-wt*[2]	At4g29260	Col-0	SALK-087041
KO200	*vnpp1/ hadIIIb4*	At4g29260	Col-0	SALK-087041
KO199	*HADIIIB1*-wt[2]	At4g25150	Col-0	SALK_128131
KO199	*hadIIIb1*	At4g25150	Col-0	SALK_128131
KO198	*HADIIIB7*-wt[2]	At2g38600	Col-0	SALK_025761
KO198	*hadIIIb7*	At2g38600	Col-0	SALK_025761
KO197	*HADIIIB2*	At5g51260	Col-0	SAIL_899B10
KO126	*pap26*	At5g34850	Col-0	GABI-144B01
KO118	*rns2*	At2g39780	Col-0	SALK_069588C
KO109	*ent1*	At1g70330	Col-0	SALK025174C
-	Wild type	-	*Brassica napus*	CS29005

[1]Laboratory's internal refrence number. [2]wild type obtained from a segregating population of the corresponding mutant line.

2.1.8. Arabidopsis thaliana Crosses

Table 12. *Arabidopsis thaliana* **crosses.**

Number[1]	Name	Pollen donor	Pollen recipient
C363	*vnpp1*pap26*	*vnpp1*	*pap26*
C332[2]	*vnpp1*hadIIIb1*	*vnpp1*	*hadIIIb1*
C136	*pap26*xdh*	*pap26*	*xdh*

[1]Laboratory's internal refrence number, [2]homozygous double mutant plant could not be obtained

2.1.9. *Arabidopsis thaliana* mutants generated by CRISPR/Cas9

Table 13. CRISPR/*Cas9* mutant lines generated in this study.

Number [1]	Target locus	genetic background used	Number of lines screened	Editing events found	Success of the gRNA (gRNA 1) (gRNA 2)	editing observed	Position in the gene (bp)
R15	*HADIIIB3*	*vnpp1*[2]	1	1	1	Ins1 C	176
R16	*HADIIIB2*	*vnpp1*pap26*[3]	10	1	2	Del 1 T	149
R17	*HADIIIB2*	*hadIIIb1*[2]	20	-	-	No editing found	-
R18	*HADIIIB2*	*VNPP1*-wt[2]	5	3	1	Ins 1 T	77
					1+2	Del 70 bp	77-147
					2	Ins 1 T	149
R19	*HADIIIB2*	*vnpp1*[2]	3	3	1+2	Del 70 bp	77-147
					1+2	Del 102 bp	45-147
					1	Ins I C	77
R20	*HADIIIB2*	*pap26*[2]	10	1	2	Insertion of 1 T	149

[1] laboratory's internal number, [2] refer to Table number 11, [3] refer to Table number 12, [4] refer to Table number 6, construct number H1070 was used for the generation of all CRISPR/Cas9 mutants except for R15 where H1068 was used. Insertion (Ins), Deletion (Del), base pair (bp).

2.1.10. Buffers

Table 14. Protein extraction buffers

Buffer	Composition
Extraction	100 mM HEPES buffer pH 8; 100 mM NaCl; 5 mM EDTA; 0.005% (w/v) TritonX 100; 15 mM DTT; 100 μg mL^{-1} avidin.
Washing	100 mM HEPES buffer pH 8; NaCl 100 mM, 0.5 mM EDTA; 0.005% (w/v) TritonX 100; 2 mM DTT.
Elution	100 mM Bis-Tris buffer pH 6.8; NaCl 100 mM, 0.5 mM EDTA; 0.005% (w/v) TritonX 100; 2 mM DTT; 10 mM biotin.

Table 15. Transient expression buffer

Buffer	Composition
Agroinfiltration Buffer	10 mM MES (pH 5.6, adjusted with KOH), 10 mM MgCl$_2$, 150 μM acetosyringone.

Table 16. Fivefold concentrated SDS buffer

Buffer	Composition
SDS loading buffer (five fold concentrated)	500 mM DTT; 300 mM Tris-HCl (pH 6.8); 50% (v/v) glycerol; 10% (w/v) SDS; 0.2% bromophenol blue.

Table 17. Colloidal Coomassie staining

Buffer	Composition
Running buffer	25 mM Tris-HCl; 192 mM glycine; 0.1% (w/v) SDS.
Fixation	40% (v/v) ethanol; 10% (v/v) acetic acid.
Colloidal Coomassie dye stock	0.1% (w/v) Coomassie Brilliant Blue G-250; 10% (w/v) ammonium sulfate; 1% (v/v) phospshoric acid.
Staining solution	80% (v/v) Colloidal Coomassie dye stock; 20% (v/v) methanol.

Table 18. Western blot buffers

Buffer	Composition
Blotting buffer	48 mM Tris-HCl (pH 9.2); 0.5 mM SDS; 40 mM glycine; 20% (v/v) methanol.
TBS1	20 mM Tris-HCl (pH 7.6); 150 mM NaCl.
TBS-T	20 mM Tris-HCl (pH 7.6); 150 mM NaCl; 0.1% (v/v) Tween 20.
Blocking solution	5% (w/v) milk powder in TBS-T.
Alkaline phosphatase buffer (AP buffer)	100 mM Tris-HCl (pH 9.5); 100 mM NaCl; 5 mM $MgCl_2$.
BCIP (5-bromo-4-chloro-3'-indolyl phosphate p-toluidine salt)	50 mg mL^{-1} in Dimethylformamide (DMF).
NBT (nitro blue tetrazolium chloride)	50 mg mL^{-1} in 70% (v/v) DMF.

Table 19. Phosphatase assay buffers

Buffer	Composition
Malachit green solution	0.045% (w/v) malachit green carbinol hydrochlorid
Ammonium molybdate solution	4.2% (w/v) ammonium heptamolybdate in 4 M HCl
Color working solution	malachit green solution : ammonium molybdate solution (3 : 1), 0.1% Triton-X100
Sodium citrate solution	34% (w/v) sodium citrate

Table 20. Phosphatase assay solutions

Buffer	Composition
Phosphatase reaction buffer (five fold concentrated) pH 6.8	200 mM (pH 6.8) Bis-Tris propane; 500 mM NaCl; 50 mM $MgCl_2$
Phosphatase reaction buffer (four fold concentrated) pH 5.2	320 mM (pH 5.2) sodium acetate; 400 mM NaCl; 40 mM $MgCl_2$
Colorimetric determination of phosphate	0.8% (v/v) colour working solution; 0.1% (v/v) sample, 0.1% (v/v) sodium citrate

Table 21. Buffer for metablomics

Buffer	Compounds to detect	Composition
Extraction buffer	Xanthine	7.5 mM ammonium acetate, pH 7, adjusted with ammonium hydroxide solution
Mobile phase A	Xanthine	7.5 mM ammonium acetate, pH 7, adjusted with ammonium hydroxide solution
Mobile phase B	xanthine	methanol (MeOH)

2.2. Methods

2.2.1. Molecular biology methods

2.2.1.1. DNA extraction

DNA for molecular biology techniques was extracted following the method of Edwards et al., 1991. One small leaf taken from a young seedling was ground in a retch mill with 200 µL of extraction buffer and five 1 mm metal beads at 28 Hz for 1 minute (min), and 10 µL of 10% SDS solution was added. The sample was incubated for 1 min, and the cell debris were centrifuged at 15000g for 3 to 5 min. Then 100 µL supernatant was transferred into a new clean centrifuge vial and the DNA was precipitated by adding 75 µL isopropanol. The precipitated DNA was pelleted by centrifugation at 15000g for 10 min. The DNA pellet was washed with 70% v/v ethanol solution and dried on the benchtop. Finally, the DNA pellet was dissolved in 100 µL of double-distilled water. The extraction procedure was done at room temperature.

2.2.1.2. RNA extraction and cDNA synthesis

RNA extraction was performed from 100 mg of plant material of young leaves and roots. The plant material was ground with a Retch mill using 1 mm metal beads, and phenol/chloroform extraction protocol was followed. The RNA was treated with 1 µL (1 U/µL) of DNase I (routinely RQ1 RNase free DNase from Promega) for 10 min at 37°C. The quality and quantity of RNA was checked by agarose gel electrophoresis and spectrophotometry (NanoDrop). 1 µg of RNA was used for cDNA synthesis.

2.2.1.3. Polymerase Chain Reaction (PCR)

The complete coding sequence (CDS) for the candidate genes was amplified using gene-specific primers (Table 3). Young leaf or young root cDNA was used according to the expression profile of the gene determined *in silico*, and 1 µg of the template was used for PCR amplification. In all reactions, the Phusion High-Fidelity (HF) DNA Polymerase from New England Biolabs (NEB, USA) was used. A total of 50 µL reaction contained 10 µL of fivefold concentrated HF buffer for the enzyme, 0.2 mM dNTPs, 0.2 µM of each primer, and 1 unit of Phusion polymerase.

Table 22. PCR profile

Step	Temperature (°C)	Time
Denaturation	98	2 min
Denaturation	98	15 s
Annealing	according to primer[1]	30 s
Elongation	72	30 s kb^{-1}
Final elongation	72	10 min

[1]the annealing temperature was routinely 5°C below the theoretical melting temperature of the primer, for reference please see Section 2.1.3.

2.2.1.4. Cloning of candidate genes

The quality and quantity of the amplified CDS were checked by agarose gel electrophoresis and spectrophotometry (NanoDrop), respectively. The sequences were excised from the gel and purified via the Gel and PCR Clean-up Kit (Macherey-Nagel). The excised DNA fragments were ligated into the pJet1.2 cloning vector and transformed into chemo-competent cells. The ligation mixture was mixed with competent cells and placed on ice for 10 min, a heat shock was given at 42°C for 45 s, and the cells were placed back on the ice for 2 min. The ligation mix was incubated with 500 µL of LB medium for 1 h at 22°C at a heat block, and the cell culture was pelleted. The pellet was then resuspended in 100 µL of fresh LB medium and the cell suspension was plated on LB solid medium plates with appropriate antibiotics and incubated overnight at 37°C. The following day, individual cell colonies were grown in 3 mL liquid LB medium with appropriate

antibiotics in the 37°C shaker. After an additional 24 h, the plasmid DNA was extracted by the GenJet Plasmid Miniprep Kit (Thermo Fisher Scientific, Waltham, USA) and send for out-of-house sequencing. Plasmids with the correct sequence and destination vectors were digested with appropriate restriction enzymes as mentioned in the Table 8. The digested fragments were ligated and transformed into *Escherichia coli*. The plasmid was extracted from *E. coli* after amplification and confirmed by test digest for the correct size of the insert band.

2.2.1.5. Lumen marker construction

For the visualization of the candidate proteins in the vacuole, a lumen marker was constructed. The coding sequences (CDS) for CFP and mCherry were amplified from the pXCS-CFP (V37) and pXCSnpt-mCherry (V115) plasmids as template, respectively, using gene specific primers (Table 3). The amplified PCR products were cloned into pJet1.2 vector and the CDS was analysed by out-of-house sequencing. In parallel, two complementary oligonucleotides (Table 4) were annealed, the oligonucleotide P1059 as sense strand and oligonucleotide p1060 as the antisense strand for the signal peptide from pumpkin 2S albumin were annealed. The resultant double stranded DNA fragment encoding the signal peptide contained an *EcoRI* overhang on the N-terminus and *XbaI* overhang on the C-terminus. The destination vector pXCS-CFP (V37) was digested with *EcoRI* and *XbaI* and the annealed primers were cloned there. The resultant vector encoded a CFP protein N-terminally tagged with a signal peptide (H851, Table 8). Another two complementary oligonucleotides were annealed encoding the vacuolar targeting sequence (VTS; 18-amino-acid sequence of pumpkin 2S albumin). These were the P1061 as sense strand and oligonucleotide p1062 as the antisense strand. The resultant double stranded DNA molecule encoded a GlyGlyGly linker at the N-terminus of the VTS and had *XbaI* overhangs on both termini. The H851 construct generated in the previous step was digested with *XbaI* and dephosphorylated and the annealed VTS primers were cloned in. The orientation of the VTS fragment was checked by the commercial sequencing and the resultant construct was named H852. However, the H852 could not be used for the vacuolar lumen studies because the CDS for the CFP protein in the initial vector pXCS-CFP (V37) contained a stop codon. Therefore, the CFP encoding fragment in H852 was replaced with fragments encoding CFP and mCherry lacking a stop codon from pJet1.2 clones (H849, H850, respectively) using *XmaI* and *XbaI*. Thereby two vacuolar lumen marker constructs encoding either CFP (H853) or mCherry (H854) were generated.

45

Table 23. Attributes of the fluorescent proteins

	YFP	mCherry
Size	26.9 kDa	26.7 kDa
PKa	6.9	4.5
Oligomerization	Dimer	Monomer
Excitation energy	514	552
Emission energy	524-550	595-622
Organism	*Aequorea victoria*	*Discosoma sp.*
	(Jellyfish)	(Coral anemones)

The final constructs were transformed into competent cells of the *Agrobacterium tumefaciens* (*Rhizobium radiobacter*) strain GV3101pMP90RK via electroporation. For this the constructs were mixed with competent cells into a pre-cooled electroporation cuvette. A 2.2 kV electric pulse was given for transformation. 500 µL of YEB medium was added and the mixture transferred to a 1 mL centrifuge vial and incubated at 28 °C for 1 h. 15 µL of culture was plated on YEB agar plates with suitable antibiotics. The plates were incubated at 28°C for two days. Individual colonies were grown in YEB liquid medium. Glycerol stocks were prepared with 30 to 40% v/v glycerol and stored at -80°C in the freezer.

2.2.1.6. CRISPR/Cas9 cloning

The constructs to generate the CRISPR/Cas9-mediated HADIIIB knockouts were cloned using the MoClo system (Weber et al., 2011; Engler et al., 2014). This required the creation of a variety of different intermediate vectors that were used in combination with previously published vectors. The final level 2 vectors used for plant transformation to generate the knockout was made using four independent level 1 vectors. To construct level 1 vectors various level 0 vectors were generated.

For Level 0 vectors, (i) DNA form *Brassica napus* seedlings was extracted following the method of Edwards et al., 1991. The *napinA* promoter from the genomic DNA was amplified using the primer P767 and P768 (Table 5). The resulting PCR product and pICH41295 (V137) vector were digested and ligated in a single step using the *BpiI* restriction enzyme. The resulting vector was

named pICH41295_Pro+5U_napinA (V139) (ii) the egg cell specific promotor and the rbcs-E9t terminator were amplified from pHEE2E-TRI (V122), and (iii) the *CAS9* coding sequence was amplified from pB330p6i2xoR-ucas-U6os4 (V130) and sequenced (for sequencing primers see Table 5). In a restriction/ligation reaction using *BpiI*, the egg cell specific promotor was cloned into pICH41295 (V137), the rbcs-E9t Terminator was ligated into pICH41276 (V138), and the Cas9 coding sequence was ligated into pICH41308 (V125). The resulting vectors were named pICH41295_Pro+5U_egg-cell-specific (V140), pICH41276_rbcS-E9t (V141), and pICH41308_CDS1_Cas9WT+Intron (V150), respectively. Next the CRISPR/Cas9 arrays were generated containing sequences encoding two gRNAs for editing each gene in the first exon. The guide RNAs were generated according to Xie et al., 2015. The gRNA sequence used for mutation of *HADIIIB* genes were selected based on the criteria proposed by Doench et al. (2014). The guide array under the control of the ATU6-26 promoter was generated by first amplifying the two halves of the array with the specific primers P293/P982 and P870/P272 on pGTR (V113) and then merging them in a one-step *BsaI* cut/ligation reaction. This fused guide array was reamplified with P294/P274. The guide array was then cloned into the MoClo-compatible gRNA shuttle vector (Streubel, unpublished) upstream of the ATU6-26 promoter in a *BbsI* cut ligation. Subsequently, this vector was cloned into pICH47751 (V145) by a *BsaI* cut/ligation, resulting in H1057. This procedure was used for the generation of level 1 vectors for all target loci.

For the Level 1 vectors, a Basta resistance cassette was generated using the pICH47732 (V126), pICH87633_nos-Promotor (V142), pICH43844_Basta_Resistence_Gene (V143), and pICH41421 (V132) in a one-step restriction digestion and ligation reaction using the *BsaI* restriction enzyme. The final vector form this step was named pICH47732_Basta_pos1_fwd (V183).

A level 1 Cas9 cassette was generated using pICH47742 (V144), pICH41295_Pro+5U_egg-cell-specific (V140), pICH41308_CDS1_Cas9WT+Intron (V150), and pICH41276_rbcS-E9t (V141) in one step restriction digestion/ligation reaction using *BsaI* restriction enzyme. The final vector from this step was named pICH47742_Cas9WT+Intron_pos2_fwd (V182).

A CRISPR/Cas9 array was generated using vector pICH47751 (V145) and the guide RNA generated for each gene from H1048 to H1053 (Table 8) in one step restriction digestion and ligation reaction using *BsaI* restriction enzyme. The vectors form this step were named H1057 to H1062.

A fluorescent marker cassette was generated using pICH47761_level_1_pos_4 (V147), pICH41295_Pro+5U_napinA, (V139), pICH41308_Turbo-GFP+Intron (V134), and pICH41432_ocs_Terminator (V148) in a one-step restriction/digestion using the *BsaI* restriction enzyme. The final vector from this step was named pICH47761_napinA_tGFP_pos4_fwd (V181).

The final constructs of Level 2 were generated by ligating pAGM4723 (V147), pICH47732_Basta_pos1_fwd (V183), pICH47742_Cas9WT+Intron_pos2_fwd (V182), pICH47761_napinA_tGFP_pos4_fwd (V181), end linker_1 pICH41780 (V149), and the guide RNA cassette for each gene (H1057-H1062 see Table 6 for details) using *BpiI* restriction enzyme. The final vectors form this step were named H1066 to H1071 (Table 8). The final constructs were transformed into the *Agrobacterium tumefaciens*. The transgenic bacteria were used to stably transform *Arabidopsis thaliana* plants for the generation of CRISPR/Cas9 edited plants.

2.2.2. Plants related mothods

2.2.2.1. Growth of *Nicotiana benthamiana*

N. benthamiana seeds were sown (one seed per pot) on soil and grown under long-day conditions (16 h light and 8 h dark). The plants were used for the transient expression of proteins after four weeks approximately. The plants used for confocal microscopy were placed on the lab benchtop after infiltration for three days. The leaf discus form lower epidermal cells of the infiltrated leaf were visualized under the confocal microscope.

2.2.2.2. Growth of *Arabidopsis thaliana*

Arabidopsis seeds were sterilized with 70% v/v ethanol and dried on a clean bench on sterilized filter paper. The seeds were either sown on half strength MS medium plates or on soil. Pots were transferred to 4°C for 48 h and then shifted to a plant growth chamber with long-day conditions (16 h light and 8 h dark).

For studies including a prolonged night, the plants were grown as mentioned above for 2 to 3 weeks, depending upon the experiment. At the onset of the next day just before the lights turned on, the plants were covered with a tray and a black cloth to block the light completely. Plant material was harvested and weighed in a dark room.

For experiments with allopurinol treatment, the plants were grown as mentioned above for 2 to 3 weeks. Before the start of the daylight, the plants were sprayed with 500 µL of 200 µM allopurinol per plate. In the case of soil-grown plants, three to four pump strokes of allopurinol from a hand-held mini-dispenser were sprayed until the plants were completely wetted, and samples were taken according to a time course.

2.2.2.3. Genotyping of *Arabidopsis thaliana*

The T-DNA insertion lines (Table 11) required for this study were ordered from the Nottingham Arabidopsis Stock Centre (NASC). PCR experiments were performed using genomic DNA as template to identify homozygous mutant lines and gene-specific primers were used as mentioned in Table 3. Only those lines were selected where the PCR reaction was positive for the T-DNA amplification. Additionally, for each T-DNA line, a wild type plant was also identified from the segregating population to be used as a control.

2.2.2.4. Crossing of *Arabidopsis thaliana*

T-DNA lines were crossed to obtain double mutants. The T-DNA lines were grown in individual pots for 4-5 weeks. Once plants were flowering, the anther of one line was used as the pollen donor to fertilize the ovary as pollen recipient of another line by hand. The ovary was marked with a thread. Once the crossed silique was fully matured and dry, three seeds were grown and the resulting plants were genotyped to assess the presence of the mother's and the father's T-DNA alleles.

2.2.2.5. Stable transformation of *Arabidopsis thaliana*

For the preparation of complementation lines and other transgenic plants, Arabidopsis was stably transformed. First, the plants were grown according to the protocol described in Section 2.2.2.2. Once the plants were flowering, a 100 mL YEB liquid culture of the bacteria to be used for transformation was grown. The following day, the bacteria were pelleted at $2600g$ for 15 min and resuspended in 5.0% sucrose solution together with 0.05% Silwet as a surfactant. The flowering

shoots were dipped in this cell suspension and incubated for 16 to 24 h in the dark. The floral dipped shoots were covered with a plastic bag to keep them humid. After incubation, the plants were returned to a plant growth chamber set to long-day conditions. After seed set, seeds were harvested, germinated, and plantlets selected by Basta[R] or seeds were screened by fluorescence in case a fluorescent marker was present using a fluorescence binocular. Transgene expression was further confirmed by immunoblotting.

3.2.2.6. Transient expression in *N. benthamiana*

For transient expression of proteins, cells from glycerol stocks of the required constructs were streaked on YEB solid medium plates with appropriate antibiotics and grown for two days. Two to three loops of bacteria (on an inoculation loop) were used to inoculate a 12 mL YEB liquid medium culture with the appropriate antibiotics and grown overnight at 28°C and 180 rpm. Bacteria carrying a construct containing the coding sequence of the p19 protein of Tomato Bushy Stunt Virus were grown in parallel. This p19 construct conferred resistance to Rif and Kan. The p19 inhibits post-transcriptional gene silencing in the plant (Voinnet et al., 2003). The following day, the cells were harvested by centrifugation at *5000g* for 15 min. The cells were resuspended in resuspension buffer (Table 15) to a final optical density of 0.5 (at 600 nm) for cells carrying the respective construct and of 0.1 for cells carrying the p19 vector.

The plants were grown according to the protocol mentioned in 2.2.2.1 and infiltrated with the required constructs for vacuolar localization. After infiltration, the plants were kept on the lab bench for three days. On the third day, before the plants were exposed to any source of light, they were placed into an S1 transport box covered with a plain black cloth blocking any light. After 40 h of darkness, leaf discs were inspected under the confocal microscope.

2.2.3. Biochemical methods

2.2.3.1. Protein extraction and purification

The transiently expressed proteins were extracted and purified with StrepII affinity chromatography. First, 0.75 mg of leaf material was harvested in a pre-cooled pestle and mortar,

1500 µL of extraction buffer was added, and the mixture was ground to a fine slurry. After centrifugation at 20000g for 10 min, the supernatant was transferred to a centrifuge vial. To obtain a sample (sample S1), 40 µL of supernatant was transferred into a separate centrifuge vial with 10 µL of fivefold concentrated SDS loading buffer. Next, 20 µL of Strep-Tactin Macroprep 50% suspension beads (IBA, Göttingen, Germany) were added to the supernatant and the sample was incubated on a rotating wheel for 10 min at 4°C. The supernatant was then centrifuged at 700g for 30 s and another sample (sample S2) was drawn by placing 40 µL of supernatant in a centrifuge vial with 10 µL of 5x SDS-loading buffer. The remaining supernatant was discarded from the Macroprep matrix and 1000 µL of washing buffer was added, briefly mixed, and the slurry centrifuged at 700g. The wash step was repeated four times. A sample was drawn from the last wash buffer as before (sample S3). The proteins were then eluted from the Macroprep matrix in 75 µL of elution buffer by incubating on a heat block at 30°C and 900 rpm for 5 min. The elution was done twice, and both elution fractions were combined in a single centrifuge vial. Here again a sample was drawn as before (sample S4). To control whether any protein was still bound to the beads, 1000 µL of wash buffer was added to the beads after elution, the beads resuspended, and sample drawn from the slurry as before (sample S5). The expression and purification of protein was assessed by analysing the samples S1 to S5 on immunoblots.

2.2.3.2. Colloidal Coomassie stain and protein quantification

To quantify the purified proteins, the S4 sample was loaded on an SDS gel. Before the loading of the gel, the S4 sample and BSA (bovine serum albumin) was boiled at 95°C for 5 min. A concentration range of 0.2, 0.1, 0.05, 0.025, 0.0125, 0.00625 and 0.00312 mg mL^{-1} of BSA was used as standards. The gel was run at 80 V for the stacking phase and 120 V for the resolving phase. The gel was then placed into a fixation solution (40.0% methanol, 10.0% acetic acid v/v) for 1 h, followed by brief washing with distilled water and incubation with staining solution for 4 h or overnight. The gel was washed with distilled water to remove excess staining solution and documented. The ImageJ software was used for quantification. Bands intensities were quantified and a plot with a regression line was generated. With the equation of the regression line the sample band intensity was converted into a concentration.

2.2.3.3. Immunoblots

To visualize the purification pattern and quality of the purified protein, the samples from S1 to S5 were loaded on a denaturing gel, as mentioned above. After the electrophoresis, the gel was transferred to a nitrocellulose membrane using the semi-dry blotting method. Afterward, the membrane was incubated with the blocking solution for 20 min. The gel was removed from the blocking solution and washed quickly with distilled water. Next, the gel was incubated with avidin for 10 min, and the Strep-Tactin alkaline phosphatase (AP) antibody was added to the TBS-T buffer and incubated for 1 h to overnight. The membrane was washed with TBS-T buffer thrice to eliminate the antibody solution. The detection was performed with 10 mL AP buffer containing 33 µL BCIP and 66 µL NBT solutions for 10 min.

2.2.3.4. Phosphatase activity assay

The phosphatase assay was performed according to Lanzetta et al., 1979, but the assay volumes were slightly changed. The enzymatic assays were conducted at 30°C and a total volume of 100 µL was usually used. Reactions contained 20 µL of fivefold concentrated reaction buffer and 10 µL of purified enzyme. The substrate concentrations were adjusted according to the assay. For initial substrate scanning, 1 mM of the substrates were used. For enzyme kinetics studies, a broad range of substrate concentrations ranging from half K_M to ten K_M were used. For the assay, the heat block was set to 30°C. A reaction mixture including buffer, enzyme, and water was warmed up for 3 min and simultaneously the substrate was also warmed up. A 96 well plate was used for sampling. 200 µL of color reagent was added to each well. After 3 min, an appropriate amount of the substrate was taken and mixed quickly into the reaction mixture. Immediately, 20 µL of sample was drawn out of the reaction mixture and placed into the color reagent in the 96 well plate followed by the addition of 20 µL of sodium citrate to stabilize the color. This sample was noted as the sample at 0 min. Then, further samples were taken with the same protocol depending on the respective time course. The plate was analyzed with a spectrophotometer at 660 nm wavelength.

2.2.4. Metabolomics methods

2.2.4.1. Sample preparation for LC-MS

Samples were prepared for metabolite analysis by taking either 100 mg fresh or 10 mg freeze-dried material. Such samples were ground with one 7 mm and five 5 mm steel beads for 1.5 min at 28 Hz in a 1.5 mL safe lock centrifuge vial using a Retsch mill. The dry material was ground at room temperature and the fresh material in liquid nitrogen. Next, 500 µL of extraction buffer, including the internal standard (ISTDs) ^{15}N5-xanthine was added and samples were incubated on a heat block at 95°C for 10 min at 1000 rpm. Samples were then centrifuged at a speed of 20000g for 20 min. The supernatant was carefully transferred to a new centrifuge vial without disturbing the cell debris at the bottom. To ensure clean samples, samples were either centrifuged again at 20000g for 20 min and the supernatant was transferred to a clean centrifuge vial or passed through micro spin filters (Thermo scientific, PVDF, 0.2 µm). Finally, 50 uL of the sample was used for the MS analysis out of which 10 µL was injected into the LC-MS.

Table 24. Acquisition method report for LC-MS

Compound Name	ISTD	Precursor Ion	Product Ion	collision energy (V)	Retention Time (min)	Polarity
^{15}N5-xanthine	Yes	155	137	15	1.54	Positive
^{15}N5-xanthine	Yes	155	110.9	15	1.54	Positive
^{15}N5-xanthine	Yes	155	56.2	33	1.54	Positive
Xanthin	No	153.1	136	15	1.54	Positive
Xanthin	No	153.1	109	15	1.54	Positive
Xanthin	No	153.1	55.2	33	1.54	Positive

Table 25. Source parameters for LC-MS

Parameter	Value (+)	Value (-)
Gas Temp (°C)	300	300
Gas Flow (l/min)	12	12
Nebulizer (psi)	30	30
Sheath Gas Heater	300	300
Sheath Gas Flow	11	11
Capillary (V)	4000	2500
V Charging	1500	1000

Table 26. Solvent flow parameters for LC-MS

	Time (min)	A (ammonium acetate; %)	B (MeOH; %)
1	1.50	95.0	5.0
2	3.50	85.0	15.0
3	6.00	0.0	100.0
4	7.00	0.0	100.0
5	7.10	95.0	5.0

2.2.4.2. Metabolomic analysis for 3'-NMPs

A more refined procedure was followed for the sensitive measurement of 3'-NMPs (Straube et al., 2021). Plant material (80-120 mg) frozen in liquid nitrogen was ground in a Retsch mill at the frequency of 28 Hz for 2 min. The sample was ground again after adding 1000 µL of 15.0% Trichloroacetic acid (TCA) solution. The mixture was then centrifuged at 20000g for 15 min. The supernatant was transferred to a clean centrifuge vial and 1000 µL of dichlormethan/trioctylamin

(DCM/TOA 78 : 22) was added and vortexed for 12 s. The mixture was centrifuged for 2 min at 2000g and 4°C. The upper phase was transferred into a clean centrifuge vial and 1000 µL acetic acid was added. The extraction column (Phenomenex Strata-X-AW) was equilibrated with 1 mL of 100.0% MeOH, formic acid/methanol/H$_2$O (2 : 25 : 73) and 10 mM ammonium acetate (NH$_4$Ac) each. The sample was loaded onto the equilibrated column and the flow-through containing the nucleosides was collected in clean centrifuge vial. The column was washed with 1 mM NH$_4$Ac and 100% MeOH and column bound nucleotides were eluted with a solution of ammonia and methanol (20 : 80).

Table 27. Acquisition method report for NMPs analysis

Compound Name	Precursor Ion	Product Ions	Fragmentor	collision energy (V)	Retention Time (min)	Polarity
3'-AMP	348.1	136	132	25	11.2	Positive
5'-AMP	348.1	136	132	25	11.5	Positive
3'-CMP	324	112	90	12	13.9	Positive
		97		28		
5'-CMP	324	112	90	12	13.2	Positive
		97		28		
3'-GMP	364.07	152	80	13	11.3	Positive
		135		45		
5'-GMP	364.07	152	80	13	14.4	Positive
		135		45		
3'-UMP	325.01	212.9	98	3	11.6	Positive
		97		10		
5'-UMP	325.01	212.9	98	3	8.3	Positive
		97		10		

Table 28. Source parameters for for NMPs analysis

Parameter	Value (+)	Value (-)
Gas Temp (°C)	250	250
Gas Flow (l/min)	12	12
Nebulizer (psi)	20	20
SheathGasHeater	395	395
SheathGasFlow	12	12
Capillary (V)	3000	3000
VCharging	500	500

Table 29. Solvent parameters for NMPs analysis

	Time	A	B
		(Ammonium acetate 5mM; %)	(Acetonitrile pH 9.5; %)
1	3.00	100.00	0.00
2	18.00	70.00	30.00
3	19.00	0.00	100.00
4	22.00	0.00	100.00
5	22.50	100.00	0.00

3. **Results**

According to our current understanding, RNA degradation in the vacuole involves three steps. First, the RNA is transported into the vacuole by various forms of autophagy (Figure 4), then the ribonucleases degrade the RNA into nucleotides and via mononucleotide phosphatases the phosphate groups are removed and nucleosides are released. Finally the nucleosides are transported out of the vacuole by nucleoside transporters (Figure 5). Vacuolar RNA degradation occurs during senescence or (nutrient) stress because plants thereby recycle resources which are mostly stored in organelles like the chloroplasts or in the ribosomes. However, vacuolar RNA degradation is also a regular process in younger unstressed cells performing housecleaning metabolism, for example removing damaged ribosomes.

An important vacuolar ribonuclease, RNS2, and a central nucleoside transporter, ENT1, of this metabolic pathway were identified and characterized a decade ago. By contrast, the acid mononucleotide phosphatases (NMPs) for nucleotide dephosphorylation in vacuoles have not been identified to date. This may be due to the difficulty of visualizing fluorescent-tagged candidate proteins in the acidic environment of the vacuole, the often broad substrate specificities of the APs, and the lack of state-of-the-art technology to quantify nucleotides in plant extracts. In this study, we attempted to identify and characterize the NMPs in vacuoles. We analyzed three families of enzymes with known mononucleotide phosphatase activity (HADIIIB, PAP, and S1/P1-type endonucleases) because of these at least some members had either been found in vacuoles in proteome studies or had the potential to localize in vacuoles since they were targeted to the secretory pathway. Initially, the list of candidates comprised 44 candidates. Several selection criteria were applied to reduce the list of candidates. The selection steps are reflected in the six main sections of the results chapter:

Section 1: Bioinformatic analyses to identify conserved members of the HADIIIB, PAP, and S1/P1-type endonuclease protein families. Because vacuolar nucleotide degradation is a housekeeping function required in every plant, only evolutionary conserved proteins were considered to be good candidates. In the case of the PAPs also the expression profile was already considered at this stage, because with 29 PAPs in total, the number was too high for any detailed experimental analysis. This analysis reduced the number of candidates from 44 to 24.

Section 2: Subcellular localization of the remaining candidates by expressing the enzymes *in planta* as versions with a C-terminal fluorescent proteins tag. Only candidate proteins present in the vacuole come into question as potential vacuolar NMP. Only 6 candidates fulfilled this criterium. However, one should note that when a protein could not be successfully localized at all, it was also excluded.

Section 3: Candidate enzymes found in the vacuolar lumen were subjected to enzymatic activity and substrate specificity analysis to identify potential 3'-NMP nucleotidases. This reduced the list to 5 candidates..

Secction 4: Two parallel analyses were performed. First, the bioinformatic analysis of expression profiles of the remaining candidates. It is likely, that genes encoding enzymes for such a housekeeping function are expressed in every tissue. Thus, only genes with ubiquitous expression patterns were considered. Such transcript profiling reduced the list from 5 to 3 candidates. Second, to study the *in vivo* function of the candidate proteins, different combinations of double and triple mutants were generated in this section. This reduced the candidate list down to only two candidates.

Secction 5: The last two candidates met all selection criteria, i.e. they were evolutionarily conserved, present in the lumen, had 3'-NMP enzyme activity, and were ubiquitously expressed in the plants. Therefore, the candidates were fully evaluated *in vitro* for their kinetic parameters.

Secction 6: *In vivo* metabolite analyses were performed employing genetic variants of the two candidates using various experimental settings. Alterations in the catabolism of 3'-NMPs are expected for genetic variants of vacuolar APs.

3.1. Bioinformatic studies

3.1.1. HADIIIB family

In a vacuolar proteome survey study (Carter et al., 2004), a HADIIIB-family enzyme from Arabidopsis encoded at locus At4g29260 was found in the vacuole. An orthologous enzyme from *Phaseolus vulgaris*, called PvNTD1, was identified and was shown to have 5'-nucleotidase activity while 3'-nucleotidase activity was not tested (Cabello-Díaz et al., 2015). Based on this data enzymes of the HADIIIB family were considered potential candidates for the sought vacuolar phosphatase activity.

Using the protein sequence encoded at the locus At4g29260 as query in BLAST (Basic Local Alignment Search Tool) searches of the Phytozome database (https://phytozome-next.jgi.doe.gov/), other related HADIIIB proteins of Arabidopsis and of further 11 plant species were identified. The Arabidopsis genome contains ten HADIIIB enzymes encoded at the loci At1g04040, At2g38600, At2g39920, At4g29260, At4g29270, At2g25150, At5g242770, At5g24780, At5g44020, and At5g51260. From eight dicotyledons and four monocotyledons species, the HADIIIB enzymes were also identified. The dicotyledons included *Phaseolus vulgaris* (common bean), *Solanum lycopersicum* (tomato), *Cucumis sativus* (cucumber), *Theobroma cacao* (cocoa beans), *Populus trichocarpa* (poplar), *Citrus sinensis* (orange) and *Aquilegia caerulea* (Colorado blue columbine flower). The monocotyledons included *Oryza sativa* (rice), *Sorghum bicolor* (millet), *Setaria italica* (foxtail millet) and *Brachypodium distachyon* (stiff brome grass). A phylogenetic study was conducted to elucidate the conservation of HADIIIB enzymes among plants, because it was hypothesized that only well conserved enzymes present in all plants are good candidates for the sought vacuolar mononucleotide phosphatases. A multiple protein sequence alignment was generated by Muscle hosted at the EBI website (https://www.ebi.ac.uk/Tools/msa/muscle/) and a phylogenetic tree was constructed using the Molecular Evolutionary Genetics Analysis (MEGA6) software, which is suited to conduct statistical analysis of molecular evolution and also used for constructing phylogenetic trees.
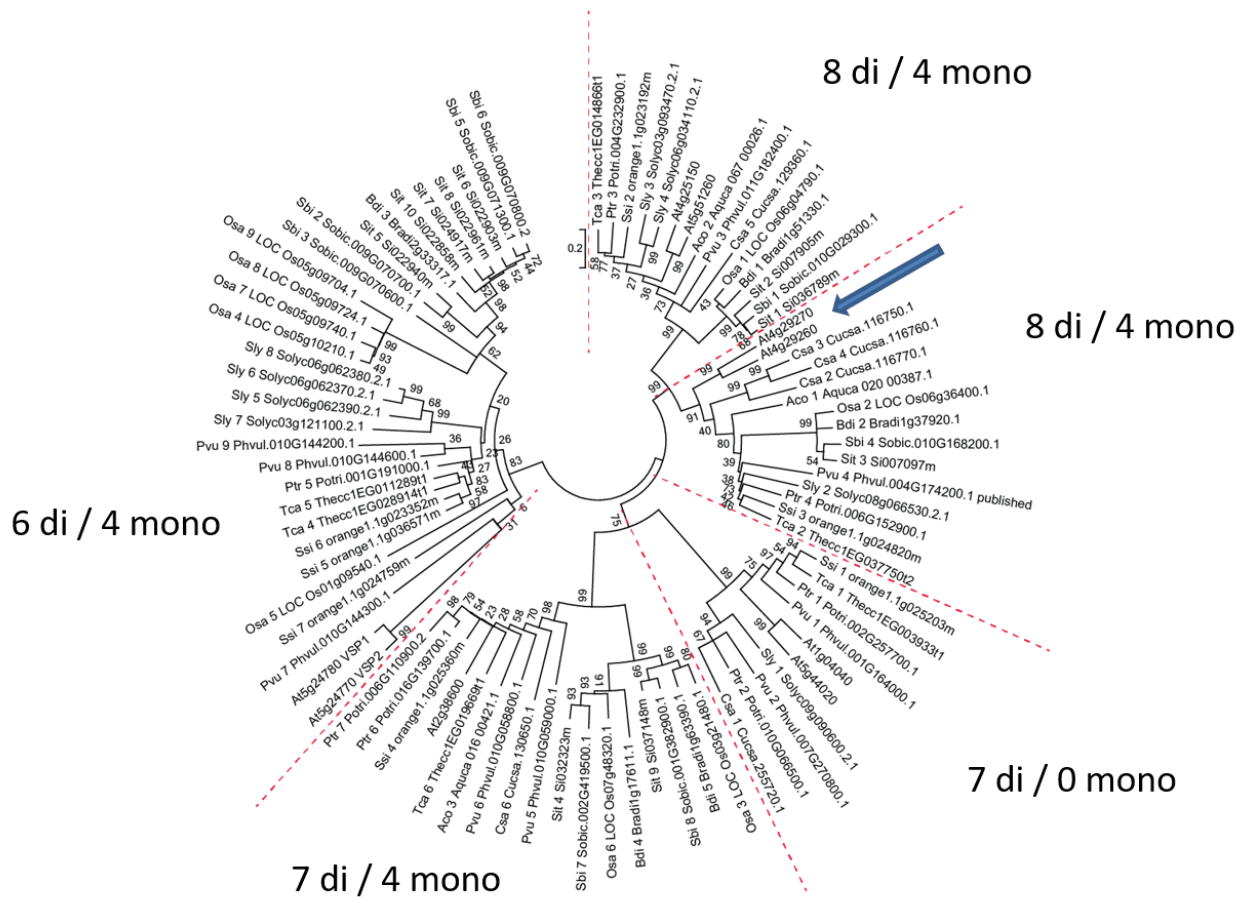
Figure 7. Molecular phylogenetic analysis of plant HADIIIB phosphatases. The phylogenetic tree was constructed by the maximum likely-hood method using MEGA6. Branch lengths represent the number of substitutions per site. The tree can be divided into five clades. Each clade contains one or two proteins from the Arabidopsis HADIIIB family. The species are as following *Arabidopsis thaliana* (At, mouse-ear cress), *Phaseolus vulgaris* (Pvu, common bean), *Solanum lycopersicum* (Sly, tomato), *Cucumis sativus* (Csa, cucumber), *Theobroma cacao* (Tca, cocoa beans), *Populus trichocarpa* (Ptr, poplar), *Citrus sinensis* (Csi, orange), *Aquilegia caerulea* (Aco, Colorado blue columbine flower), *Oryza sativa* (Osa, rice), *Sorghum bicolor* (Sbi, millet), *Setaria italica* (Sit, foxtail millet), and *Brachypodium distachyon* (Bdi, stiff brome grass). The orthologous protein of Arabidopsis to PvNTD1 of Phaseolus vulgaris is indicated with a blue arrow.

In the phylogenetic tree (Figure 7), five main branches can be discerned, containing sequences from different species. Possibly, enzymes within the same branch from different species have ortholgous functions in the respective organisms. Only in two clades enzymes from all investigated plant species are present. Therefore, these contain the most promising candidates. This is the clade containing the Arabidopsis enzymes encoded at the loci At4g25150 and At5g51260 and the clade

containing the candidates encoded at At4g29260 and At4g29270. As mentioned above, the HADIIIB enzyme encoded by At4g29260 has been found in the vacuole (Carter et al., 2004) and the bean ortholog has 5'-NMP activity (Cabello-Díaz et al., 2015). The clade comprising the Arabidopsis enzymes encoded at At1g04040 and At5g44020 lacks enzymes from monocotelydons and from the dicot *Aquilegia caerulea* (colorado blue columbine flower). The clade containing the enzyme encoded at At2g38600 contains proteins from all investigated plant except for *Solanum Lycopersicum* (tomato). The last clade contains two VSPs, encoded at At5g24780 (VSP1) and At5g24770 (VSP2), which are not present in two of the investigated dicotyledons. The VSP enzymes did not show any significant activity with 5'- or 3'-NMPs (Chen et al., 2012). One protein with similarity to HADIIIB enzymes encoded at At2g39920 was not included in the phylogenetic analysis because it lacked sequence regions conserved in this protein family and also did not have a signal peptide (Liu et al., 2005). Nonetheless, the protein from locus At2g39920 contains the DXDXT motif generally conserved in in most APs from other eukaryotes and bacteria (Collet et al., 1999; Thaller et al., 1998a) (Figure 8).
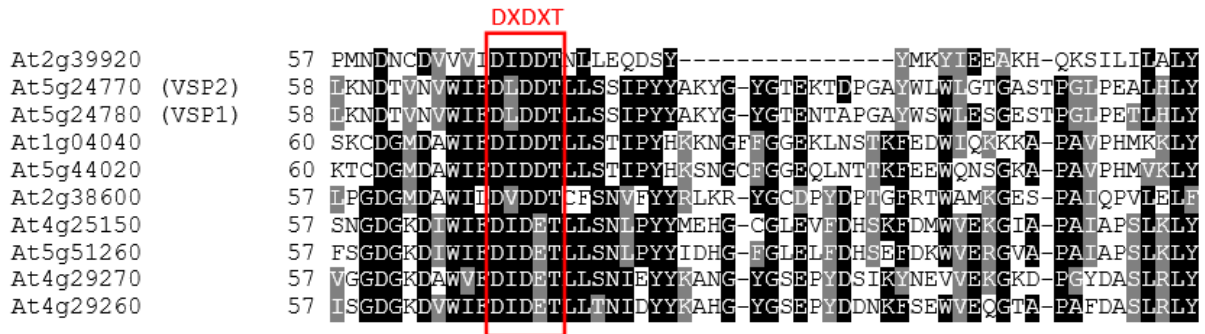
Figure 8. DXDXT motif in the HADIIIB protein family. Section of an amino acid alignment of the ten members of the HADIIIB gene family. The conserved DXDXT motif is highlighted with a rectangle. The first Asp in the motif is essential for phosphatase activity.

3.1.2. Purple acid phosphatase (PAP) family

PAP26 is a member of the PAP gene family and was included in this study because it was known to be involved in phosphate remobilization. Loss of function of PAP26 in Arabidopsis leads to significant effects in the form of delayed leaf senescence and impaired phosphate remobilization that cannot be compensated by other PAPs. PAP26 is upregulated by phosphate starvation and during leaf senescence (Robinson et al., 2012). It has not yet been demonstrated that PAP26 resides in the vacuole but PAP26 has been found in lytic vacuoles of the Arabidopsis leaves (Hurley et al., 2010). Nonetheless, some lines of evidence suggests that PAP26 is localized in central vacuoles: (i) PAP26 was found in the intact vacuoles of Arabidopsis during the proteome analysis of cells in suspension culture (Shimaoka et al., 2004), (ii) the presence of a 30-amino acid signal peptide at the N terminus suggests that PAP26 is associated with vacuoles and the secretory pathway (Vasko et al., 2006), and (iii) the optimum acidic pH of PAP26 activity is consistent with a role in vacuoles. Several of the plant APs, including those of *Brassica nigra,* are present in vacuoles (Duff et al., 1991). Based on this data, PAP26 was considered a potential candidate for the sought vacuolar NMP activity. Since there are 29 *PAP* genes in the Arabidopsis genome, it appears possible that also other PAPs are potentially involved in nucleotide degradation in the vacuole. Similarity to PAP26, evolutionary conservation, and ubiquitous expression are possible parameters to select other PAP candidates.
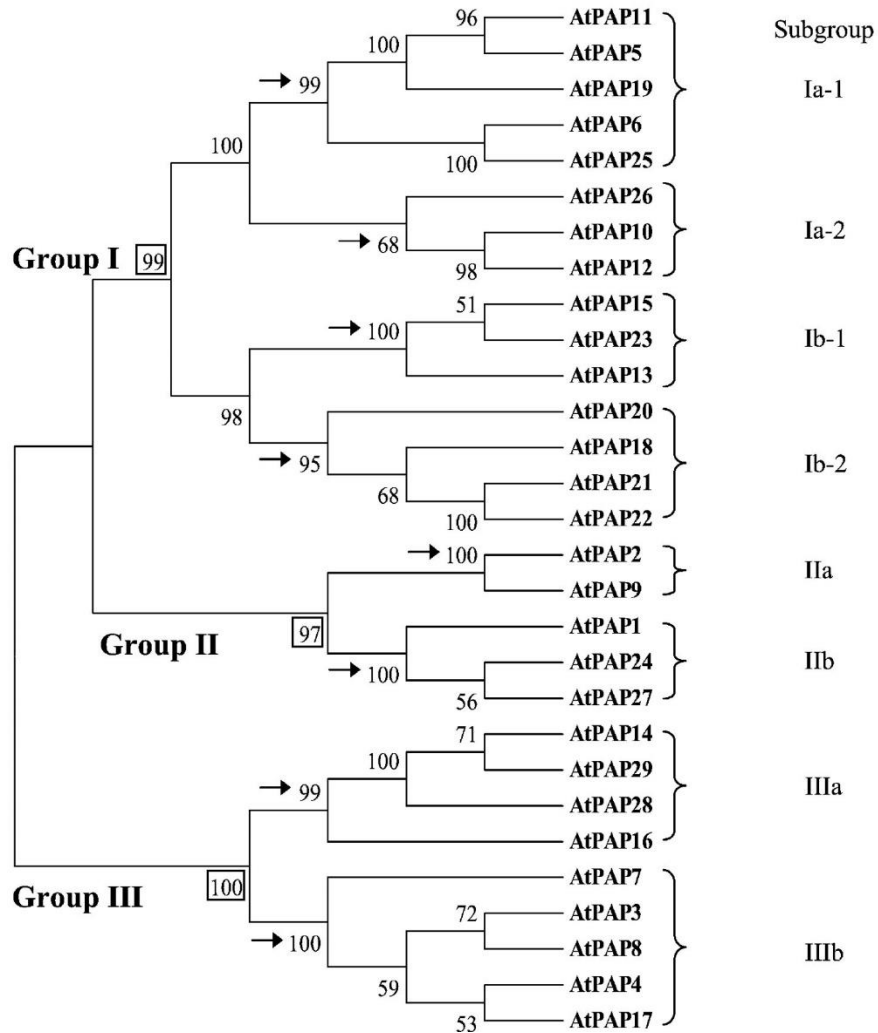
Figure 9. Phylogenetic analysis of Arabidopsis thaliana PAP enzymes. PAP26 is present in clade Ia-2 together with PAP10 and PAP12. The phylogenetic tree was reproduced from Li et al., 2002.

PAPs from Arabidopsis were categorized using phylogenetic analysis methods by (Li et al., 2002) (Figure 9). Three main groups (I, II, and III) were found which were separated with high confidence (95% bootstrap values). PAP26, PAP10 and PAP12 are present in the same clade indicating that these three enzymes are similar in sequence and might have similar function.

Since only well conserved enzymes present in all plant species are considered to be the good candidates for the desired vacuolar mononucleotide phosphatases, the conservation PAPs is a candidate selection criterion. Yin and colleges have conducted a phylogenetic study including PAPs from five dicotyledon and two monocotyledon species. The dicotyledons included *Arabidopsis thaliana* (mouse-ear cress), *Camellia sinensis* (tea), *Glycine max* (soybean), *Cicer*

arietinum (chickpea), and *Jatropha curcas* (physic nut). The monocotyledons included *Oryza sativa* (rice), and *Zea mays* (maize).

822
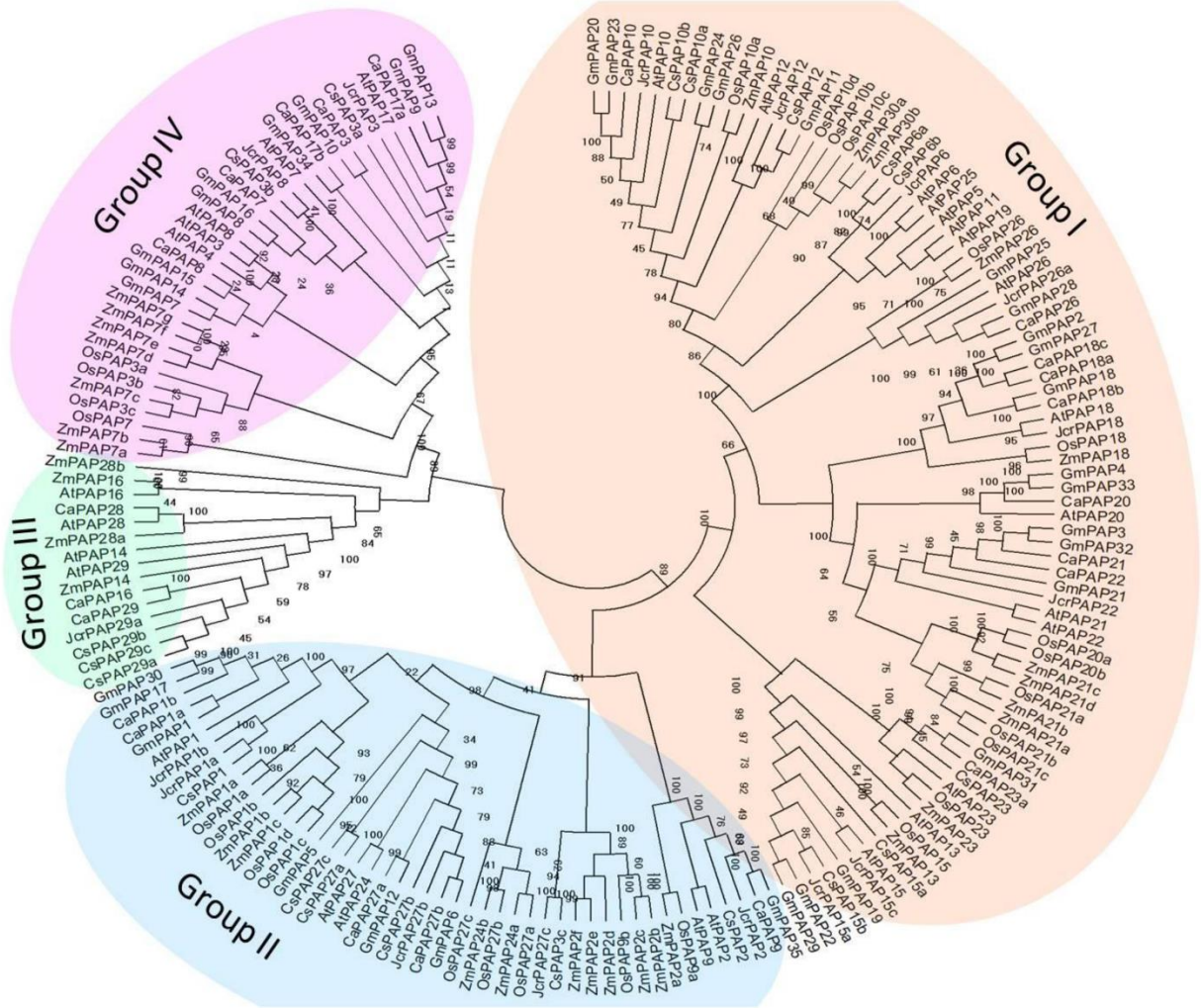
Figure 10. Molecular phylogenetic analysis of plant purple acid phosphatases. The amino acid sequences of PAPs from different plant species were used to construct the phylogenetic tree. The tree was constructed according to the neighbor-joining method and five different monocotyledons and two dicotyledons were analyzed. The dicotyledons included *Arabidopsis thaliana* (At), *Camellia sinensis* (Cs), *Glycine max* (Gm), *Cicer arietinum* (Ca), and *Jatropha curcas* (Jcr). The monocotyledons included *Oryza sativa* (Os), and *Zea mays* (Zm). The phylogenetic was reproduced from Yin et al., 2019.

In the phylogenetic analysis comprising 29 AtPAPs, 19 CsPAPs, 26 OsPAPs, 33 ZmPAPs, 25 CaPAPs, 35 GmPAPs, and 18 JcrPAPs four major clades (groups I-IV) can be discerned. PAP10 is conserved in all seven plant species, PAP26 is present in all plant species except the *Camellia sinensis* (tea) whereas PAP12 is confined only to the dicotyledons with the exception of *Cicer arietinum*. The lack of PAP26 in tea might be explained with a possible incomplete annotation or missing sequence in the tea genome, which was sequenced relatively recently. Regarding the other PAPs, PAP1 is present in all analyzed plant species while PAP2, PAP3, PAP7, PAP8, PAP18, PAP21, PAP23, PAP27, PAP28, and PAP29 are all well conserved enzymes but are apparently missing in one or two plant species (Yin et al., 2019). The other PAPs are less well conserved.

The expression of the 29 PAP genes was used as an additional criterion to select possible candidates. An ubiquitous expression pattern would be expected for the general vacuolar NMPs. The Klepikova Atlas in the Arabidopsis eFP Browser (http://bar.utoronto.ca/efp/cgi-bin/efpWeb.cgi?dataSource=Klepikova_Atlas) is a web tool that was used to obtain transcriptional data. The Klepikova Atlas is based on RNA-seq data obtained from the Arabidopsis developmental transcriptome (Klepikova et al., 2016). The authors extracted the total RNA from different developmental tissues and generated cDNA libraries. The cDNA libraries were then sequenced with a read length of 50 bp and aligned against TAIR10 (Lamesch et al., 2012) using Tophat, a sequencing method for mRNA (Trapnell et al., 2009), and reads per gene were counted with default Tophat parameters. The transcript expression profiles and levels for all 29 *PAPs* are summarized in Appendix A 1.

Using (i) conservation to PAP26, (ii) evolutionary conservation and (iii) transcriptional profiles as selection critera, 12 PAPs in addition to PAP26 were selected as candidates. The criteria were not always applied stringently, that means that even if only two of the three criteria matched the candidate profile, in some cases the corresponding PAP was still maintained in the candidate list. For example, PAP12 was in the list despite being only conserved in the dicotyledons. The reason was that PAP12 is most similar to PAP26 on sequence basis. The final candidate list comprised PAP1, PAP2, PAP3, PAP4, PAP7, PAP8, PAP10, PAP12, PAP17, PAP18, PAP26, PAP27, and PAP28.

3.1.3. S1/P1-type endonucleases

The S1/P1-type endonucleases belong to the essential nucleases for the degradation of genomic material in cells. The Arabidopsis genome codes for five S1/P1-type endonucleases called Endo1 to Endo5 (Triques et al., 2007), which are similar in catalytic activity to the well-characterized P1 and S1 nucleases from *Penicillium citrinum* and *Aspergillus oryzae*, respectively. These bifunctional enzymes mainly degrade single-stranded DNA (ssDNA) and RNA but can also function as 3'-NMP nucleotidases (Fujimoto et al., 1974; Hanson and Fairley, 1969). Amino acid analysis of the S1/P1-type endonuclease family indicates the presence of a signal peptide at the N-terminus of each member. A phylogentic analysis of the Arabidopsis S1/P1-type endonuclease family together with the nucleases from *Penicillium citrinum* and *Aspergillus oryzae* indicated that the fungal enzymes are present in one clade, Endo 3, 4, and 5 are present in one clade (*Endo4* is considered as a pseudogene because the mRNA transcript could not be detected for this gene) , and Endo 1 and 2 are present in two independent clades. Endo 3 to 5 are most similar to each other with sequence similarities of more than 74% (Triques et al., 2007). Since there were only five S1-type endonuclease present in the Arabidopsis genome, all of them were included in the second screening step investigating their subcellular localization.

3.1.4. Overview of the selected candidates

At the end of the first candidate selection stage, seven members of the HADIIIB family (At1g04040, At2g38600, At4g29260, At4g29270, At2g25150, At5g44020, and At5g51260) were selected based on the presence of a signal peptide and the conservation of the enzymes in other plant species. VSP1, VSP2, and At2g39920 were not included because the first two did not have acid phosphates activity (Chen et al., 2012; Liu et al., 2005) while later did not contain a signal peptide (Liu et al., 2005). After the first screen, working titles were assigned to the HADIIIB family members based on the phylogenetic studies. The enzymes encoded at the loci At4g25150 and At5g51260 present in the first clade were named HADIIIB1 (At4g25150) and HADIIIB2 (At5g51260). The enzymes encoded at the loci At4g29270 and At4g29260 present in the clade number two were named HADIIIB3 (At4g29270) and HADIIB4 (At4g29260). Similarly, the names HADIIIB5 (At1g04040), HADIIIB6 (At5g44020), and HADIIIB7 (At2g38600) were assigned.

For the PAP family, 12 members were included. Since the Arabidopsis genome encodes for 29 PAP proteins several selection criteria were applied as outlined in Section 3.1.2 without being too dogmatic to avoid that important enzymes from this family might be missed. Only evolutionary well conserved, ubiquitously expressed enzymes or enzymes with strong sequence similarity to PAP26 were selected. The list includes PAP1, PAP2, PAP3, PAP4, PAP8, PAP10, PAP12, PAP17, PAP18, PAP26, PAP27, and PAP28.

For the S1/P1-type endonucleases all five members were included.

3.2. Subcellular localization studies

Plant cells contain many compartments that exhibit structural and functional differences. Subcellular localization of the candidate proteins was essential to understand where they exhibit their function. Whereas phylogenetic conservation and expression profile are softer criteria for selecting possible vacuolar 3'-nucleotidase enzymes, the presence in the vacuole is a hard criterion which must be fulfilled.

The tonoplast contains two proton pumps that produce an acidic pH in the vacuolar lumen (Figure 2). Most fluorescent proteins do not fluoresce in this acidic environment probably because they are partially unfolded or degraded. To investigate the subcellular localization in vacuoles using fluorescent protein tagging, it is necessary to ensure that the fluorescence will be visible in the vacuolar lumen. It has been shown that this is possible when plants are kept in the dark for two days, because then the vacuolar lumen is not as acidic, and vacuolar fluorescent proteins become detectable (Tamura et al., 2003). For these experiments, a construct expressing a vacuolar lumen marker was generated (see section 2.2.1.5) which was co-expressed with constructs for the candidate proteins.

3.2.1. Subcellular localization of the HADIIIB acid phosphatases

Confocal microscopy was performed on transiently transformed *Nicotiana benthamiana* leaves expressing C-terminal yellow fluorescent protein (YFP)-tagged candidate proteins of the HADIIIB family of acid phosphatases (Figure 11, upper panel) to assess if these are located in the vacuole. All candidate genes were cloned as described in the Materials and Methods section 2.2.1.4 and transiently expressed along with lumen marker constructs. A C-terminal tag position was chosen because at the N-terminus of the HADIIIB protein family members the signal peptide for targeting

to the secretory pathway is located. To generate a lumen marker, a construct encoding the mCherry fluorescent protein N-terminally tagged with a signal peptide (SP), and C-terminally tagged with a vacuolar targeting signal (VTS) was made (Mitsuhashi et al., 2000). The SP directs the mCherry protein into the secretory pathway, whereas the VTS directs it into the vacuolar lumen (Figure 11, lower panel).

N-terminus	Candidate protein	YFP-Tag	C-terminus

N-terminus	SP	mCherry	VTS	C-terminus
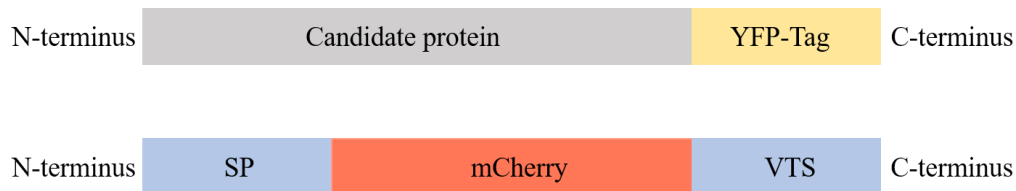
Figure 11. Schematic diagram of the candidate proteins C-terminally fused with YFP and of a vacuolar lumen marker. SP, signal peptide; VTS, vacuolar targeting sequence.

Infiltrated plants were treated in two ways: (i) plants were kept in under long-day conditions for four days (16 hours light, 8 hours dark) and served as light control, (ii) plants were kept in the light for two days (16 hours light, 8 hours dark) followed by a prolonged night of 40 h. The prolonged night ensured that the vacuolar lumen environment was less acidic, stabilizing the fluorescence of the tagged proteins. The fluorescence signal was recorded from the lower epidermal cells of the infiltrated leaf using a confocal microscope.

In the light, none of the HADIIIB enzymes showed a clear localization in the vacuolar lumen but rather in speckles close to the cell periphery and surrounding the nucleus. Also the mCherry lumen marker was confined to the cell periphery (Figure 12). By contrast, the marker labelled the lumen when the plants had been exposed to prolonged darkness of 40 hours, which also led to yellow fluorescence in the vacuolar lumen for several HADIIIB-YFP fusion proteins (Figure 13). Namely, the enzymes HADIIIB2, HADIIIB3, HADIIIB4 and HADIIIB6 were located in the vacuolar lumen under these conditions.
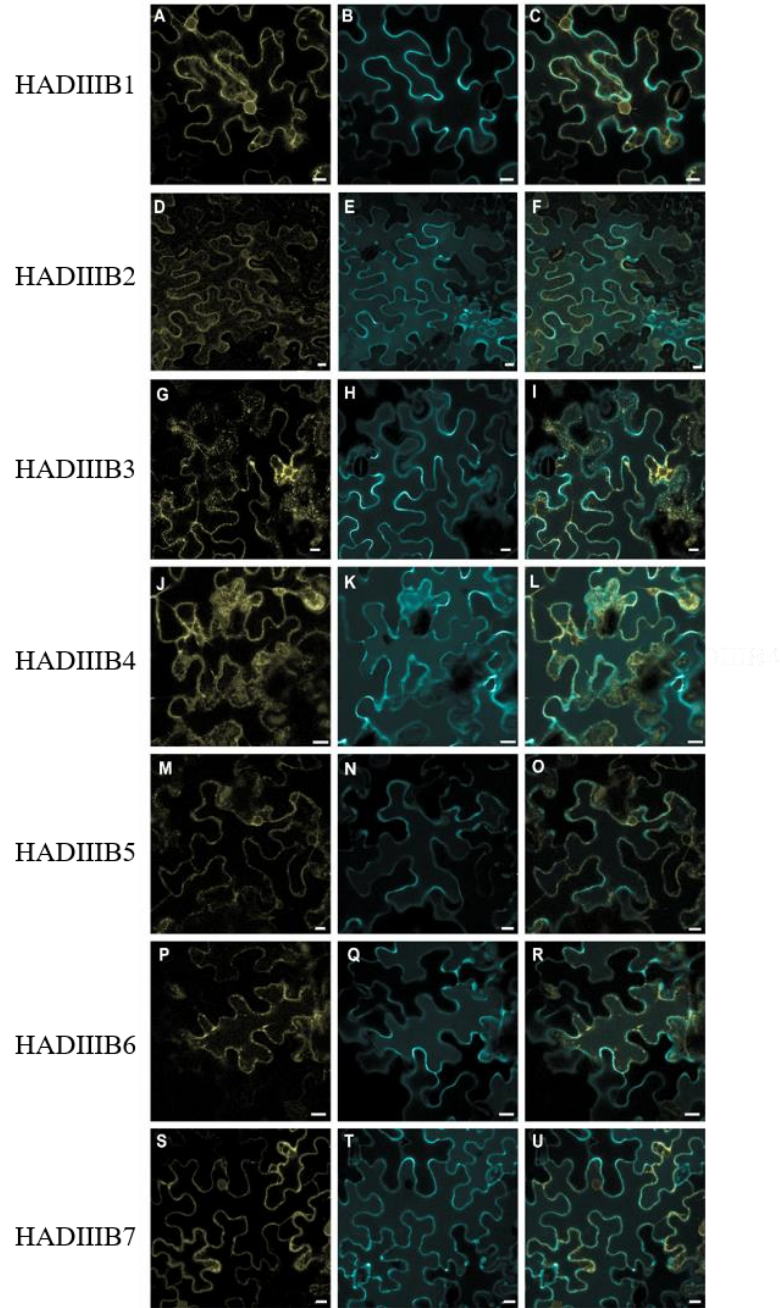
Figure 12. Subcellular localization of the transiently expressed HADIIIB family members in leaves of *N. benthamiana* harvested during the day from long-day grown plants. First row, YFP signal from the HADIIIB-YFP fusion proteins; second row, mCherry signal from the vacuolar marker; third row, overlay of first and second row. A, B, C: HADIIIB1 (At4g25150); D, E, F: HADIIIB2 (At5g51260); G, H, I: HADIIIB3 (At4g29270); J, K, L: HADIIIB4 (At4g29260); M, N, O: HADIIIB5 (At1g04040); P, Q, R: HADIIIB6 (At5g44020); S, T, U: HADIIIB7 (At2g38600). The *N.benthamiana* plants were co-infiltrated with agrobacteria containing the lumen marker construct and the respective candidate gene construct. Four days after the infiltration, leaf discs were inspected under the confocal microscope. The excitation and emission wavelengths for the florescent proteins are provided in Table 23. Scale bars, 10 µm.

Figure 13. Subcellular localization of the transiently expressed HADIIIB family members in leaves of *N. benthamiana* harvested after a prolonged night of 40 h from plants that before had been grown under long-day conditions. First row, YFP signal from the HADIIIB-YFP fusion proteins; second row, mCherry signal from the vacuolar marker; third row, overlay of first and second row. A, B, C: HADIIIB1 (At4g25150); D, E, F: HADIIIB2 (At5g51260); G, H, I: HADIIIB3 (At4g29270); J, K, L: HADIIIB4 (At4g29260); M, N, O: HADIIIB5 (At1g04040); P, Q, R: HADIIIB6 (At5g44020); S, T, U: HADIIIB7 (At2g38600). The *N. benthamiana* plants were co-infiltrated with agrobacteria containing the lumen marker construct and the respective candidate gene construct. Four days after the infiltration a prolonged night of 40 h was given, leaf discs were

inspected under the confocal microscope. The excitation and emission wavelengths for the florescent proteins are provided in Table 23. Scale bars, 10 µm.
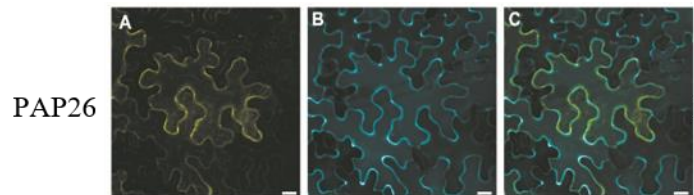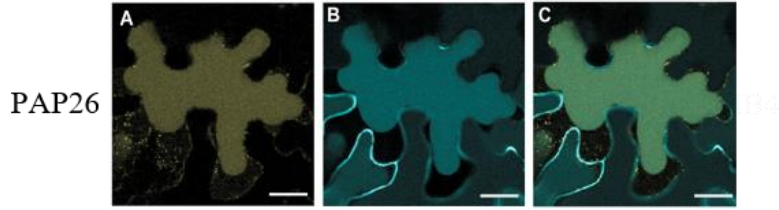
3.2.2. Subcellular localization of the Purple acid phosphatases

For the twelve PAP candidates selected by phylogenetic and transcript profile analysis, cDNAs were cloned. Constructs encoding C-terminally YFP-tagged variants were prepared and transiently expressed in *Nicotiana benthamiana*. In contrast to the strong fluorescence signals obtained during the analysis of the HADIIIB-YFP fusion proteins (Figures 12 and 13), most of the PAP-YFP proteins showed weak or no fluorescence (not shown). This was independent of the light regime. However, an exception was PAP26-YFP, which was detected in the vacuolar lumen when plants were exposed to a prolonged night of 40 hours but not when plants were grown in a day-night regime (Figures 14 and 15).

In a BSc study conducted by Patrick Kaland in our laboratory, an improved vector system was developed and tested for the localization of the PAPs (Kaland, 2021). Using this system, it could be shown that also PAP8 is located in the vacuolar lumen. However, this enzyme could not be tested further in this work due to the lack of time. Nonetheless, this finding shows that also other PAPs might be located in the vacuole.

Figure 14. Subcellular localization of transiently expressed PAP26-YFP in leaves of *N. benthamiana* harvested during the day from long-day grown plants. A, YFP signal from the PAP26-YFP fusion protein (At5g34850); B, mCherry signal from the vacuolar marker; C, overlay of A and B. The *N.benthamiana* plants were co-infiltrated with agrobacteria containing the lumen marker construct and the respective candidate gene construct. Four days after the infiltration leaf discs were inspected under the confocal microscope. The excitation and emission wavelengths for the florescent proteins are provided in Table 23. Scale bars, 10 µm.
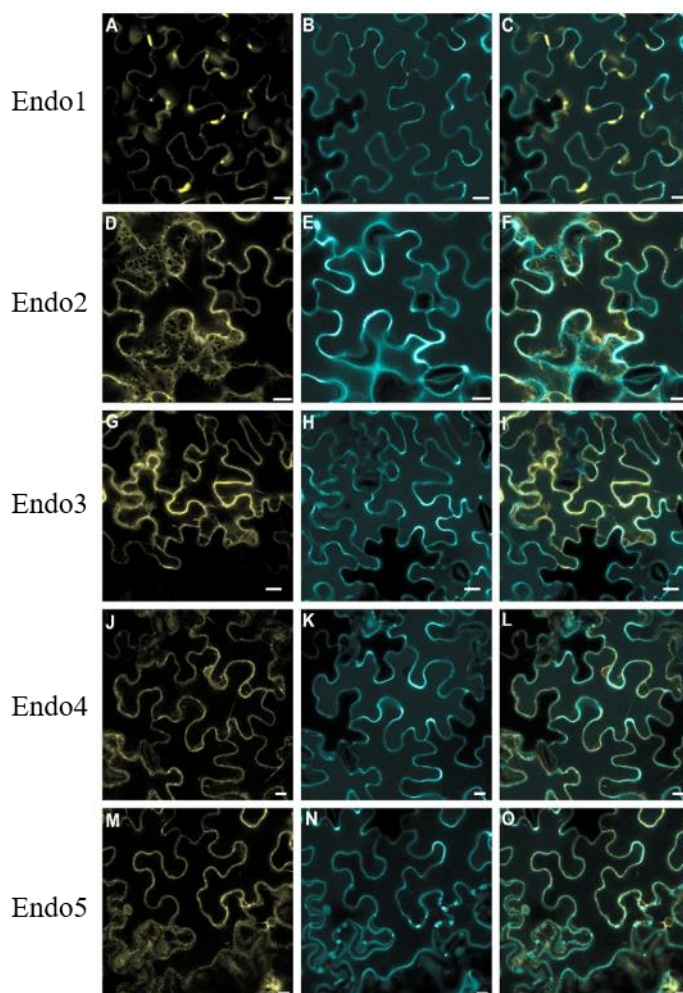
Figure 15. Subcellular localization of transiently expressed PAP26-YFP in leaves of *N. benthamiana* harvested after a prolonged night of 40 h from plants that before had been grown under long-day conditions. A, YFP signal from the PAP26-YFP fusion protein (At5g34850); B, mCherry signal from the vacuolar marker; C, overlay of first and second row. The *N.benthamiana* plants were co-infiltrated with agrobacteria containing the lumen marker construct and the respective candidate gene construct. Four days after the infiltration a prolonged night of 40 h was given, leaf discs were inspected under the confocal microscope. The excitation and emission wavelengths for the florescent proteins are provided in Table 23. Scale bars, 10 µm.

3.2.3. Subcellular localization of the S1/P1-type endonucleases

The primary function for the S1 endonucleases is to degrade single-stranded nucleic acids and release 5'-phosphoryl mono- or oligonucleotides. Nonetheless, they can also act as 3'-nucleotide monophosphatases (Fujimoto et al., 1974; Hanson and Fairley, 1969). Additionally, the S1 endonucleases are known to contain an N-terminal signal peptide for targeting to the secretory pathway and are therefore potentially also imported into the vacuole (Lesniewicz et al., 2013; Triques et al., 2007). For these reasons the five Arabidopsis S1 endonucleases, Endo1 to Endo5, were also included in the screening process for vacuolar targeting.

Similar to the results for the HADIIIB enzymes, none of the Endo-YFP fusion proteins was found in the vacuolar lumen when the plants were grown in a long-day regime (Figure 16). However, when the plants were placed into darkness of 40 h, Endo5 but none of the other Endos was located in the vacuolar lumen (Figure 17). Therefore only Endo5 was considered further.

Figure 16. Subcellular localization of the transiently expressed S1/P1-types endonuclease family members in leaves of *N. benthamiana* harvested during the day from long-day grown plants. First row, YFP signal from the Endo-YFP fusion proteins; second row, mCherry signal from the vacuolar marker; third row, overlay of first and second row. A, B, C: Endo1 (At1g11190); D, E, F: Endo2 (At1g68290); G, H, I: Endo3 (At4g21590); J, K, L: Endo4 (At4g21585); M, N, O: Endo5 (At4g21600). The *N. benthamiana* plants were co-infiltrated with agrobacteria containing the lumen marker construct and the respective candidate gene construct. Four days after the infiltration, leaf discs were inspected under the confocal microscope. The excitation and emission wavelengths for the florescent proteins are provided in Table 23. Scale bars, 10 µm.

Figure 17. Subcellular localization of the transiently expressed S1/P1-types endonuclease family members in leaves of *N. benthamiana* harvested after a prolonged night of 40 h from plants that before had been grown under long-day conditions. First row, YFP signal from the Endo-YFP fusion proteins; second row, mCherry signal from the vacuolar marker; third row, overlay of first and second row. A, B, C: Endo1 (At1g11190); D, E, F: Endo2 (At1g68290); G, H, I: Endo3 (At4g21590); J, K, L: Endo4 (At4g21585); M, N, O: Endo5 (At4g21600). The *N. benthamiana* plants were co-infiltrated with agrobacteria containing the lumen marker construct and the respective candidate gene construct. Four days after the infiltration, leaf discs were inspected under the confocal microscope. The excitation and emission energy for the florescent protein is provide in theTable 23. Scale bar = 10 µm.

3.2.4. Overview of the selected candidates

At the end of this stage four members of the HADIIIB family, HADIIIB2 (At5g51260), HADIIIB3 (At4g29270), HADIIIB4 (At4g29260), and HADIIIB6 (At5g44020), one member of PAP family, PAP26 (At5g34850), and one member from S1/P1-type endonucleases, Endo5 (At4g21600), were selected based on subcellular localization in the vacuole. HADIIIB1 (At4g25150) was not located in the vacuole but it was continued to the next stage of the selection because it is phylogenetically related to HADIIIB2 (Figure 7).

3.3. Biochemical studies of the candidates

Mainly for those candidate enzymes which were found in the vacuolar lumen enzymatic activity and substrates specificity analyses were performed to potentially identify 3'-NMP nucleotidases. All candidate genes were cloned as described in the Materials and Methods section 2.2.1.4. The candidates were expressed as fusion proteins tagged C-terminally with the eight amino acid Strep tag (Figure 18). A C-terminal tag position was chosen because the N-terminus of the candidates comprises a signal peptide for targeting to the secretory pathway. Expression constructs were prepared for HADIIIB1, HADIIIB2, HADIIIB3, HADIIIB4, HADIIIB6, Endo5 and PAP26 (Table 8).


Figure 18. Schematic diagram of the candidate proteins C-terminally fused with StrepII tag.

3.3.1. Phosphatase assays

For the phosphatase activity measurements, purified proteins were tested with different substrates, and samples were taken in time courses. Phosphate was detected colorimetically with a malachite green method. Upon the presence of P_i the assay produces a green colour that is linearly proportional to the P_i concentration. The linearity and detection limit of the P_i assay method were validated using different phosphate standards yielding concentrations of 0, 20, 40, 100, 200, and 400 μM of KH_2PO_4 in the sample (Figure 19).

For each enzyme, the same respective purification batch was used for the substrate studies. Eight mononucleotides were selected for an initial substrate scan. These included purines and pyrimidines with 3' and 5' phosphate moieties which can be dephosphorylated to nucleosides if a phosphatase with the respective activity is present (Figure 20). The substrate survey studies were performed at a final concentration of 1mM of the substrates and pH 6.8 (Bis-Tris buffer). The enzyme activity was calculated in μmol of the product formed per minute per mg of the purified enzyme ($\mu mol\ min^{-1}\ mg^{-1}$). The phosphatase activity tests were performed in triplicates using the same enzyme preparation for all substrates and for the repeats.
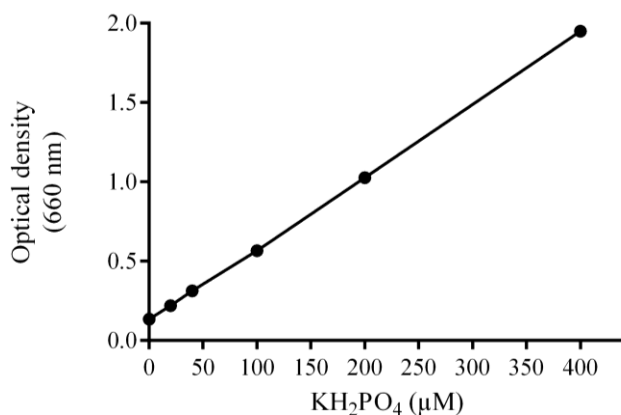
Figure 19. The linearity and detection limit of the malachite green assay. Different concentrations (0, 20, 40, 100, 200, and 400 μM) of the KH_2PO_4 were used to investigate the detection limit and linearity of the malachite green assay. The phosphate standards were first mixed with reaction buffer (Table 19) in a 96 well plate and later the malachite green solution was added. The KH_2PO_4 concentrations reflect the final Pi concentrations in the sample that was then treated with the malachite green solution. After ten minutes, the absorption at 660 nm was measured using a plate photometer.
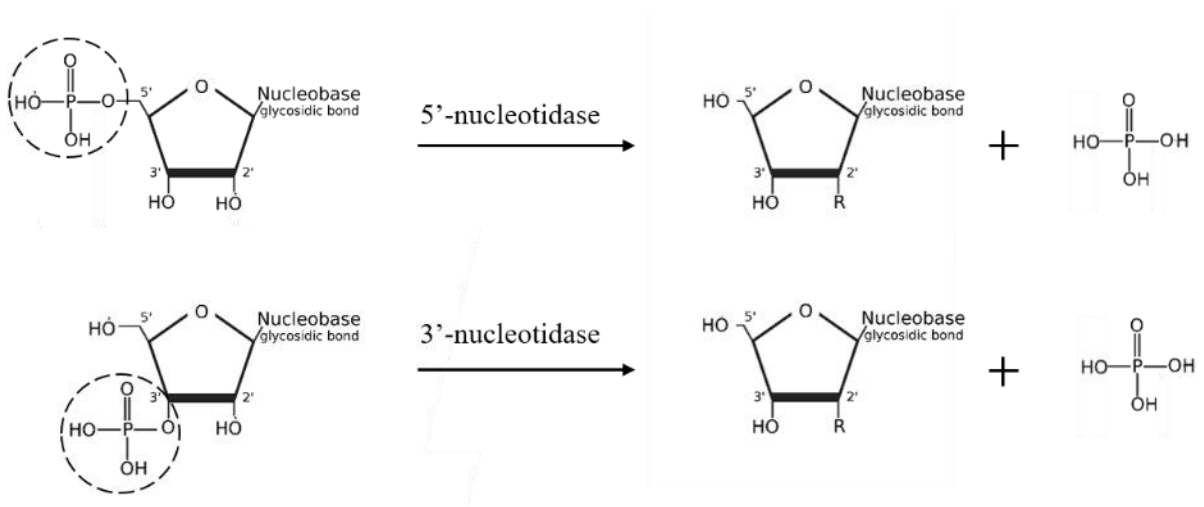
Figure 20. Dephosphorylation of the 5'-NMPs and 3'-NMPs to nucleosides. During the dephosphorylation step, the phosphate moiety present on carbon number five or three on the ribose is hydrolyzed. The free phosphate in the solution is quantified using a malachite green assay.

Table 30. Substrate specificity analysis to identify potential 3'-NMP nucleotidases [1]

	HADIIIB1	HADIIIB2	HADIIIB3	HADIIIB4	HADIIIB6	PAP26	Endo5
5'-GMP	36.1 ± 5.3	3.5 ± 0.8	12.6 ± 2.1	49.6 ± 9.2	0.2	3.2 ± 0.8	nd
5'-CMP	35.8 ± 7.4	9.2 ± 0.3	9.9 ± 0.2	15.9 ± 3.3	0.1	2.8 ± 1.1	2.4 ± 0.5
5'-AMP	8.6 ± 1.0	0.7 ± 0.0	22 ± 1.9	40.7 ± 9.3	0.1	3.5 ± 0.9	1.3
5'-UMP	43.8 ± 7.7	9.9 ± 2.2	29.8 ± 2.5	37.3 ± 6.7	0.2	1.6 ± 2.8	2.4 ± 0.3
3'-GMP	16.2 ± 4.3	1.2 ± 0.5	nd	3.3 ± 0.6	nd	16.2 ± 2.8	478 ± 5
3'-CMP	0.9 ± 0.7	0.1 ± 0.0	nd	0.4 ± 0.5	0.1	26.8 ± 7.4	0.7 ± 0.2
3'-AMP	23.2 ± 1.5	7.3 ± 1.9	7.4 ± 0.3	32.3 ± 7	0.1	16.6 ± 2.0	563 ± 5
3'-UMP	0.8 ± 0.0	0.8 ± 0.1	nd	0.6 ± 0.7	0.1	22.1 ± 3.4	134 ± 4

[1] the mean is given and units are µmol min^{-1} mg^{-1}; errors are SD , n = 3, not detected (nd)

The phosphatase activity survey showed that PAP26 exhibits stronger phosphatase activity for the 3'-NMPs as compared to the 5'-variants. PAP26 is known to have a broad spectrum phosphatase activity (Veljanovski et al., 2006) but this enzyme has not been tested with 3'-NMPs so far. HADIIIB4 (At4g29260) exhibited phosphatase activity with all 5'-NMPs offered while from the 3'-NMPs only 3'-AMP and was a good substrate. A similar activity pattern was observed for HADIIIB3 (At4g29270) but generally the activity was weaker than for HADIIIB4, for example with 3'-AMP it was 3.5 fold lower. These enzymes are encoded next to each other in the Arabidopsis genome and are phylogenetically closely related (Figure 7). Both are present in the vacuole (Figure 13).

HADIIIB1, encoded at At4g25150, and HADIIIB2, encoded at At5g51260, were also included in the substrate scan. Although HADIIIB1 was not located in the vacuole it was tested for phosphatase activity because it is phylogenetically related to HADIIIB2 (Figure 7), which was found in the vacuole (Figure 13). For HADIIIB1, all 5'-NMPs and the purine 3'-NMPs (3'-AMP and 3'-GMP) were good substrates. A similar pattern was observed for HADIIIB2 but the activity was generally weaker and 3'-GMP was not a good substrate.

HADIIIB6, encoded at At5g44020, did not show activity with any of the substrates offered. It was therefore excluded from further experiments. Other non-vacuolar enzymes from the HADIIIB family, HADIIIB5 and HADIIIB7, were also tested for the phosphatase activity but did not show activity with any of the eight substrates offered. By contrast, Endo5 exhibited a particularly strong 3'-NMP phosphatase activity except for 3'-CMP.

3.3.2. Overview of the selected candidates

At the end of this stage four members of the HADIIIB family, HADIIIB2 (At5g51260), HADIIIB3 (At4g29270), HADIIIB4 (At4g29260), one member from S1/P1-type endonucleases, Endo5 (At4g21600), and one member of PAP family, PAP26 (At5g34850) were selected based on subcellular localization in the vacuole and substrate prefrences. HADIIIB1 (At4g25150) was not located in the vacuole but it was continued to the next stage of the selection because it is phylogenetically related to HADIIIB2 (Figure 7) and exhibited a similar enzymatic preference (Table 30).

3.4. Generation of double and triple mutants of the potential candidates

The substrate scan allowed to exclude HADIIIB6 (At5g44020) from the candidate list although the enzyme is located in the vacuole, because it lacked NMP phosphatase activity. For the remaining enzymes their respective gene expression patterns were analyzed.

3.4.1. Expression patterns of the candidate genes with NMP phosphatase activity

A general vacuolar NMP phosphatase involved in housekeeping NMP turnover is expected to be ubiquitously expressed. Using publically available expression data, the expression profiles of the genes encoding the phosphatases with NMP dephosphorylating activity were analysed. The respective detailed data is presented in Appendix A. *HADIIIB2*, *HADIIIB4*, and *PAP26* have ubiquitous expression patterns and are therefore the most promising candidates for the sought function. *HADIIIB3*, which is closely related to *HADIIIB4*, is expressed during germination and most strongly in roots but only weakly in young leaves and not at all in older leaves. *Endo5* is expressed during germination and in the root but not in leaves. Both can therefore be excluded from the candidate list - at least in mature leaf tissue. *HADIIIB2* shows a broad expression pattern although at a slightly lower level than other candidates. It is strongly expressed particularly in the flower stigma.

HADIIIB1 and HADIIIB2 are phylogenetically related (Figure 7) but HADIIIB1 does not reside in the vacuole (Figure 13) and is expressed mainly in pollen (Appendix A 2). It can therefore be dismissed from the candidate list.

In summary, *HADIIIB2*, *HADIIIB4*, and *PAP26* appeared to be the most promising candidate genes. Therefore these were the primary targets in the search for corresponding mutants. However, the non-vacuolar pollen-specific enzyme HADIIIB1 was also included in the search for corresponding mutants because it is an NMP phosphatase (Table 30) and is a close relative to the vacuolar enzyme HADIIIB2 (Figure 7). Similarly, also HADIIIB3 was included because it is a vacuolar NMP phosphatase (Table 30), but with a more tissue specific expression profile (Appendix A 2).

3.4.2. Preparation of the mutant combinations

To investigate the biochemical functions *in vivo*, single, double, and triple mutant combinations were created. For the single mutants Arabidopsis T-DNA insertion lines were obtained from the Nottingham Arabidopsis Stock Centre (NASC). The following lines were screened: SALK_128131 for *HADIIIB1* (At4g25150), SALK_087041 for *HADIIIB4* (At4g29260), and GABI_144B019 for *PAP26* (At5g34850) was provided by Dr. Nieves Medina Escobar.

For mutant combinations where T-DNA insertion lines were not available or could not be used, the CRISPR/Cas9 technique was employed. With gene specific guide RNAs and the Cas9 enzyme expressed from corresponding constructs, target gene sequences were edited creating mutants. For this, a modular vector was constructed in this work (Figure 21).

| nosP | Basta | nosT | ECP | Cas9 | reT | U6P | guide RNA | CF | NapA | tGFP | T |
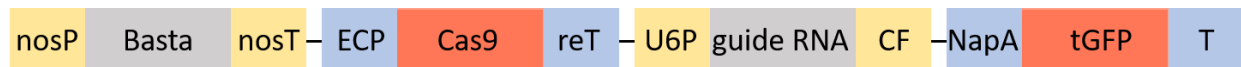
Figure 21. CRISPR/Cas9 construct for the generation mutants. nosP, nopaline synthase promoter; Basta, *phosphinotricin acetyltransferase* gene; nosT, *nopaline synthase* terminator; ECP, egg-cell-specific promoter; Cas9, Cas9 coding sequence; reT, rbcS-E9 terminator; U6P, U6-26 promoter; guide RNA, gene specific guide RNA (Table 5); CF, Cas9 scaffold; NapA, *napinA* promoter; tGFP, Turbo-GFP, fast folding green florescent protein; T, terminator.

This type of constructs was named level 2 module in the material and methods (section 2.2.1.6). The construct contained a Basta resistance (phosphinotricin acetyltransferase) gene under the control of nopaline synthase promoter for selection of transgenic plants. The Cas9 gene was placed under the control of an egg-cell-specific promoter (ECP) which ensured the expression of *Cas9* only in the ovum. This enabled the editing of genes in the ovum cells or as early as at the zygotic stage. In an ideal case this allows to identify homozygous mutants already in the first generation of transformed plants (T1). However in practice, the plants often have to be grown till the T2 generation to find homozygous mutants. The guide RNA cassettes are under the control of a U6 promoter in these construct - each gene was targeted with two independent guide RNAs fused to the *Cas9*-binding scaffold RNA. In the fourth expression cassette of these constructs, a *GFP* gene is controlled by a seed-specific napinA promoter. This cassette enables the selection of transformants and detection of the transgene by monitoring GFP fluorescence of the seeds

(Figure 22). The modules for this vector were constructed during this work. By Golden Gate cloning the modules can be combined with expression cassettes coding for gRNAs for different target genes. The guide RNAs used for the respective target genes targeted in this study are listed in Table 6. The single mutants and mutant combinations that were made are summarized in Figure 23.
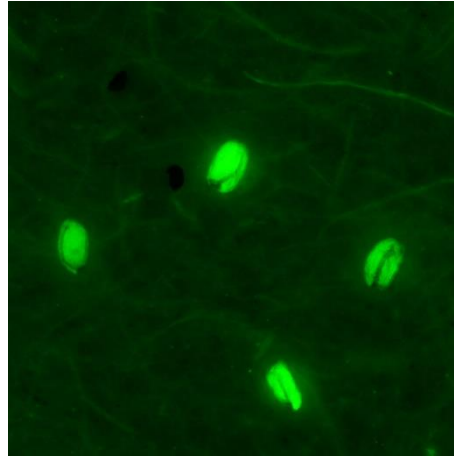
Figure 22. Selection of the transformed seeds based on a GFP signal. Seeds exhibiting a GFP signal had been successfully transformed with the CRISPR/*Cas9* vector. The CRISPR/*Cas9* editing was assessed by growing the seeds to seedlings and screening for alterations in the target sequences using DNA extracted from leaf tissue.
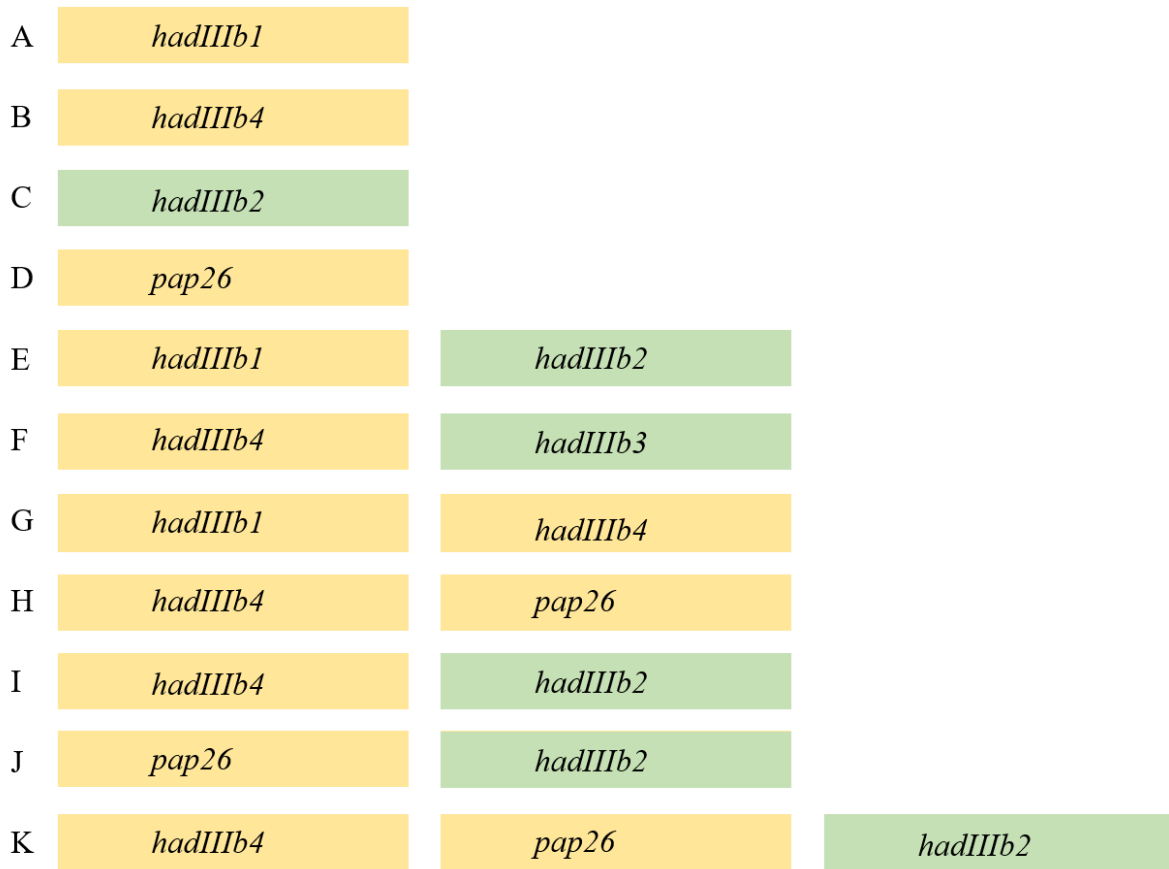
Figure 23. Schematic diagram for the generation of single, double and triple mutants. Each block represents one gene. Yellow blocks show T-DNA insertion lines, green blocks shows mutants obtained by CRISPR/Cas9 editing. A, B, D: T-DNA lines were obtained from NASC. C: *hadIIIb2* was generated by CRISPR/Cas9 editing of the wild type genetic back ground of *HADIIIB4*. E, F, I, J: double mutants were obtained by using the genetic background of *hadIIIb1*, *hadIIIb4*, and *pap26* and editing the target loci for *HADIIIB2* and *HADIIIB3* in different combinations. G, H: T-DNA line crosses for the double mutants of *hadIIIb4*pap26* and *hadIIIb1*hadIIIb4*. K: double mutant shown in (H) was used to edit *HADIIIB2* with CRISPR/Cas9 to generate *hadIIIb4*pap26*hadIIIb2*.

3.4.2.1. Single mutants

The T-DNA lines obtained from NASC were genetically characterized based on the presence and absence of the T-DNA insertion. The seeds obtained were grown to 4 leaf stage and then DNA was extracted (2.2.1.1) and gene specific primers were used to identify the wild type and homozygous and heterozygous mutant plants.

For SALK_128131 for *HADIIIB1* (At4g25150), a primer combination of P422 and P798 (Table 3) was used to amplify the wild type sequence of the gene (Wt reaction), while for the T-DNA

amplification the primer combination P422 and N61 was used (T-DNA reaction) (Figure 23 A, Figure 24). A PCR product of 876 bp could be amplified from DNA of homozygous mutant plants with the T-DNA reaction while there was no product with the Wt reaction. From DNA of wild type plants, a PCR product of 719 bp was only obtained in the Wt reaction whereas from DNA of heterozygous plants the respective products were obtained in both reactions. A wild type, a homozygous mutant, and a heterozygous plant were identified for this mutant and seeds were harvested for the next experiments. Similarly for SALK_087041 for *HADIIIB4* (At4g29260), the primers P424 and N61 were used for the T-DNA reaction (745 bp product) and the primers P424 and P799 were used for the Wt reaction (648 bp product) (Figure 21 B, Figure 22). A wild type as well as homozygous mutant and heterozygous plants were identified and seeds were harvested.
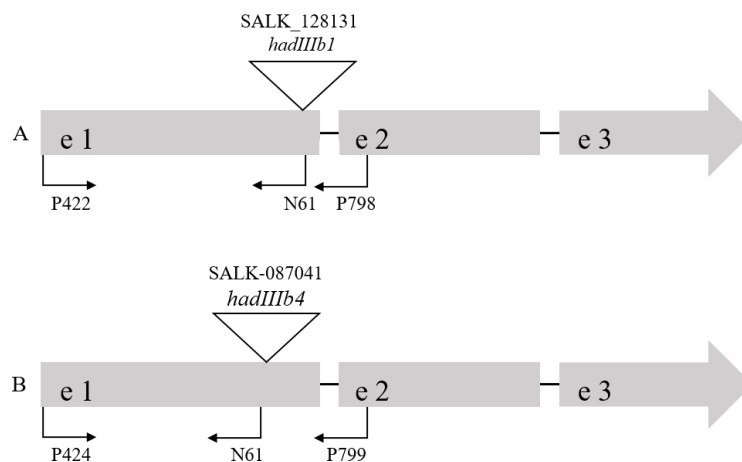
Figure 24. The genomic organization of the investigated T-DNA loci. A: At4g25150 (HADIIIB1) B: At4g29260 (HADIIIB4). The primers used for the genetic characterization are indicated by arrows. The T-DNA insert is shown by a triangle and three exons (e) are represented with e1, e2, and e3.

Although a T-DNA insertion line for *HADIIIB2* was available (SAIL_899B10) it was not analysed because SAIL lines have a BASTA resistance which would have made transformation of this line with vectors conferring BASTA resistance difficult. Therefore, the locus At5g51260 was targeted with gene specific guide RNAs in a wild type plant segregated out of the SALK_087041 line (Table 13, Figure 23 C). The background of a wild type derived from a T-DNA line was chosen, because all other mutants are in such a background. Three independent mutants for *hadIIIb2* were

generated (Table 13). The GABI_144B019 for *PAP26* (At5g34850) T-DNA line was genetically characterized in a separate study by Dr. Nieves Medina Escobar (Figure 23 D)

In summary, *HADIIIB1* (At4g25150), *HADIIIB4* (At4g29260), and *PAP26* (At5g34850) mutants were obtained as T-DNA insertion lines and mutants of *HADIIIB2* (At5g51260) were obtained by the CRISPR/Cas9 technique.

3.4.2.2.   Double and triple mutants

For the generation of double mutants, first a strategy was followed guided by the phylogenetic tree. Genes encoding verified NMPs closely related in sequence were to be mutated to eliminate subfamilies of HADIIIB phosphatases with possibly identical or overlapping function. Double mutants of *hadIIIb1*hadIIIb2* (Figure 23 E) and of *hadIIIb4*hadIIIb3* (Figure 23 F) were to be created for this purpose. For each of these double mutant combinations, the first locus carried a T-DNA insertion and the second locus was mutated by CRISPR/Cas9. Then combinations of genes coding for verified (vacuolar) NMPs were mutated irrespective of their sequence relationship. For this, T-DNA lines were crossed to generate the double mutants *hadIIIb1*hadIIIb4* (Figure 23 G) and, *hadIIIb4*pap26* (Figure 23 H). Using a T-DNA line modified by CRISPR/Cas9, the double mutants *hadIIIb4*hadIIIb2* (Figure 23 I) and *pap26*hadIIIb2* (Figure 23 J) were created (the second locus was modified by CRISPR/Cas9 in the respective T-DNA mutant of the first locus).

For the generation of a triple mutant, the locus for *HADIIIB2* was targeted by CRISPR/Cas9 in the double mutant genetic background of *hadIIIb4*pap26* (Figure 23 H) resulting in the triple mutant *hadIIIb4*pap26*hadIIIb2* (Figure 23 K).

Plant lines of the T1 and T2 generation after the transformation of the level 2 vectors were analyzed for mutations using gene specific primers. The corresponding PCR products were assessed for site specific editing. The information regarding the mutant characterization is listed in Table 13.

3.4.2.3.   Phenotypic observations in double and triple mutants

Interestingly, while attempting to create the double mutant *hadIIIb1*hadIIIb2* (Figure 23 E) no editing was found in the *HADIIIB2* locus, although the CRISPR/Cas9 construct for locus *HADIIIB2* was successfully used for editing this locus in other mutant combinations, and the editing of the target locus was followed for 4 generations selecting seeds with GFP fluorescence in each generation. HADIIIB1 and HADIIIB2 belong to the same phylogenetic clade. Since the

expression of *HADIIIB1* is highly pollen specific and *HADIIIB2* is also well expressed in pollen apart from other tissues, a double mutant of this clade might compromise pollen vigour or viability hinting to a role of NMP dephosphorylation in pollen.

The double mutant *pap26*hadIIIb2* (Figure 23 J) and the triple mutant *hadIIIb4*pap26*hadIIIb2* (Figure 23 K) showed a seed development phenotype, which was not observed in the respective single mutants (Figure 23 B, C, D) or in the *hadiiib4*pap26* (Figure 23 H) and *hadIIIb4*hadIIIb2* (Figure 23 I) double mutants. When *pap26*hadIIIb2* (Figure 21 J, K) were both mutated, up to 50% of the seeds either failed to develop or died after the maturation of the seeds. These phenotypes occurred with a variant degree of penetrance (Figure 25 B, C, D).
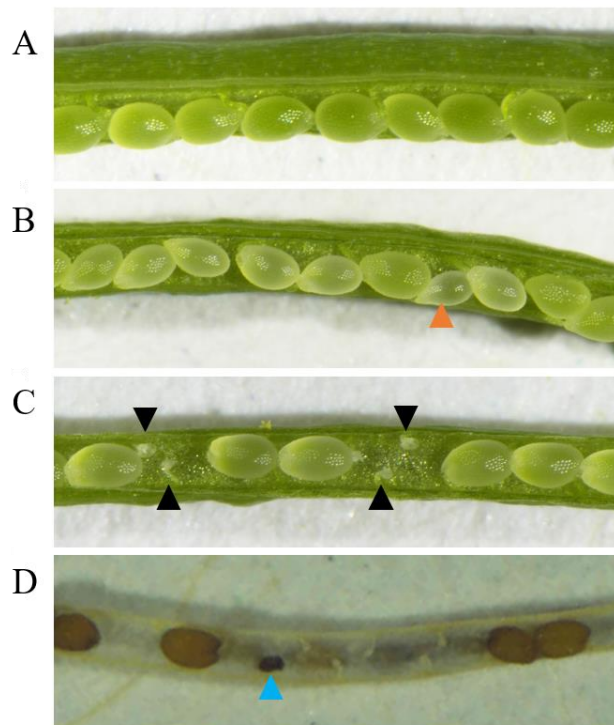
Figure 25. Different phenotypes observed in the *hadIIIb4*pap26*hadIIIb2* triple mutant. A, *hadIIIb4*pap26* double mutant containing the wild type gene for *HADIIIB2*; B, C, D, *hadIIIb4*pap26*hadIIIb2* triple mutant. Different phenotypes were observed in the same triple mutant plant. B, white seed phenotype indicated with orange triangle; C, failed seed development indicated with black triangles; D, dead seed phenotype indicated with blue triangle. A, B, C, images of siliques 10 days after pollination. D, image of silique 21 days after pollination.

The seeds either had a white colour, had died at an early developmental stage, or were completely absent while other seeds developed normally. The frequency of the phenotype was highly variable, some siliques showed no phenotype. Incomplete penetrance of a mutation is a well-known phenomenon where even genetically identical organisms can exhibit a varying phenotype under the same environmental conditions (Raj et al., 2010).

Functional loss of the vacuolar NMP *HADIIIB2* seems to be critical if combined either with abrogation of the similar but non-vacuolar NMP *HADIIIB1* or if combined with the loss of the broad spectrum vacuolar phosphatase PAP26. This indicates that *HADIIIB2* has partially overlapping functions with the other two phosphatases.

3.4.3. Overview of the selected candidates

Because the main goal of this work was to identify the general vacuolar NMPs in leaves, the further focus was not laid on a deeper investigation of the genetic variants involving *HADIIIB2* since the associated phenotypes affected the reproductive tissues. Instead, the two main vacuolar phosphatases with NMP activity and well expressed in leaves (HADIIIB4 and PAP26) were investigated in more detail.

3.5. Detailed enzymatic characterization of PAP26 and HADIIIB4

In order to better understand the functions of PAP26 and HADIIIB4, their kinetic parameters were analyzed. The proteins were transiently expressed in *N. benthamiana* as C-terminal Strep-tagged variants using the same genetic constructs as before (Section 3.2) and affinity purified. The purified enzymes were quantified using a BSA standard on SDS gels stained with Coomassie Blue and visualized by immunoblotting using anti-Strep antibodies. Enzyme preparations characterized in this way were used for enzymatic assays. Samples taken during the protein affinity purification were analysed by SDS gel electrophoresis (Figure 26). Gels shown in both panels were loaded in the same fashion. The molecular weight for the eluted proteins was calculated by measuring the migration distance of the individual marker bands and the purified proteins from the top of the gel. A plot with a regression line was generated and used to calculate the molecular weights of the purified proteins. For HADIIIB4 and PAP26 molecular weights of approximately 29 kDa and 66.6 kDa were determined, respectively. The analyses of the purified proteins (samples S4) revealed

the presence of multiple bands. Therefore, an immunoblot analysis was performed detecting the Strep-tag to assess if all bands corresponded to the respective purified Strep-tagged protein.
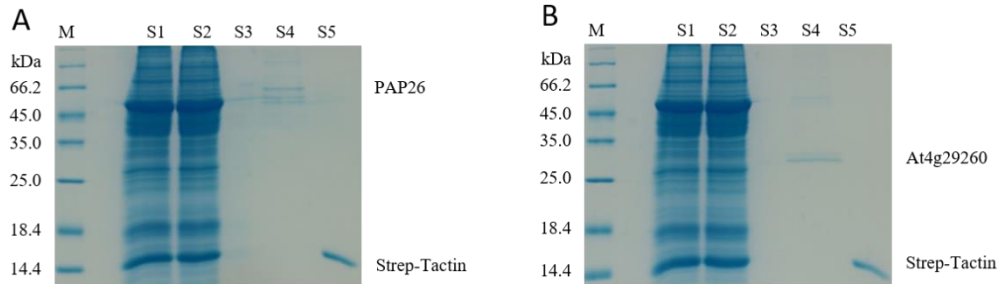
Figure 26. Purification of C-terminally Strep-tagged PAP26 and HADIIIB4. The proteins were expressed transiently in *Nicotiana benthamina* and purified by Strep affinity purification. Samples were taken at different stages of the purification procedure and loaded on an SDS gel stained with colloidal Coomassie. A, expression and purification of PAP26. B, expression and purification of HADIIIB4. M, unstained protein molecular weight marker (Thermo Scientific™ PageRuler™ Unstained Protein Ladder, 26610); S1, total soluble proteins; S2, soluble proteins not bound to the Strep-Tactin affinity matrix; S3, supernatant of the last wash step; S4, eluted protein; and S5, 50% v/v slurry of the beads and wash buffer. By boiling S5, Strep-Tactin is released from the matrix.
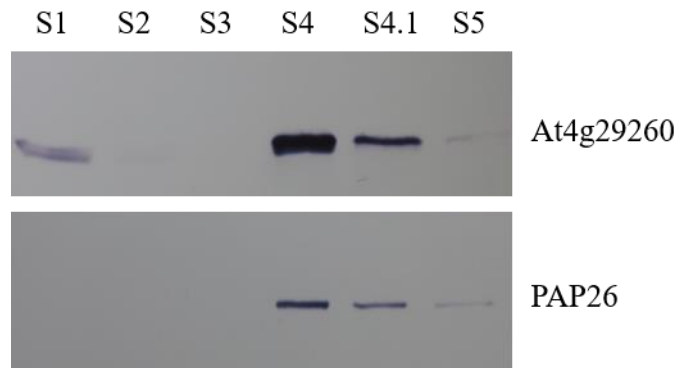
Figure 27. Expression and affinity purification of C-terminally tagged HADIIIB4 and PAP26 visualized by immunoblot. The same samples as shown in Figure 26 were loaded on an SDS gel and transferred to nitrocellulose membranes. The tag was detected with a StrepTactin alkaline phosphatase conjugate. Upper panel, expression and purification of HADIIIB4. Lower panel, expression and purificationPAP26. Sample order as described in Figure 26. The elution was performed twice generating a first and a second elution fraction sampled independently as S4 and S4.1. Only the elution sample S4 was shown in Figure 26.

The immunoblot for HADIIIB4 revealed a double band in the soluble protein extract (S1) which is possibly also present in the first elution (S4). The lower band appears weaker, maybe representing a degradation product. Alternatively, the two bands may represent different glycosylation states of the enzyme. On the immunoblot for PAP26 only a single band is present. At least one of the lower bands visible in S4 of the Coomassie stained gel may represent a contamination with the large subunit of Rubisco although eight washing steps were performed. However, in the Coomassie-stained gel there is also a faint band above the PAP26 band, which might represent an interacting protein that was co-purified. Interestingly, PAP26-Strep is not visible in the soluble protein extract (S1) on the immunoblot indicating that the over-expression of this protein was quite weak and that it was captured successfully by the purification. Arabidopsis vacuoles have an acidic pH of 5.2 (Shen et al., 2013). To assess if the pH has an influence on the phosphatase activity, a first phosphatase assay was performed comparing the specific activities at pH 6.8 and pH 5.2 for different substrates at 1 mM concentration using the purified enzyme HADIIIB4. The enzyme activities were calculated with µmol of the product formed per minute per mg ($\mu mol\ min^{-1}\ mg^{-1}$) of the purified enzyme.

Table 31. Comparison of activities of HADIIIB4 at pH 6.8 and pH 5.2

|	pH 6.8 ($\mu mol\ min^{-1}\ mg^{-1}$)	pH 5.2 ($\mu mol\ min^{-1}\ mg^{-1}$)	Factor[a]
5'-GMP	47.3	82.2	1.7
5'-CMP	14.7	56	3.8
5'-AMP	40	43.8	1
5'-UMP	31.9	73.3	2.2
3'-GMP	2.5	12.2	4.7
3'-CMP	0.04	2.1	50
3'-AMP	28	45.7	1.6
3'-UMP	0.8	4.7	5.7

[a]ratio of activities at pH 6.8 and pH 5.2

Closer to the physiolgical pH of vacuoles, HADIIIB4 showed a higher specific activity for all substrates (Table 31). For 3'-CMP a fifty-fold increase in activity at pH 5.2 was observed, but one needs to bear in mind that the activity detected at pH 6.8 was close to the assay's detection limit and therefore of low confidence. Based on these results, it was decided to determine the kinetic parameters of the enzymes at pH 5.2 which is close to the physiological pH in vacuoles.

3.5.1. Enzyme kinetic studies for the final candidate genes

The kinetic model of Michaelis-Menten describes the kinetic behavior of many enzymes and allows the determination of specific kinetic constants, the K_M and the k_{cat}. The K_M represents the substrate concentration where the enzyme reaches its half-maximal velocity. The lower the K_M, the higher is the enzyme's activity at low substrate concentrations and the lower is the amount of substrate necessary to reach the maximal velocity. The second parameter is the turnover number, the k_{cat}. This is the number of product molecules produces by the enzyme per second at full saturation. The ratio k_{cat}/K_M is called the catalytic efficiency. The catalytic efficiency rises with increasing turnover number and decreasing K_M.

Initially, the K_M of each substrate was roughly estimated using different substrate concentrations. Using the estimated K_M, kinetic measurements were made at substrate concentrations ranging from half K_M to ten times the K_M. The initial velocities were determined in triplicate at each substrate concentration, plotted against the used substrate concentrations, and fitted using the Michaelis-Menten equation to determine the kinetic parameters.
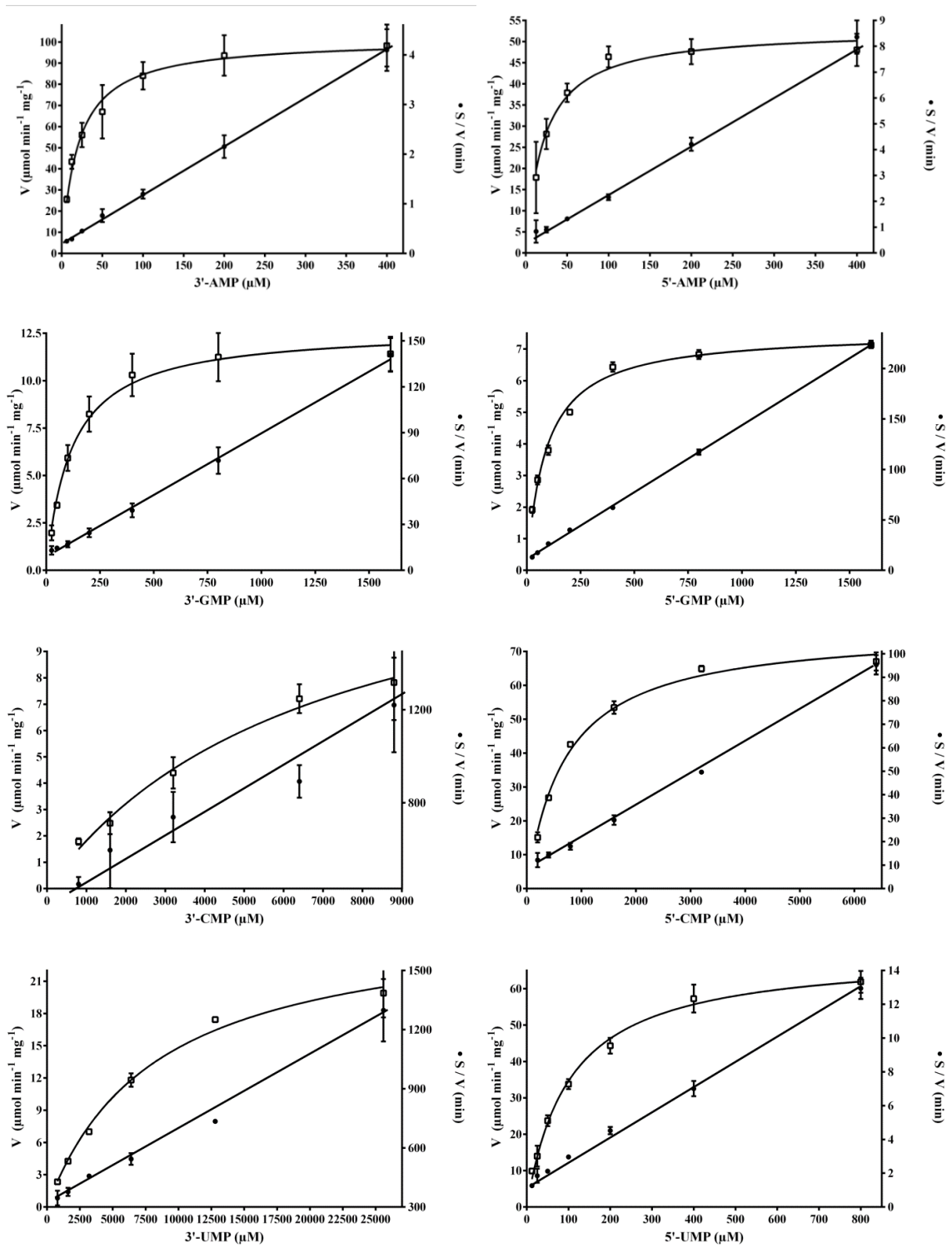
Figure 28. Determination of the kinetic constants for HADIIIB4 (At4g29260) with various substrates. In each panel: x-axis, substrate concentrations in μM; left y-axis, enzyme velocity in μmoles of product formed per minute per mg (μmol min^{-1} mg^{-1}); right y-axis, ratio of substrate to velocity (S/V). The error bars here are SD (n = 3 assay repeats using the same enzyme preparation).
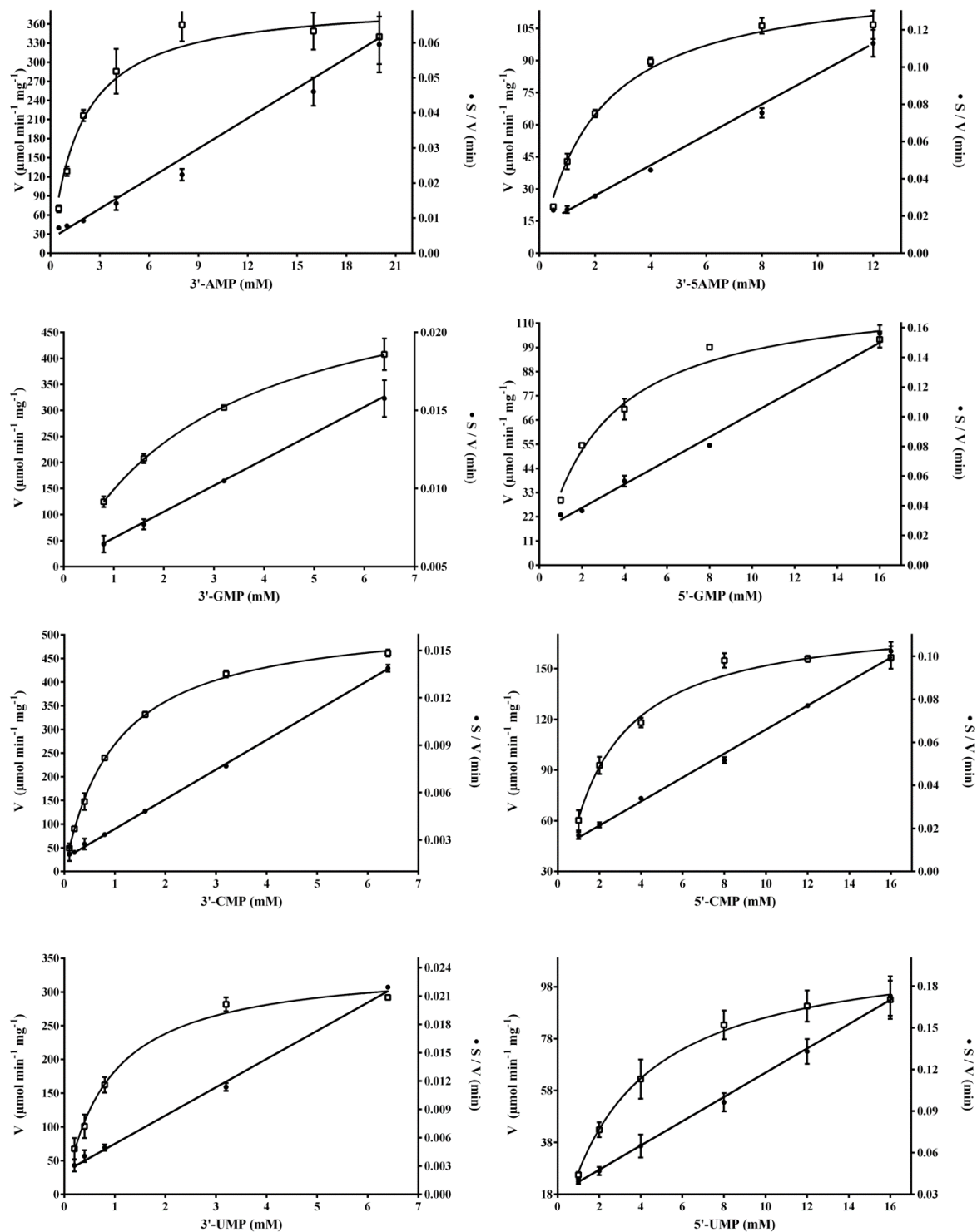
Figure 29. Determination of the kinetic constants for PAP26 (At5g34850) with various substrates. In each panel: x-axis, substrate concentrations in mM; left y-axis, enzyme velocity in µmoles of product formed per minute per mg (µmol min^{-1} mg^{-1}); right y-axis, ratio of substrate to velocity (S/V). The error bars here are SD (n = 3 assay repeats using the same enzyme preparation).

Table 32. Comparison of the kinetic constants of HADIIIB4 and PAP26

|	HADIIIB4			PAP26		
	K_M (mM)	k_{cat} (s^{-1})	k_{cat}/K_M ($s^{-1} \cdot mM^{-1}$)	K_M (mM)	k_{cat} (s^{-1})	k_{cat}/K_M ($s^{-1} \cdot mM^{-1}$)
3'-AMP	0.019 ± 0.002	24 ± 1	1242 ± 320	1.77 ± 0.26	436 ± 16	246 ± 64
5'-AMP	0.024 ± 0.003	26 ± 1	1064 ± 288	1.85 ± 0.16	140 ± 3	75 ± 23
3'-GMP	0.117 ± 0.014	6	52 ± 1	3.24 ± 0.32	676 ± 32	208 ± 101
5'-GMP	0.087 ± 0.004	3.6 ± 0.8	41 ± 1	2.79 ± 0.28	137 ± 4	49 ± 16
3'-CMP	6.8 ± 2	6.8 ± 1.1	1	1.01 ± 0.04	592 ± 8	587 ± 200
5'-CMP	0.7 ± 0.04	37 ± 0.6	52 ± 15	1.94 ± 0.15	199 ± 4	102 ± 28
3'-UMP	8.2 ± 0.8	13	1.58 ± 0.6	0.87 ± 0.08	376 ± 11	432 ± 141
5'-UMP	0.101 ± 0.007	33.7 ± 0.8	333 ± 106	3.30 ± 0.38	126 ± 4	38 ± 12

The HADIIIB4 exhibited K_M values in the very low to mid micromolar range (Table 32). The K_M values for 3'-CMP, and 3'-UMP could only be estimated. For 3'-CMP this was caused by the solubility limit 3'-CMP (only a stock up to 11 mM was possible). Thus, the initial velocity up to 7.5 mM substrate in the reaction mixture could be measured. 3'-UMP caused substrate inhibition above 25 mM of substrate offered. HADIIIB4 is a very efficient phosphatase for 5'-AMP and 3'-AMP, also catalyzes other 5'-NMPs and 3'-GMP especially due to a low K_M, but is very inefficient for the pyrimidine 3'-NMPs.In contrast to HADIIIB4, PAP26 exhibited K_M values in the low millimolar range for the offered substrates (Table 32). The K_M value for 3'-GMP could only be estimated because of the solubility the substrate (11 mM in the stock solution). Therefore the initial velocity up to 7.5 mM 3'-GMP in the reaction mixture could be measured. PAP26 is an efficient phosphatase for 3'-NMPs mainly due to a high turnover number for these substrates. For 5'-NMPs PAP26 is a very inefficient phosphatase.

3.6. Metabolomics studies

3.6.1. Indirect measurement of vacuolar nucleotide degradation by monitoring xanthine after short term blockage of the purine degradation pathway

The bioinformatic, confocal, transcript profile, and biochemical data suggest that PAP26 (At5g34850) and HADIIIB4 (At4g29260) are two vacuolar nucleotide phosphatases. Therefore, HADIIIB4 was renamed Vacuolar Nucleoside Phosphate Phosphatase 1 (VNPP1). To investigate if PAP26 and VNPP1 are involved in vacuolar nucleotide catabolism *in vivo*, an experiment was designed in which on one side purine nucleotide catabolism was boosted by a prolonged night and on the other side a short-term chemical blockage of the purine ring degradation pathway was induced. The XDH inhibitor allopurinol [4-hydroxypyrazolo-(3, 4-d) pyrimidine] was used for this purpose. XDH oxidizes the allopurinol to oxipurinol, which blocks the enzyme irreversibly, leading to the accumulation of xanthine (Figure 30) (Montalbini and Torre, 1995). Without allopurinol treatment, xanthine is undetectable in wild-type seedlings (Baccolini and Witte, 2019). The idea of this experiment was to use xanthine accumulation as a proxy to assess the activity / functionality of purine catabolism upstream of xanthine in different genotypes. The chain of events is illustrated in Figure 30. Vacuolar RNA is degraded by RNS2 releasing nucleotides that must be dephosphorylated to nucleosides for export into the cytosol by the ENT1 uniporter. Nucleosides are further catabolized in the cytosol, and in case of the purine nucleosides, xanthine is an intermediate of their degradation. According to this model, if nucleotide dephosphorylation in the vacuole is defect, nucleosides cannot be as efficiently released from the vacuole after RNA degradation and less xanthine will be produced.

For this experiment, mutants of (i) *PAP26*, (ii) *VNPP1*, (iii) *ENT1*, (iv) *RNS2*, and (v) the wild type segregated out of the *VNPP1* segregating mutant population were grown up to the middle vegetative stage (for 18 days). At the onset of day nineteen, the plants were sprayed with allopurinol and the prolonged night treatment was started for 48h. After 48h, samples were taken in a dark room, processed according to the protocol described in section 2.2.4.1, and analyzed for the xanthine content in all the genotypes.
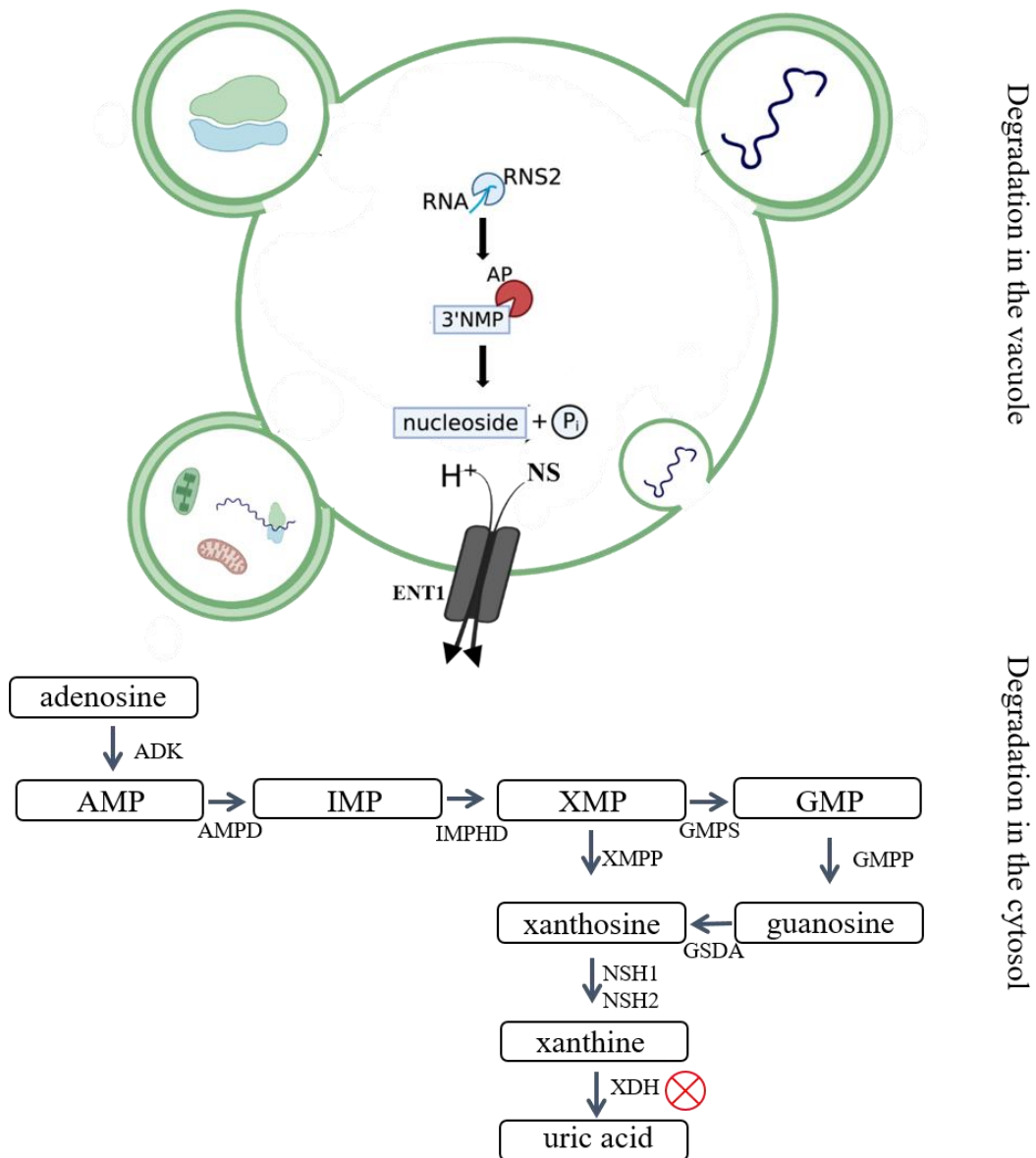
Figure 30. Model of vacuolar nucleotide release coupled with cytosolic purine nucleotide catabolism up to uric acid. The RNase RNS2 degrades vacuolar RNA into 3'-NMPs, which are hydrolyzed by acid phosphatases (APs) VNPP1 and PAP26 to the corresponding nucleosides. ENT1 mediates the translocation of the nucleosides into the cytosol. In the cytosol, nucleosides are further degraded. Here only purine nucleotide catabolism up to uric acid is shown. XDH is a central player of purine ring catabolism. When plants are sprayed with allopurinol, it temporarily blocks the activity of the XDH. As a result, xanthine accumulates over time.
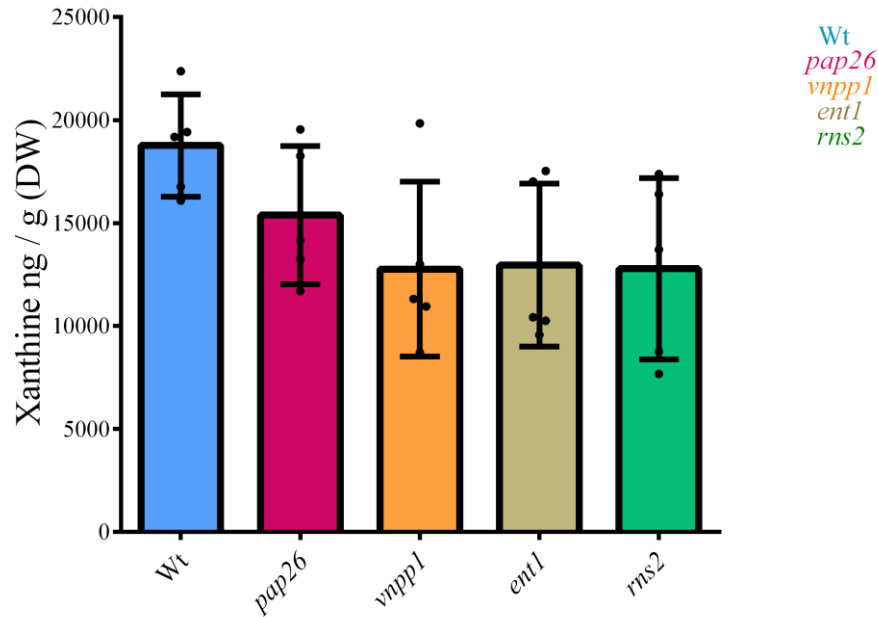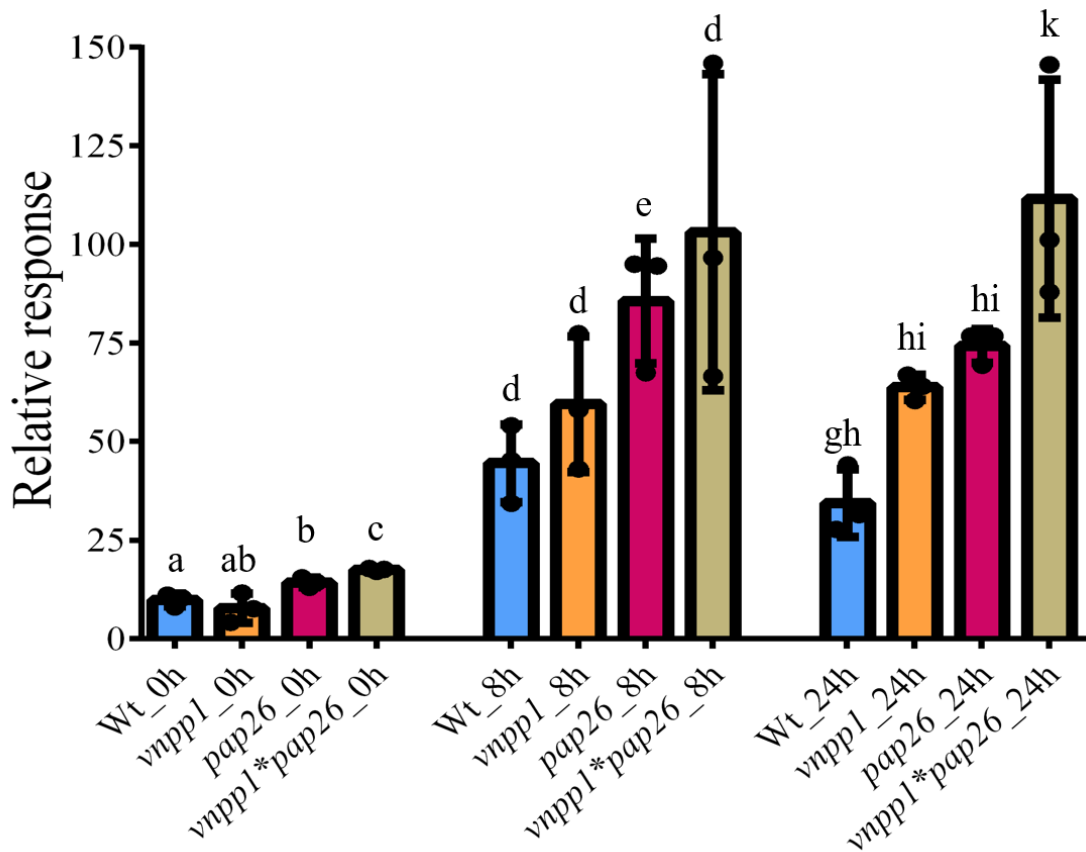
Figure 31. Xanthine accumulation in allopurinol-treated plants of different genotypes after a prolonged night of 48h. The genotypes of (i) wild type (Wt) segregated out of the mutant population of *VNPP1*, (ii) *pap26*, (iii) *vnpp1*, (iv) *ent1*, and (v) *rns2* were grown for 18 days after the imbibition. At the beginning of the day 19, allopurinol was sprayed on the rosettes and plants were exposed to additional 48 hours of darkness to boost the degradation pathway. The samples were taken 48 h after the onset of the prolonged night. The analysis was performed for the five biological repeats (n = 5 independent plants grown and treated in parallel). The error bars are SD.

It is known that in untreated plants the xanthine concentrations are usually too low to be detected. Here xanthine was well detectable in the wild type demonstrating that the allopurinol treatment was effective. For all mutants the mean xanthine accumulation was lower in tendency than in the wild type although in none of the cases the statistical significance threshold of $p < 0.05$ was reached (Table A 1 appendix). For *rns2* and *ent1* less xanthine is to be expected because the corresponding proteins are known to contribute to vacuolar RNA degradation and nucleoside export from the vacuole, respectively. These mutants served as positive control. It is promising that also *pap26* and especially *vnpp1* showed similarly decreased xanthine levels as observed in the positive control mutants. Possibly, a stronger difference in xanthine accumulation cannot be reached with the chosen experimental design for diverse reasons. RNS2 might not be the only vacuolar nucleosidase and ENT1 might not represent the only export way for vacuolar nucleosides. Similarly, PAP26 and VNPP1 might not be the only vacuolar nucleotidases. It would be interesting to repeat this experiment including the *pap26*vnpp1* double mutant.

97

3.6.2. Direct measurement of 3'-NMPs with mass spectrometry

Since RNA degradation in vacuoles presumably generates 3'-NMPs, for example by the activity of RNS2 which is known to produce 3'-NMPs, the relative concentrations of 3'-NMPs in different genotypes were analyzed *in vivo* using an adequate nucleotide extraction method (Straube et al., 2021) and sensitive mass spectrometry techniques. For this purpose, the single mutants (i) *pap26*, (ii) *vnpp1*, (iii) the double mutant *pap26*vnpp1*, and (iv) the wild type segregated from the double mutant were grown up to the mid vegetative stage (18 days) and exposed to an extended night. Samples were taken after 0 h, 8 h, and 24 h of the extended night in a dark room and analyzed by mass spectrometry. The relative concentrations of 3'-CMP and 3'-GMP could be determined (relative response in the MS). 3'-UMP and 3'-AMP could not be analyzed because the chromatographic peak of 3'-AMP was masked by a prominent 5'-AMP peak, and because of a relatively low signal for 3'-UMP.

Figure 32. 3'-CMP accumulation in rosettes of different genotypes exposed to darkness. The genotypes of (i) wild type (Wt) segregated out of the double mutant population *VNPP1*PAP26*, (ii) *vnpp1*, (iii) *pap26*, and (iv) *vnpp*pap26* were grown for 18 days after the imbibition. The sample 0 h was taken at the beginning of day 19 and plants were exposed to a prolonged night of 24 h. Samples were taken at 8 h and 24 h after the onset of dark stress. Three biological replicates, i. e. rosettes of three plants grown and treated in parallel, were analyzed (n = 3). The error bars are SD. Independent statistical analysis were performed for each time point, two-sided pairwise comparisons were performed according to Tuckey's sandwich variance estimator. Different letters indicate *p* values < 0.05. All p-values can be found in Table A 2 in the Appendix.

Already before the onset of the prolonged night (0 h), *pap26* and *pap26*vnpp1* accumulated slightly more 3'-CMP than the wild type (Figure 32). The 3'-CMP concentration rose in all genotypes upon dark treatment. At the later time points *pap26* and *pap26*vnpp1* also contained more 3'-CMP. Only after 24 h dark stress also the *vnpp1* line had more 3'-CMP than the wild type. The data is consistent with the kinetic data for 3'-CMP obtained for PAP26 (Table 32). Although VNPP1 is not an efficient 3'-CMP phosphatase (Table 32), its absence may lead to the accumulation of other nucleotides indirectly affecting the 3'-CMP concentration upon longer exposure to darkness.
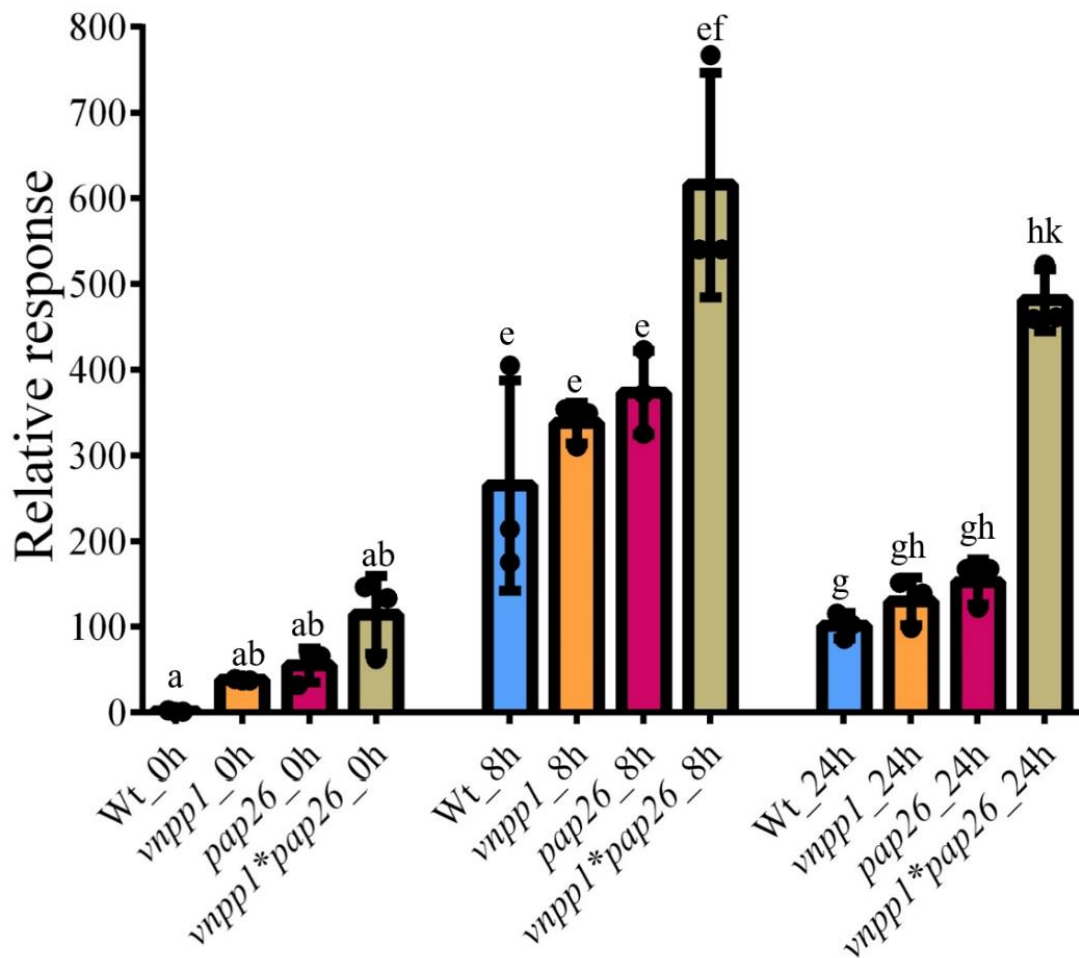
Figure 33. 3'-GMP accumulation in rosettes of different genotypes exposed to darkness. The genotypes of (i) wild type (Wt) segregated out of the double mutant population *VNPP1*PAP26*, (ii) *vnpp1*, (iii) *pap26*, and (iv) *vnpp*pap26* were grown for 18 days after the imbibition. The sample 0 h was taken at the beginning of day 19 and plants were exposed to a prolonged night of 24 h. Samples were taken at 8 h and 24 h after the onset of dark stress. Three biological replicates, i. e. rosettes of three plants grown and treated in parallel, were analyzed (n = 3). The error bars are SD. Independent statistical analysis were performed for each time point, two-sided pairwise comparisons were performed according to Tuckey's sandwich variance estimator. Different letters indicate *p* values < 0.05. All p-values can be found in Table A 3 in the Appendix.

Already before the exposure to dark stress, all mutants contained more 3'-GMP than the wild type (Figure 33). After 8 h or 24 h of darkness, the 3'-GMP concentration rose in all genotypes but the content of 3'-GMP was only higher in the *pap26*vnpp1* double mutant than in the wild type and not in the respective single mutants. The data is consistent with the 3'-GMP phosphatase activity detected for PAP26 and VNPP1 in the enzyme kinetic measurements (Table 32). Whereas for 3'-CMP PAP26 appears to be the dominant activity, both enzymes seem to be involved in the degradation of 3'-GMP.

This experiment demonstrates that PAP26 and VNPP1 are indeed required *in vivo* for the efficient degradation of 3'-NMPs. Since both enzymes are located in the vacuole and 3'-NMPs are thought to be generated mainly in the vacuole, it is plausible that these are phosphatases that act downstream of vacuolar RNA catabolism.

4. Discussion

Plants have an excellent ability to remobilize nutrients by degrading excess or harmful cellular components such as damaged organelles, RNA, proteins, and other cellular components. This is the main resource-conserving strategy of plants, and vacuoles are the most important degradation sites. Vacuoles store up to 95% intracellular inorganic phosphate (Srivastava et al., 2018). Catabolism of mononucleotides from RNA degradation also releases phosphate atoms. 80% of all cellular RNA is rRNA (Lodish et al., 2000), and RNA turnover and complete nucleotide catabolism release up to four nitrogen atoms (Melino et al., 2018). Therefore, RNA degradation plays an important role in plant survival, especially under resource-limited conditions (Melino et al., 2018). The vacuolar RNA degradation involves as first step a well-characterized ribonuclease, RNS2 (Hillwig et al., 2011), which degrades RNA to 3'-NMPs. The RNS2 is the main ribonuclease in the vacuole. (Hickl et al., 2021). The released nucleotides are substrates of vacuolar phosphatase(s) that catalyze the hydrolysis of 3'-NMPs to the corresponding nucleosides. The phosphatases for this step are still unknown and remain to be characterized. Finally, the nucleosides are exported to the cytosol by the ENT1 transporter (Bernard et al., 2011).

In this study, the aim was to identify and characterize these vacuolar 3'-mononucleotidase(s) in *Arabidopsis thaliana*. Phenotypically speaking, the *rns2* shows induction of constitutive autophagy, whereas *ent1* shows significantly reduced pollen germination and delayed plant growth. Biochemically, *rns2* accumulates rRNA (Hillwig et al., 2011), and in *ent1* ATP levels inside and outside pollen cells are significantly reduced (Bernard et al., 2011). ATP being the energy currency of the cells, can have drastic effects if the ATP pools are disturbed which impairs plant growth and survival. The biochemical and phenotypic alterations observed in the *RNS2* and *ENT1* mutants indicate that any defect in vacuolar RNA degradation can significantly affect plant fitness. The plants use the degradation machinery to survive starvation conditions. The phosphatases present in the vacuole play an important role for vacuolar RNA degradation.

Therefore, a comprehensive study was performed to identify and characterize the vacuolar 3'-nucleotidase(s). Three protein families were considered, and final candidates from these gene families were selected using some softer and some harder criteria. Only candidates that met all attributes were fully characterized *in vitro* and *in vivo*.

4.1. Candidate genes for the 3'-nucleotidases in *Arabidopsis thaliana*

The protein sequence of a known nucleotidase from *Phaseolus vulgaris* with 5'-nucleotidase activity belonging to the HADIIIB enzyme family was used as a query in protein Blast searches and several potential orthologs in *Arabidopsis thaliana* were identified. The nucleotidase from *Phaseolus vulgaris* was shown to hydrolyze 5'-NMPs, but 3'-NMPs were not tested as substrates for this enzyme (Cabello-Díaz et al., 2015). In *Escherichia coli*, several broad-spectrum phosphatases have been identified that can act on both 3'-NMPs and 5'-NMPs (Proudfoot et al., 2004), and we hypothesized here that the nucleotidase from *Phaseolus vulgaris* might also hydrolyze 3'- and 5'-NMPs. Most of the homologous HADIIIB enzymes from Arabidopsis have not yet been biochemically characterized and might represent the missing acid phosphates and can perform both 3'-NMP and 5'-NMP hydrolysis. Since this study aimed to find general plant 3'-NMP phosphatases and not only Arabidopsis-specific enzymes, other terrestrial higher plants were also included to identify HADIIIB enzymes conserved in different species. Assigning the presumed functions of genes within a group of the phylogenetic tree requires determining whether a gene arose from a duplication (paralog) or speciation (ortholog) event. Orthologs which belong to the same phylogenetic clade are likely to have the same function. In some clades potentially orthologous enzymes from all investigated plant species were found. These enzymes likely represent functions which are widely conserved and necessary in all plants, like for example vacuolar 3'-nucleotidases. In clade number five containing the vacuolar storage proteins (VSPs) most investigated plants had multiple members, indicating a duplication event (paralog) and functional redundancy. HADIIIB5 and HADIIIB6 occurred only in dicotyledons, suggesting that evolutionary divergence for this particular gene set occurred only in dicotyledons, whereas this gene set was completely absent in monocotyledons. Apparently these proteins only have a function in dicotyledons and are not necessary for monocotyledons. Thus they are likely not representing a general housekeeping function required in all plants. The PAP proteins were considered mainly because of the prominent PAP26 functions; the PAP proteins are identified and characterized in various monocotyledons and dicotyledons, this indicates that PAP proteins maintain specific roles through the whole vascular plant kingdom. The S1/P1 like endonucleases show close similarity to the well-characterized P1 and S1 nucleases from *Penicillium citrinum* and *Aspergillus oryzae* respectively indicating this protein family is specifically involved in nucleotide degaradation.

The conserved motif, DXTXT, was analyzed by aligning the amino acid sequences of the HADIIIB gene family. The DXDXT motif suggests the capability of the candidate proteins to function as phosphatases, the first amino acid Asp acts as the phosphorylation site, therefore, candidates containing the DXDXT motif can be potentially active. The motif is conserved from prokaryotes to eukaryotes including *Escherichia coli* (Thaller et al., 1998b), *Saccharomyces cerevisiae* (Reddy et al., 2008; Carman, 2011), *Vigna radiate* (Lightle et al., 2021), *Tetrahymena thermophile* (Khayyo et al., 2020), *Arabidopsis thaliana* (Reddy et al., 2010), *Caenorhabditis elegans* (Jung et al., 2020). All ten HADIIIB enzymes of Arabidopsis contain this motif indicating that all are potentially active phosphatases.s

4.2. Subcellular localization and challenges associated with the acidic environment of the vacuoles

Tagging the candidate proteins with fluorescent markers and then visualizing the organelles could help understand the actual localization of all the candidate proteins. However, the acidic environment of the vacuoles eliminates the fluorescence signals, making it impossible to categorize the candidate proteins by subcellular localization. There is no clear answer as to why is the fluorescence signal not visible in the vacuole, but several suggestions have been made. For example, the two proton pumps in the tonoplast (Figure 2) transport protons into the lumen where these protonate the fluorophore of the fluorescent markers (Tamura et al., 2003). Whether this hypothesis is correct can be determined by looking at the pKa values of the individual amino acids of the fluorophore to see if the pKa values fall within the pH-sensitive range and are actually affected by the vacuolar pH.

Since it was imperative to determine the subcellular localization of the candidate proteins, an alternative strategy was implanted to minimize the proton pump functionality. Dark conditions decreasing the activity of the proton pumps (Wang et al., 2014b). Therefore, after the agro-infiltration of the plants, the plants were placed in the dark, and then the vacuolar subcellular localization was investigated. This strategy helped in identifying the vacuolar localized candidates. This practice has been used several times for vacuolar fluorescent signal detection (Kleine-Vehn et al., 2008; Contento et al., 2005; Tamura et al., 2003; Mitsuhashi et al., 2000). ConcanamycinA an inhibitor of H^+-ATPases has also been successfully applied on *Dictyostelium discoideum* cell lines to visualize a GFP signal in vacuoles (Saheb et al., 2013). This technique was also tested for

the localization of our candidate proteins but no vacuolar localization could be observed (data not shown). This may be the case because concanmycinA inhibits only the H^+-ATPases but not the H^+-PPase. The vacuolar protein localization signal can possibly be confounded with a GFP-tagged protein that is usually located elsewhere in the call but has been transported to the vacuole for degradation. In such a case vesicle trafficking with fluorescent cargo can be observed (Kleine-Vehn et al., 2008; Dae Heon Kim et al., 2001). For the candidate proteins, 40 h of prolonged night treatment was enough to visualize the tagged proteins in the lumen and no vesicle trafficking was observed. From 24 candidates only six could be positively localized in the vacuole using this dark treatment, although some could not be localized to any subcellular compartment. However, since nucleotide degradation occurs in the vacuole, a vacuolar location was chosen as hard selection criterion.

4.3. What are the possible roles of the candidate proteins based on Transcript expression?

To further narrow down the candidate list, the transcript abundance of the candidate genes was examined in all plant tissues as an indicator for the ubiquitous expression. Since vacuolar RNA catabolism likely occurs in all tissues, good candidate genes were thought to be ubiquitously expressed. *HADIIIB2*, *VNPP1*/*HADIIIB4*, *HADIIIB6* (Figure A 2 in the appendix), and *PAP26* (Figure A 1 in the appendix) were ubiquitously expressed in all tissues indicating a housekeeping role. The transcript expression of other known genes, *ENT1* (Figure A 4 in the appendix)and *RNS2* (Figure A 5 in the appendix), involved in this pathway was explored and a similar expression pattern was observed. A common misconception is that autophagy is a process triggered by stress, but it is also a continuous process in cells that removes excess or damaged organelles and harmful cellular constituents. Cells are in a constant state of homeostasis between anabolism and catabolism (Mizushima and Komatsu, 2011; Todde et al., 2009). For this reason, vacuolar RNA degradation must be a process that occurs in every cell at any time during development and thus the transcripts of proteins involved in this process, here namely those of *RNS2*, *ENT1*, *VNPP1*, *HADIIIB6*, and *PAP26,* should be always present.

Some of the vacuolar and non-vacuolar candidates, *Endo5* (Figure A 3 in the appendix), *HADIIIB3* (Figure A 2 in the appendix), and *HADIIIB7* (Figure A 2 in the appendix), were explicitly expressed in the roots. This suggests that the corresponding proteins may have a specific function

in seedling roots or that the roots have their own nucleotide degradation machinery to which these enzymes may contribute. Consistent with this hypothesis, one study measured the accumulation of nucleotides and nucleosides in a nucleoside hydrolase mutant (*nsh1*) in roots and shoots. Metabolites related to nucleotide catabolism accumulated stronger in the roots than in the leaves. In particular, the uridine concentration was thirteen fold higher in the roots than in the shoots, and UMP concentrations were 71% higher in the roots than in the shoots (Riegler et al., 2011). The two HADIIIB candidate proteins, HADIIIB1 and HADIIIB2, present together in clade 1, are highly specific for reproductive tissues. *HADIIIB1* is specifically expressed in the anther, while *HADIIIB2* has a more ubiquitous expression pattern with highest expression in stigma tissue. The availability of an adequate phosphate supply affects pollen size and viability (Lau and Stephenson, 1994). These phosphatases are may be required to release phosphate from nucleotides to foster pollen tube growth.

4.4. *In vitro* **studies may not reflect the** *in vivo* **function**

We then assessed the substrate specificity of the vacuolar and also some non-vacuolar candidate proteins in the enzymatic assays using 3'- and 5'-NMPs. The biochemical assays showed that most of the candidates have an overlapping function.. PAP26 showed a clear preference for 3'-NMPs, demonstrating that it is present in the vacuole and hydrolyze 3'-NMPs where these substrates are generated by the ribonuclease activity of RNS2. VNPP1 preferred 3'-AMP and 3'-GMP out of the 3'-NMPs, whereas the best substrates (in terms of catalytic efficiency) were 3' and 5'-AMP. Some of the candidates did not show activity. The protein HADIIIB6, although the most highly expressed and purified phosphatase of all, showed no appreciable activity with any of the eight substrates.

Kinetic constants were then calculated for all eight substrates using the best possible biochemical parameters. PAP26 had high K_M values with 3'-NMPs, maybe suggesting that 3'-NMPs are present in the vacuole at higher concentrations. However, PAP26 is highly active with 3'-NMPs– it has a high k_{cat} for these substances, indicating that 3'-NMPs are possible *in vivo* substrates for PAP26.

On the other hand, VNPP1 indicated very low K_M for 3'-AMP and 3'-GMP, and higher k_{cat} in case of 3'-AMP, suggesting that even if the substrates are present at low levels, they are dephosphorylated efficiently. However, the actual concentrations of these substrates or enzymes in vacuoles are unknown. The mRNA transcript levels in mature leaves are 20 for *VNPP1* (Figure A 2 in the appendix) and 34 for *PAP26* (Figure A 1 in the appendix) in the units of the Klepikova

RNAseq dataset. In general, the maximum transcript abundance for *PAP26* is up to four times higher than that for *VNPP1*, but in mature leaves the transcript abundance is almost similar. Although the transcript abundance cannot predict the actual enzyme amounts, it may give an indication expecially for housekeeping enzymes. Nonetheless, it is possible that VNPP1 is a hundred times less abundant enzyme than the PAP26 and would then not contribute significantly to vacuolar nucleotide turnover. Thus, the physiological significance of these enzymes cannot be deduced only from the enzyme kinetic data and the transcription profile.

4.5.   A possible function for the other phosphatases from the HADIIIB family

The HADIIIB6 was one of the leading candidates for the possible function of a housekeeping phosphatase in *Arabidopsis thaliana*. This assumption was based on its vacuolar localization as well as the relatively high and ubiquitous expression of the corresponding gene. Nevertheless, it did not show biochemical activity with any of the eight substrates offered under the best possible *in vitro* conditions (Table 30). HADIIIB6 was also observed in the vacuolar proteome in response to stress (Carter et al., 2004). In another study, it was suggested to be a VSP. However, no biochemical analysis was performed, and no experimental evidence was provided to prove the suggestion that this protein is a VSP (Liu et al., 2005). Based on the experimental evidence in the current study, it can be assumed that it may be a VSP. The primary function of a VSP is to provide nutrients to the embryo, so transcript expression is expected to be higher in seeds. However, the expression pattern of *HADIIIB6* indicates that it is not present in the dry or imbibed seed, like the other two VSPs, VSP1, and VSP2, from the Arabidopsis. This means that the VSPs from the HADIIIB gene family might have physiological functions other than supporting seedling growth. VSPs are upregulated during biotic (Liu et al., 2005) and abiotic stresses (Neves et al., 2021), such as wounding, insect bite (jasmonic acid), and other nutritional and osmotic stresses. Whether HADIIIB6 represents a possible VSP3 still has to be tested. Since no phosphatase activity was observed despite the higher expression, it is also conceivable that it is a nucleotidase with an unknown substrate that is not 3' or 5'-NMP. Another probability is that the correct conditions for observing activity were not offered *in vitro*, maybe because some cofactors were missing in the assay for this particular enzyme. Differences between enzymatic functions *in vitro* and *in vivo* have been reported previously (Chen and Nielsen, 2021).

HADIIIB1 and HADIIIB2 are in the same cluster because they are phylogenetically related (Figure 7). According to the expression profile, this group is specific to reproductive tissue. The former candidate protein showed cytosolic localization, whereas the latter showed vacuolar localization. The expression specific to reproductive tissue suggests that this group of proteins may represent an important phosphatase activity in pollen. In this study, an attempt was made to find a double mutant of this cluster, but despite all efforts, the mutant plant could not be found. A detailed pollen-specific physiological study, such as pollen germination, pollen tube elongation, and pollen-specific nucleotide levels on individual mutants, could provide more insight into the possible function of this cluster.

Double *pap26*hadIIIb2* and triple *hadIIIb4*pap26*hadIIIb2*, mutant plants involving the *HADIIIB2* gene were generated but the plants had severe pleiotropic seed phenotypes. This might indicate that HADIIIB2 is the most important enzyme in pollen and reproductive tissues. In this context, several studies have been conducted that could explain the phenotypic observations in Arabidopsis. For example, carbohydrate deficiency induced by dark stress leads to reproductive failure (Lauxmann et al., 2016), alterations in the pyrimidine degradation pathway lead to reduced germination and seed production (Cornelius et al., 2011b), and transcriptome profile has confirmed that the nucleoside transporter ENT1 is upregulated in pollen (Bernard et al., 2011). The possible hypothesis would be that either HADIIIB2 is the major reproductive-specific nucleotidase that affects pollen viability and ultimately reduces seed production and viability, or that it is a ubiquitous phosphatase and a triple mutant of ubiquitous vacuolar phosphatases disrupts the purine and pyrimidine degradation pathway, thereby disrupting the source-sink relationship between senescent leaves and seeds.

4.6. *In vivo* phenotype

The 3'-NMPs were analyzed in vegetative rosettes of middle-aged Arabidopsis plants by mass spectrometry, and the relative response was determined with samples analyzed after 0 h, 8 h, and 24 h of a prolonged night. Significant differences between wild type and mutants were detected using the 3'-CMP data sets. VNPP1 and PAP26 are both involved in 3'-CMP recycling to different extents, although the 3'-CMP accumulation in *pap26* was higher than in *vnpp1* both before and after the onset of extended night. Nonetheless both are involved becauase the 3'-CMP accumulation was highest in the double mutant, *pap26*vnpp1*. The PAP26 and VNPP1 appear to

be important 3'-CMP phosphatases in vacuoles, but over time their absence is apparently compensated by other phosphatases, because the 3'-CMP accumulation between 8 h and 24 h is reduced. If all enzymes with 3'-CMP phosphatase activity were mutated one would expect a constant rise of 3'-CMP concentrations in the prolonged night.

For 3'-GMP accumulation, the situation was slightly different for the same genotypes and test conditions. The accumulation of 3'-GMP in wild type, *pap26*, and *vnpp1* was not much different at 8 h and 24 h, but the *pap26*vnpp1* double mutant showed a substantial increase in 3'-GMP concentration. We can hypothesize that PAP26 and VNPP1 have an overlapping function at least for 3'-GMP that is also consistent with the kintenic constants of these enzymes, both enzyme hydolyse 3'-GMP efficiently and *in vivo* thy have functional redunduncy. However, over time, the loss of function in these mutants is clearly compensated by other phosphatases because the 3'-GMP accumulation between 8 h and 24 h is significantly reduced in all genotypes.

The VNPP1 and the PAP26 have been shown to be the major 3'-NMP phosphatases in the vacuole, and mutation in these enzymes results in significant loss of 3'-nucleotide phosphatase function that is, on the other hand, recovered after some time. This suggests that other phosphatases can process the accumulated nucleotides and hydrolyze them to the nucleosides. How do plants cope with this situation? One hypotheis could be that constitutive autophagy is upregulated in the phosphatase (double) mutants like in *rns2* to ensure the regular flux of nucleosides. This should be tested in follow up experiments.

Plants have also been shown to activate autophagy as a survival mechanism when the vacuolar metabolic pathway is disrupted (Hillwig et al., 2011; Floyd et al., 2021). If PAP26 and VNPP1 are the only 3'-NMPs phosphatases in the vacuole, nucleosides should not be translocated via ENT1, even if autophagy is upregulated but over time, the loss of function in these mutants is recovered. The likelihood of other known and unknown active phosphatases present in the vacuoles cannot be ignored.

PAP8 has been shown to be present in vacuoles (Kaland, 2021). However, biochemical characterization has not yet been performed. HADIIIB2 is also present in the vacuole and has the capabilities of a phosphatase but because of the associated seed specific phenotype (Figure 25), this enzyme could not be further tested. It is also possible that the enzyme HADIIIB2, HADIIIB6, or PAP8, which has been shown to be present in the vacuole in this study, becomes biochemically

active and maintains the regular degradation process when the primary phosphatases are not present. Since Endo5 has also been localized in vacuoles, it is also possible that it is producing 5'-NMPs via RNA degradation and these 5'-NMPs maintain the regular flow of nucleosides.

The *vnpp1*pap26* double mutant of this vacuolar phosphate study shows no observable phenotype but biochemically accumulates 3'-NMPs. If the above hypothesis about up-regulated autophagy is correct, a vacuolar phosphatase and autophagy triple mutant could have drastic physiological effects on plant fitness. One way to detect the upregulation of autophagy in the double mutant is to quantify autophagosomes, which can be achieved either by transient expression of plant protoplasts with autophagosome markers or by chemical staining with DMC dye (Floyd et al., 2021). The *vnpp1*pap26*hadIIIb2* triple mutant can be characterized as a follow-up assess whether additional phosphatases are involved in 3'-NMP hydrolysis. The *Endo5* mutant could also be studied up to mid-vegetation stage, and metabolomics of roots and shoots can be reviewed to clarify whether Endo5 is involved in this process or it is indeed a root specific phosphatse.

4.7. The role of HADIIIB enzymes is still controversial

In this study, PAP26 is biochemically characterized both *in vitro* and *in vivo*, and the data on 3'-NMPs fully supports that PAP26 is indeed one of the leading vacuolar phosphatases. It has been shown to play a role in phosphate remobilization during leaf senescence (Robinson et al., 2012), and to be present in the vacuolar proteome (Shimaoka et al., 2004). There are no contradictions in the literature for the PAP26 function. On the other hand, a recent study claims a contradictory function for VNPP1; the authors claim that VNPP1 is a VSP3 although the protein has significant phosphatase activity with p-nitrophenyl phosphate (*p*NPP) (Sun et al., 2018).

VSP1 and VSP2, which are members of the HADIIIB gene family, showed activity with *p*NPP but the activity with 5'-NMPs was either undetectable or ranged from 0.1 to 2.0% compared to *p*NPP. Unfortunately, absolute quantification of acid phosphatase activities was not reported (Chen et al., 2012). Therefore, the magnitude of acid phosphatase activity with *p*NPP cannot be compared with acid phosphatase activities tested in this study. In the study in which HADIIIB4/VNPP1 is designated as VSP3, the authors compared the acid phosphatase activities of VSP1, VSP2, PAP26, and the HADIIIB4. No acid phosphatase activity for VSP1 and VSP2 could not be detected, but the acid phosphatase activity for PAP26 and HADIIIB4 (VSP3) was similar, suggesting that VSP1 and VSP2 do not have acid phosphatase activity, whereas HADIIIB4 (VSP3/VNPP1) and PAP26

have significant acid phosphatase activity (Sun et al., 2018). The ortholog of the HADIIIB4 enzyme, PvNTD1 from *Phaseolus vulgaris*, has significant acid phosphatase activity with *p*NPP and other NMPs (Cabello-Díaz et al., 2015). The amino acid sequences of VSP1 and VSP2 are 82% identical, whereas VSP2 and the claimed VSP3 (HADIIIB4) are only 38% identical (Liu et al., 2005).

In general, VSPs differ from acid phosphatases mainly by lacking AP activity. This issue was initially confused by a publication in which the authors claimed AP activity for two VSPs (VSPα and VSPß) from *Glycine max* (DeWald and Mason, 1992). However, this conflict was later resolved when AP activity was separated from VSPs and it was experimentally demonstrated that the VSPs from *Glycine max* do not exhibit AP activity (Staswick et al., 1994). Because the enzyme HADIIIB4 has acid phosphatase activity *in vitro* (Table 30) and a demonstrated biochemical phenotype *in vivo* (Figure 32, Figure 33) we can refer to this protein as acid phosphatase and call it VNPP1.

In summary, PAP26 and VNPP1 are important acid phosphatases responsible for the hydrolysis of 3'-NMPs in vacuoles. These enzymes catabolize the RNA breakdown products and release the nucleosides, which in the cytosol are either degraded or salvaged, thereby either releasing nutrients or conserving metabolic resources.

Section 2
Characterization of an engineered catabolic pathway for urea in *Arabidopsis thaliana*

Abstract

Section 2

Nitrogen is one of the most important nutrients for plants. Nitrogen deficiency leads to reduced plant growth and productivity. Urea is the most used nitrogen fertilizer in the world because it has a high nitrogen content and is easy to transport and apply in the field. However, fertilizing exclusively with urea results in reduced growth due to the toxicity of the ammonia. The urea is immediately hydrolysed to ammonia in the roots, the resulting higher ammonia concentration in the roots is toxic, and the plants excrete the excess ammonia back into the soil. In addition, the nitrogen use efficiency of nitrogen fertilizer in general and urea in particular is generally below 50% and needs improvement. Therefore, a biotechnological solution expressing heterologous transgenes in the model plant *Arabidopsis thaliana* was assessed with the aim to reduce ammonia toxicity for the plant and improve nitrogen use efficiency. For this purpose two enzymes representing an alternative urea catabolism pathway in various bacteria and fungi were investigated. In this system, urea is not immediately hydrolyzed to ammonia as in organisms employing Urease (like plants), but is first carboxylated by a Urea Carboxylase (UC) and the product allophanate is then hydrolysed by and Allophanate Hydrolase (AH) to ammonia and carbon dioxide. The performance transgenic lines expressing this system in the *Urease* mutant of Arabidopsis under the control of the 35S promoter was investigated. These lines were able to use urea demonstrating that the heterologous enzymes are functional in the plant. Since urea hydrolysis by UC and AH can occur in two steps, additional lines with wild type background (Urease positive) were investigated where the UC was expressed ubiquitously and the AH was expressed only in the shoot and in the light. In these plants ammonia release from allophanate can only occur in the shoot. Such transgenic plants performed significantly better than the wild-type with pure urea nutrition. The transgenic plants had a higher biomass and leaf area, and a higher nitrogen content. The results raise the hope that low nitrogen use efficiency and ammonia toxicity could be tackled with this system also in crop plants.

Abschnitt 2

Stickstoff ist einer der wichtigsten Nährstoffe für Pflanzen. Stickstoffmangel führt zu vermindertem Pflanzenwachstum und geringerer Produktivität. Harnstoff ist der weltweit am häufigsten verwendete Stickstoffdünger, da er einen hohen Stickstoffgehalt hat und leicht zu transportieren und auf dem Feld auszubringen ist. Die ausschließliche Düngung mit Harnstoff führt jedoch aufgrund der Toxizität des Ammoniaks zu einem geringeren Wachstum. Der Harnstoff wird in den Wurzeln durch Urease sofort zu Ammoniak hydrolysiert. Die daraus resultierende höhere Ammoniakkonzentration in den Wurzeln ist toxisch, und die Pflanzen scheiden das überschüssige Ammoniak wieder in den Boden aus. Außerdem liegt die Stickstoffnutzungseffizienz von Stickstoffdüngern im Allgemeinen und von Harnstoff im Besonderen im Allgemeinen unter 50% und muss verbessert werden. Daher wurde eine biotechnologische Lösung, bei der heterologe Transgene in der Modellpflanze *Arabidopsis thaliana* exprimiert werden, mit dem Ziel geprüft, die Ammoniak-Toxizität für die Pflanze zu verringern und die Stickstoffnutzungseffizienz zu verbessern. Zu diesem Zweck wurden zwei Enzyme untersucht, die einen alternativen Weg des Harnstoffabbaus in verschiedenen Bakterien und Pilzen katalysieren. In diesem System wird Harnstoff nicht sofort zu Ammoniak hydrolysiert, wie in Organismen, die Urease verwenden (wie Pflanzen), sondern zunächst durch eine Harnstoff-Carboxylase (UC) carboxyliert, und das Produkt Allophanat wird dann durch eine Allophanat-Hydrolase (AH) zu Ammoniak und Kohlendioxid hydrolysiert. Transgene Linien, die dieses System in der *Urease*-Mutante von Arabidopsis unter der Kontrolle des 35S-Promotors exprimierten, wurden untersucht. Diese Linien waren in der Lage, Harnstoff zu verwerten, was zeigt, dass die heterologen Enzyme in der Pflanze funktionsfähig sind. Da die Harnstoffhydrolyse durch UC und AH in zwei Schritten erfolgen kann, wurden zusätzliche Linien mit Wildtyp-Hintergrund (Urease-positiv) untersucht, bei denen UC ubiquitär und AH nur im Spross und im Licht exprimiert wurden. Bei diesen Pflanzen kann die Ammoniakfreisetzung aus Allophanat nur im Spross erfolgen. Solche transgenen Pflanzen schnitten bei reiner Harnstoffernährung deutlich besser ab als der Wildtyp. Die transgenen Pflanzen wiesen eine höhere Biomasse und Blattfläche sowie einen höheren Stickstoffgehalt auf. Die Ergebnisse geben Anlass zu der Hoffnung, dass die geringe Stickstoffausnutzung und die Ammoniaktoxizität mit diesem System auch bei Nutzpflanzen bekämpft werden könnten.

1. Introduction

## 1.1. Urea fertilization and associated problems

Plants require seventeen essential nutrients, which are categorized as either macronutrients or micronutrients depending on the requirement by the plants (Jones, Clain and Jeff Jacobsen, 2013). Nitrogen is one of the most crucial elements for plant metabolism. It is the primary building block of chlorophyll, amino acids, and nucleotides and is thus of essential importance for plant growth. At the same time, plant growth is frequently limited by nitrogen availability (Razaq et al., 2017). Nitrogen deficiency results in stunted growth and negatively affects photosynthesis (Zhao et al., 2005). Plants contain up to 5% (w/w) of nitrogen (Hawkesford et al., 2012). To optimize plant growth and achieve the highest possible productivity, generally, nitrogen fertilizers are applied in agriculture. Urea is the most widely used nitrogen fertilizer due to its high nitrogen content (46% w/w), ease of storage and transport, and dry granular texture. These advantages make it easy to use urea in the field. The worldwide demand for urea production is expected to reach 183 million metric tons in 2023 (https://www.statista.com/statistics/1063689/global-urea-production-capacity). However, the intensive use of fertilizers poses several problems. Plants use only about 30 to 50% of the nitrogen supplied (Peoples et al., 1995). The remainder is lost to the environment causing significant economic losses and environmental hazards like eutrophication, greenhouse gas emissions, and damage to the ozone layer (Hirel et al., 2011). Soil bacteria convert fertilizer nitrogen into nitrogen oxides representing potent greenhouse gases contributing to climate change. As nitrate, nitrogen can leach out of the soil leading to groundwater pollution. Nitrogen fertilizer may also reach adjacent ecosystems disturbing the ecological balance causing mineral depletion and acidification of the soil. (Vitousek et al., 1997). Due to the excessive acid rainfall, large amounts of magnesium and calcium were washed out of the soil complex and exported out with the runoff water (Likens et al., 1996).

Especially in the case of urea-based fertilizers, plants rapidly take up the urea and convert it into ammonia, which is particularly toxic to many plants and leads to a significant efflux of ammonia into the environment (Coskun et al., 2013). Ammonia is nitrified rapidly in aerobic soils, leading to soil acidification (Norton and Ouyang, 2019). Although ammonia is well bound to the soil, it can volatilize into the air and pollute nearby ecosystems. To reduce such losses, improving nitrogen utilization in plants is a particularly interesting area nowadays. Urease inhibitors are

routinely used and can reduce ammonia volatilization by 30-70% (Klimczyk et al., 2021). Nitrification inhibitors can also be used to further reduce the harmful effects of ammonia (Norton and Ouyang, 2019). These practices can keep urea stable in the soil for a while and allow the plant exclusive access to it if plant Urease is still functional despite the application of urease inhibitors. However, efficient nitrogen utilization by plant and translocation from root to shoot can address the heavy ammonia efflux from the roots into the plants. Apart from the heavy ammonia efflux into the soil, urea fertilization can also lead to an imbalance of amino acids in roots and shoots with increased accumulation of asparagine and glutamine in roots; this remarkably affects plant growth and productivity (Cao et al., 2010).

1.2. Urea catabolism in plants

Plants absorb urea with the help of unique transport systems (Kojima et al., 2007) and hydrolyze it to carbon dioxide and ammonia (NH_3) employing the nickel-dependent enzyme Urease. This particular urea catabolism is a two-step process. First, the urea is enzymatically hydrolyzed to ammonia and carbamate (Blakeley et al., 1969), and then the carbamate non-enzymatically forms ammonia and carbon dioxide (Carter et al., 2009, Figure 34). Urease is a ubiquitously expressed enzyme in all plant tissues (Witte et al., 2001).
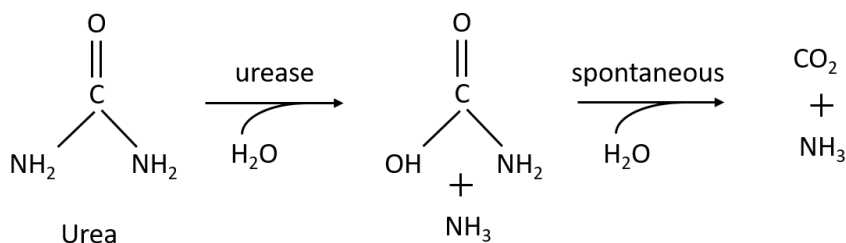
Figure 34. Urea hydrolysis by the plant Urease. Urea is first enzymatically hydrolyzed to carbamate and ammonia and then the carbamate is non-enzymatically broken down producing ammonia and carbon dioxide.

The NH_4^+ is one of the primary compounds required for synthesizing amino acids and proteins in all living organisms. However, it can be toxic at higher concentrations, and to avoid toxicity, plants need to balance NH_4^+ the uptake and translocation of assimilated nitrogen into the shoots. Any imbalance results in higher NH_4^+ levels in the roots and NH_4^+ leaving the plant again (Coskun et

al., 2013). The toxicity of NH_4^+ in plants is not a new issue; the harmful visual effects of the NH_4^+ nutrition on roots, leaves, and plant growth were first reported more than a century ago (Darwin, 1882). Much work has since been done to understand the mechanisms underlying the toxicity of NH_4^+ nutrition and avoiding the toxicity. For example development of slow-release brown coal-urea, which reduces environmental pollution but at the same time slows the availability of urea to plants (Saha et al., 2021), the use of *N*-(*n*-butyl) thiophosphoric triamide (NBPT), which significantly reduces soil microbial activity but at the same time negatively affects plant Urease and ultimately impairs urea uptake and assimilation (Zanin et al., 2015), investigation of long-distance translocation of urea in *Arabidopsis thaliana* (Bohner, 2012), foliar urea application (Witte et al., 2002), characterization of uptake and assimilation of urea (Gupta et al., 2014) identification of urea transporters (Zanin et al., 2014).

1.3. Alternative urea catabolism in some bacteria, algae, and fungi

Interestingly, the hydrolysis of urea does not rely in all organisms on the enzyme Urease. Some algae, fungi, and bacteria employ an alternative two-step mechanism without Urease. Here urea is first carboxylated to N-carboxylurea (allophanate) in an ATP-dependent reaction mediated by the enzyme urea carboxylase (UC). Then allophanate is hydrolyzed to ammonia and carbon dioxide catalyzed by allophanate hydrolase (AH) (Kanamori et al., 2004a; Maitz and Haas, 1982; Roon and Levenberg, 1972). UC belongs to the biotin dependent carboxylase family. These enzymes function as the carboxylases for several substrates with the aid of a prosthetic biotin group (Kanamori et al., 2004b). Also, UC needs to be biotinylated to be functional (Sumrada & Cooper, 1982). The AH belongs to the amidase signature family, which participates in diverse biological functions, including the catabolism of neuromodulatory fatty acids in mammals, the synthesis of indole-3-acetic acid in plants, the formation of Gln-tRNA^{Gln} in some bacteria, and the hydrolysis of malonamate from bacteroid to the plant in symbiotic relation during the nitrogen fixation. Although urea is hydrolyzed by most ureolytic organisms via Urease, the UC and AH functions are employed for this purpose in several bacteria, algae, and fungi. Interestingly, some fungal species like *Fusarium oxysporum*, *Nectria haematococca*, *Magnaporthe oryzae*, and *Fusarium verticilloides* have both systems (Navarathna et al., 2010). Plants naturally contain neither UC nor AH.
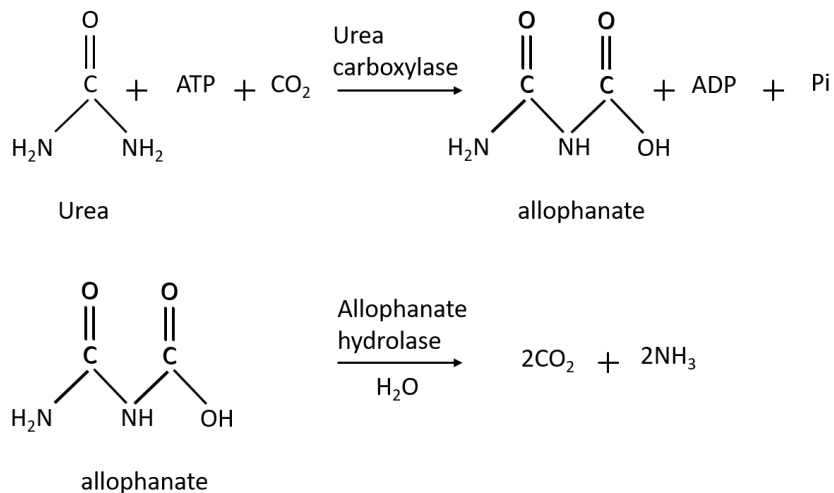
Figure 35. Urea hydrolysis via urea carboxylase and allophanate hydrolase in some bacteria and fungi.

Phylogenetic studies indicate a gene duplication event for the UC from a common prokaryotic origin. The UC present in current eukaryotes must have undergone an independent evolution (Strope et al., 2011). The UC and AH functions are either present on a single polypeptide or encoded by two separate genes. In *Saccharomyces cerevisiae*, the UC and AH functions are present on a single polypeptide, whereas, in Ascomycetes, UC and AH are encoded by individual genes. Separate genes for these enzymes are also found in several green algae, such as Chlorella and Chlamydomonas (Hodson et al., 1975; Adair et al., 1980).

1.4. Photorespiratory ammonia assimilation in C3 plants

Ribulose-1,5-bisphosphate carboxylase-oxygenase (Rubisco) catalyzes the first step of atmospheric carbon fixation where a ribulose-1,5-bisphosphate (RuBP) acceptor molecule is carboxylated and decays into two molecules of 3-phosphoglycerate. Using reduction equivalents made during photosynthesis, these molecules are reduced, resulting further downstream in the generation of glucose. On the other hand, in an unwanted reaction, RuBP is oxygenated resulting in the production of one molecule 3-phosphoglycerate and one molecule 2-phosphoglycolate. This process is called photorespiration because it uses oxygen under photosynthetic conditions. It accounts for about 25% of **Rubisco** activity. 2-phosphoglycolate cannot be used in the regular carbon fixation cycle. Therefore, it must be recycled, which involves the conversion of two glycine

molecules to serine releasing one carbon dioxide and one ammonia. Because photorespiratory oxygen assimilation is a frequent process, high amounts of ammonia are released during the recycling process of 2-phosphoglycolate. Terrestrial C3 plants re-assimilate this nitrogen through the photorespiratory nitrogen cycle (Keys, 2006), which means that they are well adapted to ammonia assimilation in the shoots. *Arabidopsis thaliana* is a C3 plant and can therefore assimilate high amounts of ammonia in the leaves.

1.5. Proposed model of alternative urea catabolism in plants

Because of the associated problems with the urea fertilizer in plants, alternative urea catabolism has great potential if successfully implemented. For alternative urea catabolism, urea in the roots will be carboxylated with the help of UC engineered into plants. The resulting allophanate (carboxylated urea) may be transported to the shoot. Then allophanate will be hydrolyzed to ammonia and carbon dioxide in the shoots by AH transformed into plants (Figure 36).
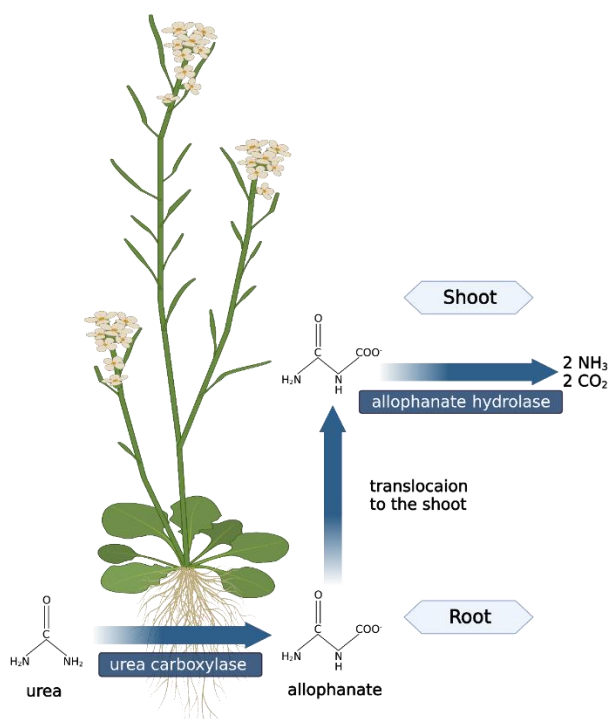
Figure 36. Overview of proposed particular separation of urea carboxylase and allophanate hydrolase in Arabidopsis thaliana. According to the proposed model, the roots will take up urea which will be carboxylated to allophanate. Then, the allophanate will be translocated to the shoots. There, the AH expressed specifically in the shoot from a transgene under a shoot-specific promoter will hydrolyze it to ammonia and carbon dioxide.

119

The concept involves the heterologous expression of the urea catabolism found in some bacteria, algae, and fungi, for example, Saccharomyces cerevisiae or Pseudomonas syringae. In C3 plants, the shoot is well adapted to ammonia assimilation because it re-assimilates high amounts of ammonia released during photorespiration. Thus, an amino acid imbalance and ammonia toxicity might be avoided. Additionally, the carbon dioxide released from allophanate in the shoot may be beneficial for increasing photosynthetic carbon fixation and suppressing the oxygenase reaction of Rubisco. Ideally, the allophanate hydrolysis should mainly occur in the light because then carbon from photosynthesis is available for ammonia-N assimilation. To achieve this, a photo responsive and shoot-specific promoter such as the Rubisco Activase (pRCA) promoter has been used to direct the transcription of the allophanate hydrolase. Another advantage is that Urease inhibitors do not affect such an engineered system allowing the plant to assimilate urea efficiently while the soil Urease is inhibited.

1.6.　Aim of this study

An alternative system was proposed to avoid urea-related ammonia toxicity in the plants. The first goal of this project was to investigate whether the alternate degradation system based on UC and AH from *Pseudomonas syringae* could be installed in *Arabidopsis thaliana*. This research further aimed to assess whether plants possessing the alternative urea degradation system show improved growth and yield and use urea fertilizers more efficiently than the wild type – first under sterile conditions and later under non-sterile growing conditions on soils that contain urea as the sole nitrogen source. For this, a nitrogen-free solid medium was required to test the growth advantage, which needed to be developed in the course of this project.

2. Materials and Methods

2.1. Materials

2.1.1. Primers

Table 33. Primers

Number[1]	Description	Sequence
N0390	Forward primer for the amplification of the RCA promoter	ACTCGAGATGTTGGTGTGAGCAAG
N0391	Reverse primer for the amplification of the RCA promoter	TTTAATTAACCACATGAGAGAATGGTTG
N0215	Forward primer for the amplification *AH* from *P. syringae*	GCCATGGGCGACACAGCTCTGC
N0216	Reverse primer for the amplification *AH* from *P. syringae*	TCCCGGGTCACAGCTGTTGCAGGTAG
N0312	Forward primer for the amplification *UC* from *P. syringae*	TCATATGTTCGACAAACTGCTGA
N0313	Reverse primer for the amplification *UC* from *P. syringae*	TCATATGGGGTTCGACAAACTGCTGA

[1]Laboratory's internal reference number

2.1.2. Vectors

Table 34. **Vectors**

Number[1]	Name	Description	Resistance
-	pJet1.2	Blunt end vector for the cloning of PCR products	Amp^R
U166	pXS1pat-mcs2	*UC* and *AH* expressed under the control of a 35S promoter.	$Amp^R/Basta^R$
U172	pXS1pat-mcs2	*UC* expressed under the control of a 35S promoter, and *AH* expressed under the control of a shoot specific RCA promoter	$Amp^R/Basta^R$

[1]Laboratory's internal reference number

2.1.3. Nutrient composition for Mourashige and Skoog (MS) medium

Table 35. **Nutrient composition for MS medium**

Nutrient	Salt	Molecular weight of the salt (g mol^{-1})	Molarity in the nutrient solution (mM)
Macronutrients			
N	CH_4N_2O	60.08	5.0
P, K	KH_2PO_4	136.09	1.2
Mg, S	$MgSO_4*7H_2O$	246.48	1.5
Ca	$CaCl_2*2H_2O$	147.02	3.0
Micronutrients			
Fe, S	$FeSO_4*7H_2O$	278.01	0.1
	$Na_2.EDTA*2H_2O$	372.24	0.1
Zn	$ZnSO_4*7H_2O$	287.56	0.03
Mn	$MnSO_4*H_2O$	169.02	0.13
Mo	$Na_2MoO_4*2H_2O$	241.95	10^{-3}
Cu	$CuSO_4*5H_2O$	249.68	10^{-4}
Ni	$NiCl_2*6H_2O$	237.69	10^{-4}
B	H_3BO_3	61.83	0.1

2.1.4. Substrate composition for coco-peat based soil medium

Table 36. Substrate composition for coco-peat based soil medium

Substrate	Coco-peat	Vermiculite	Perlite	Clay
Composition v/v	60%	20%	10%	10%

2.1.5. Nutrient composition for coco peat-based soil medium

Table 37. **Nutrient composition for coco peat-based soil medium**

Nutrient	Salt	Molecular weight of the salt (g mol^{-1})	Molarity in the nutrient solution
Macronutrients			
N	CH_4N_2O	60.08	9 mM
P, K	KH_2PO_4	136.09	8 mM
Ca	$CaCl_2*2H_2O$	147.02	10 mM
Ca, S	$CaSO_4*2H_2O$	172.17	10 mM
Mg	$MgCl_2*6\ H_2O$	203.3	8 mM
Micronutrients			
Fe	Sequestren	435.2	128.4 µM
Zn	$ZnSO_4*7H_2O$	287.5	10.8 µM
Mn	$MnSO_4*H_2O$	169.0	65.2 µM
Mo	$Na_2MoO_4*2H_2O$	241.9	7.2 µM
Cu	$CuSO_4*5H_2O$	249.6	45 µM
Ni	$NiCl_2*6H_2O$	237.6	7.2 µM
B	H_3BO_3	61.8	130.8 µM

2.2. Methods

2.2.1. Previous work conducted before this thesis by Till Myrach

The coding sequences (CDS) of *UC*, *AH*, and pRCS were amplified by polymerase chain reaction (PCR) and ligated into the pJet1.2 vector and sequenced. The CDS were then cloned into the expression vectors pXS1pat-mcs2 (Table 2). The transiently expressed proteins were purified and tested for the ureolytic activity for (i) UC, (ii) AH, and (iii) both enzymes together. The Col-0 (wild type) and *urease* plants were transformed using the floral dip method with the U172 and U166 (Table 2), respectively. For the experimental details, see till myrch thesis (Myrach, 2015).

2.2.2. Work continued in this study

For this study, a segregating wild type (Wt) population transformed with U172 (Table 2) expression construct was taken over, and the project was continued. First, homozygous transgenic lines were identified and grown on sterilized half-strength MS medium and other controls, and urea was used as the sole nitrogen source. Next, the same experimental setup was used for non-sterilized soil conditions, and then plant performance was characterized.

The alternative urea catabolism system studied in this project will be called the Alternative Urea Degradation System (AUDS). The *urease* transformed with U166 (Table 2) expression construct will be called Alternative Urea Degradation System 1 (AUDS1), and the wild type plants transformed with U172 (Table 2) expression construct will be known as the Alternative Urea Degradation System 2 (AUDS2).

2.2.3. Screening for homozygous transgenic lines

Homozygous plants for AUDS2 were segregated out by selecting transformants under the selection pressure of Basta. T3 generation seeds were screened in this experiment. Seeds were surface sterilized with 70% v/v ethanol and sown on half-strength MS agar plates. Approximately 100 seeds per transgenic line were placed equally distant from each other on plates. When the seedlings were well established, all the plates were sprayed with Basta (1:1000 dilution) one week after the germination. Seedlings with a 100% survival rate were homozygous for the AUDS2 and were used

for the production of a uniform seed batch. In the end, Different genotypes of (i) wild type, (ii) *urease,* (iii) two independent transgenic lines of AUDS1, and (iv) two independent transgenic lines of AUDS2 were grown in turf pots in a long day chamber (16 h light 8 h night), and the seeds were harvested.

2.2.4. Growth analysis of sterile Arabidopsis seedlings

The growth experiment was conducted on sterile half-strength MS media using 5 mM urea (Table 35) as a sole N source. Different genotypes of (i) wild type, (ii) *urease,* (iii) AUDS 1, and (iv) AUDS2 were surface sterilized with 70% v/v ethanol and sown on the same plate (that contains 30 mL of MS media) to assess the growth phenotypes and documented after four weeks.

2.2.5. Growth analysis of semi-sterile Arabidopsis seedlings

To analyze the different genotypes on soil, a combination of coco-peat (Pet Food TRIXIE Heimtierbedarf GmbH & Co. KG), perlite, vermiculite, and clay (ton; *Florisol® B-extra)* was prepared for 10 pots according to the v/v % composition mentioned in Table 5. To avoid any nitrate contamination from the tap water, all the equipment was washed with ultra-pure milli-Q water. 1.91 g of $CaSO_4*2H_2O$ was measured in 1 Liter (L) of water and stirred overnight ($CaSO_4*2H_2O$ has a maximum solubility of 2 g L^{-1}). The following day an appropriate amount of coco-peat, clay, and perlite were weighed and mixed in a clean box. The vermiculite was not added at this stage because of the robust mixing of nutrient solution and the solid substrates, which would have led to a loss of the spongy nature of vermiculite. Once the $CaSO_4*2H_2O$ was dissolved, the appropriate amounts of macro and micronutrients were added according to Table 6. A total of 1100 mL nutrient solution was prepared for 10 pots that was sufficient to provide the macro and micronutrients mention in Table 6. The coco-peat was then allowed to expand for two hours in the nutrient solution. The coco-peat brick has the ability to expand its initial volume up to eightfold. After two hours, the expanded substrate and nutrient mixture were once again mixed and vermiculite was added and mixed carefully not to damage the spongy nature of vermiculite. The final substrate-nutrient mixture was weighed and divided equally into ten 8 cm pots. The sterilized seeds were placed in the middle of the pot. Pots were watered every other day from the top of the pot and plants were documented every week.

126

2.2.6. ImageJ analysis

The plants from half-strength MS agar plates (2.2.4) were documented and analyzed for leaf greenness and total leaf area using the ImageJ software (https://imagej.nih.gov). For the greenness of the seedlings, a full plate image was uploaded to ImageJ, and then the color threshold window was opened in the image toolbar. The color threshold bar identifies each color pixel with a particular digit. For example, the yellow pixels were present between 42-48, while the green pixels were present between 49-65 on the color threshold digit bar. Next, individual pixels for green and yellow were calculated for each genotype on the same plate. The genotype in question was then analyzed while other genotypes present on the same plate were masked with black pixels using the drawing tool. To calculate the total leaf area, the yellow and green pixels were combined. First, the total number of pixels in the 1 cm^2 disc of paper were calculated. Then, the number of pixels on a 1 cm^2 disc were divided by the combined yellow-green pixels from the plate. To get the leaf area per plant, the resulting pixels were then divided by the total number of seedlings on the plate.

2.2.7. CNS analysis

To determine the nitrogen content of the plants grown with urea as the sole source of nitrogen, an elemental analyzer (EA3000, HEKAtech GmbH) was used. First, the plant material from the previous experiment (2.2.4) was harvested. Each plate served as a replicate. The plant material was dried in a 60°C oven, and the dry weight was determined. The samples were homogenized with 2 steel balls (5 mm) in the Retsch vibrating mill for 2 min at 30 Hz, and about 2.5 mg of the ground material was used for the analysis.

3. Results

3.1. Urea carboxylase and allophanate hydrolase expression in plants and enzymatic activity

The coding sequences of UC and AH from *Pseudomonas syringae* were cloned into expression vectors. The protein expression was investigated by transiently expressing untagged UC and C-terminal HA Strep-tagged AH in *Nicotiana benthamiana*. Expression was followed by an immunoblot (Figure 37, upper two panels). For the ureolytic activity, the desalted leaf extracts from plants expression only UC or AH or both enzymes together were tested with urea as substrate, and NH_4^+ release was examined. Only the leaf extracts containing both UC and AH expressed proteins could degrade urea. (Figure 37, lower panel).
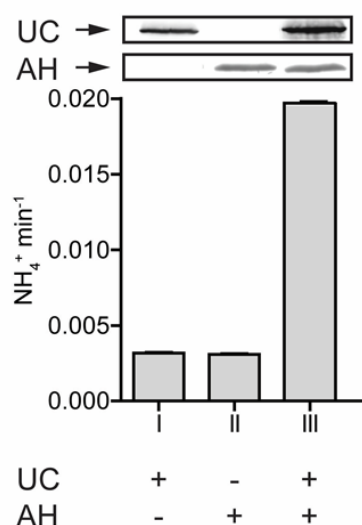
Figure 37. Expression of urea carboxylase and allophanate hydrolase from Pseudomonas syringae in Nicotiana benthamiana and activity assay. Upper two panels: immunoblot with biotin detection (via Streptavidin-alkaline phosphatase conjugate) for UC and StrepII-tag detection (via Streptactin-alkaline phosphatase conjugate) for the C-terminally StrepII-tagged AH. Plant leaves either expressed only UC or AH or both. Lower panel: Ammonia release from urea as substrate using leaf extracts from leaves either expressing only UC or AH or both enzymes together. Reproduced from the Ph.D. thesis of Till Myrach.
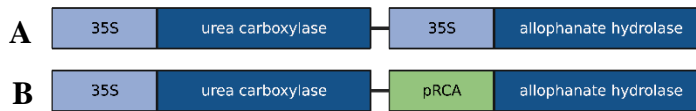
Figure 38. Constructs generated for the AUDS systems. A, Construct allowing ubiquitous constitutive expression of UC and AH (AUDS1); B, construct limiting expression of AH to the shoot in the light by using the shoot-specific, light-inducible promoter of Rubisco activase (AUDS2). Reproduced from the Ph.D. thesis of Till Myrach.

For the first analysis of the system *in vivo*, two constructs were generated (Figure 38): (a) a construct containing the coding region of UC and AH-StrepII, both under the transcriptional control of 35S promoters named as AUDS1 (Figure, 5A), and (b) a similar construct, with the AH-StrepII gene placed under the control of RCA instead of 35S named as AUDS2 (Figure, 5B). AUDS1 was used to transform *urease* from *Arabidopsis thaliana* that cannot use urea as a nitrogen source. AUDS2 was transformed into wild type Arabidopsis plants that can use urea as a nitrogen source. In order to avoid ammonia toxicity, the RCA promoter was also introduced specifically. The experiments described in this chapter were performed by a former Ph.D. student, Till Myrach (Myrach, 2015).

3.2. Arabidopsis seedlings grown in sterile conditions

A uniform seed batch was harvested after the selection of homozygous lines had been achieved. The growth rate of the seedlings of (i) wild type, (ii) AUDS2, (iii) *urease,* and (iv) AUDS1 were compared on half-strength MS agar plates in two independent experimental setups. Each setup contained 5 mM urea as a sole nitrogen source (Table 35), and the plants were documented after four weeks. In setup 1 (i) the wild type, (ii) *urease,* and (iii) AUDS 1 were compared, while in setup 2 (i) the wild type and (ii) AUDS2 were compared in terms of growth.

3.2.1. Analysis of the differential growth of the Arabidopsis plants for AUDS1

In this setup, (i) wild type, (ii) *urease,* and (iii) AUDS1 were tested for the differential growth of the different genotypes on plates with urea as the sole nitrogen source. One representative plate out of six replicates is shown in Figure 39. The wild type plants could grow on urea, whereas the *urease* line could not consume urea resulting in a clear difference between the wild type and the *Urease* mutant in growth. When the *Urease* mutant was complemented with the AUDS1 system,

where *UC* and *AH* are under the control of the 35S promoter, the transgenic line 1.2 showed growth comparable to the wild type, while line 1.1 did not complement the *urease*-negative phenotype, supposedly because the transgene(s) were silenced. In the *Urease* mutant, all the seeds germinated. However, they did not pass the two-leaf stage and died due to the unavailability of a nitrogen source. By contrast, the wild type plants could consume urea as a nitrogen source and grew. Although the *Urease* mutant transformed with the AUDS1 did not contain active Urease, they still grew comparable to the wild type because the AUDS1 enabled them to consume the urea. The expression of the urea carboxylase and the allophanate hydrolase under the control of the 35S promoter thus complemented the negative growth phenotype of the *Urease* mutant.
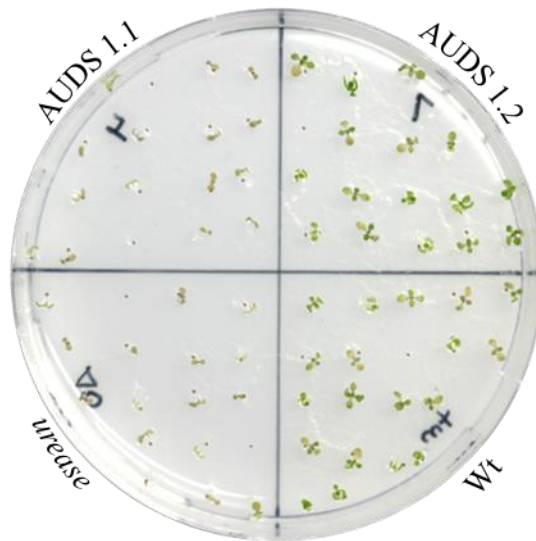
Figure 39. Differential growth of transgenic lines of AUDS1 in comparison to wild type and *urease*. The distinct ureolytic systems of (i) wild type (Wt), (ii) *urease,* and (iii) two transgenic lines of AUDS1 1.1 and 1.2 with urea as the sole nitrogen source under sterile conditions are shown here. The plates were documented four weeks after the imbibition. The plate is a representative example of a total of 6 replicates (all are shown in Figure A 6 in the appendix).

Table 38. Number of individual seedlings per plate for wild type, urease, and AUDS1 transgenic lines

	Wild type	*urease*	AUDS1.1	AUDS 1.2
	(number of seedlings)	(number of seedlings)	(number of seedlings)	(number of seedlings)
Replicate 1	19	16	15	16
Replicate 2	10	12	16	13
Replicate 3	13	13	13	15
Replicate 4	13	13	15	14
Replicate 5	14	14	10	14
Replicate 6	14	12	14	13
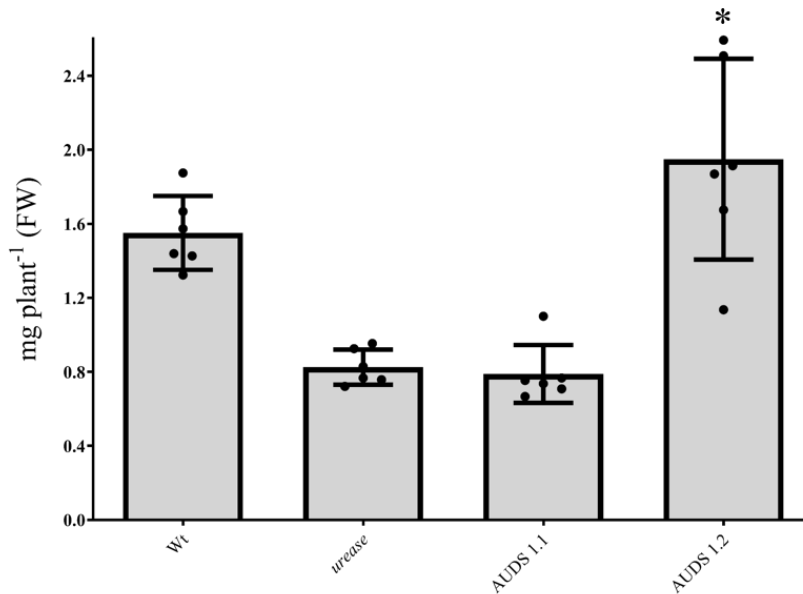
Figure 40. Determination of the fresh weight of the transgenic lines of AUDS1 in comparison to wild type and urease. The plants of (i) wild type (Wt), (ii) urease, and (iii) two transgenic lines of AUDS1 1.1 and 1.2 were grown for four weeks after imbibition on sterile MS medium with 5mM urea as the sole nitrogen source and then harvested. The joined fresh weight of the plants from each genotype was measured for each of the six repeats (n = 6) (Figure 6; appendix figure A 6). The number of individuals varied slightly between plates as detailed in Table 7. The error bars here are SD (standard deviation). For the statistical analysis, two-sided pairwise comparisons were

performed according to Tuckey's sandwich variance estimator. * indicates p-values < 0.05. The p-value refers to the comparison with *urease*. All p-values can be found in Table A 4 in the Appendix. The joined fresh weight of the plants from each genotype can be found in Table A 6 in the Appendix.

To quantify the observations, the fresh weight of the different genotypes was assessed (Figure 40). The wild type plants had an average fresh weight of 1.5 mg plant^{-1}, the u*rease* showed an average weight of 0.8 mg plant^{-1}, and the transgenic line 1.2 showed an average fresh weight of 1.9 mg plant^{-1}, which is twice as much as its corresponding background genotype. Line 1.1 showed similar growth as the *Urease* mutant probably because the transgene(s) were silenced and line 1.1 had 0.78 mg plant^{-1} fresh weight which is equal to the background.

In the example plate (Figure 6) apparent differences between different genotypes could be seen, the observations were proven quantitatively as well (Figure 7) because of the AUDS1 system, the urea can be catabolized into ammonia, and the plants can use the nitrogen contained in it; this can also be seen in Figure 40. Determination of the fresh weight of the transgenic lines of AUDS1 in comparison to wild type and urease. Where fresh weight plant^{-1} is shown quantitatively. The function of the bacterial enzymes in the context of the plant was thus demonstrated clearly. In the transgenic line 1.2, the urea capture and ammonia release metabolism occur in the same tissue. The result is immediate ammonia release from urea in the roots which potentially leads to ammonia toxicity. This is similar to the situation in wild type plants which hydrolyze the urea employing urease.

3.2.2. Analysis of the differential growth of the Arabidopsis plants with AUDS2

It is evident that the bacterial AUDS1 system can complement the growth defect of the *Urease* mutant and is thus functional in a plant context. When constitutively expressed, it captures the urea and releases the ammonia in the same tissue, potentially leading to ammonia toxicity or ammonia efflux. However, the AUDS2 system allows to separate urea capture and ammonia release in different tissues, which was explored in the next experiment. For this wild type plants were transformed with the AUDS2, where UC is ubiquitously expressed using a 35S promoter and AH is only expressed in the shoot during the day using the RCA promoter. This system enabled wild type plants to capture urea in roots and release the ammonia in the shoots, potentially avoiding the

toxicity and/or efflux problems. A prerequisite for the system to work is that the long distance transport of allophanate (the urea carboxylate produced by UC) from root to shoot is possible somehow. One should note that AUDS2 was implemented in the wild type, thus urease also participated in urea hydrolysis in these plants.
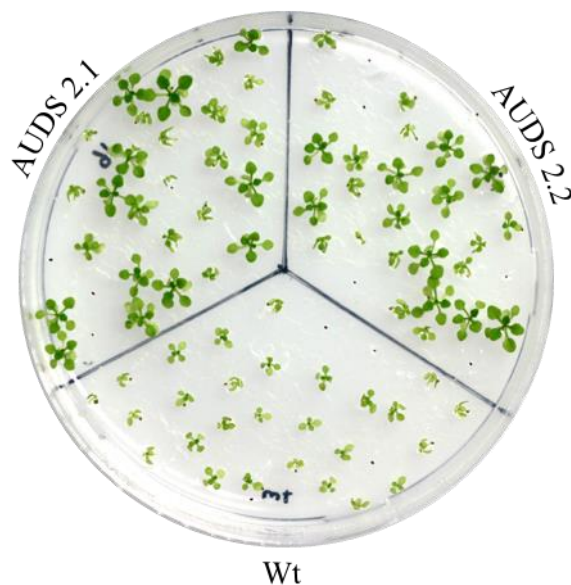
Figure 41. Differential growth of the transgenic lines of the AUDS2 in comparison to the wild type. The distinct ureolytic systems of (i) wild type (Wt) and (ii) two transgenic lines of AUDS2 2.1 and 2.2 with 5 mM urea as the sole nitrogen source under sterile conditions are shown here. The plates were documented four weeks after imbibition. The plate is a representative example of a total of 6 replicates (all are shown in Figure A 7 in the appendix)

Plants from both transgenic lines grew better than the wild type on urea as the sole N-source (Figure 8), presumably because they could consume urea more efficiently or avoid urea-associated toxicity. Some of the seeds of the transgenic lines did not germinate or germinated but the seedlings did not pass the 2 to 4 leaf stage. In such cases often the leaves were in contact with the growth medium. Because plant leaves have the ability to absorb urea, this may have caused excessive urea and ammonia concentrations in the shoot leading to toxicity and growth arrest (Krogmeier et al., 1989).

The plants on the plates were documented and harvested after 4 weeks for quantification. The dry and fresh weight, the leaf area, the greenness of the leaves, and the nitrogen content were measured.

Each plate of the six plates served as one biological replicate for each genotype. The number of seedlings on each plate varied slightly (Table 8). The two-leaf stage seedlings were ignored for the analysis.

Table 39. Number of individual seedlings per plate for wild type and AUDS2

	Wild type (number of seedlings)	AUDS2.1 (number of seedlings)	AUDS 2.2 (number of seedlings)
Replicate 1	27	27	24
Replicate 2	21	21	19
Replicate 3	23	25	18
Replicate 4	24	24	21
Replicate 5	22	23	15
Replicate 6	18	17	22

3.2.2.1.　Fresh and dry weight for AUDS2 in comparison to wild type
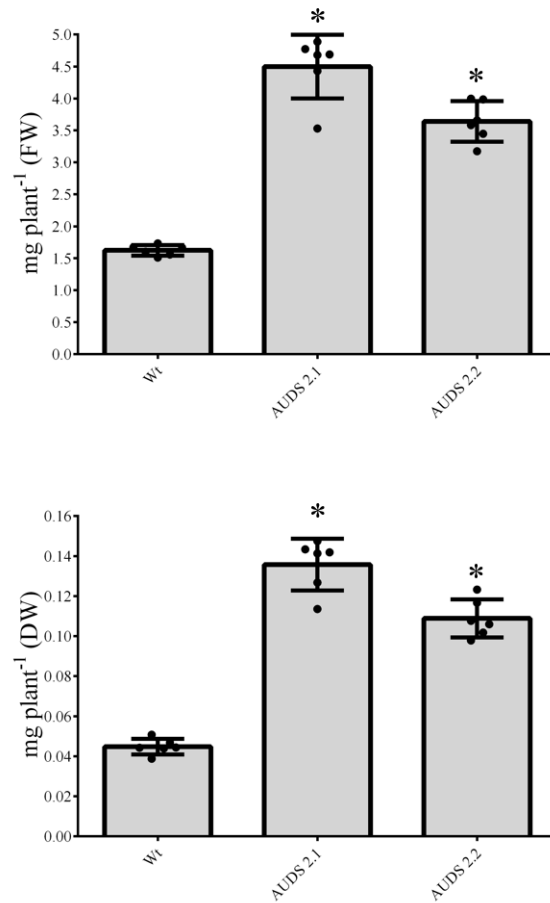
Figure 42. The fresh and dry weight of the transgenic lines of AUDS2 in comparison to wild type. The plants of (i) wild type (Wt) and (ii) two transgenic lines of AUDS2 2.1 and 2.2 were grown for four weeks after imbibition on sterile MS medium agar plates with 5 mM urea as the sole nitrogen source and then harvested. The joined fresh and dry weights of all plants from the same genotype were measured for each plate. In total there were six plates (n = 6) (Figure 8; appendix figure A 7), with varying numbers of individuals for each genotype (Table 8). Error bars are SD. For statistical analysis, two-sided pairwise comparisons were performed according to Tuckey's sandwich variance estimator. * indicates p-values < 0.05. p-value refers to comparison with wild type. All p-values can be found in Table A 5 in the Appendix. The joined fresh and dry weight of the plants from each genotype can be found in Table A 7 and Table A 8 in the Appendix.

A significant fresh and dry weight differences between the wild type and the two independent transgenic lines of AUDS2 was observed (Figure 42). The wild type plants had an average fresh weight of 1.5 mg plant$^{-1,}$ and transgenic lines 2.1 and 2.2 showed an average fresh weight of 4.5 mg and 3.6 mg plant^{-1}, respectively, which is 3.0 and 2.4 times higher than the wild type plants.

While the wild type plants had an average dry weight of 0.044 mg plant^{-1} and the transgenic lines showed an average of 0.113 and 0.108 mg plant^{-1}, which is consistent with the fresh weight observations.
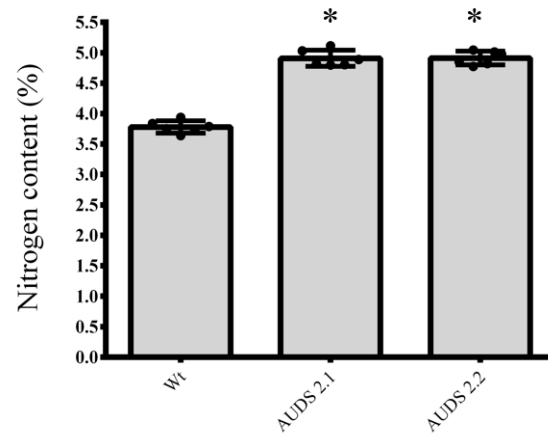
3.2.2.2. Leaf area for AUDS2 in comparison to wild type
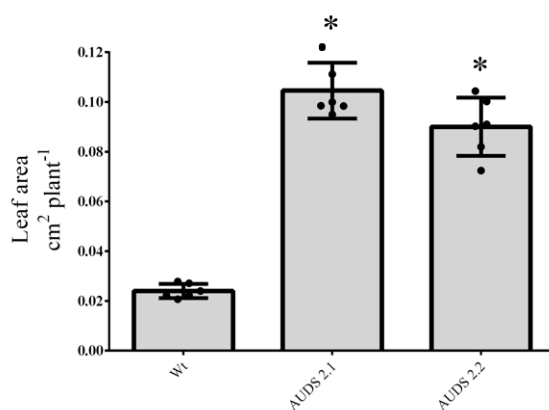
Figure 43. Leaf area per plant of the transgenic lines of AUDS2 in comparison to wild type. The plants of (i) wild type (Wt) and (ii) two transgenic lines of AUDS2 2.1 and 2.2 were grown for four weeks on sterile MS medium agar plates with 5 mM urea as the sole nitrogen source and then plants were documented and the total leaf area analyzed with the ImageJ software from all plants of each genotype and then divided by the number of individuals to determine a mean leaf area. This analysis was performed for the six biological repeats (n = 6). Each replicate consisted of a different number of seedlings (Table 8, Figure 8, appendix Figure A 7). Error bars are SD. For the statistical analysis, two-sided pairwise comparisons were performed according to Tuckey's sandwich variance estimator. * indicates p-values < 0.05. p-value refers to comparison with wild type. All p-values can be found in Table A 5 in the Appendix. The leaf area cm^2 plant^{-1} from each genotype can be found in Table A 9 in the Appendix.

The total leaf area of all plants of the same genotype was determined using the ImageJ software on each plate and then divided by the number of individuals to obtain the mean leaf area per plant. A greater leaf area was observed for the transgenic lines compared to the wild type (Figure 10). The wild type plants had an average leaf area of 0.02 cm^2 plant^{-1} and the leaf areas of the transgenic lines 2.1 and 2.2 were approximately five-fold greater with 0.10 and 0.09 cm^2 plant^{-1}, respectively.

3.2.2.3.   Leaf greenness for AUDS2 in comparison to wild type
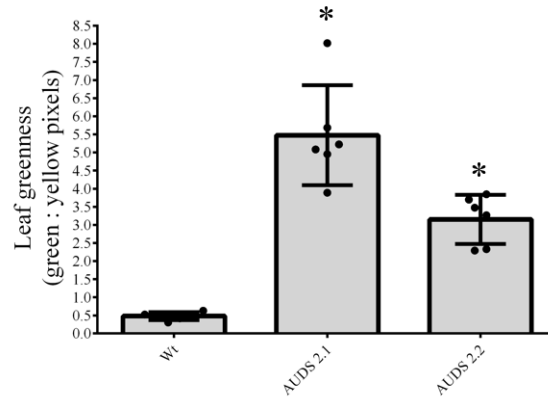
Figure 44. The leaf greenness per plant of the transgenic lines of AUDS2 in comparison to wild type. The plants of (i) wild type (Wt) and (ii) two transgenic lines of AUDS2 2.1 and 2.2 were grown for four weeks after imbibition on sterile MS medium agar plates with 5 mM urea as the sole nitrogen source and then plants were documented and the leaf greenness was analyzed with the ImageJ software from all plants of each genotype and then divided by the number of individuals to determine a mean leaf greenness. This analysis was performed for the six biological repeats (n = 6). Each replicate consisted of a different number of seedlings (Table 8, Figure 8, appendix Figure A 7). Error bars are SD. For the statistical analysis, two-sided pairwise comparisons were performed according to Tuckey's sandwich variance estimator. * indicates p-values < 0.05. p-value refers to comparison with wild type. All p-values can be found in Table A 5 in the Appendix. The leaf greenness plant^{-1} from each genotype can be found in Table A 10 in the Appendix.

The greenness of the plants was assessed by calculating the ratio of green to yellow pixels in the total leaf area. The transgenic lines had more green pixels compared to the wild type plants (Figure 11). Quantitatively speaking, the wild type plants had a green to yellow pixel ratio of 0.48 whereas the transgenic plants had pixel ratios of 5.40 and 3.10, respectively. Very likely this result reflects the leaf chlorophyll content (Tucker, 2015) and indicates a better nitrogen status of the transgenic plants. Chlorophyll contains four nitrogen atoms and thus requires nitrogen for its synthesis.

3.2.2.4. Nitrogen content for AUDS2 in comparison to wild type

Figure 45. The nitrogen content of the transgenic lines of AUDS2 in comparison to wild type. The plants of (i) wild type (Wt) and (ii) two transgenic lines of AUDS2 2.1 and 2.2 were grown for four weeks after imbibition on sterile MS medium agar plates with 5 mM urea as the sole nitrogen source and then plants were harvested. The joined dry weight of the plants from each genotype was measured for each of the six repeats (n = 6, Figure 8, appendix Figure A 7). And the nitrogen content was analyzed using an elemental analyzer. The error bars here are SD. For statistical analysis, two-sided pairwise comparisons were performed according to Tuckey's sandwich variance estimator. * indicates p-values < 0.05. The p-value refers to comparison with wild type. All p-values can be found in Table A 5 in the Appendix. The combined nitrogen content from each plate from each genotype can be found in Table A 11 in the Appendix.

Leaf greenness and better growth indicated an improved nitrogen status of the transgenic AUDS2 lines. Therefore, the total nitrogen content of the plants was measured using a CNS analyzer. The wild type had an average nitrogen content of 3.7% (w/w), whereas the transgenic line AUDS 2.1 and 2.2 contained over 30% more nitrogen with an average content of 4.9% (w/w).

3.3. Arabidopsis seedlings grown in non-sterile conditions

Under sterile conditions, urea as the sole nitrogen source will not be converted to other nitrogen forms in the growth medium. This is different under non-sterile conditions, where soil microbes can convert urea nitrogen to ammonia and nitrate. It is thus interesting to compare the growth of AUDS1/2 transgenic plants with the wild type and the *Urease* mutant under non-sterile conditions on soil with urea as N-fertilizer.

To perform this experiment, it was necessary to use a solid growth medium that is completely nitrogen-free but can sustain plant growth like turf-peat media when nitrogen is supplied. This is critical because *Arabidopsis thaliana* is a plant that produces little biomass and even small concentrations of nitrogen present in the growth medium support substantial growth. A coco-peat solid growth medium not containing any turf-peat was developed in our laboratory that fulfilled this criterion (Grove, 2019). All genotypes were grown on this medium supplemented with 58 mg of urea. Plants of all genotypes germinated in the first week and developed fine initially (Figure 13).
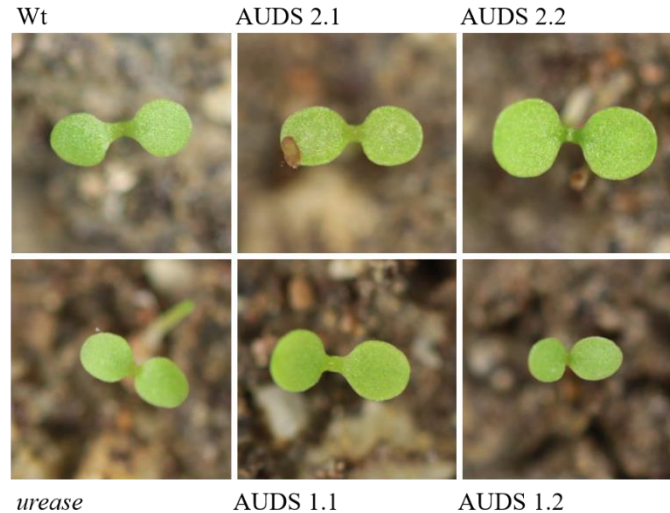
Figure 46. Seedling establishment of plants with different ureolytic systems on the coco-peat substrate supplemented with urea. The (i) wild type (Wt), (ii) urease, (iii) two transgenic lines of AUDS2 (2.1, 2.2), and (iv) two transgenic lines of AUDS1 (1.1, 1.2) are shown. The coco-peat medium contained 58 mg of urea as the sole nitrogen source. Pots were watered carefully to avoid any leaching of nutrients. The seedlings were documented one week after imbibition. The seedlings set is a representative example of a total of 3 replicates (all are shown in Figure A 8 in the appendix).
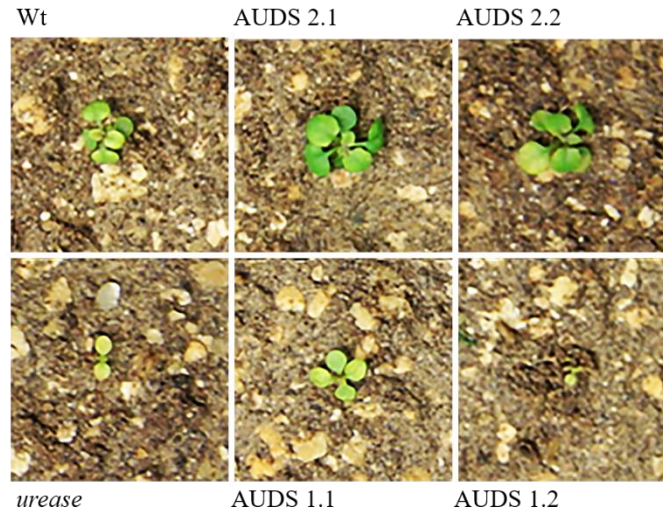
Figure 47. Differential growth of plants with different ureolytic systems on the coco-peat substrate. The substrate medium was supplemented with 58 mg of urea. The plants were documented three weeks after imbibition. Genetic variants and conditions as described in Figure 13. The plants are a representative example of a total of 3 replicates (all are shown in Figure A 9 in the appendix).

However, over time phenotypic differences arose (Figure 14). The *Urease* mutant was not able to grow beyond the two leaf stage, which is typical for Arabidopsis grown without a nitrogen source. This indicates that the offered urea was not converted in the soil to other nitrogen sources in sufficient quantities to support the growth of the *Urease* mutant. The wild type and the plants containing the AUDS1 system grew better although the growth varied between individuals. This shows that these plants were using some of the offered nitrogen, but growing conditions seemed not to be optimal probably because urea and ammonia resulting from urea hydrolysis via urease or AUDS1 were toxic. The growth of the AUDS2 lines surpassed that of the other genotypes indicating that these lines were most efficient in exploiting the offered nitrogen source. The observations on soil were similar to those from the MS medium experiment. It appears that implementing ammonia release from urea mainly in the shoot as in the AUDS2 lines boosts the growth efficiency of plants offered urea as the sole nitrogen source.

4. Discussion

Plants have a fundamental dependence on nitrogen, one of the most expensive nutrients supplied as commercial fertilizers in crop production. Urea is a widely used fertilizer and its consumption is expected to increase in the future. Usually, more than half of the nitrogen from fertilization is lost to the environment causing significant economic losses and environmental hazards like eutrophication, greenhouse gas emission, damage to the ozone layer (Hirel et al., 2011). However, externally supplied urea fertilizer might sometimes cause reduced growth, which affects the yield. Therefore, improving nitrogen use efficiency for urea has great potential to reduce the global environmental impact of nitrogen fertilization and increase productivity.

Plants fertilized with urea sometimes show reduced growth (Faustino et al., 2015; Yagoub et al., 2012), which might have been caused by (i) the nitrogen content imbalance in different parts of the plant - the roots might have excess nitrogen whereas the shoots suffer from nitrogen deficiency, (ii) the plant *Urease* readily hydrolyzes the urea, and the resultant ammonia quickly reaches toxic levels and leaves the roots (Coskun et al., 2013), and (iii) since less nitrogen is assimilated in the urea fertilized plants, less amino acids are formed also reducing the amounts of aromatic amino acids, which serve as precursors for the biosynthesis of growth hormones and protectants against biotic and abiotic stress. This can indirectly affect plant performance (Tzin and Galili, 2010). It is known that urea is not an ideal nitrogen source for *Arabidopsis* and many other plants when it is supplied as only nitrogen source. Growth on pure urea is compromised compared to ammonium nitrate and the reason is probably ammonia toxicity rather than inefficient urea transport or hydrolysis (Witte et al., 2005).

Here an alternative urea catabolic pathway was studied, where a urea sink in the plant is created by urea carboxylation which can be separated from ammonia release. This has the potential to prevent an amino acid imbalance in the roots and shoots and to lead to more efficient ammonia assimilation in the shoot which is better prepared than the root for this reaction.

To assess the functionality of this bipartite system stemming from a bacterium in planta, *UC* and *AH* were stably expressed under the 35S promoter in the *Urease* mutant. The plants did not contain any active urease and were grown on urea as a sole nitrogen source. To utilize urea, the plants could use only the alternative degradation system, which was called Alternative Urea Degradation

System 1 (AUDS1). Plants containing AUDS1 in the *urease* background grew like the wild type on urea as the sole nitrogen source (Figure 6, Figure 40.). The growth defect of the *Urease* Mutant was fully complemented by AUDS1 demonstrating that *UC* and *AH* from *Pseudomonas syringae* were functional in Arabidopsis. This is interesting because it also shows that the biotinylation machinery of the plant was capable of recognizing the bacterial UC as the target. After all, this post-translational modification is absolutely required for UC function. AH was expressed as C-terminal HA-Strep tagged variant. Thus, the result shows that the tags do not interfere with the enzymatic activity.

To assess the possible advantages of the AUDS system, the ammonium release reaction by AH was confined into the shoot in the light by using the shoot specific and light inducible promoter of the Rubisco activase gene to drive the *AH* transgene. The *UC* transgene remained under 35S promoter control. Wild type plants were transformed with this construct which thereby gained an additional pathway for urea nitrogen usage apart from urease. Potentially an amino acid imbalance in the root and shoot could and ammonia toxicity be avoided in plants using the AUDS2 system. These ideas were supported by the presented results. The AUDS2 plants developed better, had more fresh and dry weight (Figure 42), higher leaf surface area (Figure 43), and greener leaves (Figure 44) compared to the wild type plants. Moreover, the relative nitrogen content of the plants with the AUDS2 was 30% higher than for wild type plants (Figure 45). The increased growth yield together with the increased relative nitrogen content demonstrates that the AUDS2 plants had a significant advantage over the wild type in assimilating urea nitrogen.

In continuation of the sterile MS plate experiment, another experiment was conducted on the soil where the plants were directly competing with the soil microbes. In general, the seeds are well packed with all nutrients, enough for germination and establishment of initial growth of the seedling. At this early stage, the seedlings are not dependent on nutrients available in the soil. This can be observed in the soil experiment because regardless of genotype and concentration of the urea fertilizer applied, all seeds germinated and seedlings were well established to the two-leaf stage (Figure 13). Nevertheless, upon continued growth, differences in plant performance for the respective genotypes were observed (Figure 14). The coco-peat is a nitrogen-free medium, and the only available nitrogen source was urea here. Additionally, the co-applied Urease inhibitor NBPT inhibited the soil urease activity. In this situation, the *Urease* mutant did not pass the two-leaf stage

and later turned yellow and died, proving that urea was the only nitrogen source and plants could not use it. In the corresponding transformants AUDS1 1.1 and 1.2, the transgenic line no 1.1 showed no different growth pattern than the *Urease* mutant, which is in line with the experiment on sterile MS plates indicating this line might have a gene silencing effect. Line number 1.2, on the other side, showed some vegetative production similar to the wild type. However, the plants soon died probably due to the strong amino acid imbalance and the inability to separate the urea capture and nitrogen assimilation in root and shoot. In the case of wild type plants, the plants showed slight vegetative growth compared to the *Urease* mutant. However, likely due to the amino acid imbalance and ammonia toxicity the plants ultimately died. By contrast, the plants survived and appeared greener and vegetatively productive in the corresponding transformants carrying AUDS2.

It seems that urea is efficiently carboxylated to allophanate in the roots of the AUDS2 plants, and is then relocated into the shoots, where it is hydrolyzed to ammonia and carbon dioxide. The C3 plants are adapted to ammonia assimilation in the shoot because they re-assimilate high amounts of ammonia released from photorespiration in the shoots (Keys, 2006). It is possible that urea entering the roots of AUDS2 plants is mainly carboxylated and not hydrolyzed by Urease because *UC* is strongly overexpressed in these plants. Apart from creating a strong urea sink, which might increase the urea influx into the roots, this may avoid the accumulation of toxic amounts of ammonia originating from the urease reaction. This in turn may reduce the amino acid imbalance between roots and shoots which results from the ammonia assimilation in the roots. Additionally, ammonia from urea is released in the shoot in AUDS2 plants leading to amino acid production there, further avoiding a root / shoot amino acid imbalance. In addition, carbon dioxide is consumed in the roots by the UC reaction, which might increase root respiration and metabolic activity. Carbon dioxide is released in the shoot from allophanate, which is potentially beneficial for the photosynthetic carbon fixation rate suppressing the oxygenase reaction of Rubisco. Because the *AH* transcription is probably increased in the light in AUDS2 plants, allophanate hydrolysis might increase during the light phase. This is advantageous because during the day carbon from photosynthesis is available for ammonia-N assimilation and also the photorespiratory ammonia assimilation will be more active.

In the non-sterile soil, microbes are present that can readily hydrolyze urea. Therefore, to suppress the ureolytic activity of soil urease, most commercial urea fertilizers are coated with the urease inhibitor NBPT, which inhibits the soil urease but also affects the plant urease (Zanin et al., 2015). In this scenario, the resultant artificial/transient urease-inhibited plants could still consume urea when they possess an AUDS2, avoiding urea toxicity to the maximum level. Thus, even if urease activity is severely suppressed, such plants could make efficient use of fertilizer urea without being intoxicated by excess ammonia. At the same time, fertilizer loss might be minimized because soil urease is inhibited. It would be interesting to further optimize the AUDS2 system and to implement it in important C3 crop plants like wheat, rice, cotton, potato, or sugar beet. With this modification, it may be possible to create crop plants with significantly better nitrogen use efficiency when urea is used as nitrogen fertilizer.

References

Abel, S., Blume, B., and Glund, K. (1990). Evidence for RNA-oligonucleotides in plant vacuoles isolated from cultured tomato cells. Plant Physiol. **94**: 1163–1171.

Abel, S. and Glund, K. (1986). Localization of RNA-degrading enzyme activity within vacuoles of cultured tomato cells. Physiol. Plant. **66**: 79–86.

Adair, W.S., Monk, B., Hwang, C., and Goodenough, U.W. (1980). Purification and properties of chlamydomonas reinhardii sexual agglutinins. Eur. J. Cell Biol. **22**: 228.

Baccolini, C. and Witte, C. (2019). AMP and GMP catabolism in Arabidopsis converge on xanthosine, which is degraded by a nucleoside hydrolase heterocomplex. Plant Cell **31**: 734–751.

Bernard, C., Traub, M., Kunz, H.H., Hach, S., Trentmann, O., and Möhlmann, T. (2011). Equilibrative nucleoside transporter 1 (ENT1) is critical for pollen germination and vegetative growth in Arabidopsis. J. Exp. Bot. **62**: 4627–4637.

Blakeley, R.L., Hinds, J.A.J., Kunze, H.E., Webb, E.C., and Zerner, B. (1969). Jack bean urease (EC 3.5. 1.5). Demonstration of a Carbamoyl-Transfer Reaction and Inhibition by Hydroxamic Acids. Biochemistry **8**: 1991–2000.

Bohner, A. (2012). Membrane transport and long-distance translocation of urea in Arabidopsis thaliana.

Boller, T. and Kende, H. (1979). Hydrolytic Enzymes in the Central Vacuole of Plant Cells. Plant Physiol. **63**: 1123–1132.

Burroughs, A.M., Allen, K.N., Dunaway-Mariano, D., and Aravind, L. (2006). Evolutionary Genomics of the HAD Superfamily: Understanding the Structural Adaptations and Catalytic Diversity in a Superfamily of Phosphoesterases and Allied Enzymes. J. Mol. Biol. **361**: 1003–1034.

Cabello-Díaz, J.M., Gálvez-Valdivieso, G., Caballo, C., Lambert, R., Quiles, F.A., Pineda, M., and Piedras, P. (2015). Identification and characterization of a gene encoding for a

nucleotidase from Phaseolus vulgaris. J. Plant Physiol. **185**: 44–51.

Cañizares, M.C., Liu, L., Perrin, Y., Tsakiris, E., and P, L.G. (2006). A bipartite system for the constitutive and inducible expression of high levels of foreign proteins in plants. Plant Biotechnol. J. **4**: 183–193.

Cao, F., Werner, A., Dahncke, K., Romeis, T., Liu, L., and Witte, C. (2010). Identification and characterization of proteins involved in rice urea and arginine catabolism. Plant Physiol. **154**: 98–108.

Carman, G.M. (2011). The discovery of the fat-regulating phosphatidic acid phosphatase gene. Front. Biol. (Beijing). **6**: 172–176.

Carstensen, A., Herdean, A., Schmidt, S.B., Sharma, A., Spetea, C., Pribil, M., and Husted, S. (2018). The Impacts of Phosphorus Deficiency on the Photosynthetic Electron Transport Chain. Plant Physiol. **177**: 271–284.

Carter, C., Pan, S., Zouhar, J., Avila, E.L., Girke, T., and Raikhel, N. V (2004). The Vegetative Vacuole Proteome of Arabidopsis thaliana Reveals Predicted and Unexpected Proteins W. Plant Cell **16**: 3285–3303.

Carter, E.L., Flugga, N., Boer, J.L., Mulrooney, S.B., and Hausinger, R.P. (2009). Interplay of metal ions and urease. Metallomics **1**: 207–221.

Chen, M., Herde, M., Physiology, C.W.-P., and 2016, U. (2016). Of the nine cytidine deaminase-like genes in Arabidopsis, eight are pseudogenes and only one is required to maintain pyrimidine homeostasis in vivo. Plant Physiol. **171**: 799–809.

Chen, M. and Witte, C.-P. (2020). A Kinase and a Glycosylase Catabolize Pseudouridine in the Peroxisome to Prevent Toxic Pseudouridine Monophosphate Accumulation. Plant Cell **32**: 722–739.

Chen, Y. and Nielsen, J. (2021). In vitro turnover numbers do not reflect in vivo activities of yeast enzymes. Proc. Natl. Acad. Sci. **118**.

Chen, Y., Wei, J., Wang, M., Shi, Z., Gong, W., and Zhang, M. (2012). The Crystal Structure of Arabidopsis VSP1 Reveals the Plant Class C-Like Phosphatase Structure of the DDDD

Superfamily of Phosphohydrolases. PLoS One **7**: e49421.

Collet, J., Stroobant, V., and Schaftingen, E. Van (1999). Mechanistic studies of phosphoserine phosphatase, an enzyme related to P-type ATPases. J. Biol. Chem. **274**: 33985–33990.

Contento, A.L., Xiong, Y., and Bassham, D.C. (2005). Visualization of autophagy in Arabidopsis using the fluorescent dye monodansylcadaverine and a GFP-AtATG8e fusion protein. Plant J. **42**: 598–608.

Cornelius, S., Witz, S., Rolletschek, H., and Möhlmann, T. (2011a). Pyrimidine degradation influences germination seedling growth and production of Arabidopsis seeds. J. Exp. Bot. **62**: 5623–5632.

Cornelius, S., Witz, S., Rolletschek, H., and Möhlmann, T. (2011b). Pyrimidine degradation influences germination seedling growth and production of Arabidopsis seeds. J. Exp. Bot. **62**: 5623–5632.

Coskun, D., Britto, D.T., Li, M., Becker, A., and Kronzucker, H.J. (2013). Rapid ammonia gas transport accounts for futile transmembrane cycling under NH3/NH4+ toxicity in plant roots. Plant Physiol. **163**: 1859–1867.

Crozier A, Kamiya Y, G, B., and Yokota, T. (2000). Biosynthesis of hormones and elicitor molecules. In Biochemistry and Molecular Biology of Plants (The American Society of Plant Physiologists), pp. 850–929.

Dae Heon Kim, Eu, Y.J., Cheol Min Yoo, Kim, Y.W., Kyeong Tae Pih, Jing Bo Jin, Soo Jin Kim, Stenmark, H., and Hwang, I. (2001). Trafficking of Phosphatidylinositol 3-Phosphate from the trans-Golgi Network to the Lumen of the Central Vacuole in Plant Cells. Plant Cell **13**: 287–301.

Dahncke, K. and Witte, C.-P. (2013). Plant Purine Nucleoside Catabolism Employs a Guanosine Deaminase Required for the Generation of Xanthosine in Arabidopsis. Plant Cell **25**: 4101–4109.

Darwin, C.R. (1882). The action of carbonate of ammonia on the roots of certain plants. Bot. J. Linn. Soc. **19**: 239–261.

Dégut, C., Ponchon, L., Folly-Klan, M., … P.B.-B., and 2016, U. (2016). The m1A58 modification in eubacterial tRNA: An overview of tRNA recognition and mechanism of catalysis by TrmI. Biophys. Chem. **210**: 27–34.

DeWald, D. and Mason, H. (1992). The soybean vegetative storage proteins VSP alpha and VSP beta are acid phosphatases active on polyphosphates. J. Biol. Chem. **267**: 15958–15964.

Doench, J.G., Hartenian, E., Graham, D.B., Tothova, Z., Hegde, M., Smith, I., Sullender, M., Ebert, B.L., Xavier, R.J., and Root, D.E. (2014). Rational design of highly active sgRNAs for CRISPR-Cas9–mediated gene inactivation. Nat. Biotechnol. **32**: 1262–1267.

Duff, S.M.G., Lefebvre, D.D., and Plaxton, W.C. (1991). Purification, characterization, and subcellular localization of an acid phosphatase from black mustard cell-suspension cultures: Comparison with phosphoenolpyruvate phosphatase. Arch. Biochem. Biophys. **286**: 226–232.

Edwards, K., Johnstone, C., and Thompson, C. (1991). A simple and rapid method for the preparation of plant genomic DNA for PCR analysis. Nucleic Acids Res. **19**: 1349–1349.

Endler, A., Meyer, S., Schelbert, S., Schneider, T., Weschke, W., Peters, S.W., Keller, F., Baginsky, S., Martinoia, E., and Schmidt, U.G. (2006). Identification of a Vacuolar Sucrose Transporter in Barley and Arabidopsis Mesophyll Cells by a Tonoplast Proteomic Approach. Plant Physiol. **141**: 196–207.

Engler, C., Youles, M., Gruetzner, R., Ehnert, T.M., Werner, S., Jones, J.D.G., Patron, N.J., and Marillonnet, S. (2014). A Golden Gate modular cloning toolbox for plants. ACS Synth. Biol. **3**: 839–843.

Farré, J. and Subramani, S. (2004). Peroxisome turnover by micropexophagy: an autophagy-related process. Trends Cell Biol. **14**: 515–523.

Faustino, L.I., Moretti, A.P., and Graciano, C. (2015). Fertilization with urea, ammonium and nitrate produce different effects on growth, hydraulic traits and drought tolerance in Pinus taeda seedlings. Tree Physiol. **35**: 1062–1074.

Feys, B.J., Wiermer, M., Bhat, R.A., Moisan, L.J., Medina-Escobar, N., Neu, C., Cabral,

A., and Parker, J.E. (2005). Arabidopsis SENESCENCE-ASSOCIATED GENE101 Stabilizes and Signals within an ENHANCED DISEASE SUSCEPTIBILITY1 Complex in Plant Innate Immunity. Plant Cell **17**: 2601–2613.

Floyd, B.E., Kazibwe, Z., Morriss, S.C., Mugume, Y., Liu, A.-Y., Ridout, V., Luo, X., MacIntosh, G.C., and Bassham, D.C. (2021). An active RNA transport mechanism into plant vacuoles. bioRxiv: 2021.07.28.454214.

Fujimoto, M., Kuninaka, A., and Yoshino, H. (1974). Identity of Phosphodiesterase and Phosphomonoesterase Activities with Nuclease P1 (a Nuclease from Penicillium citrinum). Agric. Biol. Chem. **38**: 785–790.

Gatica, D., Lahiri, V., and Klionsky, D.J. (2018). Cargo recognition and degradation by selective autophagy. Nat. Cell Biol. 2018 203 **20**: 233–242.

Grove, R.P. (2019). Der Beitrag des Purin- und Pyrimidinkatabolismus zur Stickstoffremobilisierung in Arabidopsis.

Gupta, R., Hou, Z., Loussaert, D.F., Shen, B., and Wood, L.K. (2014). Engineering plants for efficient uptake and utilization of urea to improve crop production.: 491.

Hanson, A., Biology, J.G.I.-C. opinion in plant, and 2002, U. (2002). Synthesis and turnover of folates in plants. Curr. Opin. Plant Biol. **5**: 244–249.

Hanson, D.M. and Fairley, J.L. (1969). Enzymes of nucleic acid metabolism from wheat seedlings. I. Purification and general properties of associated deoxyribonuclease, ribonuclease, and 3'-nucleotidase activities. J. Biol. Chem. **244**: 2440–2449.

Haran, S., Logendra, S., Seskar, M., … M.B.-P., and 2000, U. (2000). Characterization of Arabidopsis acid phosphatase promoter and regulation of acid phosphatase expression. Plant Physiol. **124**: 615–626.

Hawkesford, M., Horst, W., Kichey, T., Lambers, H., Schjoerring, J., Møller, I.S., and White, P. (2012). Functions of Macronutrients. In Mineral Nutrition of Higher Plants (Academic Press), pp. 135–189.

Heinemann, K.J., Yang, S.-Y., Straube, H., Medina-Escobar, N., Varbanova-Herde, M.,

Herde, M., Rhee, S., and Witte, C.-P. (2021). Initiation of cytosolic plant purine nucleotide catabolism involves a monospecific xanthosine monophosphate phosphatase. Nat. Commun. **12**: 1–9.

Herz, S., Eberhardt, S., Phytochemistry, A.B.-, and 2000, U. (2000). Biosynthesis of riboflavin in plants. The ribA gene of Arabidopsis thaliana specifies a bifunctional GTP cyclohydrolase II/3, 4-dihydroxy-2-butanone 4. Phytochemistry **53**: 723–731.

Hickl, D. et al. (2021). Differential degradation of RNA species by autophagy-related pathways in Arabidopsis. J. Exp. Bot. **72**: 6867–6881.

Hickl, D. et al. (2019). Differential degradation of RNA species by autophagy related pathways in plants. bioRxiv: 793950.

Hillwig, M.S., Contento, A.L., Meyer, A., Ebany, D., Bassham, D.C., and MacIntosh, G.C. (2011). RNS2, a conserved member of the RNase T2 family, is necessary for ribosomal RNA decay in plants. Proc. Natl. Acad. Sci. **108**: 1093–1098.

Hirel, B., Tétu, T., Lea, P.J., and Dubois, F. (2011). Improving Nitrogen Use Efficiency in Crops for Sustainable Agriculture. Sustainability **3**: 1452–1485.

Hirota, T., Izumi, M., Wada, S., Makino, A., and Ishida, H. (2018). Vacuolar protein degradation via autophagy provides substrates to amino acid catabolic pathways as an adaptive response to sugar starvation in arabidopsis thaliana. Plant Cell Physiol. **59**: 1363–1376.

Hodson, R.C., Williams 2nd, S.K., and Davidson Jr, W.R. (1975). Metabolic control of urea catabolism in Chlamydomonas reinhardi and Chlorella pyrenoidosa. J. Bacteriol. **121**: 1022–1035.

Huang, H., Kawamata, T., Horie, T., Tsugawa, H., Nakayama, Y., Ohsumi, Y., and Fukusaki, E. (2015). Bulk RNA degradation by nitrogen starvation-induced autophagy in yeast. Eur. Mol. Biol. Organ. J. **34**: 154–168.

Hurley, B.A., Tran, H.T., Marty, N.J., Park, J., Snedden, W.A., Mullen, R.T., and Plaxton, W.C. (2010). The Dual-Targeted Purple Acid Phosphatase Isozyme AtPAP26 Is Essential for Efficient Acclimation of Arabidopsis to Nutritional Phosphate Deprivation. Plant

Physiol. **153**: 1112.

Irie, M. (1999). Structure-function relationships of acid ribonucleases: lysosomal, vacuolar, and periplasmic enzymes. Pharmacol. Ther. **81**: 77–89.

Johansen, T. and Lamark, T. (2020). Selective Autophagy: ATG8 Family Proteins, LIR Motifs and Cargo Receptors. J. Mol. Biol. **432**: 80–103.

Jones, Clain and Jeff Jacobsen (2013). Plant nutrition and soil fertility. Nutr. Manag. Modul. **2**: 1–11.

Jung, B., Flörchinger, M., Kunz, H.-H., Traub, M., Wartenberg, R., Jeblick, W., Neuhaus, H.E., and Möhlmann, T. (2009). Uridine-Ribohydrolase Is a Key Regulator in the Uridine Degradation Pathway of Arabidopsis. Plant Cell **21**: 876.

Jung, Y. et al. (2020). Caenorhabditis elegans Lipin 1 moderates the lifespan-shortening effects of dietary glucose by maintaining ω-6 polyunsaturated fatty acids. Aging Cell **19**: e13150.

Kaland, P.J. (2021). Untersuchung der subzellulären Lokalisation einiger Purple Acid Phosphatasen und S1 Endonukleasen von Arabidopsis thaliana, sowie die biochemische Charakterisierung der Endonuklease Endo5.

Kanamori, T., Kanou, N., Atomi, H., and Imanaka, T. (2004a). Enzymatic Characterization of a Prokaryotic Urea Carboxylase. J. Bacteriol. **186**: 2532–2539.

Kanamori, T., Kanou, N., Atomi, H., and Imanaka, T. (2004b). Enzymatic Characterization of a Prokaryotic Urea Carboxylase. J. Bacteriol. **186**: 2532–2539.

Katahira, R. and Ashihara, H. (2002). Profiles of pyrimidine biosynthesis, salvage and degradation in disks of potato (Solanum tuberosum L.) tubers. Planta 2002 2155 **215**: 821–828.

Keys, A.J. (2006). The re-assimilation of ammonia produced by photorespiration and the nitrogen economy of C3 higher plants. Photosynth. Res. **87**: 165–175.

Khayyo, V.I., Hoffmann, R.M., Wang, H., Bell, J.A., Burke, J.E., Reue, K., and Airola, M.V.V. (2020). Crystal structure of a lipin/Pah phosphatidic acid phosphatase. Nat. Commun. **11**: 1–11.

Kirkin, V. (2020). History of the Selective Autophagy Research: How Did It Begin and Where Does It Stand Today? J. Mol. Biol. **432**: 3–27.

Kleine-Vehn, J., Leitner, J., Zwiewka, M., Sauer, M., Abas, L., Luschnig, C., and Friml, J. (2008). Differential degradation of PIN2 auxin efflux carrier by retromer-dependent vacuolar targeting. Proc. Natl. Acad. Sci. U. S. A. **105**: 17812–17817.

Klepikova, A. V., Kasianov, A.S., Gerasimov, E.S., Logacheva, M.D., and Penin, A.A. (2016). A high resolution map of the Arabidopsis thaliana developmental transcriptome based on RNA-seq profiling. Plant J. **88**: 1058–1070.

Klimczyk, M., Siczek, A., and Schimmelpfennig, L. (2021). Improving the efficiency of urea-based fertilization leading to reduction in ammonia emission. Sci. Total Environ. **771**: 145483.

Klionsky, D.J. and Emr, S.D. (2000). Autophagy as a Regulated Pathway of Cellular Degradation.

Kojima, S., Bohner, A., Gassert, B., Yuan, L., and Wirén, N. Von (2007). AtDUR3 represents the major transporter for high-affinity urea transport across the plasma membrane of nitrogen-deficient Arabidopsis roots. Plant J. **52**: 30–40.

Koncz, C. and Schell, J. (1986). The promoter of TL-DNA gene 5 controls the tissue-specific expression of chimaeric genes carried by a novel type of Agrobacterium binary vector. Mol. Gen. Genet. **204**: 383–396.

Kraft, C., Deplazes, A., Sohrmann, M., and Peter, M. (2008). Mature ribosomes are selectively degraded upon starvation by an autophagy pathway requiring the Ubp3p/Bre5p ubiquitin protease. Nat. Cell Biol. 2008 105 **10**: 602–610.

Krogmeier, M.J., McCarty, G.W., and Bremner, J.M. (1989). Phytotoxicity of foliar-applied urea. Proc. Natl. Acad. Sci. U. S. A. **86**: 8189–8191.

Kumar, S. and Mohapatra, T. (2021). Deciphering Epitranscriptome: Modification of mRNA Bases Provides a New Perspective for Post-transcriptional Regulation of Gene Expression. Front. Cell Dev. Biol. **9**: 550.

Lamesch, P. et al. (2012). The Arabidopsis Information Resource (TAIR): improved gene annotation and new tools. Nucleic Acids Res. **40**: D1202–D1210.

Lanzetta, P.A., Alvarez, L.J., Reinach, P.S., and Candia, O.A. (1979). An Improved Assay for Nanomole Amounts of Inorganic Phosphate.

Lau, T.C. and Stephenson, A.G. (1994). Effects of soil phosphorus on pollen production, pollen size, pollen phosphorus content, and the ability to sire seeds in Cucurbita pepo (Cucurbitaceae). Sex. Plant Reprod. **7**: 215–220.

Lauxmann, M.A. et al. (2016). Reproductive failure in Arabidopsis thaliana under transient carbohydrate limitation: flowers and very young siliques are jettisoned and the meristem is maintained to allow successful resumption of reproductive growth. Plant. Cell Environ. **39**: 745–767.

Lazo, G.R., Stein, P.A., and Ludwig, R.A. (1991). A DNA Transformation–Competent Arabidopsis Genomic Library in Agrobacterium. Nat. Biotechnol. **9**: 963–967.

Lemasters, J.J. (2005). Selective mitochondrial autophagy, or mitophagy, as a targeted defense against oxidative stress, mitochondrial dysfunction, and aging. Rejuvenation Res. **8**: 3–5.

Lesniewicz, K., Karlowski, W.M., Pienkowska, J.R., Krzywkowski, P., and Poreba, E. (2013). The Plant S1-Like Nuclease Family Has Evolved a Highly Diverse Range of Catalytic Capabilities. Plant Cell Physiol. **54**: 1064–1078.

Li, D., Zhu, H., Liu, K., Liu, X., Leggewie, G., Udvardi, M., and Wang, D. (2002). Purple Acid Phosphatases of Arabidopsis thaliana: COMPARATIVE ANALYSIS AND DIFFERENTIAL REGULATION BY PHOSPHATE DEPRIVATION *. J. Biol. Chem. **277**: 27772–27781.

Lightle, H., Fosco, S., … R.G.-A.J. of, and 2021, U. (2021). Vigna radiata (mung bean) acid phosphatase is difficult to purify and may have a role as a vegetative Storage protein. African J. Biotechnol. **20**: 275–286.

Likens, G.E., Driscoll, C.T., and Buso, D.C. (1996). Long-Term Effects of Acid Rain: Response and Recovery of a Forest Ecosystem. Science (80-.). **272**: 244–246.

Lim, E.K. and Bowles, D.J. (2004). A class of plant glycosyltransferases involved in cellular homeostasis. EMBO J. **23**: 2915–2922.

Liu, Y., Ahn, J.E., Datta, S., Salzman, R.A., Moon, J., Huyghues-Despointes, B., Pittendrigh, B., Murdock, L.L., Koiwa, H., and Zhu-Salzman, K. (2005). Arabidopsis vegetative storage protein is an anti-insect acid phosphatase. Plant Physiol. **139**: 1545–1556.

Lodish, H., Berk, A., Zipursky, S.L., Matsudaira, P., Baltimore, D., and Darnell, J. (2000). Molecular Cell Biology (W. H. Freeman).

MacIntosh, G., Autophagy, D.B.-, and 2011, undefined (2011). The connection between ribophagy, autophagy and ribosomal RNA decay. Taylor Fr. **7**: 662–663.

Mackerell, A.D. (2004). Empirical force fields for biological macromolecules: Overview and issues. J. Comput. Chem. **25**: 1584–1604.

Maitz, G.S. and Haas, E.M. (1982). Purification and properties of the allophanate hydrolase from Chlamydomonas reinhardii. Biochim. Biophys. Acta (BBA)-General Subj. **714**: 486–491.

Makino, S., Kawamata, T., Iwasaki, S., and Ohsumi, Y. (2021). Selectivity of mRNA degradation by autophagy in yeast. Nat. Commun. **12**: 1–10.

Masclaux-Daubresse, C., Daniel-Vedele, F., Dechorgnat, J., Chardon, F., Gaufichon, L., and Suzuki, A. (2010). Nitrogen uptake, assimilation and remobilization in plants: challenges for sustainable and productive agriculture. Ann. Bot. **105**: 1141–1157.

Melino, V.J., Casartelli, A., George, J, Rupasinghe, T., Roessner, U., Okamoto, M., and Heuer, S. (2018). RNA Catabolites Contribute to the Nitrogen Pool and Support Growth Recovery of Wheat. Front. Plant Sci. **9**: 1539.

Michaeli, S. and Galili, G. (2014). Degradation of Organelles or Specific Organelle Components via Selective Autophagy in Plant Cells. Int. J. Mol. Sci. **15**: 7624–7638.

Mitsuhashi, N., Shimada, T., Mano, S., Nishimura, M., and Hara-Nishimura, I. (2000). Characterization of Organelles in the Vacuolar-Sorting Pathway by Visualization with GFP in Tobacco BY-2 Cells. Plant Cell Physiol. **41**: 993–1001.

Mizushima, N. and Komatsu, M. (2011). Autophagy: Renovation of Cells and Tissues. Cell **147**: 728–741.

Montalbini, P. and Torre, G. Della (1995). Allopurinol metabolites and xanthine accumulation in allopurinol-treated tobacco. J. Plant Physiol. **147**: 321–327.

Mü, K. (2007). Protein dynamics and proteolysis in plant vacuoles. J. Exp. Bot. **58**: 2391–2407.

Myrach, T. (2015). Harnstoffabbau in Arabidopsis thaliana und Oryza sativa: Untersuchung der katalysierten Aktivierung von Urease und biotechnologischer Ansatz zur Verbesserung der Harnstoffnutzung.

Nasb, M., Kirberger, M., and Chen, N. (2021). Molecular Processes and Regulation of Autophagy. Exerc. Autophagy Chronic Dis.: 1–27.

Navarathna, D.H.M.L.P., Harris, S.D., Roberts, D.D., and Nickerson, K.W. (2010). Evolutionary aspects of urea utilization by fungi. FEMS Yeast Res. **10**: 209–213.

Neves, J., Sampaio, M., Séneca, A., Pereira, S., Pissarra, J., and Pereira, C. (2021). Abiotic Stress Triggers the Expression of Genes Involved in Protein Storage Vacuole and Exocyst-Mediated Routes. Int. J. Mol. Sci. **22**: 10644.

Norton, J. and Ouyang, Y. (2019). Controls and Adaptive Management of Nitrification in Agricultural Soils. Front. Microbiol. **10**: 1931.

Paris, N., Stanley, C.M., Jones, R.L., and Rogers, J.C. (1996). Plant cells contain two functionally distinct vacuolar compartments. Cell **85**: 563–572.

Pedley, A.M. and Benkovic, S.J. (2017). A New View into the Regulation of Purine Metabolism – The Purinosome. Trends Biochem. Sci. **42**: 141–154.

Peoples, M.B., Freney, J.R., and Mosier, A.R. (1995). Minimizing gaseous losses of nitrogen. In Nitrogen fertilization in the environment, pp. 565–602.

Del Pozo, J.C., Allona, I., Rubio, V., Leyva, A., De La Peña, A., Aragoncillo, C., and Paz-Ares, J. (1999). A type 5 acid phosphatase gene from Arabidopsis thaliana is induced by phosphate starvation and by some other types of phosphate mobilising/oxidative stress conditions. Plant J. **19**: 579–589.

Proudfoot, M., Kuznetsova, E., Brown, G., Rao, N.N., Kitagawa, M., Mori, H., Savchenko, A., and Yakunin, A.F. (2004). General Enzymatic Screens Identify Three New Nucleotidases in Escherichia coli: BIOCHEMICAL CHARACTERIZATION OF SurE, YfbR, AND YjjG. J. Biol. Chem. **279**: 54687–54694.

Raj, A., Rifkin, S.A., Andersen, E., and Van Oudenaarden, A. (2010). Variability in gene expression underlies incomplete penetrance. Nature **463**: 913–918.

Rathore, S.K. and Pati, P. (2021). RNA–Protein Interaction Analysis. Bioinforma. Rice Res.: 335–359.

Razaq, M., Zhang, P., Shen, H., and Salahuddin (2017). Influence of nitrogen and phosphorous on the growth and root morphology of Acer mono. PLoS One **12**: 1–13.

Rea, P.A. and Sanders, D. (1987). Tonoplast energization: Two H+ pumps, one membrane. Physiol. Plant. **71**: 131–141.

Reddy, V.S., Rao, D.K.V., and Rajasekharan, R. (2010). Functional characterization of lysophosphatidic acid phosphatase from Arabidopsis thaliana. Biochim. Biophys. Acta - Mol. Cell Biol. Lipids **1801**: 455–461.

Reddy, V.S., Singh, A.K., and Rajasekharan, R. (2008). The Saccharomyces cerevisiae PHM8 gene encodes a soluble magnesium-dependent lysophosphatidic acid phosphatase. J. Biol. Chem. **283**: 8846–8854.

Riegler, H., Geserick, C., and Zrenner, R. (2011). Arabidopsis thaliana nucleosidase mutants provide new insights into nucleoside degradation. New Phytol. **191**: 349.

Roberts, P., Moshitch-Moshkovitz, Kvam, E., O'Toole, E., Winey, M., and Goldfarb, D.S. (2003). Piecemeal microautophagy of nucleus in Saccharomyces cerevisiae. Mol. Biol. Cell **14**: 129–141.

Robinson, D. (2003). The Golgi apparatus and the plant secretory pathway. In Sorting of lytic enzymes in the plant Golgi apparatus (OxfordBlackwell Publishing), pp. 114–140.

Robinson, W.D., Carson, I., Ying, S., Ellis, K., and Plaxton, W.C. (2012). Eliminating the purple acid phosphatase AtPAP26 in Arabidopsis thaliana delays leaf senescence and

impairs phosphorus remobilization. New Phytol. **196**: 1024–1029.

Roon, R.J. and Levenberg, B. (1972). Urea Amidolyase: I. PROPERTIES OF THE ENZYME FROM CANDIDA UTILIS. J. Biol. Chem. **247**: 4107–4113.

Saha, B.K., Rose, M.T., Zwieten, L.V., Wong, V.N.L., and Patti, A.F. (2021). Slow Release Brown Coal-Urea Fertilizer Potentially Influences Greenhouse Gas Emissions, Nitrogen Use Efficiency, and Sweet Corn Yield in Oxisol. ACS Agric. Sci. Technol. **1**: 469–478.

Saheb, E., Biton, I., Maringer, K., and Bush, J. (2013). A functional connection of Dictyostelium paracaspase with the contractile vacuole and a possible partner of the vacuolar proton ATPase. J. Biosci. **38**: 509–521.

Schenk, G., Mitić, N.Š., Hanson, G.R., and Comba, P. (2013). Purple acid phosphatase: A journey into the function and mechanism of a colorful enzyme. Coord. Chem. Rev. **257**: 473–482.

Sharma, S., Watzinger, P., Kötter, P., and Entian, K.D. (2013). Identification of a novel methyltransferase, Bmt2, responsible for the N-1-methyl-adenosine base modification of 25S rRNA in Saccharomyces cerevisiae. Nucleic Acids Res. **41**: 5428–5443.

Shen, J., Zeng, Y., Zhuang, X., Sun, L., Yao, X., Pimpl, P., and Jiang, L. (2013). Organelle pH in the arabidopsis endomembrane system. Mol. Plant **6**: 1419–1437.

Shimaoka, T., M, O., T, S., N, M., I, H.-N., K, S., M, M., A, Y., K, T., and T, M. (2004). Isolation of intact vacuoles and proteomic analysis of tonoplast from suspension-cultured cells of Arabidopsis thaliana. Plant Cell Physiol. **45**: 672–683.

Shishido, K. and Ando, T. (1975). Action of Single-strand-specific S1 Endonuclease on Locally Altered Structures in Double-stranded DNA. Agric. Biol. Chem. **39**: 673–681.

Staswick, P., Papa, C., and Huang, J. (1994). Purification of the major soybean leaf acid phosphatase that is increased by seed-pod removal. Plant Physiol. **104**: 49–57.

Straube, H., Witte, C.P., and Herde, M. (2021). Analysis of Nucleosides and Nucleotides in Plants: An Update on Sample Preparation and LC-MS Techniques. Cells **10**: 689.

Strope, P.K., Nickerson, K.W., Harris, S.D., and Moriyama, E.N. (2011). Molecular

evolution of urea amidolyase and urea carboxylase in fungi. BMC Evol. Biol. **11**: 1–15.

Sultenfuss, J.H. and Doyle, W.J. (1999). Functions of Phosphorus in Plants. In Better crops with plant food, pp. 6–7.

Sumrada, R.A. and Cooper, T.G. (1982). Urea Carboxylase and Allophanate Hydrolase Are Components of a Multifunctional Protein in Yeast. J. Biol. Chem. **25**: 9119–9127.

Sun, L., Wang, L., Zheng, Z., and Liu, D. (2018). Identification and characterization of an Arabidopsis phosphate starvation-induced secreted acid phosphatase as a vegetative storage protein. Plant Sci. **277**: 278–284.

Sun, Z. and Brodsky, J.L. (2018). The degradation pathway of a model misfolded protein is determined by aggregation propensity. Mol. Biol. Cell **29**: 1422–1434.

Tamura, K., Shimada, T., Ono, E., Tanaka, Y., Nagatani, A., Higashi, S.I., Watanabe, M., Nishimura, M., and Hara-Nishimura, I. (2003). Why green fluorescent fusion proteins have not been observed in the vacuoles of higher plants. Plant J. **35**: 545–555.

Tatosyan, K.A., Ustyantsev, I.G., and Kramerov, D.A. (2020). RNA Degradation in Eukaryotic Cells. Mol. Biol. **54**: 485–502.

Thaller, M.C., Schippa, S., and Rossolini, G.M. (1998a). Conserved sequence motifs among bacterial, eukaryotic, and archaeal phosphatases that define a new phosphohydrolase superfamily. Protein Sci. **7**: 1647–1652.

Thaller, M.C., Schippa, S., and Rossolini, G.M. (1998b). Conserved sequence motifs among bacterial, eukaryotic, and archaeal phosphatases that define a new phosphohydrolase superfamily. Protein Sci. **7**: 1647–1652.

Thuynsma, R., Kleinert, A., Kossmann, J., Valentine, A.J., and Hills, P.N. (2016). The effects of limiting phosphate on photosynthesis and growth of Lotus japonicus. South African J. Bot. **104**: 244–248.

Todde, V., Veenhuis, M., and van der Klei, I.J. (2009). Autophagy: Principles and significance in health and disease. Biochim. Biophys. Acta - Mol. Basis Dis. **1792**: 3–13.

Trapnell, C., Pachter, L., and Salzberg, S.L. (2009). TopHat: discovering splice junctions with

RNA-Seq. Bioinformatics **25**: 1105–1111.

Triques, K., Sturbois, B., Gallais, S., Dalmais, M., Chauvin, S., Clepet, C., Aubourg, S., Rameau, C., Caboche, M., and Bendahmane, A. (2007). Characterization of Arabidopsis thaliana mismatch specific endonucleases: application to mutation discovery by TILLING in pea. Plant J. **51**: 1116–1125.

Tucker, T.C. (2015). Diagnosis of Nitrogen Deficiency in Plants. In Nitrogen in Crop Production, pp. 247–262.

Tzin, V. and Galili, G. (2010). New Insights into the Shikimate and Aromatic Amino Acids Biosynthesis Pathways in Plants. Mol. Plant **3**: 956–972.

Urarte, E., Esteban, R., Moran, J.F., and Bittner, F. (2015). Established and Proposed Roles of Xanthine Oxidoreductase in Oxidative and Reductive Pathways in Plants. React. Oxyg. nitrogen species Signal. Commun. plants: 15–42.

Veljanovski, V., Vanderbeld, B., Knowles, V.L., Snedden, W.A., and Plaxton, W.C. (2006). Biochemical and molecular characterization of AtPAP26, a vacuolar purple acid phosphatase up-regulated in phosphate-deprived Arabidopsis suspension cells and. Plant Physiol. **142**: 1282–1293.

Vitousek, P.M., Aber, J.D., Howarth, R.W., Likens, G.E., Matson, P.A., Schindler, D.W., Schlesinger, W.H., and Tilman, D.G. (1997). Human alteration of the global nitrogen cycle: sources and consequences. Ecol. Appl. **7**: 737–750.

Voinnet, O., Rivas, S., Mestre, P., and Baulcombe, D. (2003). An enhanced transient expression system in plants based on suppression of gene silencing by the p19 protein of tomato bushy stunt virus. Plant J. **33**: 949–956.

Wang, L., Li, Z., Qian, W., Guo, W., Gao, X., and Huang, L. (2011). The Arabidopsis purple acid phosphatase AtPAP10 is predominantly associated with the root surface and plays an important role in plant tolerance to phosphate. Plant Physiol. **157**: 1283–1299.

Wang, L. and Liu, D. (2012). Arabidopsis purple acid phosphatase 10 is a component of plant adaptive mechanism to phosphate limitation. Plant Signal. Behav. **7**: 306–310.

Wang, L., Lu, S., Zhang, Y., Li, Z., Du, X., and Liu, D. (2014a). Comparative genetic analysis of Arabidopsis purple acid phosphatases AtPAP10, AtPAP12, and AtPAP26 provides new insights into their roles in plant adaptation to phosphate deprivation. J. Integr. Plant Biol. **56**: 299–314.

Wang, Y., Noguchi, K., Ono, N., Inoue, S.I., Terashima, I., and Kinoshita, T. (2014b). Overexpression of plasma membrane H+-ATPase in guard cells promotes light-induced stomatal opening and enhances plant growth. Proc. Natl. Acad. Sci. U. S. A. **111**: 533–538.

Weber, E., Engler, C, Gruetzner, R., Werner, S., and Marillonnet, S. (2011). A Modular Cloning System for Standardized Assembly of Multigene Constructs. PLoS One **6**: e16765.

Witte, C.-P., Isidore, E., Tiller, S.A., Davies, H. V., and Taylor, M.A. (2001). Functional characterisation of urease accessory protein G (ureG) from potato. Plant Mol. Biol. **45**: 169–179.

Witte, C.-P., Rosso, M.G., and Romeis, T. (2005). Identification of Three Urease Accessory Proteins That Are Required for Urease Activation in Arabidopsis. Plant Physiol. **139**: 1155–1162.

Witte, C.P. and Herde, M. (2020). Nucleotide metabolism in plants. Plant Physiol. **182**: 63–78.

Witte, C.P., Tiller, S.A., Taylor, M.A., and Davies, H. V. (2002). Leaf urea metabolism in potato. Urease activity profile and patterns of recovery and distribution of 15N after foliar urea application in wild-type and urease-antisense transgenics. Plant Physiol. **128**: 1129–1136.

Xie, K., Minkenberg, B., and Yang, Y. (2015). Boosting CRISPR/Cas9 multiplex editing capability with the endogenous tRNA-processing system. Proc. Natl. Acad. Sci. U. S. A. **112**: 3570–3575.

Yagoub, S.O., Ahmed, W.M.A., and Mariod, A.A. (2012). Effect of Urea, NPK and Compost on Growth and Yield of Soybean (Glycine max L.), in Semi-Arid Region of Sudan. ISRN Agron.: 1–6.

Yang, S.Y., Huang, T.K., Kuo, H.F., and Chiou, T.J. (2017). Role of vacuoles in phosphorus storage and remobilization. J. Exp. Bot. **68**: 3045–3055.

Yin, C., Wang, F., Fan, H., Fang, Y., and Li, W. (2019). Identification of Tea Plant Purple Acid Phosphatase Genes and Their Expression Responses to Excess Iron. Int. J. Mol. Sci. **20**: 1954.

Yorimitsu, T. and Klionsky, D.J. (2005). Autophagy: molecular machinery for self-eating. Cell Death Differ. **12**: 1542–1552.

Yorimitsu, T. and Klionsky, D.J. (2007). Eating the endoplasmic reticulum: quality control by autophagy. Trends Cell Biol. **17**: 279–285.

Zamani, K., Sabet, M., Lohrasebi, T., Mousavi, A., and Malboobi, M. (2012). Improved phosphate metabolism and biomass production by overexpression of AtPAP18 in tobacco. Biologia (Bratisl). **67**: 713–720.

Zanin, L., Tomasi, N., Wirdnam, C., Meier, S., Komarova, N.Y., Mimmo, T., Cesco, S., Rentsch, D., and Pinton, R. (2014). Isolation and functional characterization of a high affinity urea transporter from roots of Zea mays. BMC Plant Biol. **14**: 1–15.

Zanin, L., Tomasi, N., Zamboni, A., Varanini, Z., and Pinton, R. (2015). The Urease Inhibitor NBPT Negatively Affects DUR3-mediated Uptake and Assimilation of Urea in Maize Roots. Front. Plant Sci. **6**: 1007.

Zhao, D., Reddy, K.R., Kakani, V.G., and Reddy, V.R. (2005). Nitrogen deficiency effects on plant growth, leaf photosynthesis, and hyperspectral reflectance properties of sorghum. Eur. J. Agron. **22**: 391–403.

Zrenner, R., and Ashihara, H. (2011). Nucleotide Metabolism. In Plant Metabolism and Biotechnology, pp. 135–162.

Zrenner, R., Riegler, H., Marquard, C.R., Lange, P.R., Geserick, C., Bartosz, C.E., Chen, C.T., and Slocum, R.D. (2009). A functional analysis of the pyrimidine catabolic pathway in Arabidopsis. New Phytol. **183**: 117–132.

Zrenner, R., Stitt, M., Sonnewald, U., and Boldt, R. (2006). Pyrimidine and Purine Biosynthesis and Degradation in Plants. Annu. Rev. Plant Biol. **57**: 805–836.

Appendix of Figures

Figure A 1. Expression profile of *PAPs* in *Arabidopsis thaliana* according to the publicly available Klepikova Atlas data in the Arabidopsis eFP Browser (http://bar.utoronto.ca/efp/cgi-bin/efpWeb.cgi?dataSource=Klepikova_Atlas). The level of transcript expression is indicated by a color code (yellow = low expression, red = high expression), and an absolute scale is also available on the left side of the image.
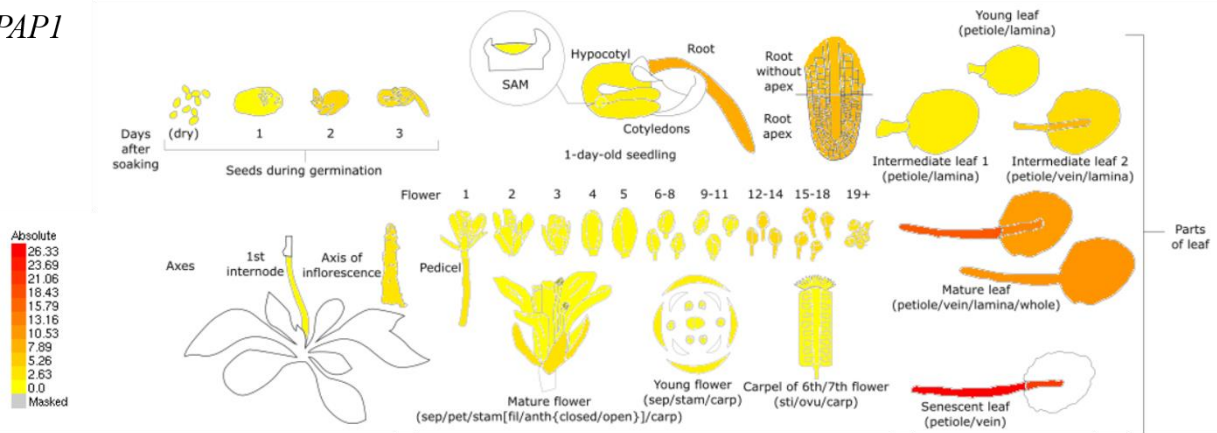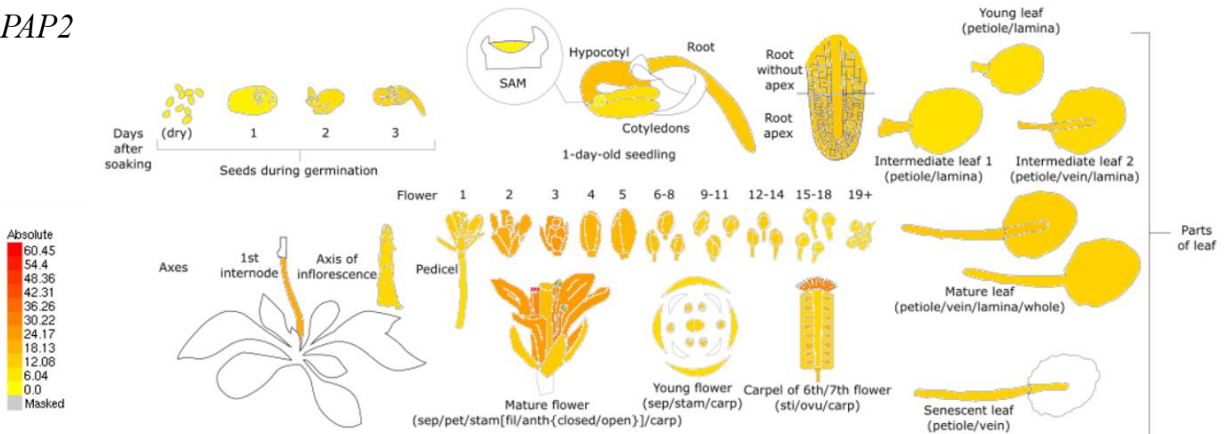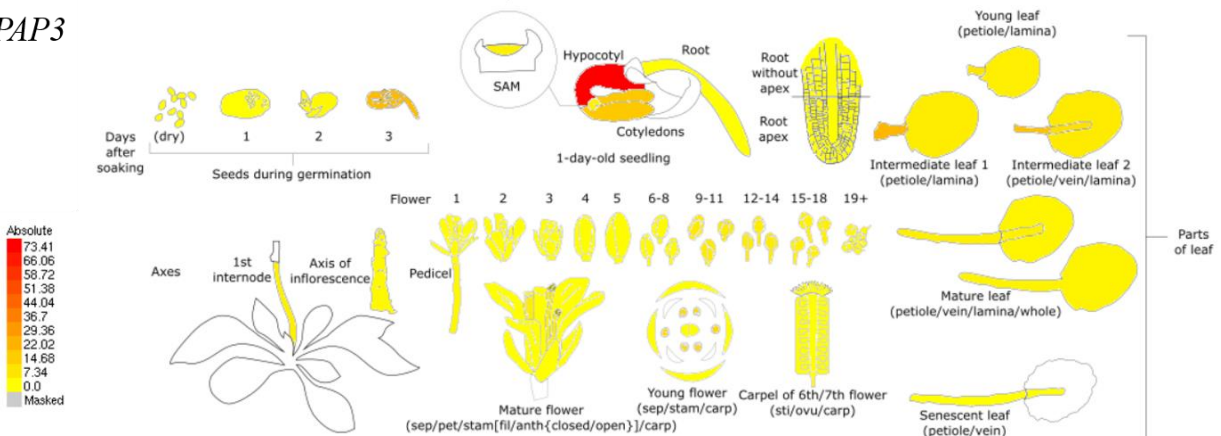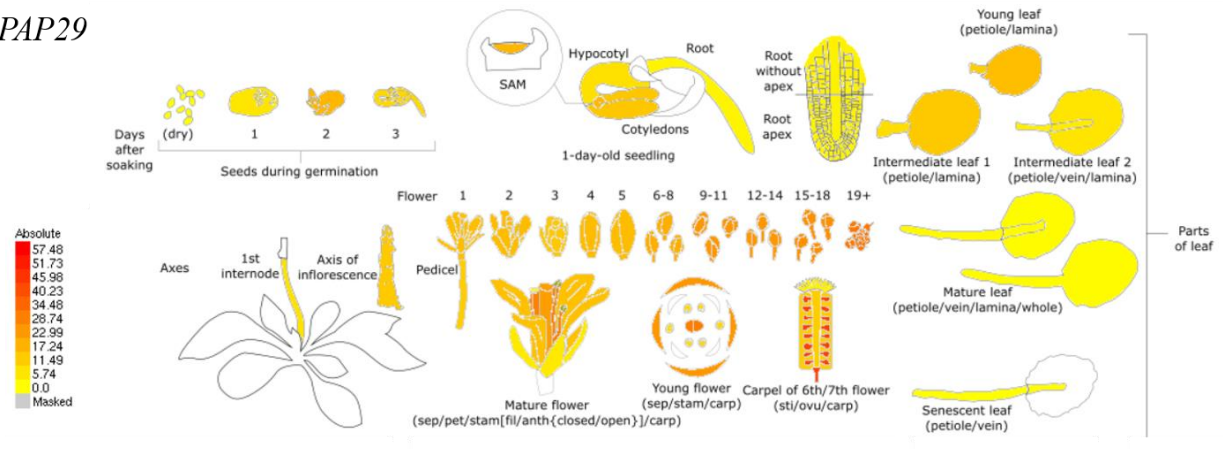
PAP4
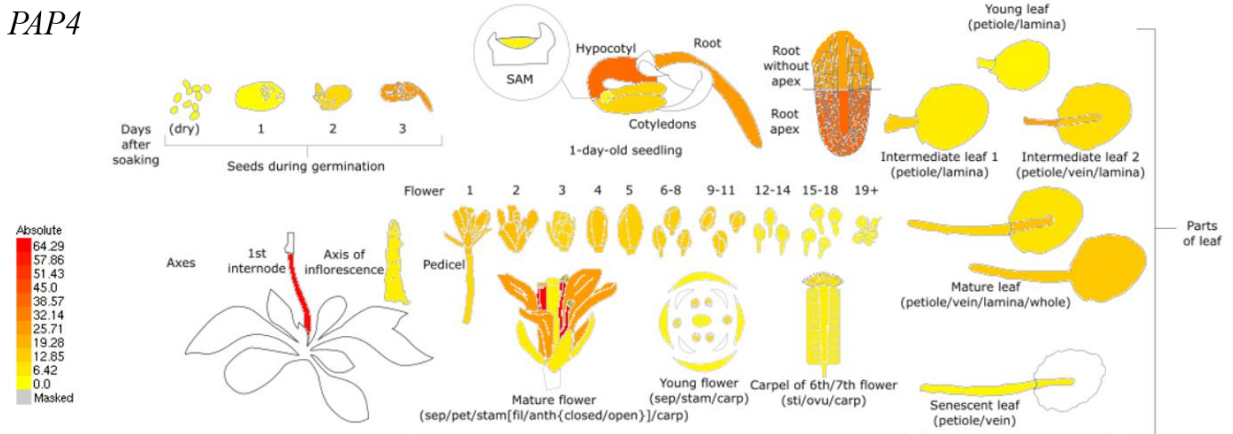
PAP5
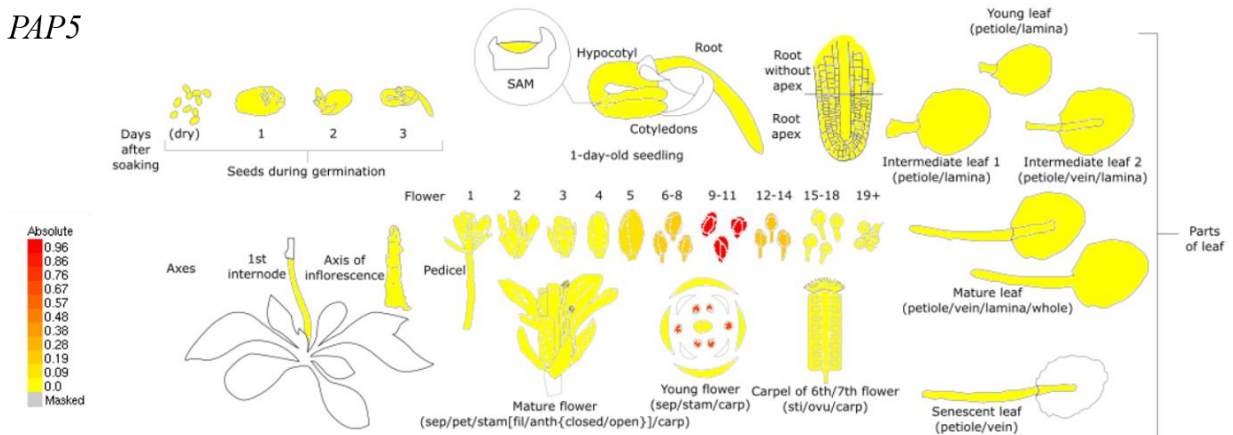
PAP6

PAP7

PAP8

PAP9

164

PAP10

PAP11

PAP12

165
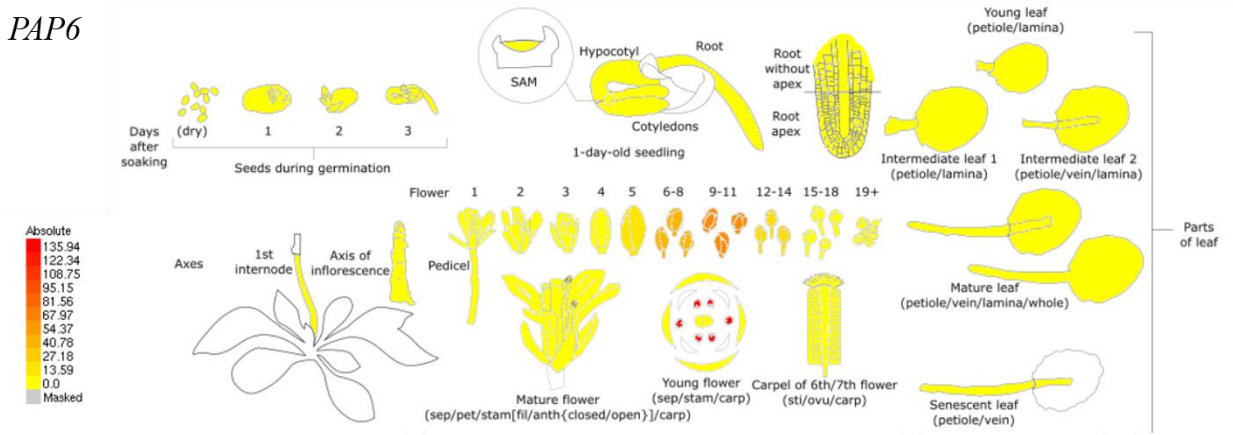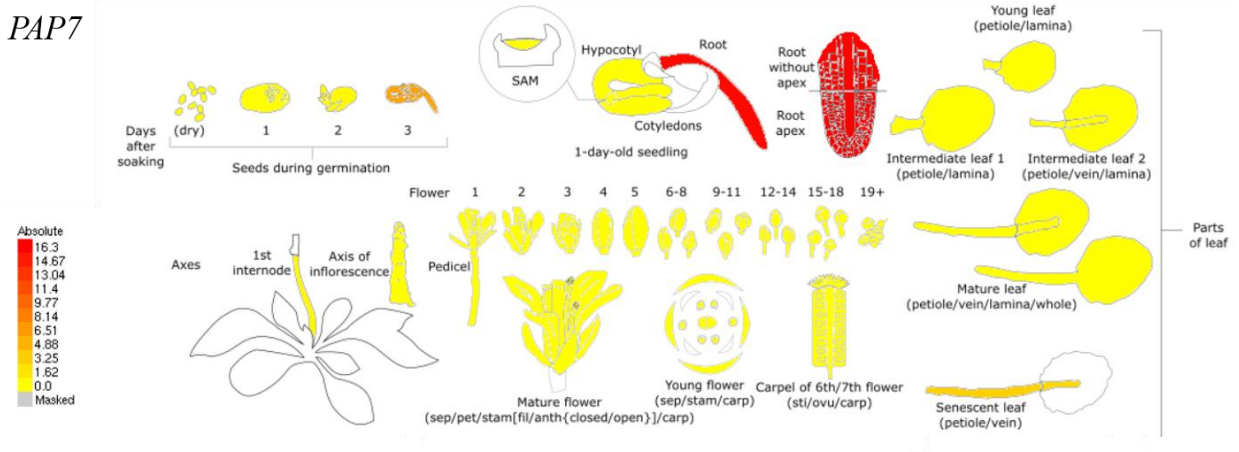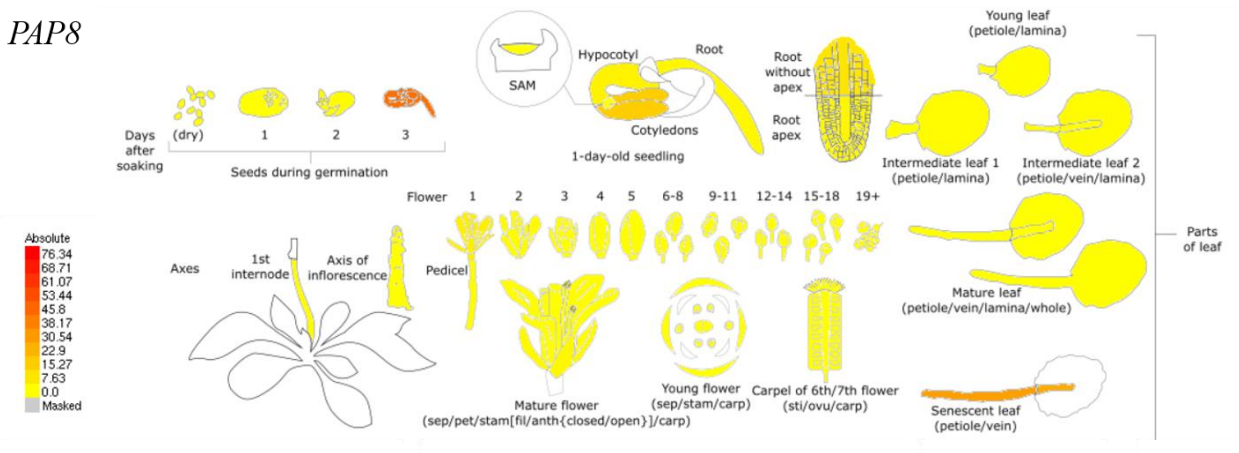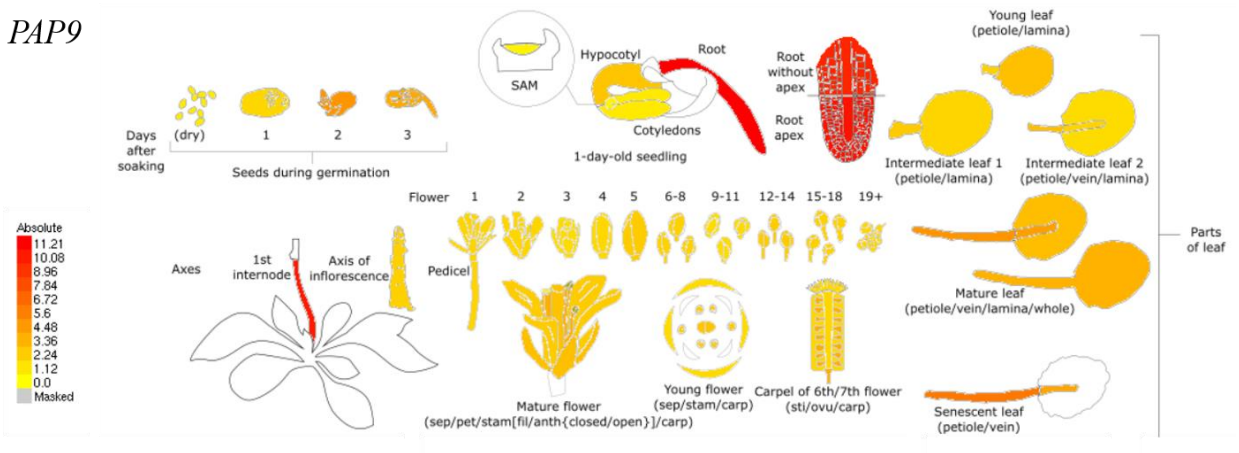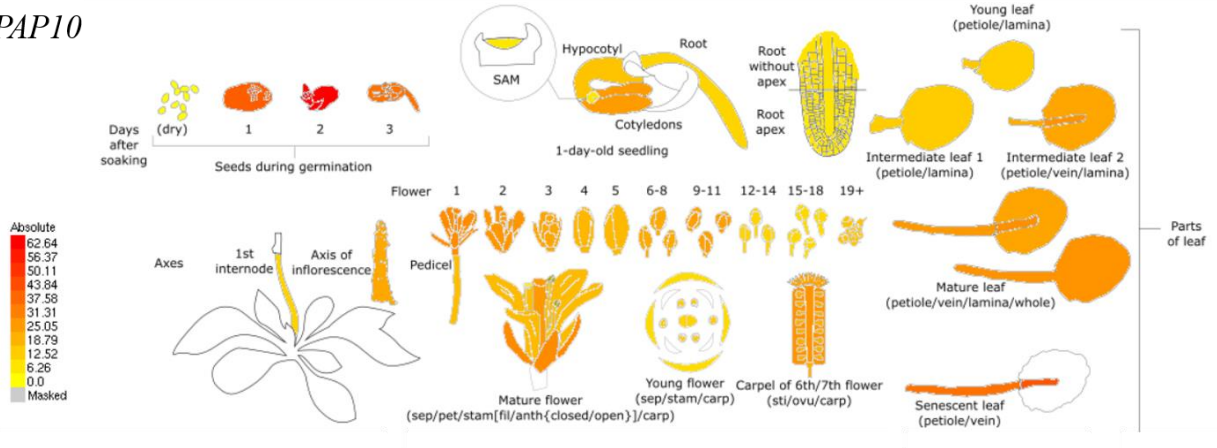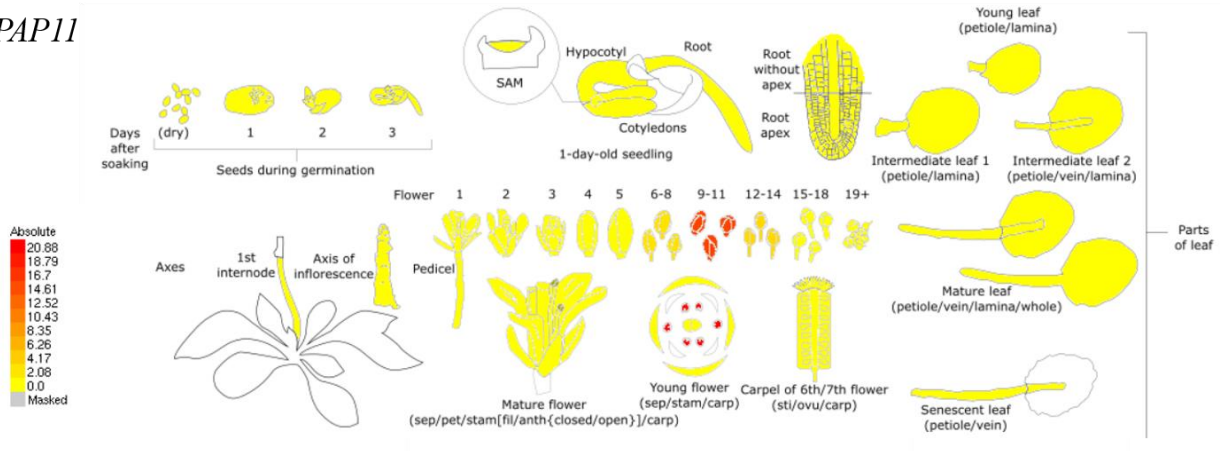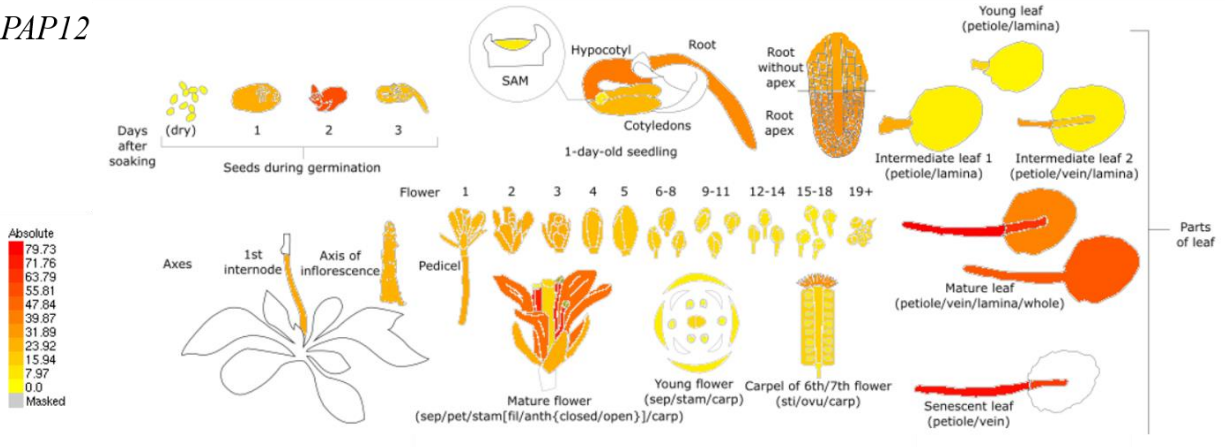
PAP13
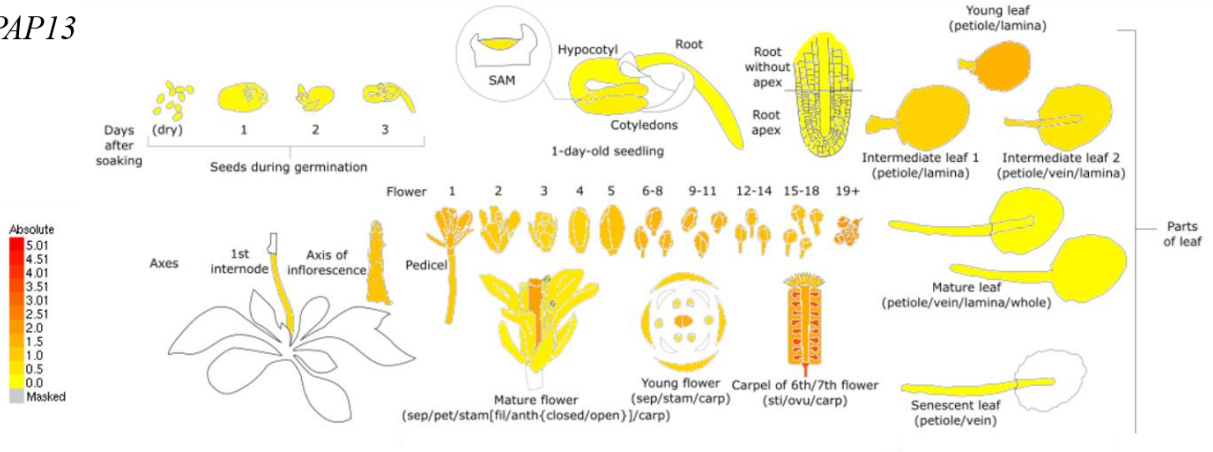
PAP14
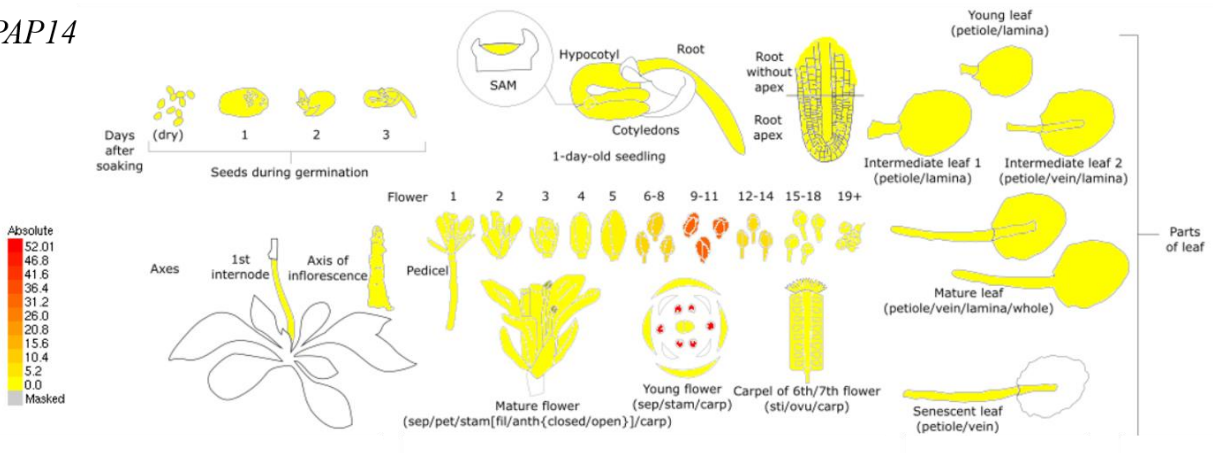
PAP15

PAP16

PAP17

PAP18

167

PAP19

PAP20

PAP21

168
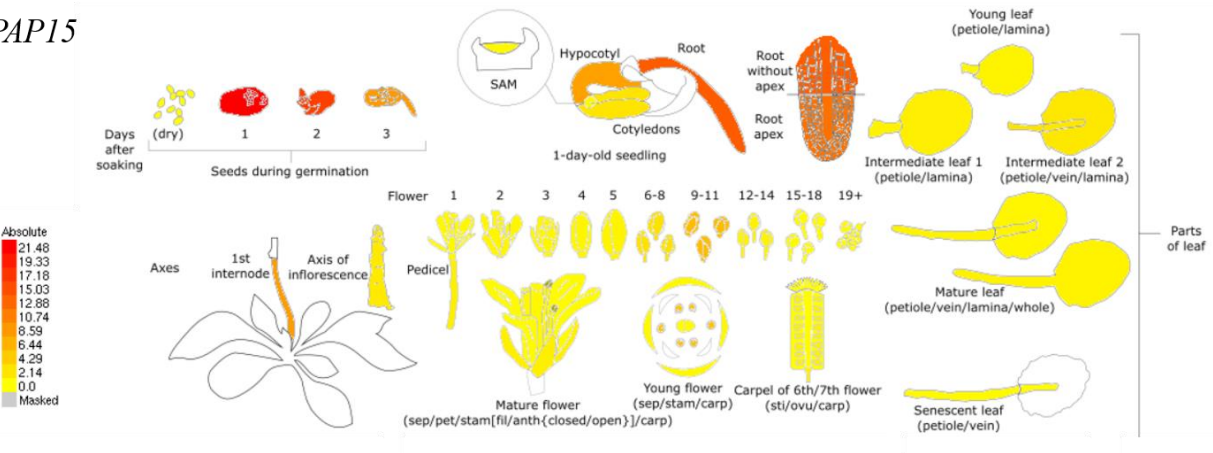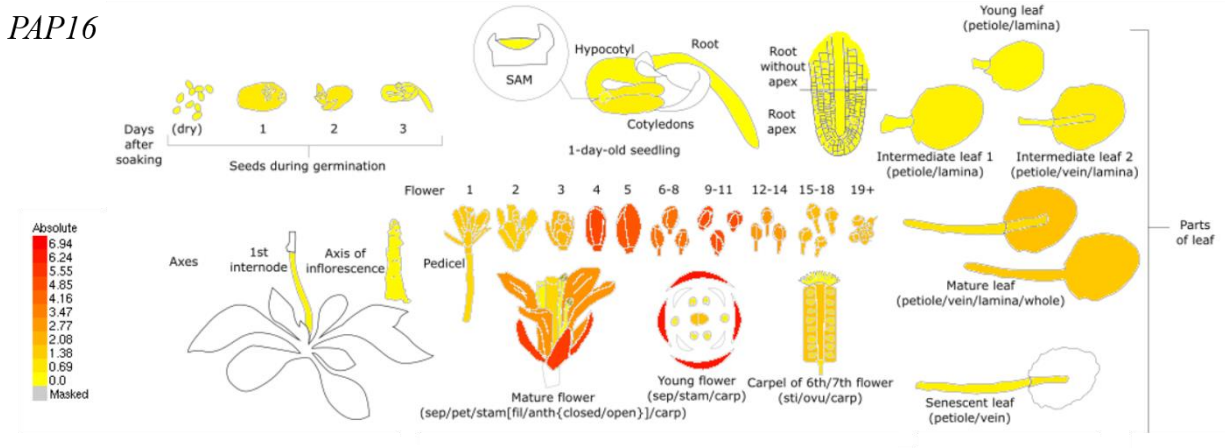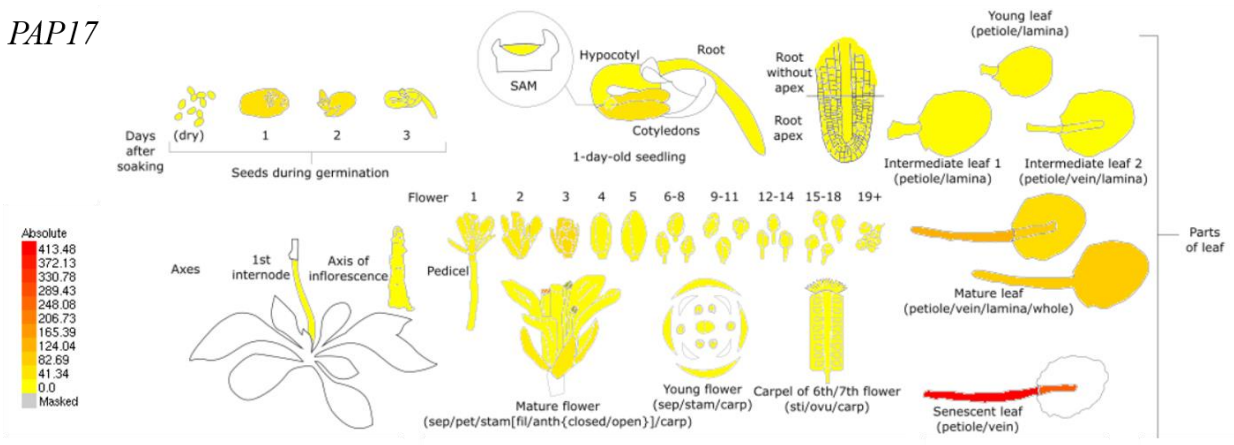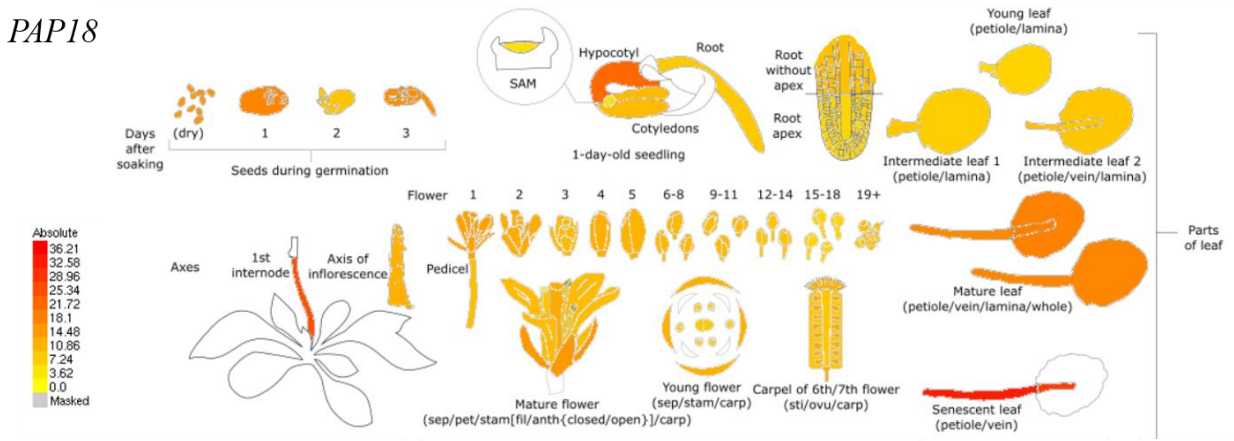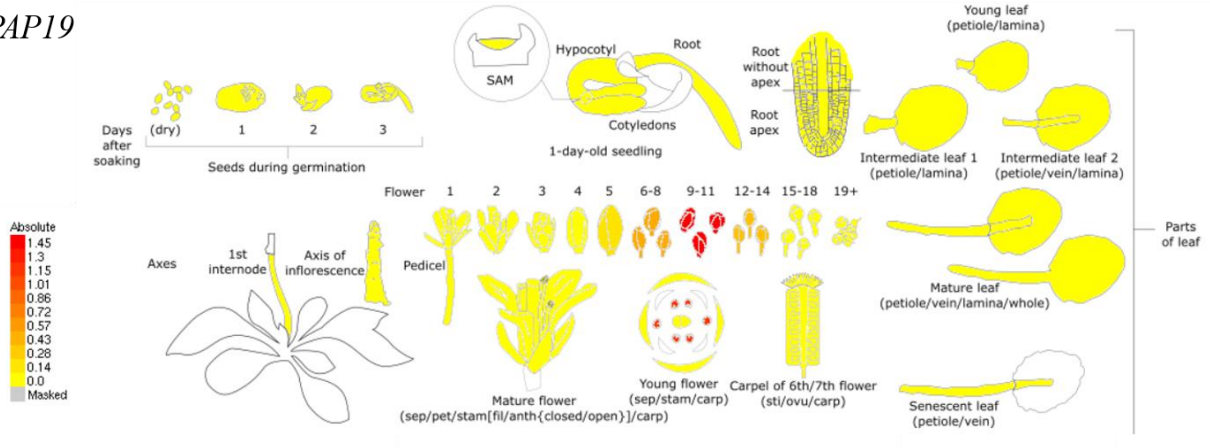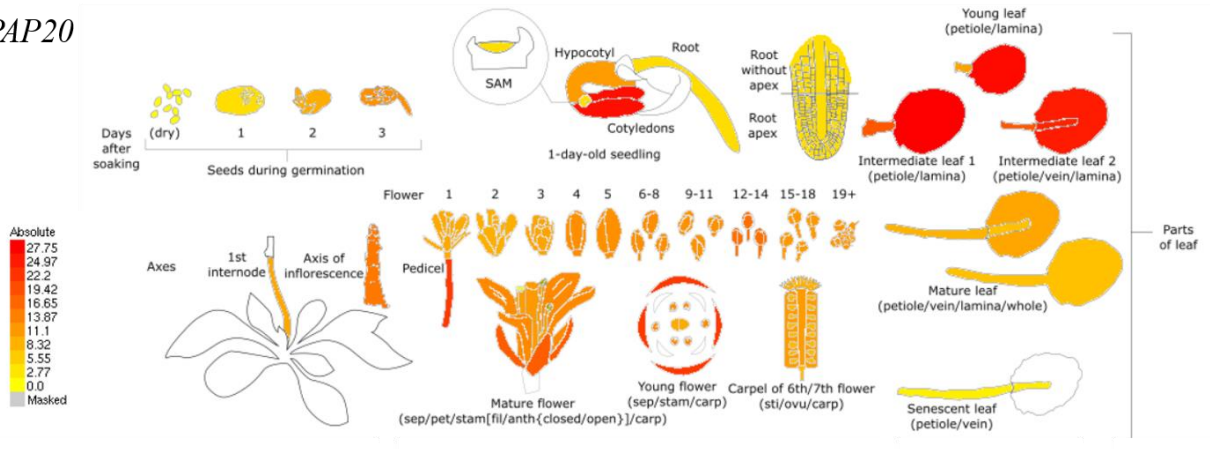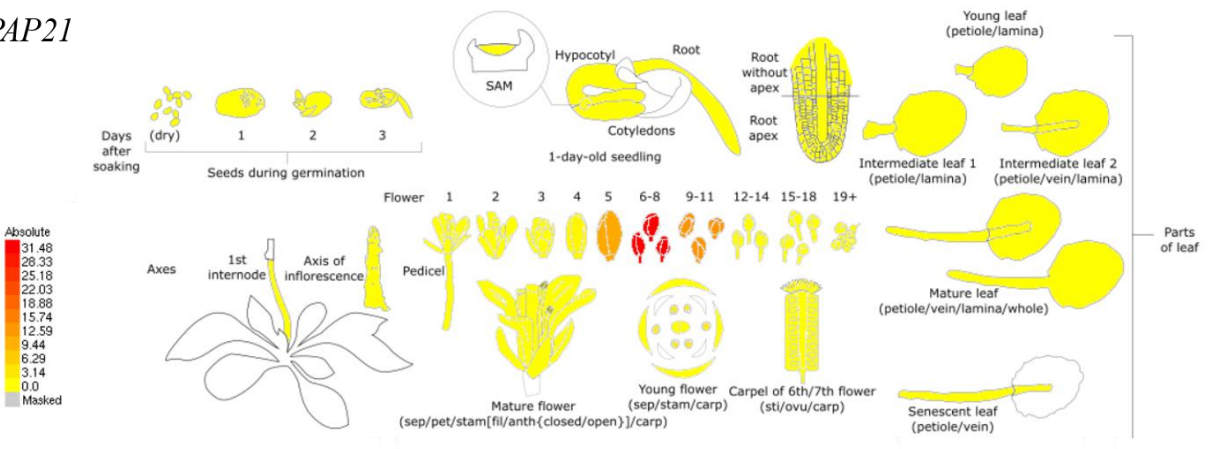
PAP22
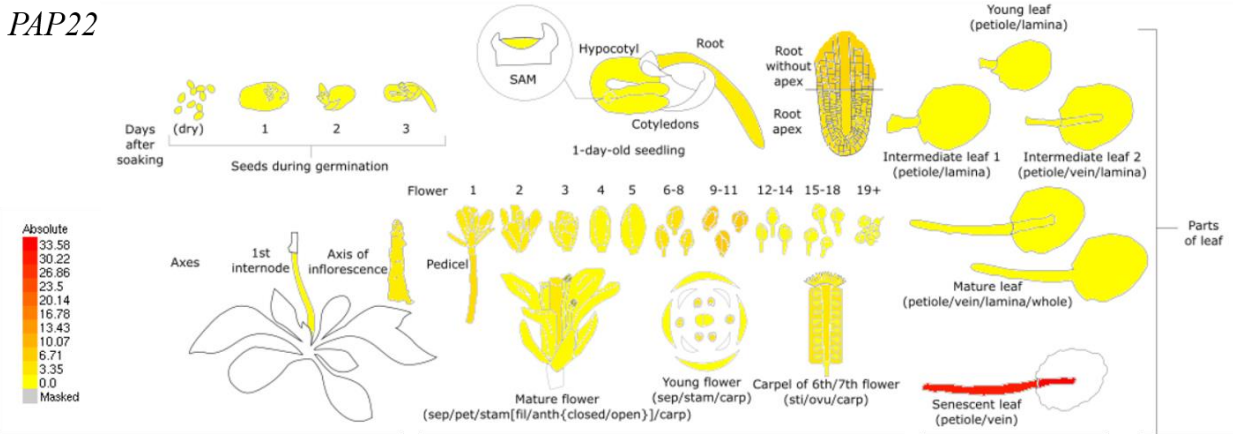
PAP23
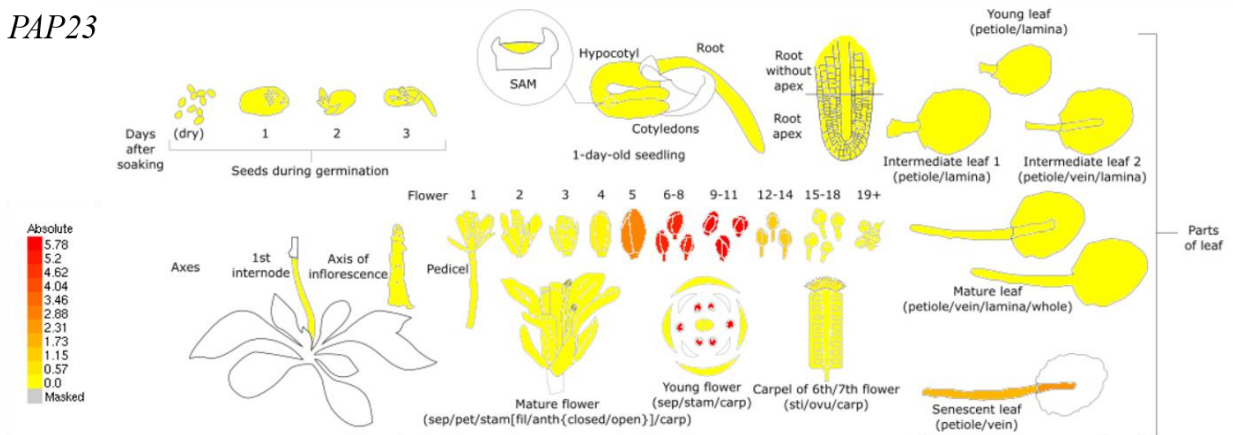
PAP24

PAP25

PAP26

PAP27

170

PAP28

PAP29

171
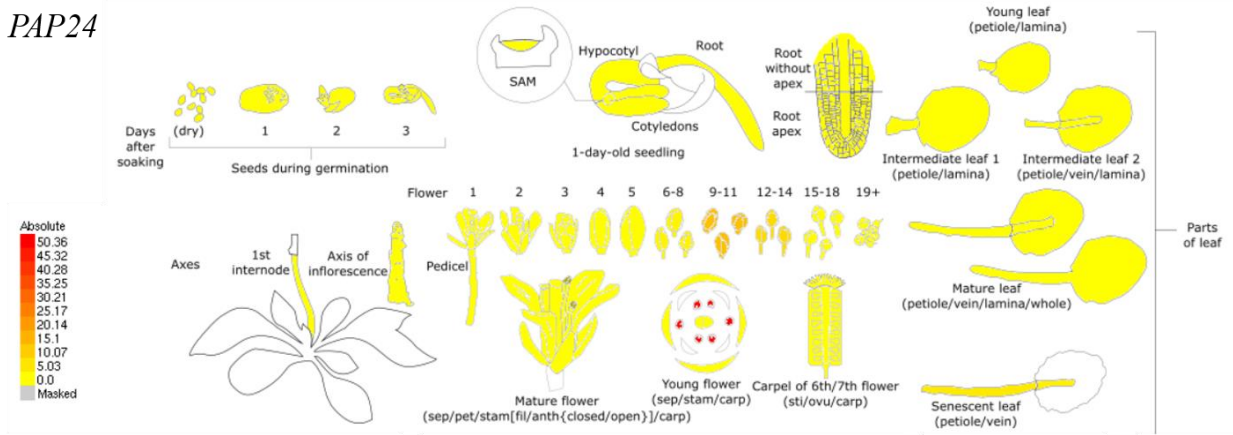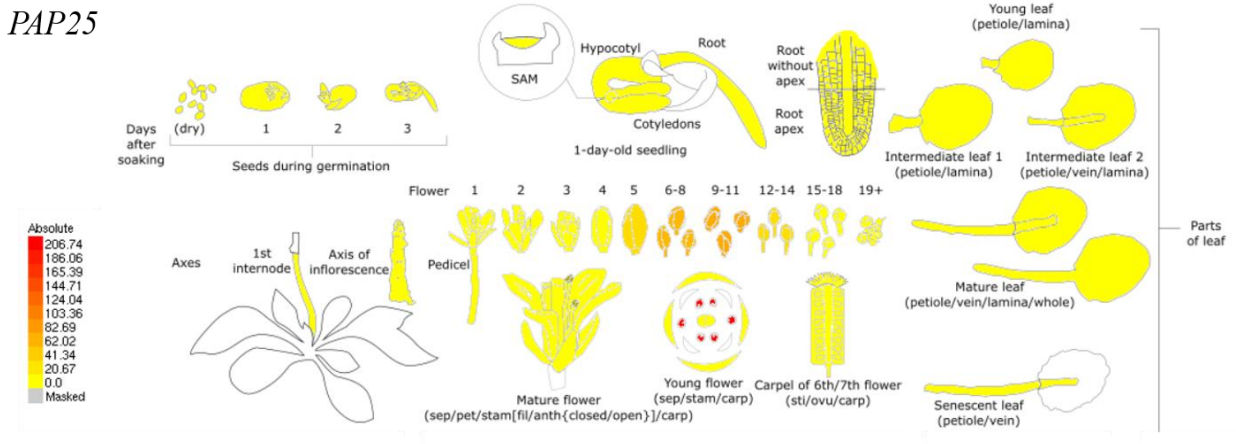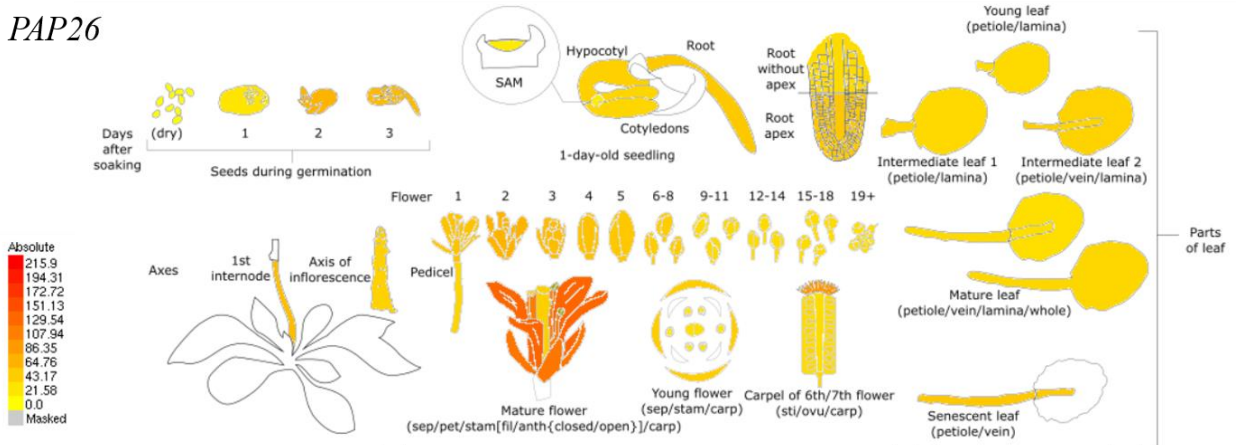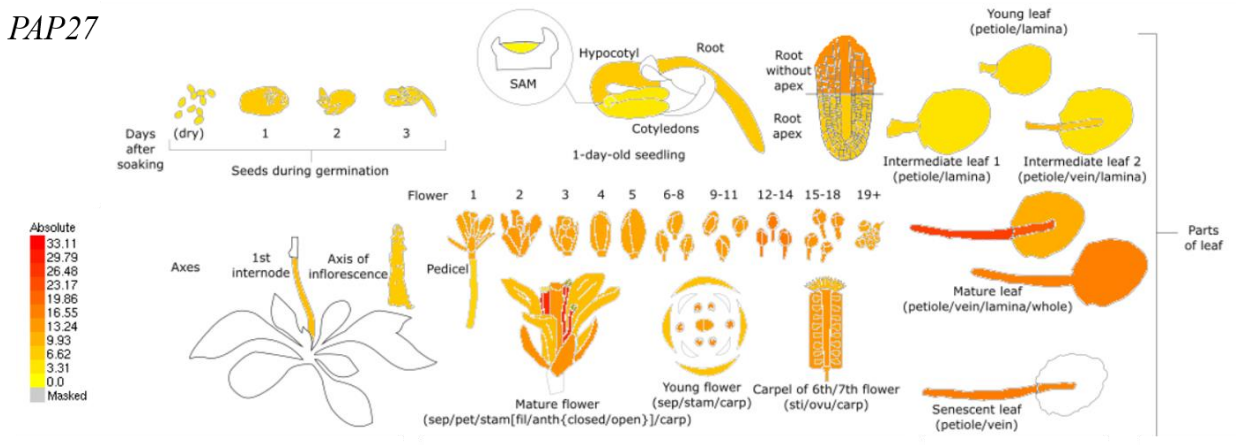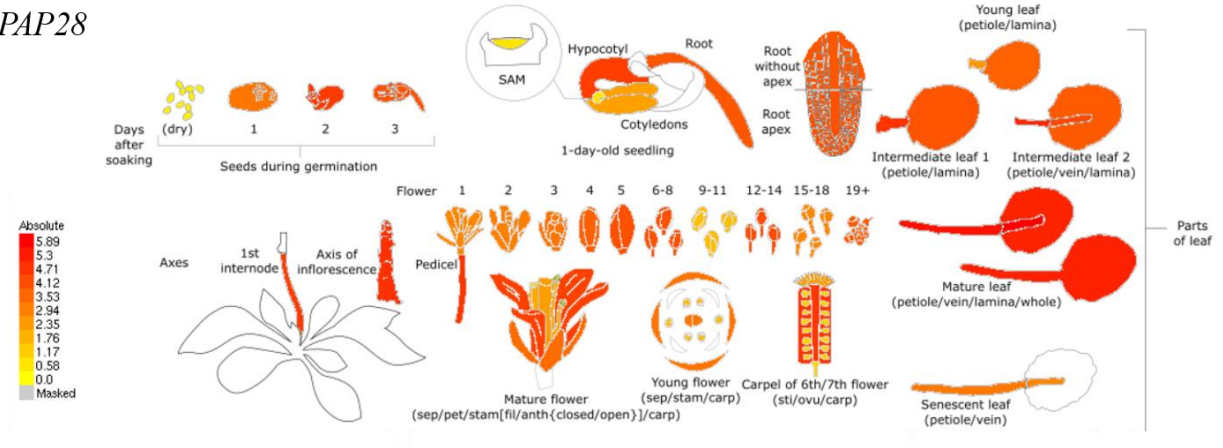
Figure A 2. Expression profile of *HADIIIBs* in *Arabidopsis thaliana* according to the publicly available Klepikova Atlas data in the Arabidopsis eFP Browser (http://bar.utoronto.ca/efp/cgi-bin/efpWeb.cgi?dataSource=Klepikova_Atlas). The level of transcript expression is indicated by a color code (yellow = low expression, red = high expression), and an absolute scale is also available on the left side of the image.
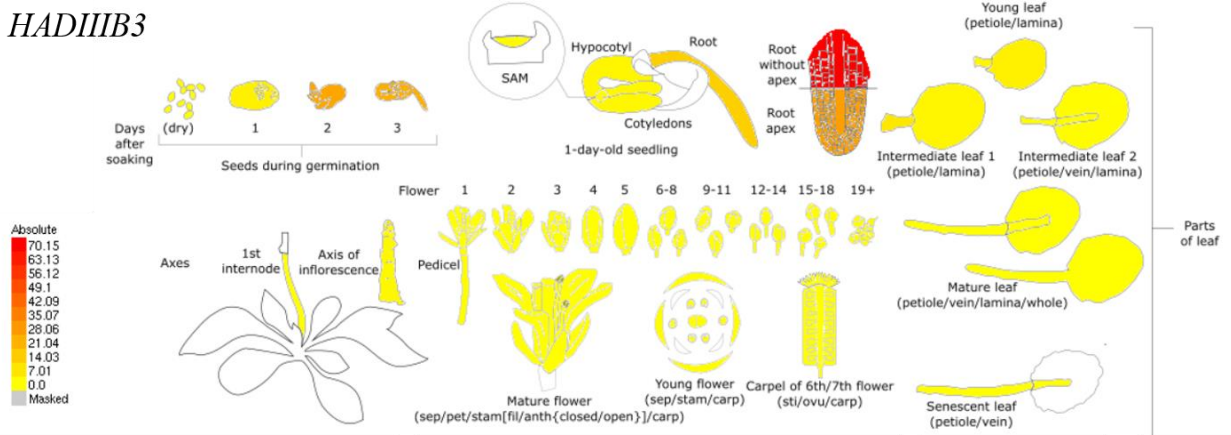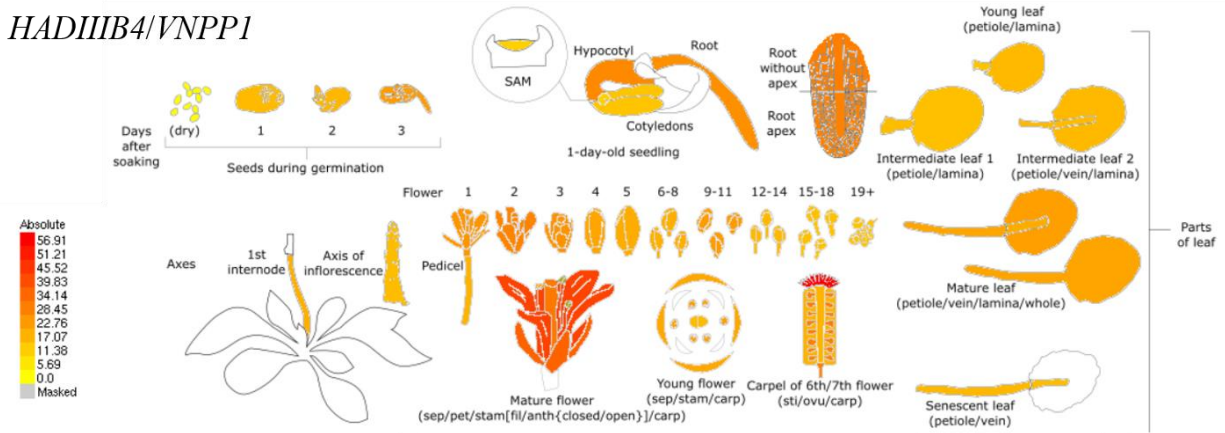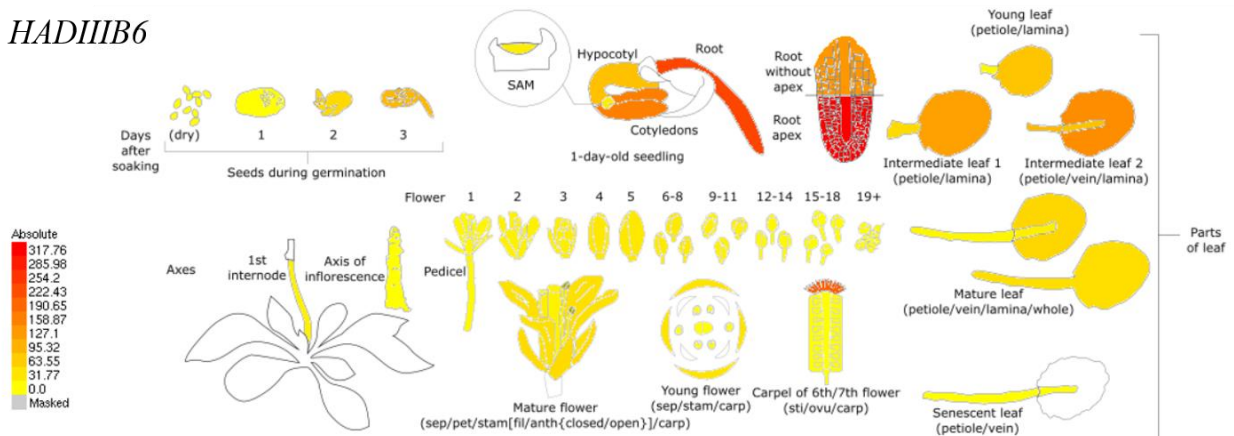
HADIIIB4/VNPP1

HADIIIB6

HADIIIB7

173
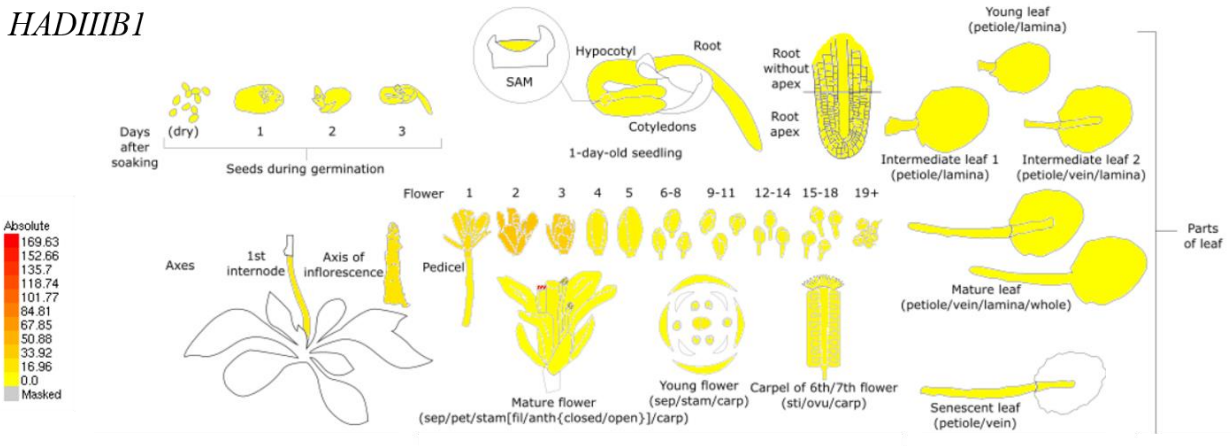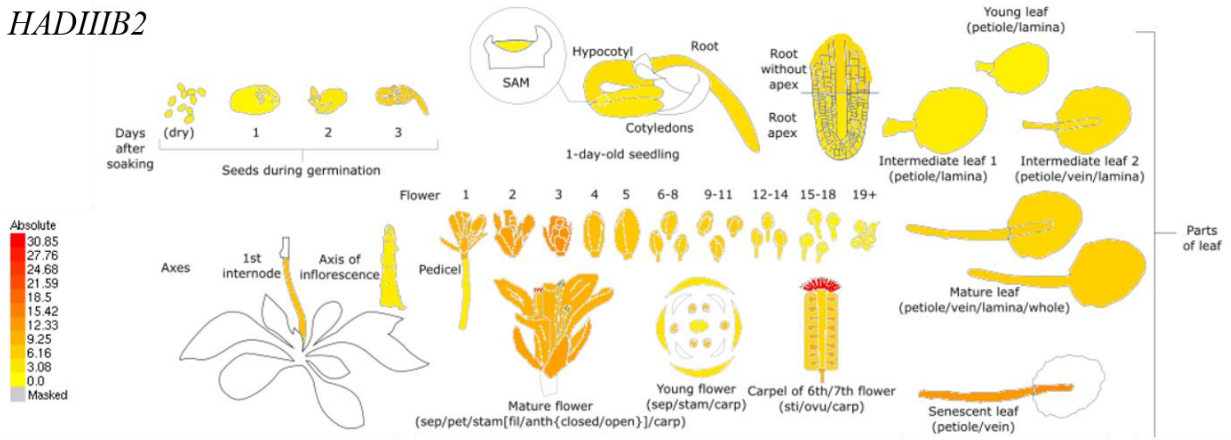
Figure A 3. Expression profile of *Endo5* in *Arabidopsis thaliana* according to the publicly available Klepikova Atlas data in the Arabidopsis eFP Browser (http://bar.utoronto.ca/efp/cgi-bin/efpWeb.cgi?dataSource=Klepikova_Atlas). The level of transcript expression is indicated by a color code (yellow = low expression, red = high expression), and an absolute scale is also available on the left side of the image.
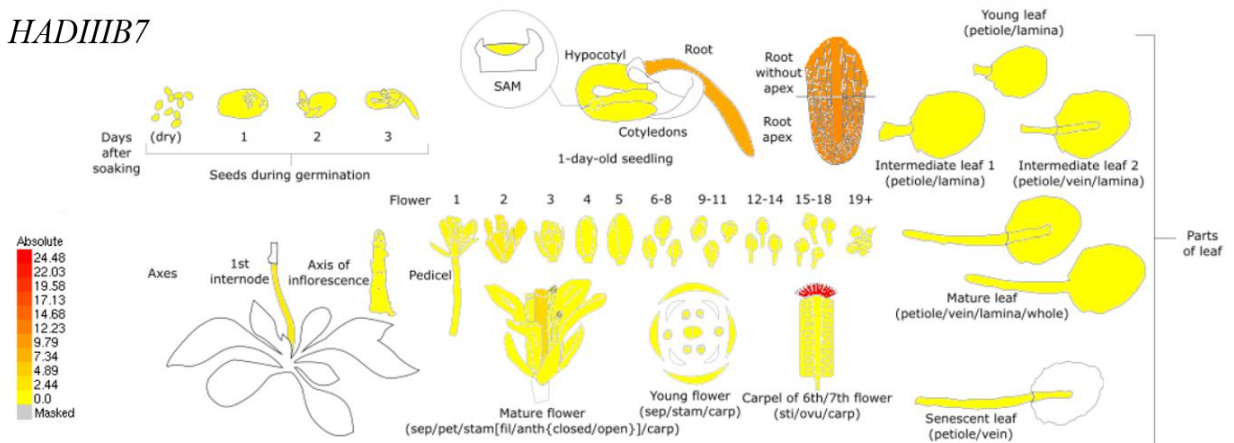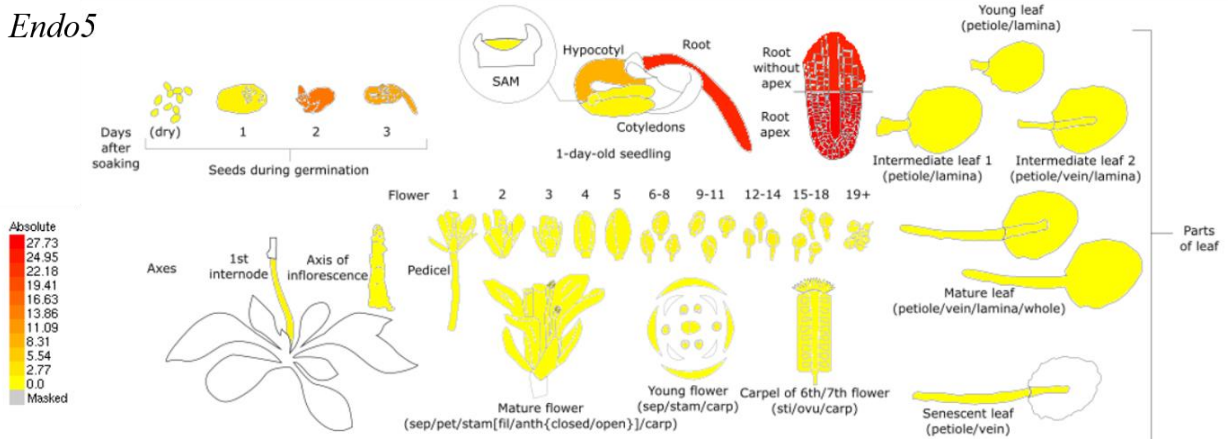

Figure A 4. Expression profile of *ENT1* in *Arabidopsis thaliana* according to the publicly available Klepikova Atlas data in the Arabidopsis eFP Browser (http://bar.utoronto.ca/efp/cgi-bin/efpWeb.cgi?dataSource=Klepikova_Atlas). The level of transcript expression is indicated by a color code (yellow = low expression, red = high expression), and an absolute scale is also available on the left side of the image.

174

Figure A 5. Expression profile of *RNS2* in *Arabidopsis thaliana* according to the publicly available Klepikova Atlas data in the Arabidopsis eFP Browser (http://bar.utoronto.ca/efp/cgi-bin/efpWeb.cgi?dataSource=Klepikova_Atlas). The level of transcript expression is indicated by a color code (yellow = low expression, red = high expression), and an absolute scale is also available on the left side of the image.
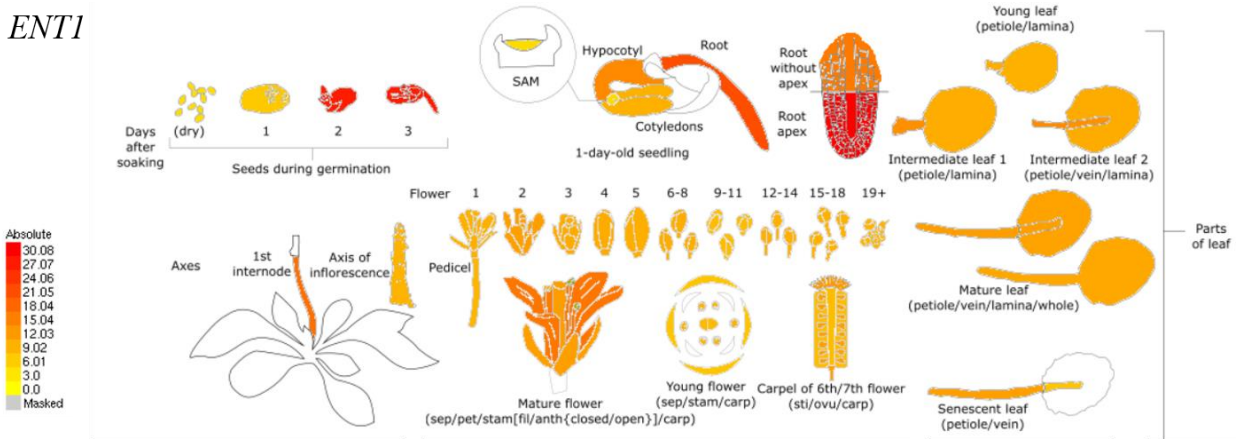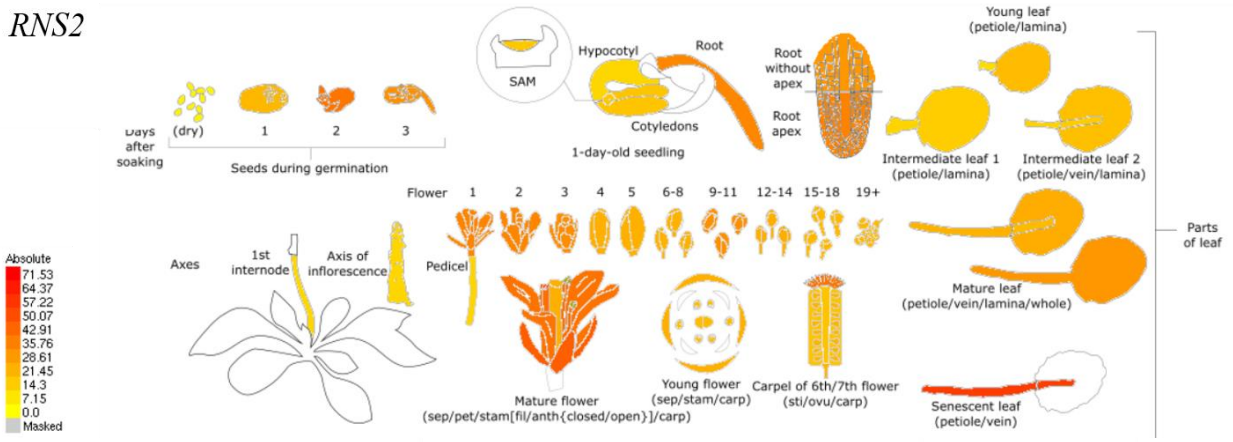
Figure A 6. Differential growth of transgenic lines of AUDS1 in comparison to wild type and *urease*. Six independent replicates from Section 2, experiment 3.2.1, and Figure 6.
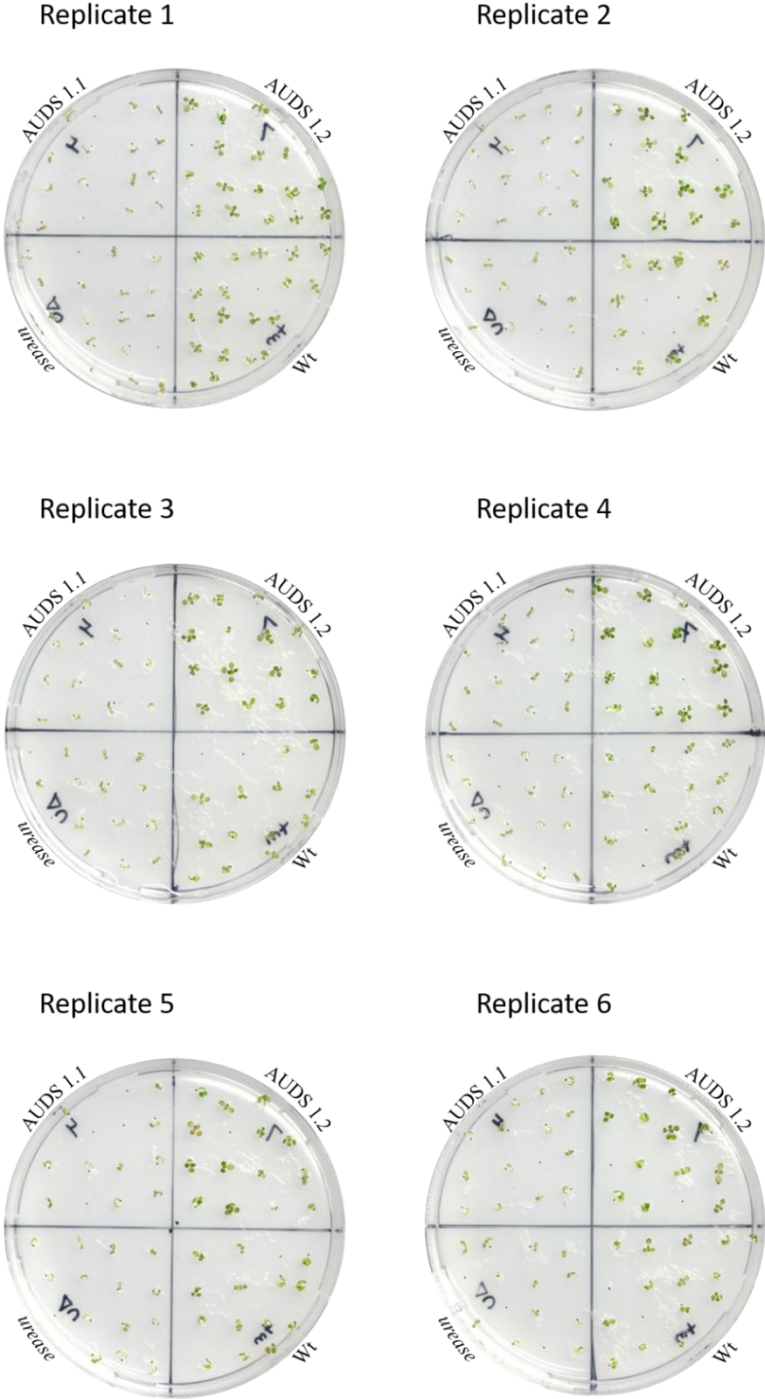
Figure A 7. Differential growth of the transgenic lines of the AUDS2 in comparison to the wild type. Six independent replicates from Section 2, experiment 3.2.2, and Figure 8.
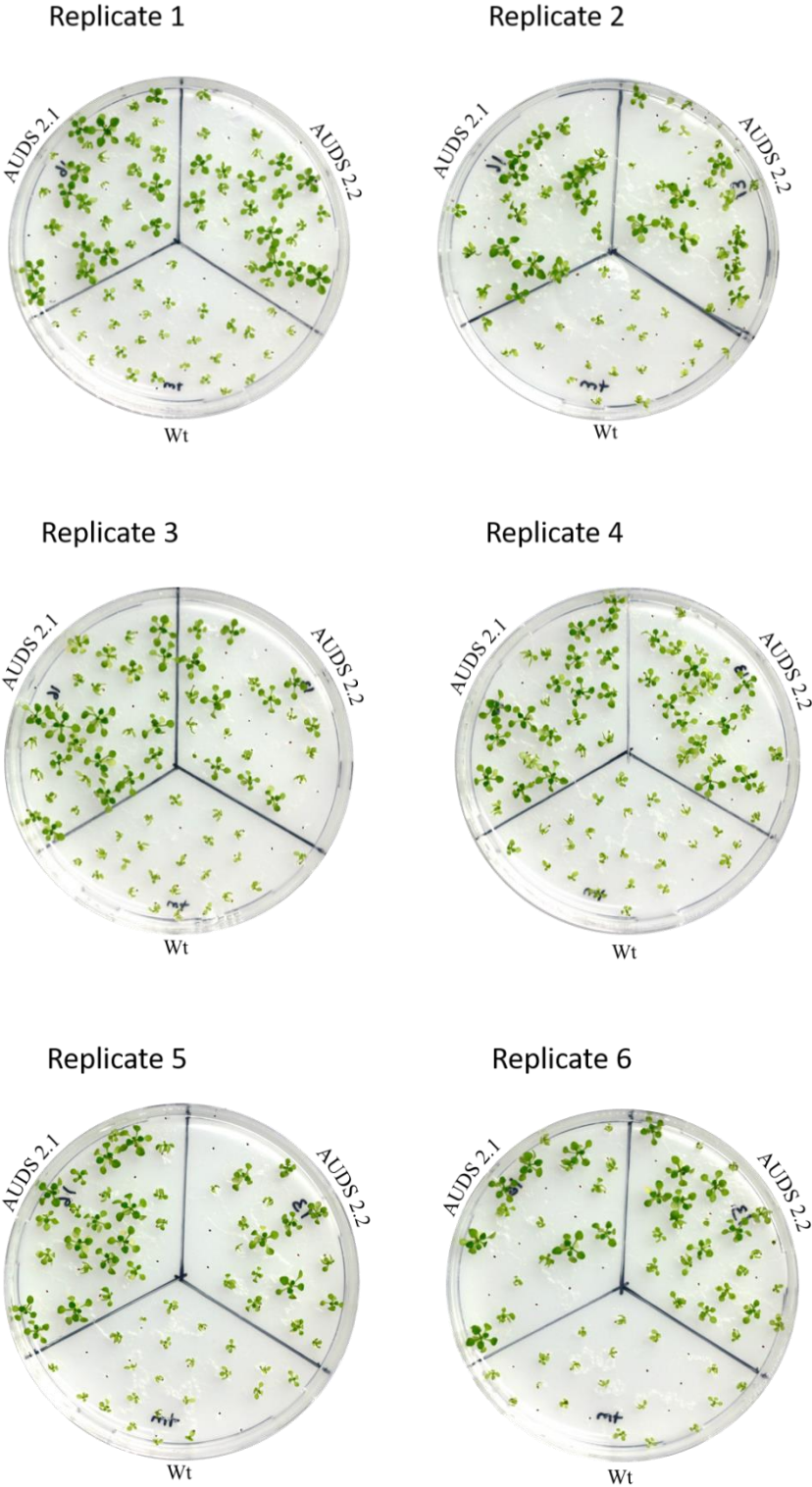
Figure A 8. Seedling establishment of plants with different ureolytic systems on the coco-peat substrate supplemented with urea. Three independent replicates from Section 2, experiment 3.3 and Figure 13.

Figure A 9. Differential growth of plants with different ureolytic systems on the coco-peat substrate, three weeks old plants. Three independent replicates from Section 2, experiment 3.3 and Figure 14.
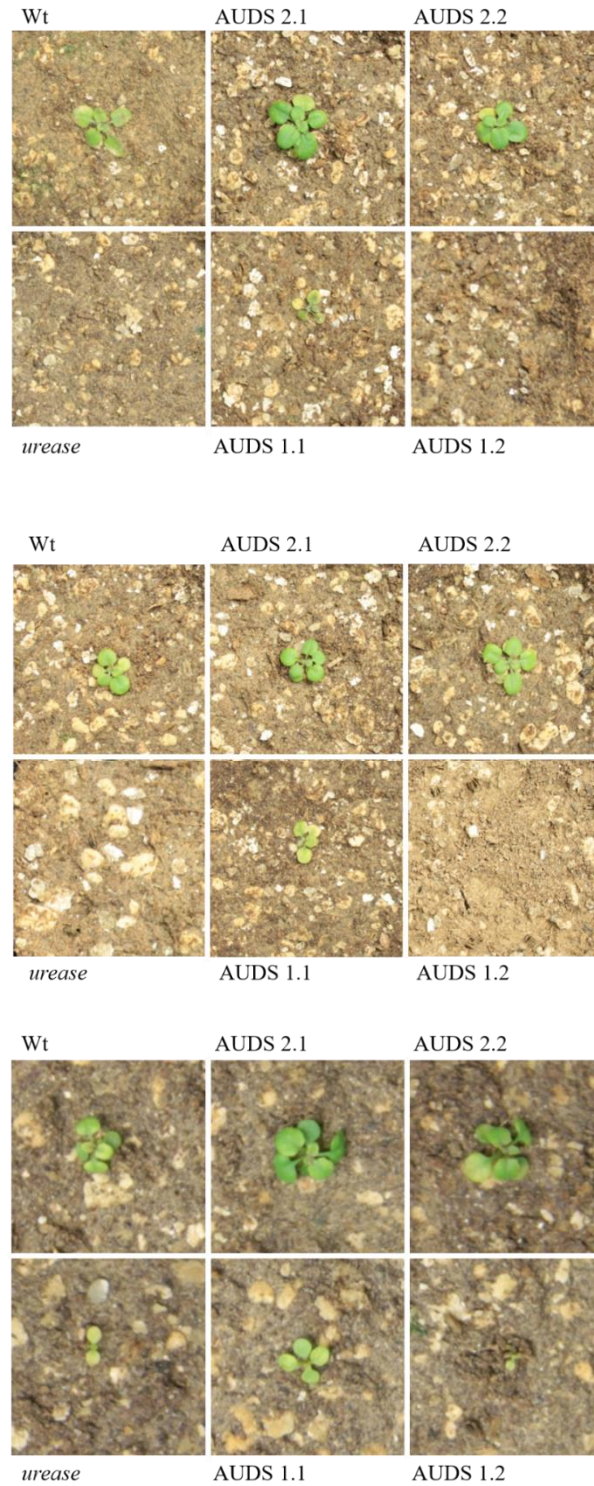
Appendix of Tables

Table A 1. Statistical analysis for xanthine concentration ng/g DW

Comparison	Test value	p value	Significance
Wt-*pap26*	1.61889434924934	0.497368708477443	NO
Wt-*vnpp1*	2.44144701341831	0.141990789133229	NO
Wt-*ent1*	2.48358000007601	0.131499570915806	NO
Wt-*rns2*	2.36829749824432	0.161874232258297	NO

Table A 2. Statistical analysis for 3'-CMP accumulation

Comparison	Test value	p value	Significance
0 h			
Wt-*vnpp1*	0.712795723371924	0.876665466958115	NO
Wt-*pap26*	-3.14951168078821	0.0475580336641529	YES
Wt-*vnpp1*pap26*	-6.70894260358007	0.000706529914182186	YES
8 h			
Wt-*vnpp1*	-1.06968657056529	0.701152446896055	NO
Wt-*pap26*	-3.13057077244595	0.050945710414906	YES
Wt-*vnpp1*pap26*	-2.00456871367692	0.24801767043147	NO
24 h			
Wt-*vnpp1*	-4.52550205630785	0.00719997864768951	YES
Wt-*pap26*	-5.87918663277105	0.00142063451165497	YES
Wt-*vnpp1*pap26*	-3.47616817033319	0.0290122275633581	YES

Table A 3. Statistical analysis for 3'-GMP accumulation

Comparison	Test value	p value	Significance
0 h			
Wt-*vnpp1*	-43.2248928986071	0	YES
Wt-*pap26*	-3.79106775194742	0.0167971184145175	YES
Wt-*vnpp1*pap26*	-3.53113403027483	0.0241993459497943	YES
8 h			
Wt-*vnpp1*	-0.824675384870919	0.826328823342792	NO
Wt-*pap26*	-1.16028303836824	0.642436541046957	NO
Wt-*vnpp1*pap26*	-2.76416732244568	0.0836260793361862	NO
24 h			
Wt-*vnpp1*	-1.27504230717732	0.593271696589451	NO
Wt-*pap26*	-2.40203223863306	0.149238846479281	NO
Wt-*vnpp1*pap26*	-13.7897149535517	8.2599612660772e-07	YES

Table A 4. Statistical analysis for AUDS1 in comparison to wild type and *urease*.

Comparison	Test value	p value	Significance
Fresh weight[-1]			
Wt-AUDS1.1	6.719439876	4.69E-06	Yes
Wt-AUDS1.2	-1.540519576	0.406993197	NO
urease-AUDS1.1	0.449504927	0.965546946	NO
urease-AUDS1.2	-4.56214493	0.000768342	Yes
Wt-*urease*	7.342602788	8.98E-07	Yes
AUDS1.1-AUDS1.2	4.595470553	0.000970247	Yes

[1] Please refer to Figure 7

Table A 5. Statistical analysis for AUDS2 in comparison to wild type

Comparison	Test value	p value	Significance
Fresh weight[-1]			
Wt-AUDS2.1	-12.74696435	4.54E-13	Yes
Wt-AUDS2.2	-13.77590022	2.01E-12	Yes
Dry weight[-1]			
Wt-AUDS2.1	-15.0443377	2.22E-16	Yes
Wt-AUDS2.2	-13.97368873	4.11E-15	Yes
Leaf area[-2]			
Wt-AUDS2.1	-15.56141232	8.88E-15	Yes
Wt-AUDS2.2	-12.24836527	6.23E-10	Yes
Leaf greenness[3]			
Wt-AUDS2.1	-8.067058728	1.39E-05	Yes
Wt-AUDS2.2	-8.662569934	4.32E-07	Yes
Nitrogen content[4]			
Wt-AUDS2.1	-15.08695873	8.88E-16	Yes
Wt-AUDS2.2	-15.08675871	8.88E-16	Yes

[1] Please refer to Figure 9, [2] please refer to Figure 10, [3] please refer to Figure 11, [4] please refer to Figure 12,

Table A 6. Fresh weight of the transgenic lines of AUDS1 in comparison to wild type and *urease*.

	Wild type (mg Plant^{-1})	*urease* (mg Plant^{-1})	AUDS1.1 (mg Plant^{-1})	AUDS1.2 (mg Plant^{-1})
Biological replicates^{-1}	1.438889	0.828571	0.735714	1.86875
	1.875	0.925	0.708333	2.592308
	1.666667	0.952941	1.1	2.507692
	1.426667	0.757143	0.666667	1.913333
	1.573333	0.721429	0.753333	1.675
	1.323077	0.766667	0.766667	1.135294

[1] Please refer to Section 4.2.3, Figure 9.

Table A 7. Fresh weight of the transgenic lines of AUDS2 in comparison to wild type.

	Wild type (mg Plant^{-1})	AUDS2.1 (mg Plant^{-1})	AUDS2.2 (mg Plant^{-1})
Biological replicates^{-1}	1.603704	3.52963	3.175
	1.509524	4.885714	3.984211
	1.665217	4.772	3.583333
	1.733333	4.429167	3.657143
	1.559091	4.678261	3.446667
	1.672222	4.688235	3.995455

[1] Please refer to Section 4.2.4, Figure 9.

Table A 8. Dry weight of the transgenic lines of AUDS2 in comparison to wild type.

	Wild type (mg Plant^{-1})	AUDS2.1 (mg Plant^{-1})	AUDS2.2 (mg Plant^{-1})
Biological replicates^{-1}	0.046740741	0.113555556	0.097875
	0.038809524	0.141857143	0.123263
	0.043913043	0.14336	0.101778
	0.05075	0.126791667	0.105952
	0.044272727	0.141347826	0.116667
	0.044388889	0.147470588	0.107682

[1] Please refer to Section 4.2.4, Figure 9.

Table A 9. Leaf area of the transgenic lines of AUDS2 in comparison to wild type.

	Wild type (cm^2 plant^{-1})	AUDS2.1 (cm^2 plant^{-1})	AUDS2.2 (cm^2 plant^{-1})
Biological replicates^{-1}	0.027807687	0.124488	0.104366304
	0.022149869	0.098381	0.081971794
	0.020717496	0.098492	0.090260845
	0.027082452	0.094973	0.100205277
	0.022202336	0.111194	0.072409625
	0.023980481	0.099969	0.091003976

[1] Please refer to Section 4.2.4, Figure 10.

Table A 10. Leaf area of the transgenic lines of AUDS2 in comparison to wild type.

	Wild type Green : yellow (Pixels raio)	AUDS2.1 Green : yellow (Pixels raio)	AUDS2.2 Green : yellow (Pixels raio)
Biological replicates[1]	0.627699	5.082917	3.843412903
	0.524551	8.020743	3.698306281
	0.304641	3.890068	2.289735461
	0.510465	4.953304	2.329219337
	0.499199	5.683479	3.475824991
	0.417516	5.22391	3.265994363

[1] Please refer to Section 4.2.4, Figure 11.

Table A 11. Nitrogen content of the transgenic lines of AUDS2 in comparison to wild type.

	Wild type w/w	AUDS2.1 w/w	AUDS2.2 w/w
Biological replicates[1]	3.788	5.012	5.112
	3732	5.042	4.888
	3.637	4.846	4.798
	3.752	4.821	4.803
	3.836	4.979	4.818
	3.937	4.774	5.031

1   Please refer to Section 4.2.4, Figure 12.

2

Table A 12. Carbon content of the transgenic lines of AUDS2 in comparison to wild type.

	Wild type w/w	AUDS2.1 w/w	AUDS2.2 w/w
Biological replicates[1]	36.80	36.59	36.36
	37.13	37.18	36.27
	35.81	35.95	35.29
	36.09	36.34	34.82
	36.28	35.10	35.33
	37.10	36.72	35.19

[1] Please refer to Section 4.2.4, data not shown in main thesis

Table A 13. Xanthine concentration ng/g DW (Figure 31)

	Wild type	*pap26*	*vnpp1*	*ent1*	*rns2*
Biological replicates	16089.35	19542.66	8712.315	10249.97	17377.63
	19185.17	14159.18	12997.28	17019.41	16393.62
	22373.47	11705.13	10953.76	10424.71	7673.148
	19418.92	18253.46	11309.67	9570.241	8756.463
	16759.42	13238.4	19839.04	17531.37	13707.75

Curriculum Vitae

Personal data

Name	Nabila Firdoos
Nationality	Pakistani
Date of birth	28-03-1989
Place of birth	Faisalabad, Pakistan

Education

04.2016–Present	PhD study in the Department of Molecular Nutrition and Biochemistry of Plants Gottfried Wilhelm Leibniz Universität Hannover Supervisor: Prof. Dr. Claus-Peter Witte Financed by a fellowship from the German Academic Exchange Service (DAAD)
10.2014–06.2015	Volunteer research work Institute: National Institute for Biotechnology and Genetic Engineering (NIBGE) Supervisor: Dr. Niaz ahmad
09.2012–12.2014	M.Phil. Biotechnology Institute: National Institute for Biotechnology and Genetic Engineering (NIBGE) Supervisor: Dr. Niaz ahmad
10.2008–07.2012	BS(Hons) Bioinformatics Institute: Government College University Faisalabad (GCUF)